TECHNICAL UNIVERSITY OF LIBEREC
Faculty of Mechatronics, Informatics
and Interdisciplinary Studies

ONE-DIMENSIONAL NANOFIBERS: APPLICATION IN MEMBRANE TECHNOLOGY

Habilitation Thesis

MSc. Fatma Yalcinkaya, PhD.

November 2020

Acknowledgment

Abstract:

This habilitation thesis is prepared based on the author's contributions to the nanofiber membranes in water treatment. First, the author tried to determine the main problems why the nanofibers cannot use in water domain applications in the market, then tried to suggest solutions, solve and clarify each problem. The thesis provides a comprehensive description of the issue based on the current state of knowledge.

The structure of the thesis is as follows: Chapter 1 is a general introduction that shows the main problems why the nanofibers cannot take place in liquid filtration. In Chapter 2, electrospinning process and parameters for the forming of the nanofiber web are introduced. We discuss the needle-free electsopinning system developed by the Technical University of Liberec (TUL). Chapter 3 focuses on membrane technology and nanofibers in membrane technology. Chapter 4 is represented the work of the author in cooperation with several authors from different institutions and countries in the field of nanofiber web formation, membrane preparation, application, and comment on their contribution to the scientific community. Chapter 5 is the conclusion of the work. In the Appendix part, the author includes scientific publications together with co-authors from the same or different institutions.

Content

CHAPTER 1-INTRODUCTION

One-dimensional (1-D) nanostructures such as rods, tubes, wires, and fibers have attracted a great deal of attention because of their numerous applications in sensors, energy storage and generation, pharmaceutical and textile industries, air filtration, water purification, and environmental remediation. These nanostructures can provide unique advantages such as specific surface area, superior mechanical properties, nanoporosity, and improved surface characteristics. 1-D electrospun nanostructures-nanofibers are rapidly emerging as key enabling components in filtration application due to their unique specific surface area, tight pore size and highly porous structure, finer degree of filtration and better filter efficiency, the low-pressure drop across the filtration media, flexibility in filter configuration, and easy to modified surface.

Currently, nanofibers have a significant market in air filtration such as turbine air filters, dust air filters, engine air intake filters, and vacuum bag filters, with an annual growth rate of around 35% [1,2]. Despite to huge potential of nanofibers in filtration technology, water domain applications are limited, require extensive investigation and development. To apply the nanofibers into water filtration, there is a great need to develop a novel nanofibrous structure with good mechanical strength and high permeability. **<u>The main problems</u>** why the nanofibers cannot take place in liquid filtration are given as;

> **P.1.** Not all polymers can form detect-free nanofibers: All polymeric materials that are currently used in membrane technology are not able to form nanofiber web.

> **P.2.** Not all the hydrophilic nanofiber is suitable to use in water filtration: Many of polymers used in nanofiber technology (polyvinyl alcohol, polyethylene oxide, polyvinyl pyrrolidone, poly(acrylic acid), cellulose acetate, chitosan, gelatin, etc.) can be dissolved, swollen or degradable underwater.

> **P.3.** Mechanical weakness of nanofibers underwater: Any slight tension can cause damage to the nanofiber surface.

> **P.4.** Higher cost compared to conventional nonwovens: significant cost differences of nanofibers compared to other traditional textile materials.

> **P.5.** Lack of selectivity for liquid-liquid separation: After forming hybrid structure, the selectivity of nanofiber membrane can be altered. In many cases, selectivity needs to improve.

> **P.6.** Life-span: Due to membrane fouling, the life-span of membranes reduces significantly.

> **P.7.** Cleaning: Cleaning is needed when the nanofibrous membranes fouled. So far, no cleaning method has been submitted for the nanofibrous membranes.

> **P.8.** Recycling and disposal: Since the final product is in a hybrid structure, recycling and disposal of the membranes are limited.

> **P.9.** Environmental effect: Chemicals and side products, risk of nanomaterials.

The main aims of this thesis are to address each problem mentioned above and try to suggest a possible solution to solve each problem. Even though many scientists have already focused on

nanofibrous membrane filtration and have appropriate extensive specialized knowledge and techniques to the issues, it is significant to continue working in this field to commercialize the application area for the future market.

The author follows a pattern to clarify each problem: First, the author introduces nanofibers and their preparation method using an industrial scale device. Then, the author's contribution to parameters on this device to improve the quality of the nanofiber web which has been mentioned. After that, membrane technology, the requirement for a membrane, membrane modules, and separation systems have been explained to clarify what are the current situation of membrane technology in the market and how to improve it. The preparation of nanofiber membranes is explained step by step. The first step is focused on the preparation of nanofiber webs; the second step is related to how to improve mechanical strength to adapt nanofiber technology in membrane technology; the third step is to characterized methods that can be used for nanofiber membranes, and the fourth step is related to the improvement of surfaces for a better flux, selectivity, and anti-fouling property. In the fifth step, some of the current studies on nanofiber membranes are chosen for discussion; the disposal and the environmental effect of nanofiber membranes. As the last step, the author included own selected publications related to nanofiber membranes, how to enhance the application of various polymeric materials, and the mechanical properties of nanofibers using the lamination method. Also, nanofiber membranes at different liquid separations from seawater to oil/water emulsion have been included. The author mainly focuses on the nanofiber membranes as microfilter and their surface modification.

The ultimate goal of the author is to clarify the problems and offer solutions for the application of nanofibers in liquid filtration. The author, therefore, publishes this thesis to introduce nanofiber webs into membrane technology. The author nevertheless extends the apologies to those scientists whose research findings have not been cited or discussed in this thesis. The present thesis shall be of interest to those scientists and company researchers engaged in nanofibers and applications in liquid separation.

CHAPTER 2-NANOFIBER TECHNOLOGY

2.1. Electrospun Nanofibers

The word "nano" comes from the Greek word "Nanos" which has meaning "dwarf". In science, nanotechnology refers to a particle size smaller than 1 micron (1000 nm). Nano dimension is a billionth of a meter. According to dimension, nanomaterials can be classified in four groups as (a) zero-dimension (0-D) in which all three dimensions are in the range of 1 to 100 nm, (b) one-dimension (1-D) in which one of the dimensions is limited to the nanometer scale, (c) two-dimension (2-D) in which two dimensions larger than 100 nm, (d) three-dimension (3-D) in which three dimensions larger than 100 nm, but components of their microstructures are at nanoscale.

Nanofibers are a 1-D structure that has a fiber diameter below 1 μm. Nanofibers have ultimate properties compared to conventional fibrous structures. Such properties are low basis weight, high specific surface area (high surface-to-volume ratio), tight pore size and pose size distribution, porous structure, high permeability and gas diffusivity, good reproducibility, tunable size, and well-controlled orientation. Envied by those unique advantages, remarkable growth and interest have been engaged in filtration applications.

Nanofibers can be fabricated using several technologies like island-in the sea, centrifugal spinning, melt-blown, phase-separation, freeze-drying, template synthesis, drawing, self-assembly, force-spinning, and electrospinning. Among all technologies, electrospinning is the most common technique which is easy and simple to fabricate nanofiber webs. Even though the first electrostatic attraction of a liquid was observed in the 1600s [3], electrospinning technology has been patented first time in 1900s [4], since then the number of patents and publications about electrospinning has been increasing exponentially.

2.1.1. Single-Needle Electrospinning System

Electrospinning is an easy set-up that contains 3 major components; high voltage supplier (AC or DC), a solution feeding unit, and a collector (charged or grounded). A lab-scale electrospinning system is demonstrated in Figure 2.1. Basically, a high voltage supply is connected to a polymer feeding unit polymer. The collector is grounded or oppositely charged to the feeding unit. Under the applied voltage, if the electrostatic field overcomes to surface tension of polymeric solution/melt, the solution is accelerated and ejected towards to collector with whipping or splitting with reducing size. The solution is evaporated during ejection, and a solid fiber is collected onto the collector.
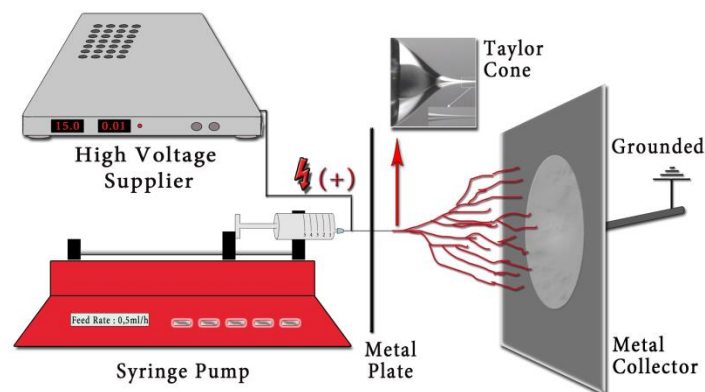
Figure 2.1. Schematic illustration of electrospinning set-up [5]

Spinnability, defect-free structure, and uniformity of the fiber diameter are challenges of electrospinning technology. To address this problem, the effect of process and the solution parameters on electrospun nanofiber are studied.

Parameters that can be changed by equipment setting are called as process parameters. These parameters are mainly applied voltage, the feed rate of the polymer solution, the distance between the collector and the needle tip, temperature of the solution, and ambient parameters. Parameters that are related to solution properties are called as solution or system parameters. Viscosity, concentration, molecular weight, surface tension, conductivity, and dielectric properties of polymer solution are the main system parameters. More information is given in the needle-free electrospinning system part.

Single needle electrospinning system is only suitable for lab-scale production; highly productive systems have been developed to fulfill industry needs. One of the important electrospinning systems for bulk production has been developed and patented by the Technical University of Liberec in 2005 [6] and commercialized in Elmarco s.r.o. Company with the trade name first generation of Nanospider. Since then, the application of nanofiber material in our daily life is fastened in the Czech Republic.

In the following sub-title, we focus on the needle-free electrospinning system in detail, which brings us to the point where we are today. There is plenty of new technology for the industrial production of the nanofiber. However, the author would like to focus on the roller electrospinning system to show each step of its' contribution to the roller electrospinning parameters to the end-use of nanofibers in membrane technology. Thanks to the developments of industrial production devices, we are able to use nanofibers in our daily life.

2.1.2. Needle-Free electrospinning system (Roller electrospinning)

In 2003, Jirsak et al. tried to develop needle-free roller electrospinning system for the bulk production of nanofibers and a new nanofiber production method was developed [6]. In roller electrospinning system, there is a rotating roller immersed in a solution bath which is connected to high voltage supplier. On the opposite side, a metallic collector (grounded or charged) is placed under a conveyer supporting material (antistatic nonwoven or silicon paper) as shown in Figure 2.2. Different from single needle, many Taylor's cone are forming on the surface of the roller at the same time to fasten production.
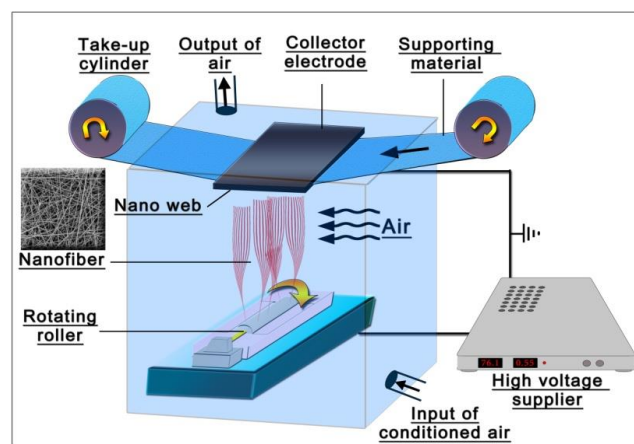
Figure 2.2. Schematic diagram of roller-electrospinning system [5].

Parameters of roller electrospinning system are more complicated compared to needle electrospinning systems due to different technological approaches. In the roller system, the parameters are classified as (a) independent parameters and (b) dependent parameters, as shown in Table 2.1. All these parameters are related to "*Chapter 1-Introduction, P1*". To solve "*P1*", one should focus on the parameters of the electrospinning system. Since there are plenty of parameters, herein, we described only selected parameters. It should be noted that, all these parameters affect the spinnability and quality of the nanofiber webs.

Table 2.1. Dependent and independent parameters of roller electrospinning system [7]

Independent Parameters	**Dependent Parameters**
• Polymer solution properties (concentration, viscosity, composition, surface tension, conductivity, molecular weight) • Applied voltage • Distance between electrodes • The velocity of rotating roller* • The velocity of take-up fabric • Geometry of electrode • Geometry of collector • Ambient conditions (temperature, relative humidity)	• Number of cones, the density of jets • Lifetime of jets • Spinning performance, spinning performance/per jet • Total average current, current/jet* • The thickness of the polymer solution layer on the surface of the roller* • Force acting on a jet* • Spinning area* • Distance between neighboring jets* • Jet length in the stable zone • Diameter and distribution of nanofiber • Non-fibrous area • Launching time of jets

*The parameters defined or studied by the author and introduced to literature.

2.1.2.1. Selected electrospinning parameters

Concentration/Molecular Weight /Viscosity: The electrospinning process requires high molecular weight polymers to initiate the spinning process. During electrospinning, a certain amount of chain entanglement is needed to keep the solution jet coherent. At low concentration or molecular weight, the jets break and create beads instead of fibers. As a result, spinning quality decreased. At high concentration or molecular weight, the charged jet does not break up into small droplets due to an increase in the viscoelastic force and thick fibers or non-fiber structures form. Shenoy et al. suggested the number of entanglements/chain must be bigger than 2.5 to fabricate nanofibers [8]. The viscosity of the solution depends on concentration, molecular weight, solvent type, shear rate, pressure, and temperature. The intrinsic viscosity [η] of many polymer solutions is given by the Mark-Houwink equation (2.1);

$$[\eta] = KM^{\alpha} \qquad (2.1)$$

where M is the molecular weight, and K and α are constants for particular kinds of polymer and solvent. The value of α varies from 0.5 for a random coil to 2 for a rigid rod [9].

The relationship between solution concentration-molecular weight and fiber structure is studied by Author [7], as shown in Figure 2.3.
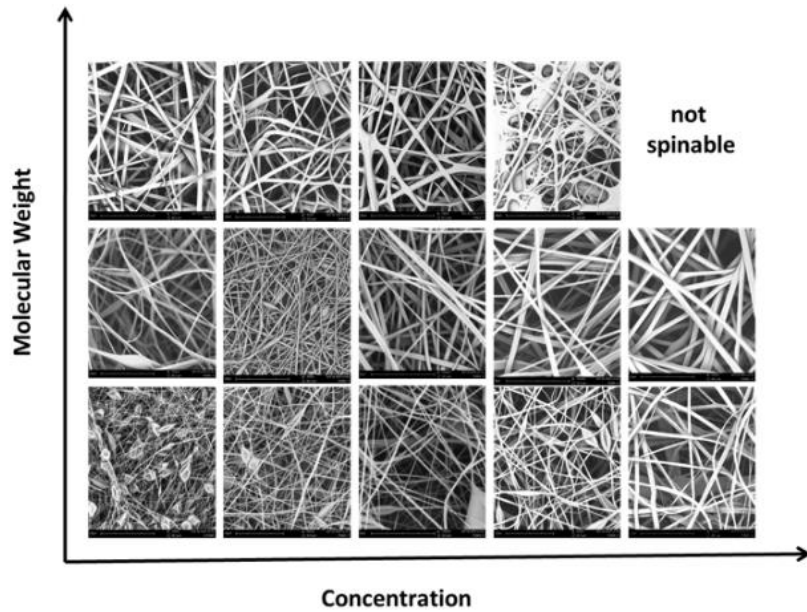
Figure 2.3. The changes in the surface morphology of nanofibers by molecular weight and concentration [7].

The image indicates that bead structure, fiber quality, and spinnability of polyvinyl butyral (PVB) nanofibers are very much changed by the molecular weight and concentration of the polymers.

Surface Tension: The electrospinning process initiates once the electrostatic force on polymeric solution overcomes to surface tension and forms a cone called as "Taylor's cone". For a higher surface tension, a stronger electric field is required. To avoid a high electric field, generally, surfactants are used in the polymer solution to reduce surface tension. A higher amount of surfactant can cause polymer droplets during spinning, which can result in a bad quality of nanofibers. The relationship between the amount of non-ionic surfactant and polyvinyl alcohol (PVA) nanofiber surface morphology is studied by the Author as shown in Figure 2.4 [7].
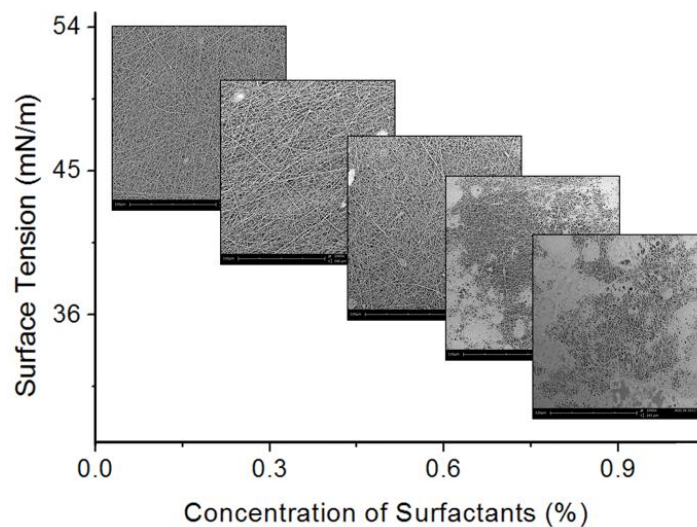
Figure 2.4. Effect of surfactant concentration on the surface morphology of PVA nanofibers.

Conductivity and permittivity: during the electrospinning, the stretching and whipping or splitting of a Taylor's cone is controlled by the Coulombic forces between charges and the electric field. The

surface charge of the Taylor's cone can be changed by changing the solution conductivity. Uniform, defect-free and thinner nanofibers can be fabricated by controlling the conductivity of the solution. In literature, it was suggested that an acceptable range of conductivity in electrospinning is changing from 10^{-6} to 10^{-2} $(\Omega.m)^{-1}$ [10]. By lowering the permittivity, the electric charge transfer is getting higher in the solution. It was also suggested that the best relative permittivity value for the electrospinning is between 5 and 30, with a limit not exceeding 100 [10]. To increase the conductivity of the polymeric solution, generally salt is used.

The velocity of rotating roller[*]: Rotating roller speed is associated with the feed-rate of the solution. High rotating speeds mean more solution can carry to the surface, but also fast-moving of roller. When the roller is too fast, there will be not enough time to born a new Taylor's cone or less amount of cones are formed. Oppositely, the low speed of the roller can cause not enough feed on the roller surface, and as a result, no fibers form (Figure 2.5). The feed rate controls the quality, spinnability and the amount of fibers formed on the support.
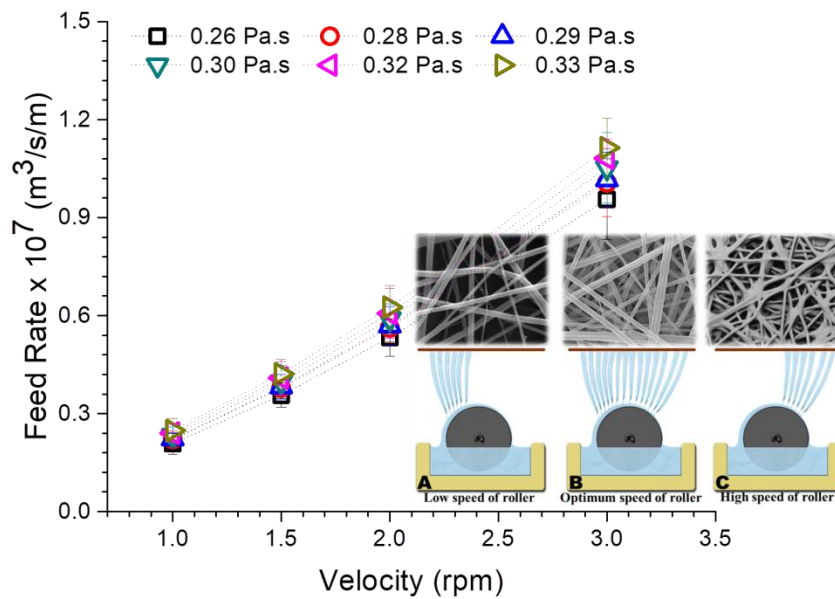
Figure 2.5. Relationship between roller speeds, feed rate fiber surface morphology [5].

The feed rate calculated by the equations 2.2-2.4:

the linear-velocity of the roller surface (v) is equal to

$$v = \omega * \pi * d / 60 \quad (m/s) \quad (2.2)$$

and the voluminous feed rate ύ

$$\acute{\upsilon} = h * v * \ell \quad = h * \omega * \pi * d * \ell / 60 \quad (m^3/s) \quad (2.3)$$

The voluminous feed rate of polymer solution per 1 meter length of roller ύ/ℓ is equal to

$$\acute{\upsilon} / \ell = h * \omega * \pi * d / 60 \quad (m^3/s/m) \quad (2.4)$$

where, h is the thickness of solution layer (m), ω is the angular speed of roller (rpm), d is the roller diameter (m), ℓ is the roller length (m).

Total average current, current/jet: Many researchers tried to focus on the current-voltage relationship in electrospinning process. Fallahi et al. used power law and showed current ~ (voltage)$^{2.53}$ [11]. In another approach, it was shown that the current did not only depend on voltage but also conductivity [12]. The relationship between current-voltage-conductivity was shown as $I\sim E*Q^{0.5}*K^{0.4}$. Some other works indicate that the feeding rate also has an importance on the jet current [13,14]. In our case, we tried to measure the total current of the electrospinning process since there is more than one Taylor's cone forming and then they are divided into the number of cones for evaluating the current per one jet. For this aim, the following set-up was built, as shown in Figure 2.6. The number of Taylor's cone on the whole surface of the roller was counted using a high-speed camera simultaneously with a digital multimeter, which measures the total current.
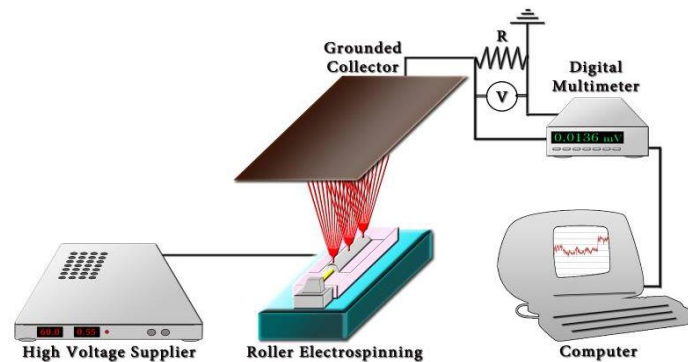
Figure 2.6. Measurement of total current on roller electrospinning system [5].

This work is currently used on nanofiber production devices to determine the stability of the spinning process. If the process is stable, the total current does not change. In case any problem happens during spinning (such as not enough feed, changes of humidity or temperature, breaking of wire on wire spinning, etc.), the total current changes are due to changes in total number of Taylor's cone. The operator generally stops the process and controls all parameters. Our contribution to the nanofiber web is to control the stability of the process.

Besides the used electrospinning technology, the type and the property of the material are very important in nanofiber preparation. For instance, not all polymeric materials can form nanofibers. To improve fiber-forming, many authors tried to change the solution properties (conductivity, viscosity, surface tension, so on), cross-linking, or prepare a polymer mixture with a suitable spinnable polymer. Polymer mixing offers not only spinnability but also an easy way to obtain new materials by combining various polymers. The polymer mixture is generally used to improve chemical and mechanical resistance, strength, and thermal stability. Using the mixture method, one can try to overcome the problem in "*Chapter 1- P1, P2*". For this purpose, the author prepared a series of experimental work published in [15]. More details are given in "*Chapter 4-4.1.1. Improving Nanofiber Quality for Water Filtration*".

2.2. Application of Nanofibers

The technology of the electrospinning was first patented in 1931 [16], since then a series of technology development has been continuing untill now. Electrospinning allows a wide range of material from natural to synthetic, ceramics, metals, metal oxides. In the past few decades, the electrospun nanofibers has been successfully exploited with a wide variety of applications includes the textile application, sensors, batteries, catalysis, biomedical application, defense, optical electronics, environmental protection, air and liquid filtration, etc. Compared to traditional fibrous materials nanofiber market has limited the growth of polymer nanofibers in the global market due to high production cost. Nowadays, highly productive industrial devices are developed to compete current materials in the market that brings the solution for the "*Chapter 1-P4*". Some of the selected

key players/manufacturers mentioned in the global market research report are; Elmarco (CZ), DuPont (US), Hollingsworth & Vose (US), Yamashin (JP), Respilon Ltd (CZ), Donaldson Company, Inc. (US), Teijin Limited (JP), Ahlstrom Corporation (Finland), ACS Material (US), Verdex Technologies (US), Inovenso (TR), eSpin Technologies (US), SNS Nano Fiber Technology (US), Finetex (Korea), Revolution Fibres (NZ), Nafigate (CZ), Toray Industries, INC. (Japan), Nanoflux Pte Ltd (Singapore), Nanovia (CZ), Nano Medical s.r.o (CZ).

Nanofibers have 80-95 % porous structure, which makes it very suitable to remove dust particles, aerosols, fine particles in micron sizes, fine liquid droplets. Consequently, nanofibers find their place in the air filtration market. There is still lack of application for liquid filtration. The reason has been discussed in "*Chapter 1*" under the main problems. Liquid filtration is a topic that is of enormous importance around the world. Only a few companies tried to commercialized nanofibers in water purification. These companies are Liquidity Nanotech Corporation, Coway, Pardam Nanotechnology, and SPUR Nanotechnologies [17]. There is a need for research on the topic of nanofibers in water filtration. In the following chapters, nanofiber in membrane technology and how to prepare nanofiber membranes are discussed in detail.

CHAPTER 3-NANOFIBROUS MEMBRANES

3.1. Membrane Technology

Membrane technology is playing an important role in chemical technology and is used in a broad range of applications, including water treatment for domestic and industrial water supply, beverages, food, dairy, paper and pulp, biotechnological, chemical, pharmaceutical, metallurgy, automotive, textile, and other separation processes. Membrane technology has a short but expedited history in commercialization. Even though the first microporous membrane was prepared in the early 1900s [18], the first asymmetric membranes have been developed in the 1960s [19] for industrial scale-application. The period from the 1960s to 1980s, membrane technology blossomed, and significant changes were produced [20]. The main problems had been studied and addressed during past years on membrane-based separation processes were too unreliable, very slow, unselective, and too expensive. Over the years, modern membrane science has been focused on the main problems, and significant improvement has been achieved.

The membrane (which is prepared from polymers, inorganics, or metals) is a permeable or semi-permeable barrier that restricts intimate contact between two homogeneous phases and prevents the movement of certain species across their structure. There are many ways to classify the membranes: (a) by composition: natural, polymeric, ceramic, and metallic, (b) by form: solid or liquid, (c) by morphology: symmetric (isotropic) or asymmetric (anisotropic) membranes (Figure 3.1) (d) by separation regime: reverse of forward osmosis, distillation, dialysis, electrodialysis, electrofiltration, pervaporation, nanofiltration, ultrafiltration, and microfiltration, (e) by geometric shape: flat, spiral, tubular, or hallow, and (f) by charge: electrically charged or neutral, [21]. Some of the membrane classifications are discussed in the following sections.
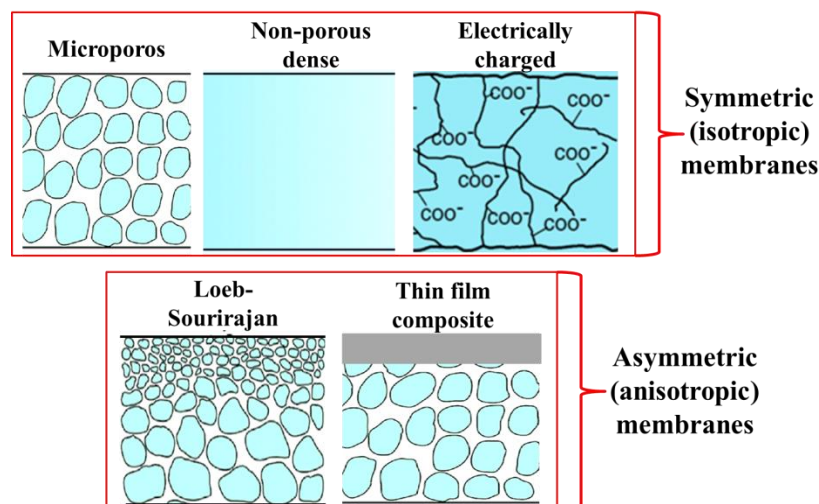
Figure 3.1. Symmetric and Asymmetric membranes

Although the membrane technology offers a solution for separation technology, there are still some problems that require to be solved, such as;

— Flux: the flux of membranes decreases in time due to fouling, which reduces membrane life-span and increases the cost.
— Lack of selectivity: in many cases, selectivity needs to improve
— High cost: Membranes and the overall separation system can be costly.

— Mechanical resistance: some of the materials cannot withstand abrasion, temperature, and pressure.

— Chemical resistance: some of the polymeric membranes cannot withstand chemicals.

More information is given in the following sections for a better understanding of membrane technology.

3.1.1. Membrane Morphology

3.1.1.1. Symmetric Membranes

Symmetric or isotropic membranes are described as the membranes with pore size, morphology, and composition close to a uniform and homogenous structure throughout the depth of the membrane and are generally used in dialysis, microfiltration (MF), and ultrafiltration (UF) applications. Symmetric membranes can be prepared in the form of microporous, non-porous dense or electrically charged, as shown in Figure 3.1.

Symmetric microporous membranes are highly voided structure, randomly distributed pores with pore diameter changes from 0.01-10 µm, and have rigid structure [22]. The pore structure is straight and sponge-like, and the membrane can be dense. Most MF and UF membranes use symmetric microporous membranes to perform the separation.

Non-porous or dense membranes have dense film through. Dense films are prepared by solution casting followed by solvent evaporation or melt extrusion. The permeate transport is controlled by diffusion under the driving force of pressure, concentration, or electrical potential gradient. These types of membranes are generally used in gas separation, pervaporation, and reverse osmosis.

Electrically charged membranes have positively or negatively charged ion in their pore walls, which have a dense and porous structure. The concentration and the charge of ions are affected by the separation process. Membranes with positively charged ions are called anion-exchange membranes due to the binding of anions in the feed solution. Membranes with negatively charged ions are called as cation-exchange membranes. These types of membranes are mostly used for processing electrolyte solutions in electrodialysis.

3.1.1.2. Asymmetric Membranes

In asymmetric membranes, the transport rate of permeate through the membrane is inversely proportional to the membrane thickness. Pore diameter and porosity change considerably through the membrane cross-section. Generally, the skin layer of 0.5-5 µm is on the top of a porous support layer of 50-200 µm thickness. The top skin layer is used as a selective layer for the separation process. Because of the thin selective layer, the flux and permeability are usually very high. The porous membrane support layer under the thin film is to provide mechanical stability. Asymmetric membranes are mostly used in reverse osmosis (RO), nanofiltration (NF), ultrafiltration (UF) and microfiltration (MF). Asymmetric membranes can be prepared in the form of Loeb-Sourirajan structure or thin-film composite structure, as shown in Figure 3.1.

In 1963, Leob and Sourirajan developed the first asymmetric membranes using the phase inversion method by applying a single polymer in which porosity and pore size changed through the wall of the membrane [19]. These membranes are prepared by casting a polymeric solution to form a film and

immersing the prepared film into a non-solvent system. Mainly hydrophobic polymers are used in the phase separation technique; water is used as non-solvent.

Thin film composite membranes usually have highly porous substrate coated with a thin dense film of a different polymer. There are several methods to prepare thin film composites which are including interfacial polymerization, plasma polymerization, solution coating, or surface treatment [21].

The disadvantages of asymmetric membranes are (a) using a single polymer, (b) preparation of high customized polymers is costly, and (c) only a small amount is produced [23]. To overcome all these problems, composite membranes are produced. In the composite structure of asymmetric membranes, at least two different layers are used, as the author uses in this thesis. The top thin layer is the selective layer, while the porous bottom layer supports mechanical stability. The advantage of the asymmetric composite layer is the high flux, and almost all commercial process uses such membranes. Compared to symmetric membranes, asymmetric membranes have several advantages such as:

— The skin layer of asymmetric membranes plays a screen filter role which not allows to particulate matter within the membrane itself.
— Asymmetric membranes seldomly block in the same way as do symmetric membranes.
— Since the residual particles collected only on the surface, not the entire membrane cross-section, that cleaning is relatively straightforward.

3.1.2. Membrane Separation Regime
The membrane separation process changes according to type and configuration, mechanism of feed component transport, pore size and, the nature of driving force [23]. Membrane operation can be categorized as;

— Pressure-driven separation process: reverse osmosis (RO), nanofiltration (NF), ultrafiltration (UF), and microfiltration (MF).
— Partial-pressure-driven processes: such as pervaporation (PV)
— Concentration-driven processes: such as dialysis and forward osmosis (FO).
— Temperature driven processes: such as membrane distillation (MD).
— Electrical-potential-driven processes: such as elctrodialysis (ED).

In this thesis, we focus on the pressure-driven separation-process for the nanofibrous membranes. For this aim, the rest of the work concentrates only on microfilters to avoid excessive information related to membrane technology. The differences in the pressure-driven membrane process are their pore size and related selectivity, as shown in Figure 3.2. Because of pressure on the feed solution, a major portion of the solution can pass through the semi-permeable pressure-driven membranes.
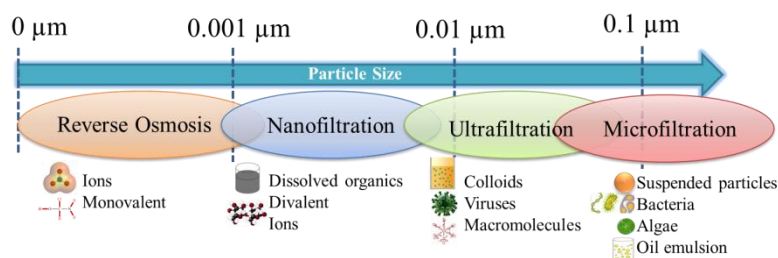
Figure 3.2. Type of membrane separation process and their selectivity according to pore size [24].

Due to the smallest pore size, RO system can remove ions and monovalent. NF system is suitable to remove ions, dissolved organics and low-molecular-weight contaminants. UF system is suitable to remove macromolecules, such as proteins and small colloids, and viruses. MF is suitable to remove particulates, bacteria, oil emulsion and other larger colloids.

3.1.2.1. Microfiltration

Microfiltration (MF) is a process mainly made from polymeric materials with a highly porous structure (80% and up) and uniform pore size. The suspended particles or molecules with the diameters ranging from 0.1-10 μm can be separated using microfilters under the pressure range 1-4 bar [25]. MF is suitable for symmetric and asymmetric membranes and separation processes typically based in the sieving mechanism (physical separation of the particle due to smaller pore size). Particle separation is influenced by interactions between the membrane surface and the solution. Since the membrane structure highly porous, the flux is high and hydrodynamic resistance is low. The membrane flux is directly proportional to the applied pressure difference. The key parameters of membrane performance are its flux and retention characteristics.

The liquid flow model is described by Poiseuille's law, equation 3.1.

$$q = \frac{\pi d^4}{128 \mu l} . \Delta p \qquad (3.1)$$

where, d is a series of cylindrical capillary pores of diameter, q is flow through a pore, Δp is the pressure difference across the pore, μ is the liquid viscosity, l is the pore length. The flux (J) is the sum of all the flows through the individual pores is given in equation 3.2, and the number of pores per square centimeter (n) is given in equation 3.3 [21].

$$J = n.\frac{\pi d^4}{128 \mu l} . \Delta p \qquad (3.2), \qquad\qquad n = \varepsilon.\frac{4}{\pi d^2} \qquad (3.3)$$

After the combination of equation 3.2 and 3.3., the flux is (3.4);

$$J = \frac{\Delta p}{32 \mu l} . d^2 \qquad (3.4)$$

Ideally, the membrane would be capable of rejecting all particulate matters above a specified size or molecular weight completely. Due to the different pore diameters in real membranes, the cut-off is imperfect, and some particles may be passing through the membrane and retentate. Membrane rejection (selectivity) is calculated according to equation 3.5.

$$R = \frac{C_r - C_p}{C_r} \qquad (3.5)$$

where, R is rejection, C_r and C_p are the concentration of particle in the retentate and the permeate at any point during the filtration process.

Dead-end filtration widely used in the microfilters. In dead-end filtration, the feed and permeate are both perpendicular to the surface of the membrane, and the retained materials accumulate on the surface. As a result, a layer of retained particles forms a cake layer—the cake layer thickness increases in time and prone to fouling. Eventually, membrane flux decreased and needs to clean (backwashing is suggested) or replaced membranes that affect the cost.

Another filtration system used in microfilters is cross-flow. In this system, the feed stream flows parallel to the membrane's surface, thereby reduces resistance to flow. The cake layer is lower than the dead-end due to the shear force exerted by the flowing feed stream on the membrane surface. To minimize the impact of the accumulation of particulate material, the velocity of the cross-flow can be lowered to several meters per second—still, membranes flux decline in time due to membrane fouling. Occasionally, membrane cleaning and sterilization is needed. Generally, organic polymers, inorganic materials (such as ceramics, carbon, metals, and glass) are used in microfiltration, which must be able to resist the mechanical, the chemical, and the thermal stresses after cleaning and sterilization.

The proper filtration mode should be selected according to fluid composition, membrane material, the selectivity of the membrane, filtration module geometry, and cleaning methods. The differences between dead-end and cross-flow filtration can be summarized in Table 3.1.

Table 3.1. Differences between dead-end and cross-flow filtration.

Dead-end system	Cross-flow system
The feed direction is perpendicular to the surface of the membrane	The feed direction is parallel to the surface of the membrane
Requires frequently backwash	Less frequent requirement for backwash
Require higher backwash flux rates	Lower backwash flux rates
Require low energy	Higher liquid removal rate
Require for higher flushing flux rates	Lower flushing flux rates
No recirculation	Higher membrane life-span

Microfiltration is suitable for;
— removing oil from oilfield-produced water,
— removing of particles from liquid and gas streams,
— clarification, separation, and purification of proteins,
— clarification and sterile filtration of heat-sensitive solutions,
— clarification of fruit juice, wine, beer, etc.
— purification, gas filtration, process solvent recovery in the chemical industry,
— production of pure water in the electronics industry,
— wastewater treatment

Microfiltration is used as a primary step for the process of drinkable water and is employed in the food and dairy industry, the metal industry, the pharmaceutical industry, and the textile industry.

In this thesis, polymeric electrospun materials are used to prepare membrane microfiltration. Suitable polymeric materials in membrane technology and their properties in terms of advantages and disadvantages are given in Table 3.2.

The selection of polymeric material should be made according to availability, stability under a range of chemical conditions, formable (withstand stretching), must be approved for food or water contact for certain markets.

Table 3.2. Commonly used polymers in membrane technology

Polymer	Properties
Polyvinylidene fluoride (PVDF)	• High chemical and thermal stability, high tolerance to oxidizing agents. • Highly hydrophobic
Polysulfone (PSf)	o Stable structure, pH and temperature resistance, good chlorine resistance, good chemical resistance and easy to prepare. o Low mechanical strength
Polyacrylonitrile (PAN)	• High resistance to oxidation, high resistance to hydrolysis, • Hydrophobic, require co-polymer to make less brittle
poly (tetrafluoroethylene) (PTFE)	o High chemical and thermal stability o Highly hydrophobic, difficult to processing in phase-inversion
Polyamide (PA)	• pH and temperature tolerance. • Not good with regards to chlorine tolerance and biofouling tendencies
Polypropylene (PP), polyethylene (PE)	o Inexpensive o Hydrophobic, low thermal stability
Cellulose acetate (CA)	• Hydrophobic, good for reducing the membrane fouling, pore size can be varied, easy to prepare, inexpensive. • Very sensitive to temperature and pressure, narrow pH range to work between 3-6, highly biodegradable.
polyethersulfone (PES)	o Favorable selectivity-permeability characteristics, easy to processing, good mechanical and thermal properties, dimensionally stable o Hydrophobic, high cost, processing at high temperature and pressure, low UV resistance.

Membrane modules are designed to achieve an efficiency of membrane fouling prevention, different characteristics on the hydrodynamic conditions, energy consumptions, etc. Four types of modules are used in membrane technology: flat-sheet, spiral wound, tubular, and hollow fiber.

The flat-sheet module is the simplest configuration, consisting of two end plates at the bottom, the selective flat sheet membrane on the top, and spacers. Compared to energy consumption, cost, and packing density, flat-sheet modules lie in between spiral-wound modules and tubular modules.

Spiral-wound modules are similar to that of flat sheet modules consisting of a membrane envelope wrapped around a perforated central collection tube in a spiral configuration. A mesh-like spacer separates two membrane sheets. Pressure drop is relatively high, high surface area, and it has the lowest capital cost compared to other systems. Also, the particles can block mesh-like spencer and feed channels easily. Therefore, this type of module requires the minimum content of suspended particles in the feed.

In tubular modules, are a certain number of membrane tubes assembled in one tube (internal diameter is 5 - 25 mm, length is 0.6 - 6 m), and the feed solution is pumped through the tube. Using mechanical or chemical cleaning methods, this type of module can be easily clean. Compares to other modules, tubular modules have the lowest surface-area-to-volume ratio.

Hollow fiber modules used for seawater desalination consist of 50–3000 individual hollow fibers, which are bundled and sealed together on each end with epoxy and placed in a pressure vessel. Compared to other modules, hollow fiber modules have the highest surface-area-to-volume ratio and economical energy consumption. However, the big particles may block the fibers in the cleaning process.

3.1.2.2. Polymeric Membrane Preparation Methods

Several parameters affect the membrane preparation method, which is depended on the selection of polymer type and the desired structure of the membrane. The preparation method can be categorized as phase inversion, interfacial polymerization, track-etching, stretching, and electrospinning. The phase-inversion method is the most common technique among all.

The phase-inversion method is a demixing process in which the process of controlled polymer transformation from a liquid phase to a solid phase. This technique allows us to prepare a porous membrane with a large form of structure, and it was first suggested in 1977 [26]. Selected polymer and additives used in the casting solution affects the membrane structure and properties. Phase inversion membranes can be prepared in various ways as (a) wet process, (b) dry process, and (c) thermal inversion process. (a) In wet phase-inversion process, the polymeric solution forms a film by casting method, and the solvent partly evaporated before immersing into a non-solvent water system. Precipitation takes place due to solvent and non-solvent exchange. Then membranes are heated to 70-90 °C to form a void structure. (b) In the dry phase-inversion method, a solvent and non-solvent in different evaporation rates are used to prepare a polymeric solution. After thin film casting, a more volatile solvent evaporates faster and creates voids and pores. (c) In the thermal phase-inversion method, a mixed or single solvent polymer solution is first heated to form a single-phase and then cooled down to induce phase separation and solidify the polymer. Later, the solvent is removed solvent extraction to form a porous structure.

The interfacial polymerization method is used to form thin film composite membranes that the method is mainly for RO and NF. This method was developed in 1980 [27]. In this method, two reactive monomers are used. First, the supporting material is immersed into an aqueous solution of diamine or polyamine, and then the amine-impregnated membrane immersed into the second monomer solution of a diisocyanate in hexane. These two reactive monomers react at the organic/aqueous interface and form a PA thin layer. The final membrane is treated with heat to form cross-linking at 100-110 °C. Generally, the thickness of the thin film is between 100-300 nm. Membrane thickness, surface roughness, morphology, and surface charge determine membrane permeability and selectivity [23,28].

The Track-etching method is used to form pores on a dense film of a polymer by producing latent tracks via irradiation with high-energy, heavy ions followed by preferential chemical etching of the particle tracks and available since the 1970s [29]. Using this technique, it is possible to form uniform pores with cylindrical geometry [30]. Porosity and the pore size are depending on the duration of irradiation, etching time, and temperature.

The stretching method is used extruded dense films of semi-crystalline polymers such as PE, PP, and PTFE to prepare porous membranes. Pores are formed due to the stretching of the film—pore size changes between 0.1-3 µm [30]. The polymer includes melt-extruded, annealing, stretching, and heat treatment. The structure of the membrane depends on the polymer type, extrusion draw ratio, stretching rate, and the temperature.

The electrospinning method is an easy and versatile method to prepare highly porous (more than 80% void structure) webs with tight pore size. Electrospun membranes show excellent performance over conventional membranes due to high porosity, tight and adjustable pore size with a narrow pore-size distribution, and functionalized surface. More information related to the preparation of electrospun nanofiber webs is given in *Chapter 2*. A separate sub-title is prepared in this chapter for the role of nanofibers in membrane technology and preparation method.

3.2. Membrane Structural Properties
Besides the membrane module configuration and operation conditions, membrane performance, selectivity, permeability, and fouling are affected by membrane crystallinity, porous structure, hydrophilicity/hydrophobicity, surface roughness, and membrane charge.

3.2.1. Polymer Crystallinity
For the non-porous membranes, the permeability and mechanical stability are mainly determined by the polymer crystallinity. The molecular weight and type of the polymer, growth condition, chain flexibility, chain configuration, chain interaction, and branch structure determines the polymer crystallinity. Most of the polymer has a semi-crystalline structure. In RO system, the liquid separation is done by sorption and diffusion through a permeable membrane. The crystallites of polymer create a compact packed structure in which liquid cannot penetrate. The liquid transports through the amorphous layer. The swelling of the membrane takes place in an amorphous state. Increasing crystallinity decreases diffusion.

3.2.2. Membrane Porous Structure
Membrane pore structure indicates pore size, pore size distribution, porosity, and pore tortuosity of the membranes. Track-etched membranes offer parallel-cylindrical pores perpendicular to the

membrane surface along with the thickness of the membranes. The relationship between this type of pore geometry and flux is given by the Hagen-Poiseuille equation as equation (3.6) [23].

$$J = \frac{\varepsilon r^2 \Delta P}{8 \mu \tau \Delta x} \qquad (3.6)$$

where, J is the flux, ε is the surface porosity, r is the pore radius, ΔP is the pressure difference across the membrane of thickness Δx, μ is the solution viscosity, and τ is the pore tortuosity. The membrane tortuosity (τ) indicates the length of the average pore compared to the membrane thickness.

In membrane technology, many membranes prepared phase inversion, stretching, solution casting, or electrospinning techniques that do not have parallel-cylindrical pores. They have irregular pore geometry and tortuosity. In this case, Kozeny-Carman model tries to explain the relationship between membrane pore geometry and flux, as shown in equation 3.7 [23].

$$J = \frac{\epsilon^3 \Delta P}{K \mu S^2 (1-\epsilon)^2 \Delta x} \qquad (3.7)$$

Where, ϵ is the volume fraction of pores, K is the Kozeny-Carman constant (depends on the shape of the pores and tortuosity), and S is the internal surface area of the membrane pores.

3.2.3. Membrane Surface Hydrophilicity/Hydrophobicity
Hydrophobic membranes tend to foul easier compared to hydrophilic membranes. In other words, hydrophobic membranes have no interaction with water but hydrophobic compounds, while hydrophilic membranes can form hydrogen-bonds with water. Hydrophilic membranes have less interaction with organic substances, microorganisms, and charged inorganic particles, which reduce membrane fouling. On the other hand, highly polar compounds can be sorbed into hydrophilic membranes via hydrogen bonding. They can cause the greatest decline in flux through pore blocking or the adsorption within the pores.

Membrane hydrophilicity is measured by water contact angle (WCA) measurement. If WCA is greater than 90C, membranes are counted as hydrophobic [31]. Hydrophilicity is related to the functional groups on the membrane surface, the roughness of the surface, and zeta-potential. The hydrophilic groups such as $-OH$, COO^-, and $-NH_2$ are mainly used to improve membrane surface hydrophilicity. Many commercial membranes are in hydrophobic nature and prone to fouling.

3.2.4 Membrane Surface Roughness
Membrane surface roughness is determined by the measurement of surface texture. Roughness plays an important role to understand the interaction between membrane surfaces in its environment. Hydrophobic membranes with surface roughness are prone to fouling compared to the hydrophilic smooth membrane surface. Higher surface roughness means a higher surface area to which foulants can be attached and caused fouling.

3.2.5 Membrane Surface Charge
Membrane surface charge determines the electrostatic interaction between charged foulant and the membrane surface. It is important for the rejection mechanism. Depend on the membrane charge, the interaction between charged foulant and membrane surface can be quantified by zeta potential measurements.

Negatively charged membrane surface helps to reject dissolved salts, microorganisms and minimize the adsorption of negatively charged organic foulants. This type of membrane surface can be prepared by sulfonic and/or carboxylic acid groups on the surface of the membrane, which may be deprotonated in feed solution by increasing the pH of feed solutions. Since the pH changes are needed, the flux, pore size, and pore structure can be affected by pH value. Charged membranes are important for the fouling resistance when the foulants are charged. Similar charged solute and membrane surface repulses each other and reduces the membrane fouling. Most of the colloidal particles are negatively charged, which requires charged membranes. Cationic charged membranes are more suitable for the cationic macromolecules in biotechnology.

3.3. Membrane Transport Theory

There is two suggested model for permeation of different species, as shown in Figure 3.3. The first model is the pore-flow model in which permeants are transported and pass through pores by the pressure-driven mechanism. The second model is the solution-diffusion model, in which permeants dissolve in the membrane material and then diffuse through the membrane cross-section. The difference between the two mechanisms is the relative size and permanence of the pores—pore-flow membranes have better flux than simple diffusion membranes.

Since this thesis is about the porous nanofiber membrane, we only focus on the pore-flow model.

The transport of permeant in the pore-flow model is explained by Darcy's law, as shown in equation 3.8 [32].

$$J_i = K' c_i \cdot \frac{dp}{dx} \quad (3.8)$$

where, J_i is the flow in a capillary or porous medium, K' is a coefficient reflecting the nature of the medium, c_i is the concentration of component i in the medium, dp/dx is the pressure gradient existing in the porous medium.
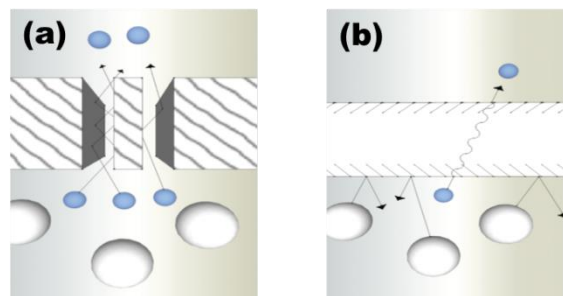
Figure 3.3. Permeation models of different membrane (a) microporous membranes separated by molecular filtration, (b) dense membranes separated by solution diffusion [33]

3.3.1. Pore-flow and Permeation in Microfiltration Membranes

Even though there are a lot of theories about diffusion membranes, no unified theory to describe the transport mechanism in microporous membranes which have been developed due to the extremely heterogeneous nature of microporous membranes. Even the microporous membranes can show similar separation, their porous structure and the mechanism of the separation can be different. For instance, the porosity of the membrane can vary from place to place or different in each layer for asymmetric membranes. As a result, the parameters to characterize the complexity of microporous membranes are incomplete. Also, the membrane tortuosity (τ) which is a cylindrical pore which has a right angle to

the membrane surface and has a tortuosity of one, which means the average length of the pores is equal to the membrane thickness. However, in asymmetric membranes, the pores take a more meandering path through the membrane cross-section and the tortuosity changes in the range from 1.5–2.5. The pore diameter is another important parameter that needs to be taken into account. The asymmetric membranes contain a range of pore sizes. In microfilters, the pore diameter is described by the biggest particle which can penetrate the membrane: and the membrane might be much smaller than the pore diameter observed under microscopic examination.
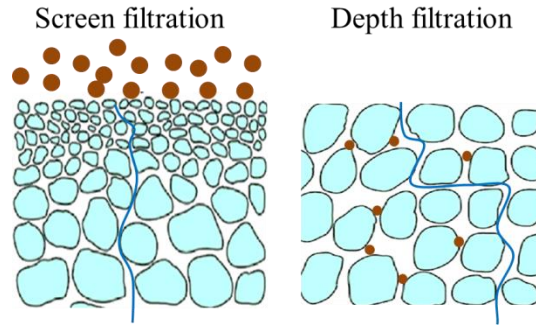
Figure 3.4. Screen and depth filtration mechanism

Based on the filtration type, membranes can filter the particle in two ways:

The surface or screen filter has surface pores smaller than the particles to be removed. As a result, particles captured and accumulate only on the surface, as shown in Figure 3.4. Particles that are smaller than the pores and able to pass through the membrane are not captured by the interior membrane pores. These types of membranes are in the asymmetric structure and generally use a tiny, porous structure layer on the top and larger pore size support at the bottom. Surface/screen filters can be used as either pre-filters or clarifying filters.

The rejection mechanism for screen filters has been developed by Ferry [34] and Renkin [35] as Ferry-Renkin equation shown in equation (3.9):

$$R = \left[1 - 2\left(1 - \frac{a}{r}\right)^2 + \left(1 - \frac{a}{r}\right)^4 \right] \times 100 \,\% \qquad (3.9)$$

where, R is the rejection percentage, a is solute molecule radius, and r is pore radius. The Ferry–Renkin model can be used to estimate the pore size of ultrafiltration membranes.

In screen filters, the initial rejection 60-70% can be achieved to 100% after the cake layer formed on the membrane surface.

The depth filter has a large pore size on the surface that allows the particles to enter the membrane and captured in the interior of the membrane (Figure 3.4). Some particles are trapped in the interior membrane; others are adsorbed in a tortuous path. Depth filters are usually symmetric and used in microfilters as pre-filters to remove particles and protect downstream equipment from fouling or clogging.

The depth filter mechanism is more complicated than the screen filter. The particles are not only captured by the membrane pore, but also adsorption can take place. Four mechanisms can be suggested for the particle capturing in the depth filters: sieving (capture of particles on small constrictions within the membrane), inertial impaction, Brownian diffusion, and electrostatic

adsorption. In every case, particles smaller than the diameter of the depth filter pores are trapped by adsorption in the interior membrane surface.

The sieving mechanism is the simple capture of particles at pore constructions in the interior of the membrane. In internal capture, particles are bigger than the membrane's tortuous pores and trapped inside the membrane. This capture mechanism is more suitable for big particles. Brownian diffusion mechanism is more suitable for small particles. While the small particles move along the pores, they are subjected to Brownian motion (random motions of particles suspended in permeate) that creates contact with pore walls. As a result, particles are captured to the surface by adsorption. Electrostatic adsorption is the capture of charged particles by a membrane which has surface-charged groups. Many colloidal particles carry a slight negative charge. A positively charged membrane can help the rejection process. During the filtration process, the adsorption capacity of the charged membrane is exhausted in time, and rejection decreases.

Screen filters are more commonly used and less expensive than depth filters. On the other hand, depth filters have a larger available surface area than a screen filter, allowing them to have higher loading capacity before fouling.

3.4. Concertation Polarization
Concentration polarization is formed as a natural consequence of membrane selectivity and negative effect on the overall process efficiency of the membrane. Concentration polarization is observed when the concentration of a specific component decreases or increases at the boundary layer closes to the membrane surface. Concentration gradients form in the fluids on both sides of the membrane. Membrane performance in ultrafiltration, electrodialysis, and some pervaporation processes is suffered by concentration polarization.

Concentration polarization has a negative effect on membrane flux and membrane separation properties due to high surface concentration that exceeds the solubility limit. Its impact on rejection is an open question. It may reduce retention for the low molecular weight solutes while opposite for macromolecular solutes [36]. The design and operating conditions of the membrane module are important to minimize the effect of concentration polarization.

Concentration polarization is affected by membrane boundary layer thickness, the membrane enrichment, the volume flux through the membrane, and the diffusion coefficient of the solute in the boundary layer fluid. Among the all, the changing of the boundary layer thickness is easy by reducing the boundary thickness minimizes the concentration polarization.

3.5. Membrane Fouling
Membrane fouling is one of the biggest problems in membrane technology. Membrane fouling is a consequence of concentration polarization and gradual decrease of flux due to blocking of pores on the surface or in the membrane with contaminants. Fouling reduces membrane performance significantly as a reduction in flux, shortening of the membrane life span, and increasing the cost.

Foulants are generally in the form of organic, inorganic, biological, and colloidal structure. The common and the most problematic fouling is colloidal one. Organic fouling forms as a consequence of natural organic matter (NOM) appear during the filtration. Inorganic fouling forms as a consequence of precipitation of deposits on the membrane, which results in bulk and membrane crystallization. Biological fouling forms as a consequence of biofilm on the surface.

The fouling layer can be grouped as reversible and irreversible parts. Reversible part consists of the easily removable portion of the foulants, and the irreversible fouling part consists of the remaining portion. During the separation process, membrane resistance increases, and flux decreases. The decrease in flux can be due to clogging of the membrane pores, adsorption in interior membrane pores, concentration polarization, and gel layer formation.

Factors that affect the fouling can be categorized as;

— Membrane properties: membrane material, pore size, pore size distribution, hydrophobicity.
— Feed properties: concentration of components in the feed, size, and nature of components.
— Operating conditions: flow rate, pressure, pH, and temperature.

Frequently membrane cleaning can reduce the membrane fouling and improve the flux. A proper cleaning method must be developed according to membrane type, structure, feed properties, and the membrane module. To maintain membrane performance, many cleaning processes have been developed as biological, chemical, and physical treatments or combinations. Biological cleaning is containing bioactive species such as enzymes to clean the membrane surface. The chemical cleaning process is used to remove the adhered particles while the physical cleaning process can remove loose particles attached on the membrane surface. Combination of both chemical and physical cleaning can be suggested for the cleaning of nanofiber membranes which may offer solution for "*Chapter 1-P7*".

3.5.1. Membrane Antifouling Mechanism

Antifouling membranes are a new trend to reduce the cost of operation, chemical and biological cleaners, and wasted time during the cleaning process. There are three ways to reduce fouling;

(a) Improve membrane hydrophilicity to minimize the adsorption and deposition of hydrophobic foulants on the membrane surface. A highly hydrophilic surface is more attractive for water molecules to attach than hydrophobic foulants.

(b) Changing of surface charge, as mentioned in sub-title "*Membrane Surface Charge*". Electrostatic repulsive force helps to reduce fouling when the foulant and membrane surface is charged similarly.

(c) Grafting of hydrophilic polymer chains on the membrane surface will exert steric repulsion to hydrophobic proteins. Due to the loss of configurational entropy, volume restriction and/or osmotic repulsion between the overlapping polymer layers results in steric repulsion [23].

Antifouling membranes are in great interest. Many polymeric membranes are hydrophobic, which cause fouling problems. For this aim, researchers have been focused on changing the surface of polymeric membranes. More details are given in the following section.

3.5.2. Surface Modification of Synthetic Polymeric Membranes

The main aim of surface modification is to prevent contact between membrane and pollutants as well as improve the selectivity and permeability by enhancing the hydrophilicity of existing polymeric membranes. Modification can be done physically or chemically: (a) by blending or adding some other component(s) into the polymeric material, (b) by coating the surface of the membrane with some other polymer including grafting and in situ polymerization, (c) by altering the membrane surface via chemical reaction (d) by radiation via high energy particles, (e) plasma treatment, and (f) by other methods [37].

Physical modification focuses on physical interaction (not covalent bonding) of hydrophilic modifiers on the polymeric membrane surface. The chemical composition of the polymeric membrane is not changed. There are two ways to produce a physical modification, (a) direct coating or depositing of hydrophilic polymer on the surface of the membrane, (b) immersion of membrane into chemically active monomer, then immobilized by crosslinking or polymerization reaction with no chemical participation of the pristine membrane.

Chemical modification focuses on a chemically modified surface by a covalent bond. The polymeric membrane chains are activated by chemical reaction or high-energy radiation. Then, hydrophilic modifiers are grafting. This method improves the membrane surface, not the bulk structure. Comparing to the physical modification, this method offers long-term chemical stability.

3.5.2.1. Blending

One of the easy methods of the modified membrane is the blending of the polymer with polymeric additives to improve surface hydrophilicity and pore interconnectivity. A hydrophilic additive adds into a hydrophobic polymer can improve the membrane hydrophilicity and reduce fouling.

Another method is the preparation of polymer/inorganic membrane by inorganic filler embedded in a polymer matrix. Incorporating nano-size particles into membranes can improve optical, mechanical, electrical, magnetic, rheological, and fire retardancy properties.

3.5.2.2. Coating

Interfacial polymerization was introduced the first time in the 1960s [38] and developed in the 1980s [27]. Using this method, a thin PA film can form on the membrane surface for a good permeability and selectivity. More details are given in the sub-section "*Polymeric Membrane Preparation Methods*".

Layer by layer coating is another method for the fabrication of ultrathin polyelectrolyte multilayer (PEM) film to prepare multilayer membranes. This method includes alternating sequential adsorption of polycations and polyanions on a substrate. After each adsorption, a rising step takes place to remove weakly associated polymer chains. The thin film is formed due to electrostatic interaction between the positive and negative charges. This type of membrane possesses high selectivity and permeability.

Sol-gel coating is used to fabricate materials from a chemical precursor solution for an integrated network (or gel) of either discrete particles or network polymers. The sol-gel process involves both physical and chemical reactions such as hydrolysis, condensation, drying, and densification. The sol is prepared by hydrolysis and condensation at room temperature. The prepared sol is deposited on the membrane surface using spray coating, dip coating, or spin coating followed by annealing, sintering, or calcination under heat. The sol-gel process is a route for preparing complex oxides at low temperatures [39]. Different sizes and shaped particles, fibers, porous materials, membranes, coatings can be produced.

The spin coating technique is suitable for composite membrane preparation but in lab-scale with the thickness in the range of 0.5–30 μm. In this technique, a polymeric solution is applied to the center of a circular plate, which rotates at a given angular velocity and duration of spinning. Due to centrifugal force, the polymeric solution flows radially and helps the solution to be ejected off the edge of the plate. An ultrathin layer of film is formed after solvent evaporation. The thin film on the plate is immersed in a water coagulation bath together with the plate in which phase inversion occurs and a

membrane is produced. To remove the residual solvent completely, the resultant membrane is immersed in another water bath.

3.5.2.4. Chemical Reaction
The chemical reaction can modify the internal surface of the pores of the membrane. This method can help to improve the hydrophilicity of the membrane.

3.5.2.4. Irradiation of High Energy Particles
UV/ozone treatment is used to increase the wettability of the polymeric membrane surface. The surface energy of the polymeric membrane increased due to oxidation of the polymer. UV/ozone irradiation can induce chain scission and crosslink on the polymer surface, thereby functional groups are formed such as hydroxyls, carbonyls, or carboxylic acids on the membrane top surface. Only the surface is modified.

Ion-beam Irradiation changes the microstructure of the surface layer of the polymer. At high irradiation, a large number of small-size microvoids can be formed on the surface. When the ions penetrate through the polymer surface, the deep valleys and tall peaks can be eliminated. As a result, surface roughness can reduce.

3.5.2.5. Plasma Treatment
Plasma treatment can create functional groups on the surface of membranes as directly or indirectly. Plasma surface modification can improve hydrophilicity, hydrophobicity, biocompatibility, and biofunctonality. Direct treatment of plasma gases (such as Ar, N_2, H_2, O_2, CO_2, CH_4, and NH_3) is used to produce functional groups (amines, COOH, and free radicals) on the membranes' surface. In contrast, indirect treatment introduces functional groups by polymer grafting [40].

3.5.2.6. Other Techniques
There are different methods that do not belong to any of the above methods. Molecular Imprinting Technology (MIT) is one of them. MIT uses polymerization or phase inversion in the presence of a template for the selectivity of the specific molecules. The surface is affected by ion implantation [41].

Heat treatment is another method for modification of the surface. Heat treatment improves the mechanical properties of the polymers and chemical stability of the modified membrane by altering the polymer chain mobility.

3.6. Nanofibers in Membrane Technology
Over the year, developments in membrane technology proceed successfully, and new and improved techniques/membranes/modules will continue to be discovered. New concepts are regularly introduced to enhance membrane performance (such as flux, selectivity, transmembrane pressure), reduce cost (operation, membrane material) and energy; also the prolonged operating life and membrane life-span. There is an excellent challenge for research scientists for further development on advanced membrane materials for highly permeable, better selectivity and resistance to both chemical and mechanical barriers, prolonging the membrane life span and induce long-term performance. Nanofibers can be one of the key solutions to address these issues. Electrospinning has become a promising technique to obtain nano-size fibrous materials in the last years. Currently, this process allows the mass production of nanofibers on the industrial scale. More details related to the electrospinning process and mass production has been given in "*Chapter 2- Electrospun Nanofibers*". The microporous structure of nanofibers makes them suitable in the microfilter membrane application.

Even though nanofibers look limitless from the applications' point of view, development is needed, especially in the water domain area. The pros and cons of nanofibers to use in liquid filtration are given in Table 3.3.

Table 3.3. The Pros and cons of nanofibers in liquid filtration.

Pros	Cons
• Highly porous structure (more than 80%) helps to improve permeability.	• Low mechanical strength requires additional support to provide strength.
• Tight pore size improves selectivity.	• High cost due to low production speed.
• Narrow pore size distribution helps to have high selectivity for the determined size of particles.	• Not all polymers can form nano-sized fibers.
• The large surface-to-volume ratio of the nanofibers can enhance their sorbent performance for heavy metals and desired pollutants.	• Not all the hydrophilic nanofibers are suitable for membrane (dissolving or swelling problem).
• Thin nanofiber layer can enhance the flux.	• Almost all spinnable polymers hydrophobic.
• Multiple choice of material (cellulose nitrate, cellulose acetate, polyvinylchloride, polyacrylonitrile, polyamide, polyurethane, polyamide, polysulfone, polycarbonate, polydimethylsiloxane, polytetrafluoro ethylene, polyvinylidene fluoride, etc) can enhance separation application depends on selectivity.	
• The possibility of incorporating a variety of polymers can improve mechanical properties, increase selectivity and flux, and a broader range of environmental applications.	

The mechanical problem of the nanofiber membranes is tried to be solved by various researchers. Heat treatment is one of the suggested processes to improve the mechanical strength of nanofiber, which can promote crystallinity. Moreover, heat treatment can remove the residual solvent in the nanofiber web. Heat treatment itself is not enough to use nanofibers in liquid separation. A support layer is needed to adhere to nanofibers. In this thesis, the author suggests the lamination method by using heat treatment to prepare mechanically stable nanofiber hybrid membranes. The lamination process may offer a solution to the problem in "*Chapter 1-P3*".

Not all the engineered polymers with unique features can form nanofibers. Thus polymer mixtures can solve this problem. Polymers with the same solvent system can be mix at various ratios. A study is submitted in the "*Presented Works and Their Novelties - Preparation of various nanofiber layers using wire electrospinning system*". Mixing of chitosan (CH) into PA6 polymeric solution improves the spinnability of the CH. The mixing/blending method may suggest a solution for the problem in "*Chapter 1-P1*".

Some of the electrospun nanofibers such as polyvinyl alcohol (PVA), polyethylene oxide (PEO), polyvinylpyrrolidone (PVP) can quickly dissolve in aqueous media. Not only dissolving but also swelling of fibers can create problems during filtration. For this reason, proper cross-linking is required, which might increase the cost of material and chemical waste. Cross-linking of water-soluble nanofibers may suggest a solution for the problem in *"Chapter 1-P2"*.

The preparation of nanofibers is costly due to low productivity. Fortunately, more and more industrial production equipment is developed addressing this issue. The wire electrode electrospinning system (Nanospider) is one of the bulk production methods. The price comparison of nanofiber webs prepared by wire electrospinning system and commercial microfilter membranes are given in Table 3.4. Information was taken from suppliers and their web pages.

Table 3.4. Comparison of cost of nanofibrous membranes and commercial microfilters.

Membrane	Price	Manufacturer	Properties
PVDF nanofibrous membrane	Estimated as 24 €/m^2	Our membranes prepared in our labs	3-3.5 g/m^2 nanofiber on PET spunbond-between 0.5-0.7 μm pore size
PA6 nanofiber	1.7-5.4 €/m^2	Elmarco	1-3 g/m^2 PA6 nanofiber without substrate
PVDF nanofiber	3.3 €/m^2	Elmarco	3 g/m^2 PVDF nanofiber without substrate
PA6 nanofiber	3.9-5.7 €/m^2	Nano Medical s.r.o.	PA6 nanofibers with 21-43 L/(m^{2}s) air permeability
Synder Flat Sheet Membrane	67.64 $/ 47 mm x5 package	Sterlitech	PVDF-0.2 μm pore size
TriSep Flat Sheet Membrane	122.99 $/ 1016 X 305 mm size	Sterlitech	PVDF-0.2 μm pore size
PVDF Transfer Membrane	365 €/m^2	Thermofisher	PVDF-0.45 μm pore size
Hydrophobic PVDF membrane-HAWP04700	129 $/m^2	Membrane Solutions, LLC.	PVDF-0.45 μm pore size
Hydrophilic PVDF membrane-MSPVDF260045L	209 $/m^2	Membrane Solutions, LLC.	PVDF-0.45 μm pore size

Nylon membrane-MSNY300080	65 \$/m^2	Membrane Solutions, LLC.	Nylon on PET -0.8 μm pore size
Nylon membrane-MSNY3000100	65 \$/m^2	Membrane Solutions, LLC.	Nylon on PET-1.0 μm pore size
Nylon membrane-MSNY300045	52 \$/m^2	Membrane Solutions, LLC.	Nylon on PET-0.45 μm pore size
MF010, MF022, MF045	30-100\$/m^2	RisingSun Membrane	PVDF-0.1 to 0.45 μm pore size

Based on the information from Table 3.4, it is possible to say that price of nanofibers (produced via Nanospider device) is comparable to commercial membranes. The prices of nanofibers in our laboratory, Elmarco and Nanomedical s.r.o are calculated by production cost, not the market price. Using an industrial scale nanofiber production device may solve the problem in "*Chapter 1-P4*".

Many polymeric nanofibers are hydrophobic that can cause membrane fouling. For this reason, hydrophilic modification is required. The attempts to surface-modified nanofiber membranes have been made, as shown in "*Presented Works and Their Novelties*". Surface modification improves the membrane permeability and selectivity, which may solve the problem in "*Chapter 1-P5*".

3.6.1. Preparation of Nanofiber Membranes

1-D structure nanofiber can be prepared by various methods mentioned in "*Chapter 2*". Either polymeric solution or melt can be used to fabricate nanofiber layers. Recently, the industrial scale nanofiber production methods have been developed drastically, allowing nanofiber preparation in bulk. Since the limitation of production is over, many end-applications have started to use nanofibers in real life. Membrane technology is one of the promising areas to conduct nanofiber webs. The structural property of nanofibers allows them to use as microfilter due to micron-size pores. Based on the additional process (such as thin-film covering), nanofibers can be used as a support layer for nanofilters, ultrafilters, and reverse osmosis. Unfortunately, the mechanical weakness and ease abrasion structure of nanofiber webs, nanofibers cannot be used in water domain applications without any support. For this reason, many researchers have been focusing on the combination of the nanofiber layer onto a support layer using various methods. These methods are discussed in the following section.

3.6.1.1. Mechanically Enhanced Nanofiber Membranes

Nanofibers are randomly oriented anisotropic structures and can filter particles by a size-exclusion mechanism that one molecule fits in the pores and can pass through the membrane. In contrast, the other type of molecule is quite big to fit in the pores. However, the weak interaction among the nanofibers results in loose fiber packing, which may result in poor mechanical properties. The mechanical weakness of the nanofiber web limited their application in liquid filtration. To improve nanofiber membrane tensile properties, various attempts have been made. Some of the methods are explained as;

Blending with other materials: polymeric, metallic, organic, or inorganic material can be mix with a polymer solution of nanofibers to change their elastic modulus, tensile strength, hardness, and so on. Plasticizers can be added to the polymeric solution to improve the flexibility and durability of the nanofibers. For instance, the mixing of low molecular weight poly(ethylene glycol) (PEG) as a plasticizer to silk fibroin solution improves the strain by 300 % times, and the stress almost doubled [42]. Gelatin was used with poly(butylene succinate) (PBS) to improve the mechanical properties of the PBS membrane due to changes in the crystallinity of PBS, the interaction between PBS and gelation or possible interaction between adjacent fibers [43]. One approach has been made by adding carbon nanotubes into the polymeric solution [44]. Functionalized single-walled carbon nanotube (SWNT) has been electrospun with polyurethane (PU) to enhance tensile strength which results in a 104% higher when it compares to the pristine polyurethane membranes. However, these methods can be complicated and costly, and for some cases, the mechanical strength cannot be strong enough to fulfill the desired membrane's condition.

Epoxy lamination: Epoxy is used to improve the mechanical properties of nanofibers via impregnation. A heat curing process is following the epoxy impregnation. Good adhesion between nanofiber and matrix in composites can be achieved. Some of the studies related to epoxy reinforced nanofibers are given in [45–48]. However, porosity and permeability can be reduced significantly. Moreover, this method is time-consuming and requires energy to cure epoxy for a long period.

Dip-coating: this method is simple and reproducible that includes the deposition of a film by immersion of the membrane into a solution. Generally, dip-coating is used to enhance the surface functionality of nanofiber webs to achieve some properties as hydrophilic, hydrophobic, antibacterial, antifouling, etc. Besides surface improvement, the dip-coating method can improve the mechanical properties of the nanofiber. The dip-coating method has been employed in fibrous materials to improve abrasion resistance during weaving [49]. Soaking of nanofiber web into solvent can enhance the bonding of junction points by welding or soldering by changing the degree of molecular orientation [50].

Thermal treatment: In this first method the nanofiber web is heated above glass transition temperature but below the melting point. As a result, inter-fiber fusion takes place that improves the welded fiber-fiber junctions and mechanical properties. For instance, the PVDF nanofibers were thermally treated at 150–160 °C [51]. Tensile strength, modulus, and elongation at break of the thermally treated PVDF nanofibers were much higher than those of the untreated pristine PVDF nanofibers due to increased crystallinity, shrinkage of the web, and nanofiber thickening. The disadvantage is that dimensional shrinkage of heat-applied membranes may be caused by entropic relaxation of stretched polymer chains [52,53].

Ultrasonic-welding: Ultrasonic seaming has been used for the first time in the textile industry in the 1960s [54]. The lamination of nanofibers using ultra-sonic welding has been reported recently [55,56]. Using this method, the fibrous materials can bond on other support materials along with defined seam areas while the other regions kept original form. During ultrasonic welding, high-frequency vibration and heat are applied to bond and seal two different materials. This method is still required optimization for the fragile nanofiber webs.

Heat-press lamination: Heat-press lamination is also a common method used in the textile industry to combine at least two different surfaces. For an adhesion, intrinsic adhesion forces need to be established between the adhesive material and substrates. Adhesion requires physical and chemical

bonding. Chemical bonding consists of covalent bonds between the molecules of the adhesive and the surface material. On the other hand, physical bonding consists of four types of theory; mechanical interlocking, adsorption, diffusion theory, and electrostatic. Mechanical interlocking is when an adhesive penetrates the pores and holes, it locks mechanically to the substrate. Adsorption theory includes intermolecular attraction (such as van der Waals bonding or permanent dipole) between the adhesive and the substrate. The diffusion model explains the adhesion concept by the compatibility between polymers and the movements of polymer chains, such as partial penetration between the materials. Electrostatic forces contain polar molecules or permanent dipoles in the adhesive and substrate that form electrostatic bonding.

In heat-press lamination, a hot-melt adhesive (such as glue, web, or powder) that has a lower melting point compared to other surfaces is applied in between two surfaces under heat and force. In this method; properties of materials, applied heat, force, and time of contact during lamination are important factors that affect the lamination quality. For instance, insufficient heat and applied force can cause less adhesion and the adhered area between nanofiber and substrate. In this case, under a slight pressure, layers can easily separate. The high applied force can cause damages or changes on the nanofiber surface. High temperatures can cause the melting of nanofiber or substrate and damage the membrane. Moreover, excessive melting of the adhesive web can fill all pores on of nanofiber web, which can reduce porosity and permeability. For proper adhesion, the adhesive web should partly over the surface of nanofibers as shown in Figure 3.5. When using the heat-lamination process, it is possible to prepare a nanofiber that is suitable to use in pressure-driven water filtration. Besides adhesion of layers, the heat lamination can help to remove residual solvents and allow crystallinity for the electrospun nanofibers, which in turn improves mechanical strength.
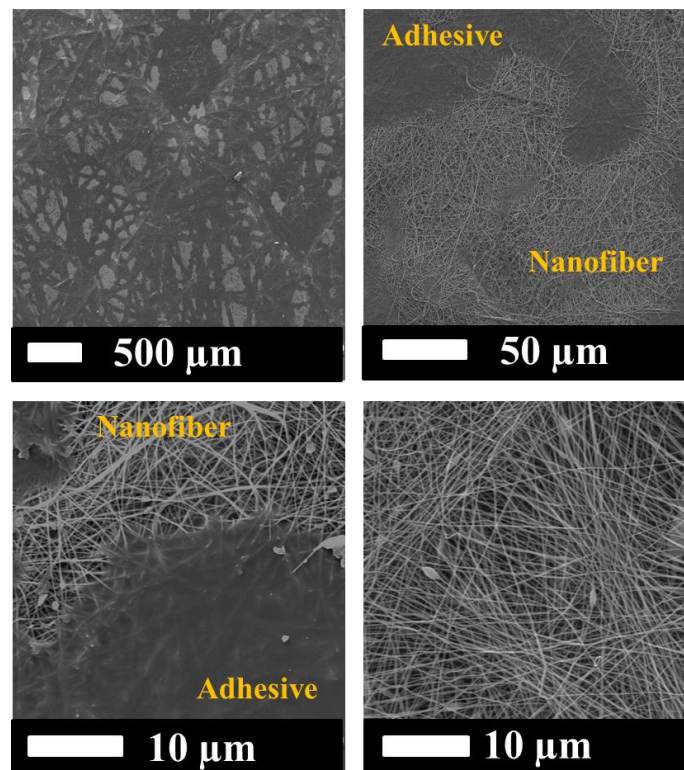

Figure 3.5. Images of laminated nanofiber webs on a substrate under a scanning electron microscope at various magnifications.

After the preparation of nanofiber membranes, characterization is needed to evaluate if the nanofiber membranes are suitable for the liquid filtration or not.

3.6.1.2. Characterization of Nanofiber Membranes

To understand the behavior of nanofiber membranes in filtration technology, characterizing is needed. The characterization methods can be divided into several groups, such as physical characteristics (morphology, mechanical properties, charge, etc.), chemical (structure and composition), transport characteristics, bulk characteristics, porosity, and surface characteristics [57]. Herein, the author discusses some of the most commonly used techniques for the characterization of nanofiber membranes.

Scanning electron microscope (SEM): SEM is a useful tool to detect membrane surface at various magnification. SEM is used to characterize membrane properties quantitatively (such as surface porosity, pore shape, pore size, and pore density) and qualitatively.

Energy-dispersive X-ray spectroscopy (EDS or EDX): EDX combined with SEM imaging can examine chemically distinct regions within composite membranes and on the surface of fouled membranes.

Water contact angle (WCA): WCA is used to determine the wettability and surface energy of the membrane surface.

Fourier-transform infrared spectroscopy (FTIR): The attenuated total reflection (ATR)-FTIR is the most popular in membrane research (ATR-FTIR). This method is suitable to detect chemical changes in the top layer of the membrane, such as hydrolysis, chlorination, irradiation, or comparison with other membranes.

Differential scanning calorimetry (DSC): DCS can indicate useful information about structural transport relationships of the membranes that can help to identify the best-performing membranes.

Atomic force microscopy (AFM): AFM performs topographic scans on the membrane surface for surface examination and characterizes the surfaces physically. Moreover, AFM may determine membrane thickness in dry and swollen states via scanning across stripes of a membrane both in dry and wet conditions.

Nuclear Magnetic Resonance (NMR): NMR is used to characterize the chemical structure of the modified membranes and the structure of the modifying agent.

Thermal Gravitational Analysis (TGA): TGA is used to determine the thermal stability of membranes or thermal degradation behavior of membranes.

Brunauer–Emmett–Teller (BET): BET is generally used to determine porosity, pore geometry, the uniformity of pore sizes, and surface area of microporous and mesoporous materials.

Membrane Fouling Tests: Dynamic and static testing modes are useful for fouling experiments with real membranes. In the dynamic test, the feed is moved along the membrane in cross-flow mode. The hydrodynamic conditions (feed velocity, pressure, the permeate flux, and concentration polarization) are important in this type of test. Deionized (DI) water is used as first feed until a constant flux is

obtained. Then the feed solution containing foulants is used in a determined time, and later the feed is again replaced with DI water. Membrane cleaning can be introduced before and after fouling. The difference between the membrane flux and rejection before and after the filtration cycle and cleaning process shows membrane fouling and reversibility and efficiency of the cleaning process. A static test is suitable for biofouling or organic fouling. In this test, the membrane is immersed in a feed solution with bacteria or foulants at defined conditions and time. Then the membrane is removed and rinsed. The grown biofilm or amount of adsorbed foulant is examined.

Bubble Point: This measurement is used to measure membrane pore size. The pore size found via bubble point corresponds to the largest pore.

Total Organic Carbon (TOC), Dissolved Organic Carbon (DOC), and Chemical Oxygen Demand (COD): These methods are used to measure organic compounds, in the total amount of carbon, organic matter, and oxygen demand within water or wastewater.

To reduce the cleaning process and to improve membrane permeability and selectivity, surface modification is needed. Surface modified nanofiber membranes can suggest a solution for the "*Chapter 1-P5, P6 and P7*".

3.6.2. Surface Modification of Nanofiber Membranes

Mechanically enhanced nanofibers are a big step for water domain applications. However, many polymeric nanofiber membranes are hydrophobic, which might cause fouling quickly during water treatment. To enhance the functionality of the nanofiber membranes and reduce the fouling, surface modification can be suggested. The high surface area of nanofibers allows better modification on the whole surface. The surface modification can be done as physically (blending or coating, high energy irradiation, heat and plasma treatments), chemically (chemical grafting, adding functional groups, chemical vapor deposition, and co-polymerization), or both physically and chemically (Figure 3.6). The main aim of surface modification is to alter surfaces by either physically or chemically altering the atoms/molecules on the surface, coating the surface with new materials, or changing the surface topography. Some of these methods are;
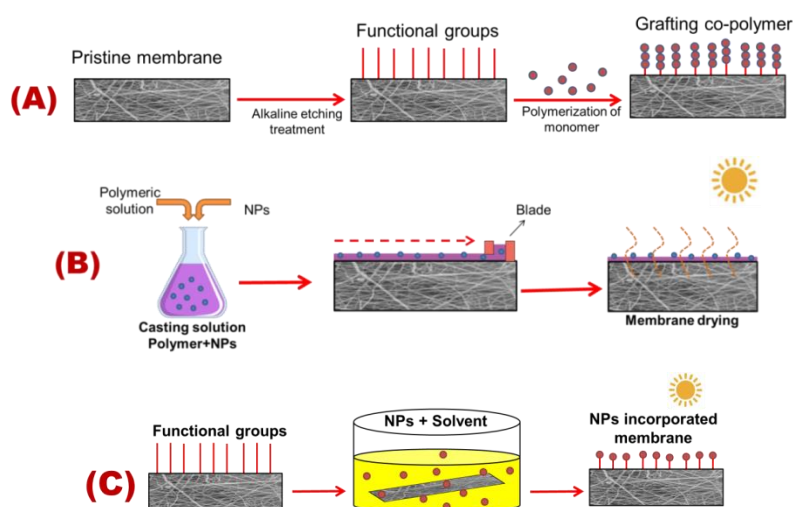

Figure 3.6. Modification of nanofiber membranes (A) co-polymer grafting, (B) NPs casting, (C) NPs grafting.

Blending and coating: It is a simple physical method, no chemical attachment or interaction between the functional material and the polymer occurs. At least two different materials are blended or surface coated to get the desired properties of functional material. Combining additives with polar groups to a nonpolar matrix in the electrospinning process can result in the forming of polar groups at the nanofibers' surface. Including hydrophilic poly(vinyl alcohol) (PVA) into hydrophobic polyvinylidene fluoride (PVDF) polymer into electrospinning solution improved not only water flux but also fouling resistance of the nanofiber membrane [58]. However, controlling and re-productivity of this method is difficult [59].

Sol-gel Method: Sol-gel process is a wet chemical method for forming inorganic structures from a colloidal suspension of inorganic or metal and organic precursors. This method consists of four steps: (a) hydrolysis of the inorganic or organic precursor in the acidic or basic mediums and condensation reactions of precursors, (b) agglomeration/clustering of sol constituents, (c) drying of the gel, (d) and sintering to form inorganic phases and structures with desired characteristics. The advantage of this method is to obtain high surface area and stable surfaces while possible disadvantages are shrinkage during drying, cracking formation problems, and relatively low production rate.

Plasma: Plasma treatment is a common method to achieve hydrophilic or hydrophobic electrospun nanofiber mats. In this technology, a reactive treatment process takes place for creating or reducing positive ions, negative ions, and radicals on polymer surfaces using various plasma sources. This method requires shorter treatment time as compared to other surface modification methods. Plasma modification forms functional groups, molecular crosslinking, graft polymerization, and coating without changing the fiber surface. The adhesion property of plasma-modified polymer surfaces can be enhanced by increasing the charge density. Previously, the author tried to improve membrane surface hydrophilicity using low vacuum microwave plasma treatment with argon (Ar) gas [60]. For this reason, various polymeric nanofiber membranes such as polyurethane (PUR), PVDF, PAN, and polyamide 6 (PA6) were used. WCA measurement was used to determine the contact angle. The water contact angle was measured occasionally during 55 days to observe the stability of surface hydrophilicity. Results showed that the stability of the contact angle is changed depend on the polymeric material. The plasma-treated PAN, PA6, and PUR membranes lost their plasma effect on 13th, 17th, and 17th days respectively; and they had similar contact angles before plasma treatment. PVDF did not show the same contact angle as neat polymeric nanofibers over 55 days. The hydrophilic effect of plasma is not long-lasting, and stability is changes depend on the polymeric material.

Graft Polymerization: Surface grafting is easy, useful, and controllable process to improve the nanofiber membrane surface. Surface modification can be achieved by grafting-to or grafting-from. In the grafting-to (grafting onto) method, a functionalized polymer must react with the membrane surface to produce polymer brushes. In the grafting-from, initiators are used and immobilized on the membrane surface that allows monomer polymerization.

Radiation-Induced Graft Co-Polymerization: This method can be grouped into two categories, such as low and high energy radiation. Visible light and UV radiation with particle energy of up to about 50 eV is called low energy radiation which is suitable for nanofibers. In high energy radiation, the ionization mechanism is induced which leads to the formation of ions with different signs. UV and high energy radiation can lead to physical and chemical modification via cross-linking and grafting on the surface of the polymers. On the other hand, it can cause the breaking of bonds and damage the

polymer, especially for biodegradable polymers. In some cases, this can be an advantage. For instance, electron beam irradiation has been used to fasten the degradation of poly L-lactide acid/ carboxymethyl starch/β-tricalcium phosphate (PLLA/CMS/β-TCP) composite nanofibers for tissue engineering [61].

Wet-Chemistry: This method is based on the reaction between the chemical compound in the solution and the surface of the nanofiber web. Hydrolysis can generate carboxyl or hydroxyl groups on the nanofiber. Potassium hydroxide (KOH) has been used to promote hydroxyl groups to the surface of PVDF nanofiber membranes, which increase water permeability and fouling resistance [62,63]. An alkaline treatment may lead to swelling of the nanofibers and reduce pore size or the destruction of the open fibrous structure and formation of gel-like materials [64,65]. In some cases, two or more modification is needed to improve wettability or provide stable modification [66,67]. In this method, degradation, non-reproducible, irregular etching, and non-uniformity are the disadvantages.

The author includes surface modified nanofiber membranes for separation of wastewater in the part "*Presented Works and Their Novelties*".

3.6.3. Current Research on Nanofiber Membranes

Nanofibers are one of the safest nanomaterials serve as a promising candidate for water treatment. Many papers have been published more recently regarding nanofiber applications in membrane technology. There is an exponential growth of documents dealing with nanofiber membranes in water applications published in the last decade (Figure 3.7.). Nanofiber webs have high porosity; almost more than 80% void structure, and tight pore size from 40nm to 1000 nm. The lower fiber diameter increases filtration efficiency and increases the pressure drop that negatively affects the quality factor of air filtration. The particles in the wastewater are mainly deposited and attach the nanofiber surface by mechanically or electrostatically. Compared to commercially available microfilters, nanofibers can have 4-100 times smaller pore size and several times higher surface area [68].

Application of nanofibers in water treatment varies from membrane distillation, microfiltration, ultrafiltration, nanofiltration, reverse osmosis, and oil/water separation.
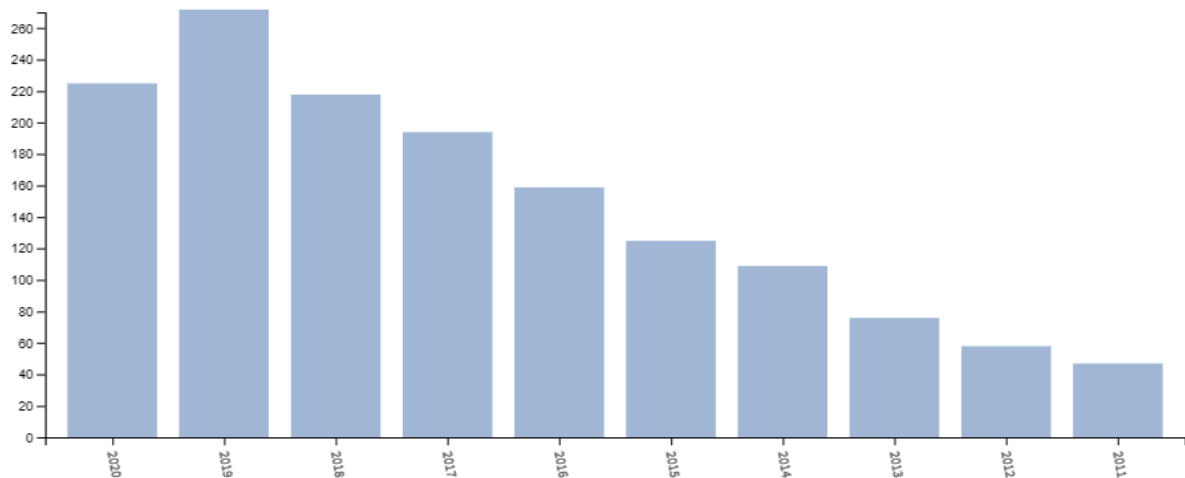
Figure 3.7. Papers on nanofiber membrane in water application (according to WoS, September 2020)

Membrane distillation (MD) is a non-isothermal membrane process driven by the vapor pressure difference across the membrane caused by the temperature gradient between feed and permeation solutions. In essence, the high cost of MD modules, relatively low permeate flux (caused by concentration polarization) in comparison with pressure-based membrane processes, water loss due to conduction through the polymeric membrane, membrane pollution, pore wetting, and high thermal energy consumption did not allow expanding of the technology. The preparation of nanofiber membranes provides better control of the membrane parameters, such as pore size, porosity, and thickness, these characteristics that are crucial for the high efficiency of MD [24]. Membrane distillation modules supported by nanofiber membranes offer significant advantages over commercial MD membranes. Specifically, nanofiber products provide an enormous amount of specific surface area and controlled porosity and narrowed pore size, which is certainly necessary for MD membranes. PVDF nanofiber surface was covered with polydimethylsiloxane (PDMS) to reduce surface energy by the dip-coating method and used in MD [69]. Improved nanofibers exhibited high water contact angle as148.7° and strong intrinsic hydrophobicity. The water flux was 30.2 kg/(m^2 h) and excellent stability in 22 hours of operation. Polyurethane nanofibers exhibited extremely high salt retention above 99% and flux up to 12 kg/(m^2 h) [70].

Nanofiber in micron size pore is suitable for microfiltration. Microfilter membranes can separate particles between 0.1 and 10 μm. Nanofibers increase the water permeability by reducing the membrane resistance against water flow. Mechanically enhanced poly(trimethylene terephthalate) (PTT) nanofiber membrane as microfiltration media is used for the separation of 100 μm TiO2 nanoparticles [71]. Apparently, heat-treated nanofibers have a particle rejection above 99.6%.

Carbonaceous microspheres were covalently attached to the PAN nanofiber surface [72]. Later silver nanoparticles were trapped via in situ reductions to form carbonaceous-silver nanofibrous membrane for separation of complex oil/water separation and removal of heavy metal ions, organic dyes, and bacteria. The membrane had high permeability of 45612 ± 430 L/(m^{2}hbar) for toluene-in-water emulsion with separation efficiency of higher than 99% and removed above 90% Pb2+ through the adsorption of covalently attached carbonaceous microspheres and nearly 100% methylene blue through the Fenton-like oxidation of embedded silver nanoparticles. Moreover, silver nanoparticles showed excellent antibacterial properties against *E. coli*.

Electrically conductive, superhydrophilic nanofiber composite membrane was prepared by acidified carbon nanotubes (ACNTs) decoration onto polyurethane (PU) nanofibers and subsequent polydopamine (PDA) modification [73]. Results indicated superior anti-fouling property with high flux (4195 L/(m^{2}h) and rejection (99.9%) and can be used for high-efficiency separation of an oil-in-water emulsion.

Manganese dioxide (MnO$_2$)-coated cellulose nanofibers have been used to remove methylene blue, resulting in high adsorption and oxidation efficiency in the decolorization of methylene blue [74].

Electrospun nanofibers are mainly used as a support layer for the thin film UF and NF. For instance, nanofiber has been used as a microporous structure for forward osmosis and membrane distillation [75]. Thin film composite (TFC) membrane was prepared from PAN nanofibers to support a hydrophilic PAN-coating layer for arsenate removal from contaminated water [76]. Due to high

porosity, the prepared membrane showed 172–520% higher flux and 1.1–1.3 times more efficient in rejecting arsenate ions than the UF membrane.

A hydrophilic poly(vinyl alcohol-co-ethylene) (PVA-co-PE) nanofiber membrane was prepared as support layer for TFC membranes for nanofiltration to separate different metal ions as NaCl, Na2SO4, CaCl2, CuCl2, CuSO4, and methyl orange solutions [77]. The rejection was found 87.9%, 93.4%, 92.0%, 93.1%, 95.8%, and 100%, respectively.

All the research shows there is an excellent potential for nanofiber membranes in the water domain application. More example related to nanofibers as microfilter is given in "*Presented Works and Their Novelties*".

3.7. Recycling and Disposal of Nanofiber Membranes

Recycling of the membranes is mainly done by the cleaning process. Nanofibers are a relatively new technology. For this reason, there is no clear policy and standard about nanofiber recycling and disposal due to the large variety of nanomaterials that exist in various applications and the varying approaches required for each.

3.8. Possible Risks

During the preparation of nanofibers, there may be little hazard posed by exposure of chemicals that users in particular need to be aware of. At the industrial level, proper training is needed for the workers. The effect of nanofibers in human health is debatable. It was found that lung cells were not affected by short fibers (less than five-thousandths of a millimeter long) while long fibers can reach the lung cavity and cause disease [78]. Nanofibers might pose a risk because they have a similar shape to asbestos. It is necessary to have more researches on nanofiber effects on environment and human health. Toxicity tests of the nanoparticles used as surface modification should be done correctly. The nano dimension of NPs makes it challenging to track and monitor both the environment and the human body and observe the hazards.

Nanofiber membrane has to have good selectivity, high mechanical, chemical, and/or thermal resistance, and reusability to increase the separation performance and to reduce the material and labor costs. Commercialization of nanofiber still needs some developments as; compatibility with the existing infrastructures, potential environmental and human risks, optimized cleaning process during filtration and operating cost. All these developments are temporary, and a considerable effort is needed between research institutions, industry, and stakeholders. In 2011, the International Organization for Standardization (ISO) developed the ISO/TR 13121:2011 (10) standard, which relates to *Nanomaterial risk evaluation* [79]. To ensure the health and safety protection of the public, consumers, workers and the environment, this standard is evaluating, addressing, making decisions about, and communicating the potential risks of developing and using manufactured nanomaterials.

There is not enough defined policy or testing methods to evaluate risks associated with nanomaterials and nanofibers. However, researchers, industrial producers, and lawmakers are collaborating to identify and eliminate potential hazards in nanotechnology.

CHAPTER 4- PRESENTED WORKS AND THEIR NOVELTIES

The last chapter includes the selected works documenting the author's contribution to nanofiber membranes in liquid filtration applications.

The represented publications in this chapter are not placed in chronological order due to different journals' publication and evaluation policy, differences in manuscript preparation time, prioritizing the publication of finished projects, etc. The publications are placed in the order of scientific research from nanofiber preparation to end application as;

— Improve fiber morphology, spinnability, and selected properties of some polymeric solutions for possible application of nanofibers include water filtration.

— Enhancement of mechanical properties of nanofiber web and investigation of lamination conditions on the nanofiber membrane.

— Surface modification and application of nanofiber membranes in various water treatment (Sea-water desalination, oily water separation, wastewater treatment, separation of racemic compounds).

The novelty of works:

4.1. Improving Nanofiber Quality for Water Filtration

Polymer blends are mainly used to obtain new material with the desired strength, chemical and mechanical resistance, thermal stability, and biological properties. Polymer blending offers an easy way to obtain new materials by combining various polymers. In electrospinning technology, polymer blending is very often used to improve nanofiber quality by incorporating the unique properties of each polymer. The blending of polymers is typically achieved by using the polymers which can be dissolved in the same solvent system.

The Author's contribution to this field is to use various water-insoluble polymers and their mixture for a better fiber surface morphology, improve spinnability, and enhance the properties of nanofiber web via an industrial-scale electrospinning device. This work shows that some of the polymers and their mixtures can be electrospun and use in industrial applications. The work has considerable practical relevance in a multidisciplinary field (e.g., pharmaceutical industry, wastewater filtering). The screening of the polymers and polymer composites from the point of their spinning ability is of impact. Although the electrospinning process has been reported several years before, the research content of the paper is still very interested because 1) the preparation of nanofibers on a large scale is a hot topic in this field presently, 2) polymer blends and solvent mixtures are explored as a way to improve electrospinnability of polymer solutions, and 3) this work does provide insight for industrial applications.

Reprint:

1. Yalcinkaya F. Preparation of various nanofiber layers using wire electrospinning system. Arabian Journal of Chemistry. 2019 Dec 1;12(8):5162-72.

King Saud University

Arabian Journal of Chemistry

www.ksu.edu.sa
www.sciencedirect.com

ORIGINAL ARTICLE

Preparation of various nanofiber layers using wire electrospinning system

CrossMark

Fatma Yalcinkaya

Centre for Nanomaterials, Advanced Technology and Innovation, Technical University of Liberec, Studentska 2, 46117 Liberec, Czech Republic

Abstract This study focuses on the preparation of various polymeric nanofibers using new indus- trial production equipment – a wire electrospinning system. The disadvantages of each polymeric nanofiber were improved by mixing suitable polymer/polymer-solvent/solvent systems. A total of 9 types of polymers (polyamide, polyvinylidene fluoride, polyacrylonitrile, polyurethane, polysul- fone, chitosan, cellulose acetate, polyvinyl butyral, and polycaprolactone) and their mixtures were electrospun using a wire electrospinning system. The resultant fiber surface morphology showed that the wire electrospinning method is suitable for the production of various polymers on an indus- trial scale. Moreover, polymer mixtures changed the adhesion properties, increased productivity and reduced the fiber diameter of nanofibers.

ELSEVIER **Production and hosting by Elsevier**

1. Introduction

The application area of polymeric nanofibers has been increased since the late 20th century due to their highly porous structure and high aspect ratio and the new design of materials. The nanofibers can be produced easily using needle and needleless electrospinning, force spin- ning, melt-blown, island-in-the-sea, drawing, etc. (Torobin and Findlow, 2001; Huang et al., 2012; Fabbricante et al., 2000; Huang, 2009; Nain et al., 2006; Jirsak et al., 2004). The biggest challenges for creating nanofibers are mass production and complicated struc- tures from multiple-fluid spinning processes (Wen et al., 2016; Yang et al., 2016a; Yu et al., 2016). Among the various techniques reported in the literature, the free surface electrospinning system using Nanospi- der electrospinning technology is one of the most demanded technolo- gies for the continuous and mass production of nanofiber layers. The Nanospider technology was firstly developed by Jirsak et al. (2004), and then the new models were improved by Elmarco (Petras et al., 2010, 2009a, 2009b). The principle of the Nanospider equipment is based on a rotating electrode immersed into a polymer bath. The role of the rotating roller electrode is to feed the solution on the surface of

38

Table 1 Polymer and polymer mixture solutions.

Polymers	Polymer ratio (% wt.)	Solvent ratio (% wt.)	Total concentration of polymer in solution (% wt.)
PA6		AA:FA (2:1)	8
PVB		AA	11
PCL		AA:FA (2:1)	12
CH		DAA	8
CA		AA	9
PSU		DMAC	10
PVDF		DMAC	13
PAN		DMAC	8
PU		DMF	13
CA:PVB	1:1	AA	10
CA:PA6	1:1	AA:FA	8.5
PA6:CH	1:1	AA:FA:DAA	8
PA6:PCL	1:1	AA:FA	10
PA6:PVB	1:1	AA:FA	9.5
PCL:PVB	1:1	AA:FA	11.5
CH:PVB	1:1	AA:DAA	9.5
PCL:CH	1:1	AA:FA:DAA	10
PU:PSU	1:1	DMF:DMAC	11.5
PVDF:PAN	1:1	DMAC	10.5

Table 2 Spinning conditions of solution on wire electrospinning system.

Solution	Applied voltage/distance (kV/cm)	Relative humidity-Temperature (%- C)	Wide of substrate (cm)	Speed of substrate (mm/min)	Diameter of wire (mm)
PA6, CA:PA6, PA6:PCL	3.28	30–22.5	40	13	0.2
PVB, CA:PVB, PA6: PVB, PCL:PVB	3.28	30–22.5	40	13	0.2
PCL	3.28	30–22.5	40	13	0.2
CH, PA6:CH, PCL:CH	3.28	30–22.5	40	13	0.2
CA	3.28	30–22.5	40	13	0.2
PSU, PU:PSU	3.88	26–22.0	40	13	0.2
PVDF, PVDF:PAN	3.80	33–22.5	40	13	0.2
PAN	3.80	33–22.5	40	13	0.2
PU	3.88	26–22.0	40	13	0.2
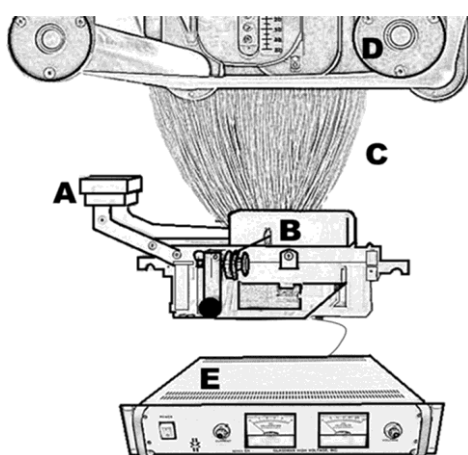
Figure 1 Schematic illustration of a Nanospider new generation electrospinning device, (A) a solution tank feeds the solution toward the wire, (B) wire electrode, (C) spinning area, (D) take-up cylinder connected to backing material, and (E) high voltage supply.

Table 3 Spinning performance of nanofiber webs.

Polymers	Aw (g/m^2)
PA6	0.800
PVB	3.53
PCL	5.00
CH	Not spinnable
CA	3.50
PSU	8.20
PVDF	6.80
PAN	3.50
PU	5.40
CA:PVB	3.62
CA:PA6	3.83
PA6:CH	0.40
PA6:PCL	1.70
PA6:PVB	8.20
PCL:PVB	7.10
CH:PVB	Solution precipitate
PCL:CH	Droplets, no fiber
PU:PSU	13.80
PVDF:PAN	6.98

Figure 2   Preparation of nanofiber webs to calculate *Aw*.
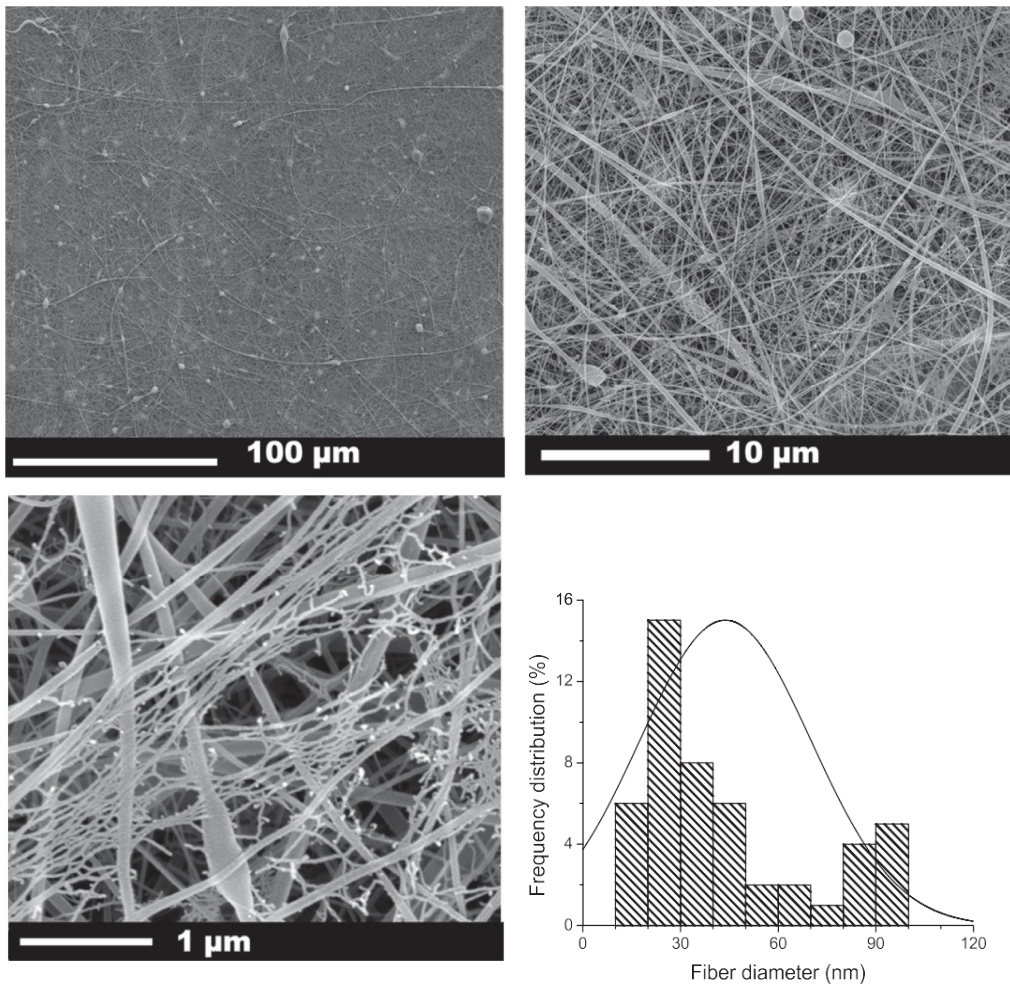
Figure 3   SEM images of the PA6/CH mixture electrospun nanofiber.

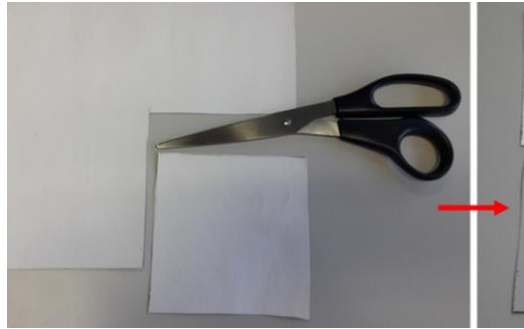the roller. The biggest difference between the first (roller electrospinning) and the new generation Nanospider (wire electrospinning) is the type of electrode and feeding unit. In new generation technology, there is a conveyor wire electrode and a close bath unit conveyed on the wire for the feeding of the solution. The effective electrostatic field on a thin wire is higher than roller surface which might affect the spinnability of various polymeric solutions. Moreover, the closed feeding system makes it possible to keep solution viscosity stable over time. On the open surface, some hygroscopic polymer solutions can easily absorb the humidity and change the viscosity and properties of the solution over time. Using a wire electrode the Nanospider equipment prevents the undesirable variations in the polymer solution during

long-term usage. The use of the conveyor wire can easily remove the ex-solution, and the new fresh solution is always supplied to the electrode.

The wire electrospinning system has great advantages compared to many mass production methods. Roller, disk or spring electrospinning systems have high productivity rates, with the fiber diameters varying between 80 and 700 nm with a standard deviation of ±50 nm. However, the solution is on an open surface and it is difficult to maintain the solution's viscosity stable over time. In the force spinning method, productivity is very high but the controlling of the fiber diameter and diameter distribution is not easy. In melt electrospinning, productivity is high but the fiber diameter and diameter distribution are wide. The drawing method has very low productivity rates while the fiber diameter is high. In the island-in-the-sea method, the fibers are produced in entanglement form and the fiber diameter varies between 800 and 2500 nm with a standard deviation of ±200 nm.
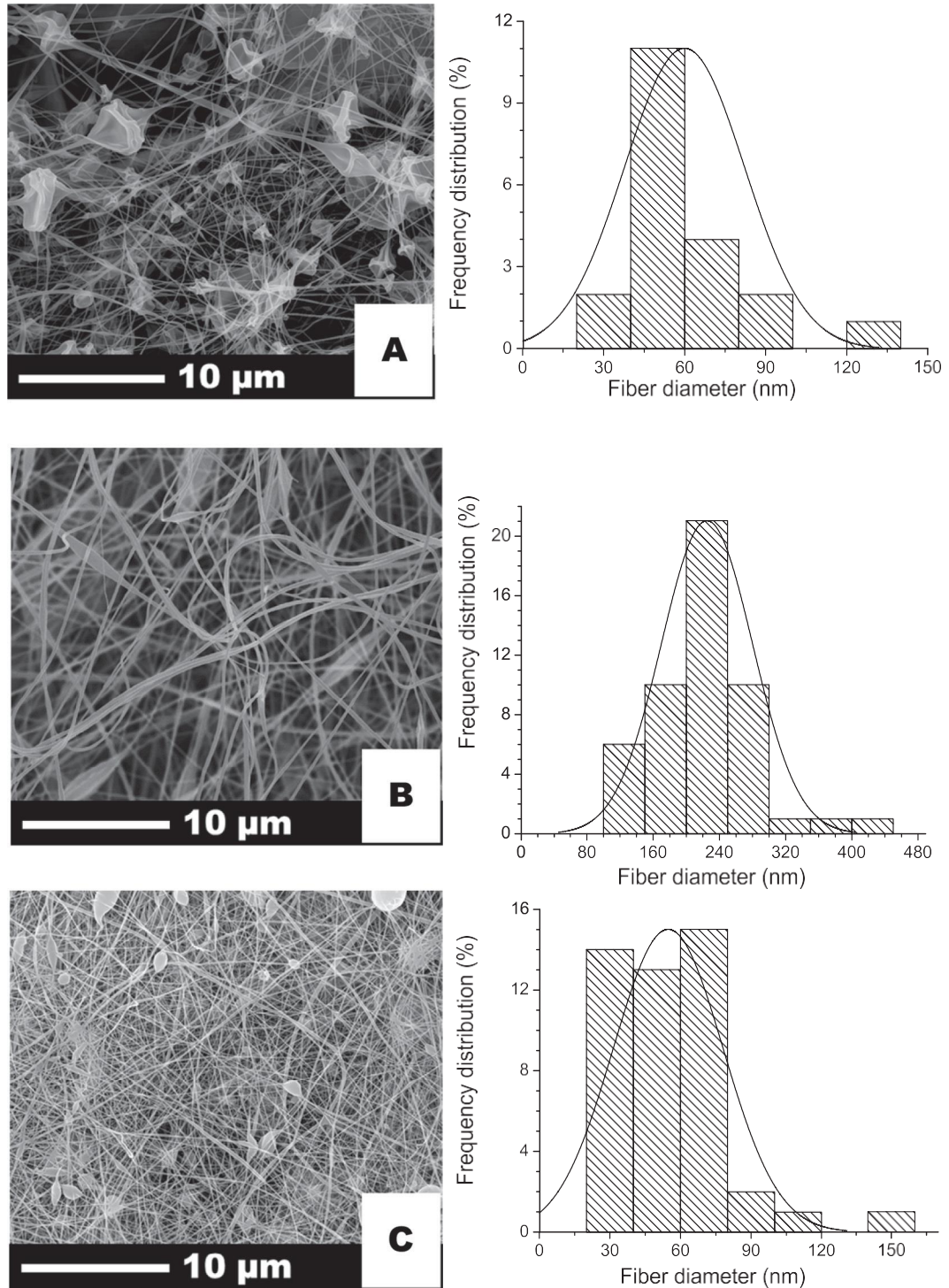

Figure 4   SEM images of (A) CA, (B) CA + PVB, (C) CA + PA6.

The advantage of using the wire electrode Nanospider equipment is the easy formation of nanofibers on a thin wire (0.2 mm). The productivity rate is very high; the fibers are thin (80–700 nm) and have a narrow standard deviation (±30 nm).

In this study, various electrospun polymeric nanofibers were fabricated using wire electrospinning. Unlike in the case of roller electrode Nanospider electrospinning (Yalcinkaya et al., 2014, 2016a, 2016b, 2015; Yener et al., 2013; Yener and Jirsak, 2012; Cengiz et al., 2010; Sasithorn and Martinova, 2014; Jirsak et al., 2010), there is not enough information about the production of nanofibers using wire electrospinning in the literature. Herein, a wide range of polymer and polymer mixtures were fabricated and the disadvantages of each polymer were eliminated and new features added by using polymer mixtures. The improvement of the various nanofiber webs' disadvantages was studied for the first time.

The fiber diameter of nanofibers can be changed through electrospinning parameters. However, controlling the fiber diameter is not an easy process. Changing the spinning parameters (applied voltage,
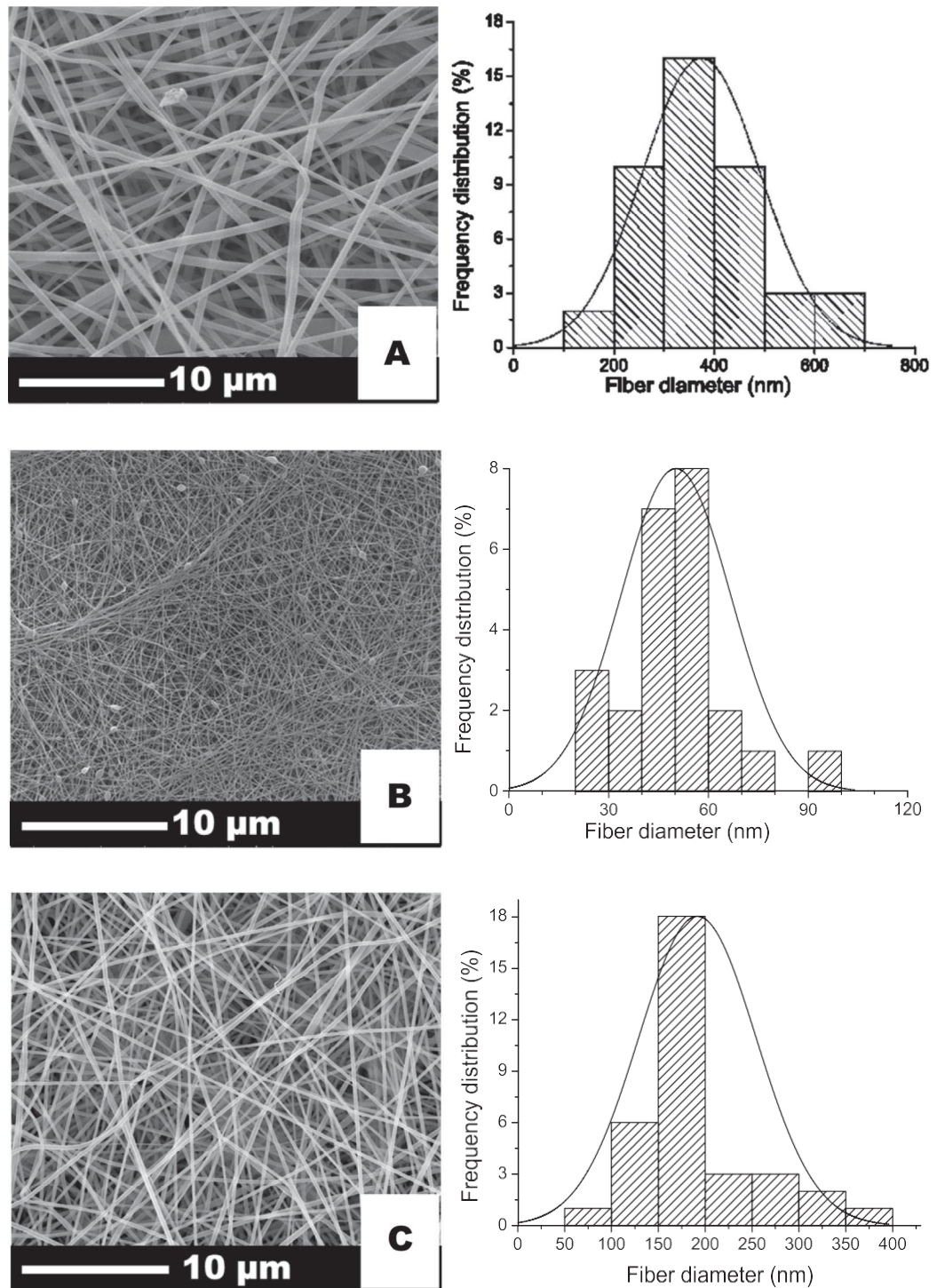
Figure 5   SEM images of (A) PVB, (B) PA6, (C) PA6 + PVB nanofibers.

distance between electrodes, solution properties and speed of carriage) can make changes on the fiber diameter but parameters alone are not sufficient to obtain nanofibers without beads. Herein, some of the polymer mixtures were used to change the surface morphology of the nanofiber layers.

The diversity of spinnable polymers showed that the use of the wire electrode Nanospider equipment had big advantages for the continuous mass production of nanofibers. The resulting nanofibers are suitable for application in air filtration, water filtration, ion-battery separation, bio-medical application, cosmetics, etc. (Bella, 2015;

Figure 6   SEM images of (A) PCL, (B) PCL + PA6, (C) PCL + PVB nanofibers.

Figure 7   SEM images of (A) PSU, (B) PU, (C) PVDF, (D) PAN nanofibers.

Bella et al., 2015; Yalcin Enis and Gok Sadikoglu, 2016; Yalcinkaya et al., 2016a, 2016b; Yang et al., 2016b). The aim of the preparation of mixture fibers was to eliminate disadvantages such as weakness, abrasion, hydrophilicity/hydrophobicity, and oleophilicity/oleophobicity and improve and combine the advantages of polymers. The blended nanofibers are more ad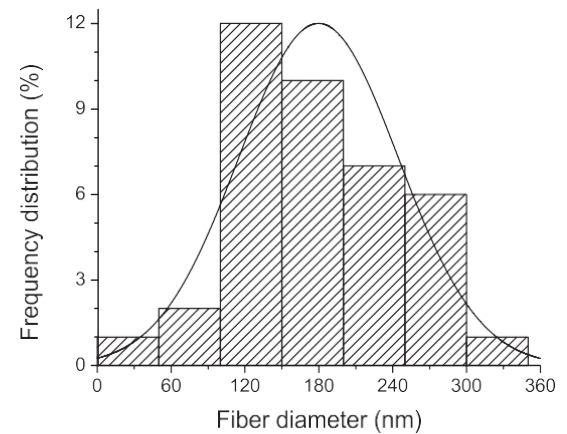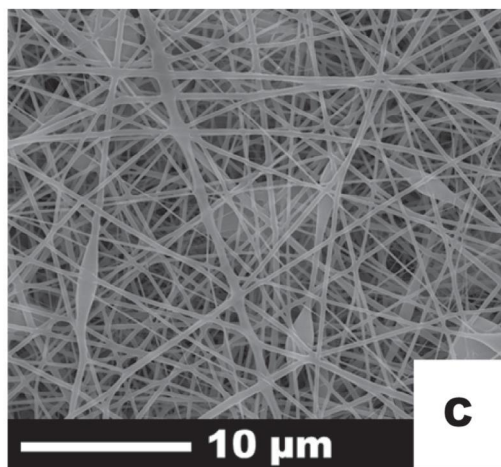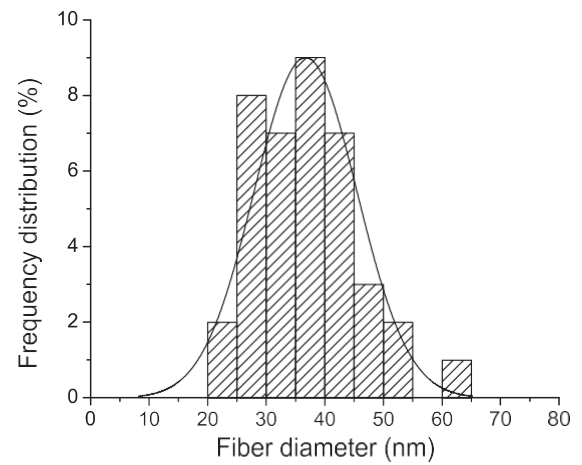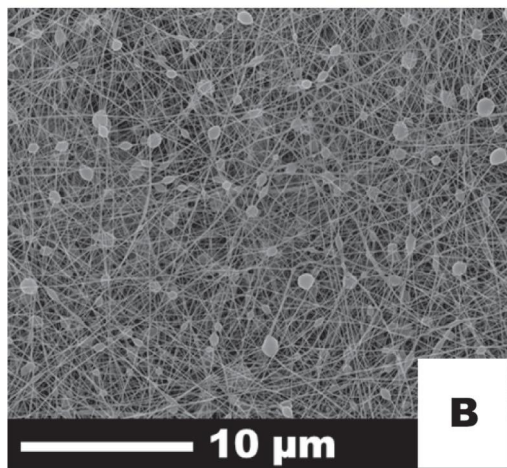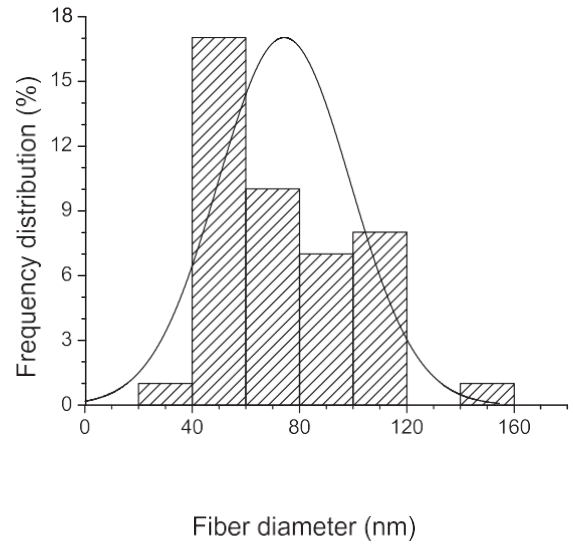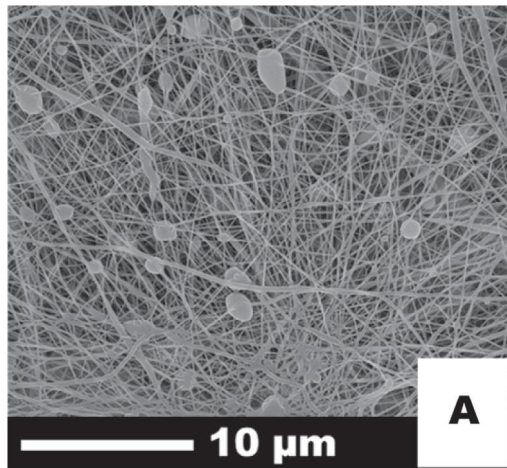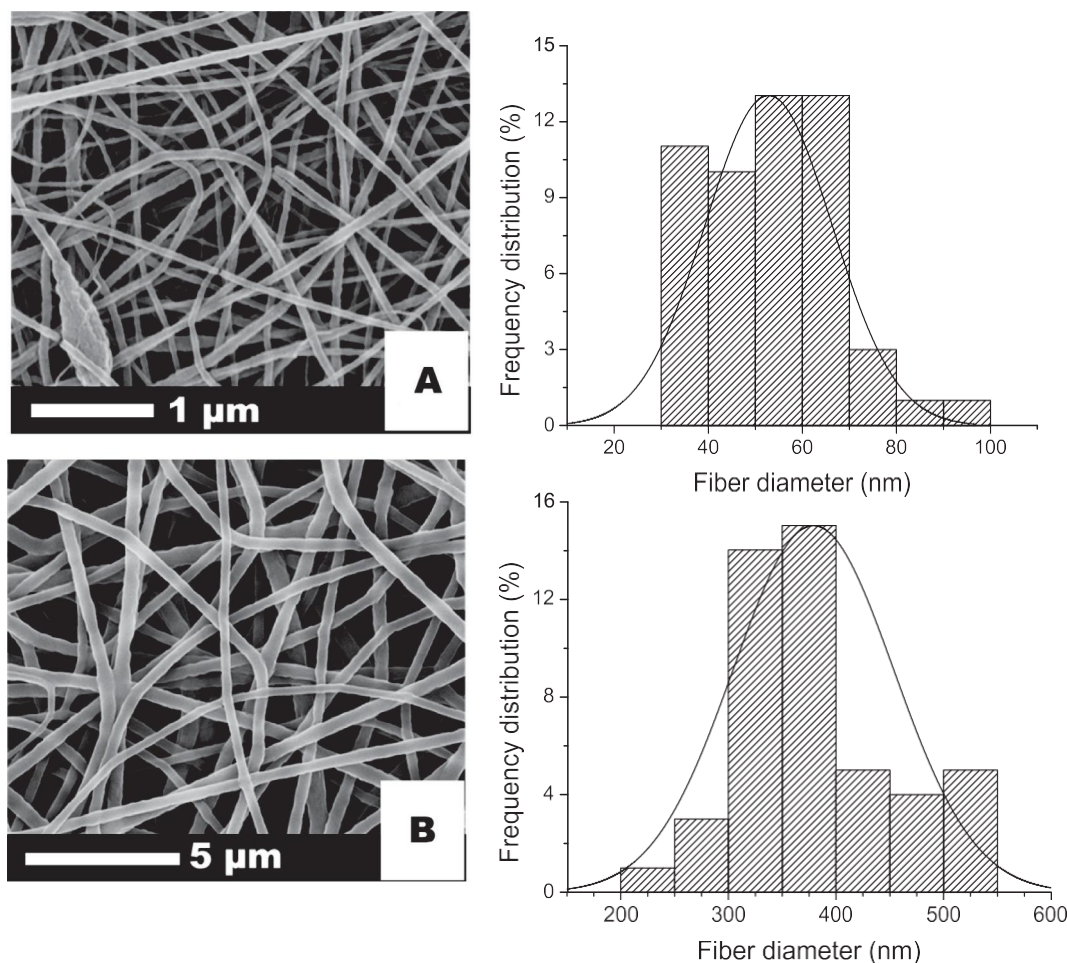vantageous compared to single electrospun nanofibers for improving the mechanical, structural, antibacterial, biocompatible and engineered properties of materials.

1. Experimental

50.000 g/mol cellulose acetate (CA) and 45.000 g/mol polycaprolactone (PCL) were purchased from Sigma–Aldrich; vegetal chitosan (CH) was purchased from KitoZyme; 60.000 g/mol polyvinyl butyral was purchased from Mowital; ultra-aramid B24 polyamide 6 and Ultrason E600P polysulfone (PSU) were purchased from BASF; Polyvinylidene fluoride (PVDF) was donated by Kynar 761A; polyurethane was purchased from Larithane LS 1086; 150.000 g/mol polyacrylonitrile (PAN) was purchased from Dimachema Pigment Corporation. The solvents, %99 acetic acid (AA) and %56 diluted acetic acid (DAA), formic acid (FA), dimethylformamide (DMF), and dimethylacetamide (DMAC) were purchased from Penta s.r.o. The polymers were dissolved in the solvent for 30 h and mixed to form a homogenous solution. The per-

centages of the prepared solutions and mixtures are shown in Table 1. For the solution mixtures, first the single polymer solution was prepared, and then the polymer blends were prepared at a given weight ratio according to Table 1 and mixed overnight. The concentration ratio was determined according to our previous experiments and known-how.

The spinning conditions kept stable during process are shown in Table 2. The schematic figure of the new generation Nanospider equipment is shown in Fig. 1.

The solution is placed into a feed unit (A, B). The wire is placed in the middle of the solution tank. The feed unit is moving back and forth and the solution is feeding on the wire. The upward part has a second wire electrode, which generally has the opposite charge to the downward wire electrode or is grounded. If the electrical field between the electrodes overcomes the surface tension of the polymer solution, fibers are formed (C). A conveyer backing/supporting material is placed in between the two electrodes to collect the fibers, moving at a desired speed using take-up cylinders (D).

The nanofibers were analyzed using a scanning electron microscope (SEM, Tescan Vega3 SB). All samples were goldcoated for 60 s and 7 nm thickness before SEM imaging to reduce the effect of charging. The Image-J software was used to measure the average fiber diameter from more than 50 different randomly selected fibers.
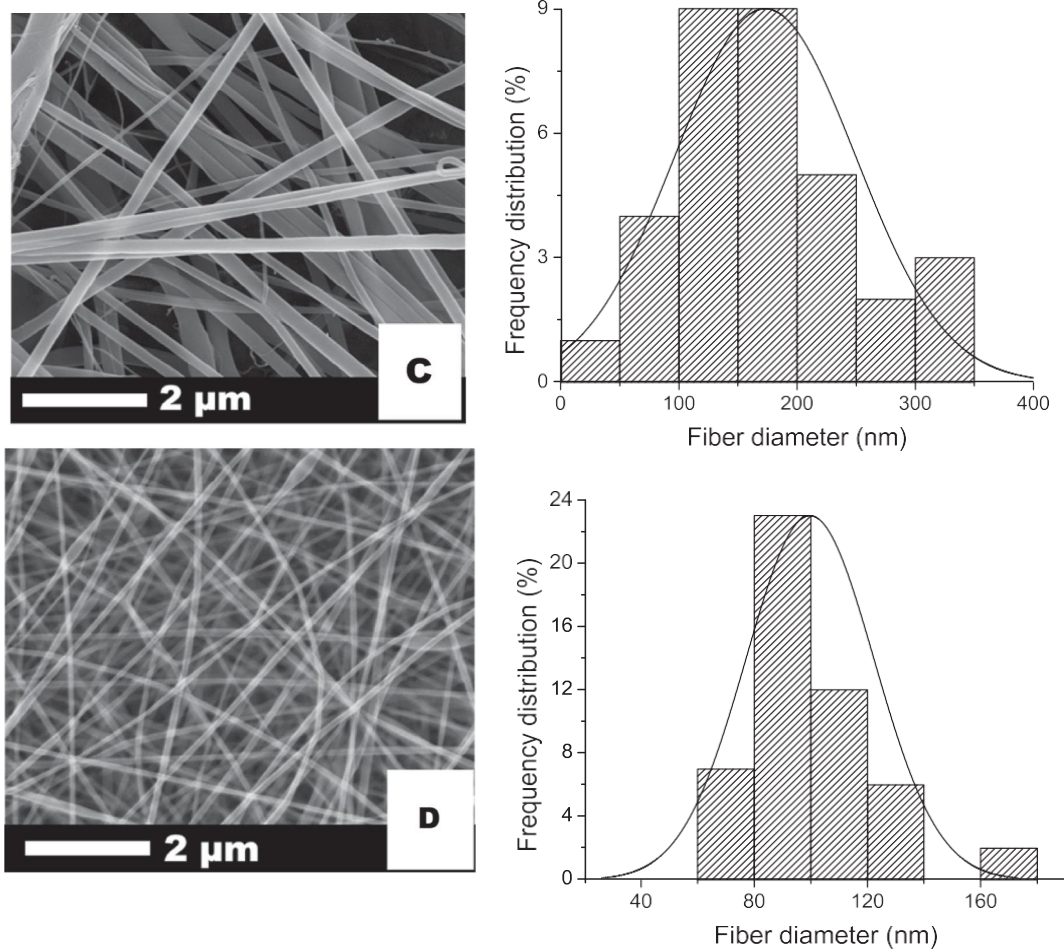
Figure 7 (*continued*)

The productivity of the nanofiber webs can be compared calculating the area weight (basis weight) of the samples. Table 3 shows the area weight of each polymeric nanofiber web. The area weight of the nanofibers was calculated according to Eq. (1):

$$Aw = \frac{G}{A} \; g=m^2 \qquad (1)$$

where *Aw* is the area weight of the nanofiber web, *G* is the weight of nanofibers at a given area (gram), and *A* is the measured area of the web (m²). The samples were cut into sheets of 10 10 cm² (3 for each sample), separated and weighted as shown in Fig. 2.

1. Result and discussion

The results showed that some of the polymers and their mixtures did not form fibers as shown in Table 3. Each polymer solution showed different spinnability and spinning performance. Spinning performance is an important parameter for the productivity.

The spinning of a pristine chitosan polymer solution is quite difficult due to high viscosity. Gel-like networks prevent the formation of electrospun fibers. Chitosan nanofiber is a good candidate for biomedical application and adsorbent materials to remove dyes from industrial wastewater (Iqbal et al., 2011; Sobahi et al., 2014; Kenawy et al., 2015). The idea of mixing chitosan with other polymers is to improve spinnability and mechanical and biocompatible properties. The results showed that only the mixture of a chitosan and polyamide 6 solution forms nanofiber structures with a low area weight and fiber diameter.

The results of chitosan and polyamide 6 mixture nanofibers are given in Fig. 3.

Fig. 3 shows that there are two types of fiber in polymer mixture nanofibers. It can be observed that the average fiber diameter is less than 100 nm. Moreover, some fibers have broken ends. The reason can be explained as follows: chitosan has low concentration (8%) with very high viscosity, which prevents the continuous fiber forming, with the drops breaking following fiber formation. The entanglement between the chitosan macromolecules is not strong enough to produce continuous nanofibers. Chitosan has an effective volume fraction that is much greater than its actual volume fraction, which means physical properties equivalent to higher concentrations of less complex molecules (LeCorre-Bordes et al., 2016). It can be suggested that chitosan nanofibers can be produced with a mixture of PA6 for possible application of microfiltration,
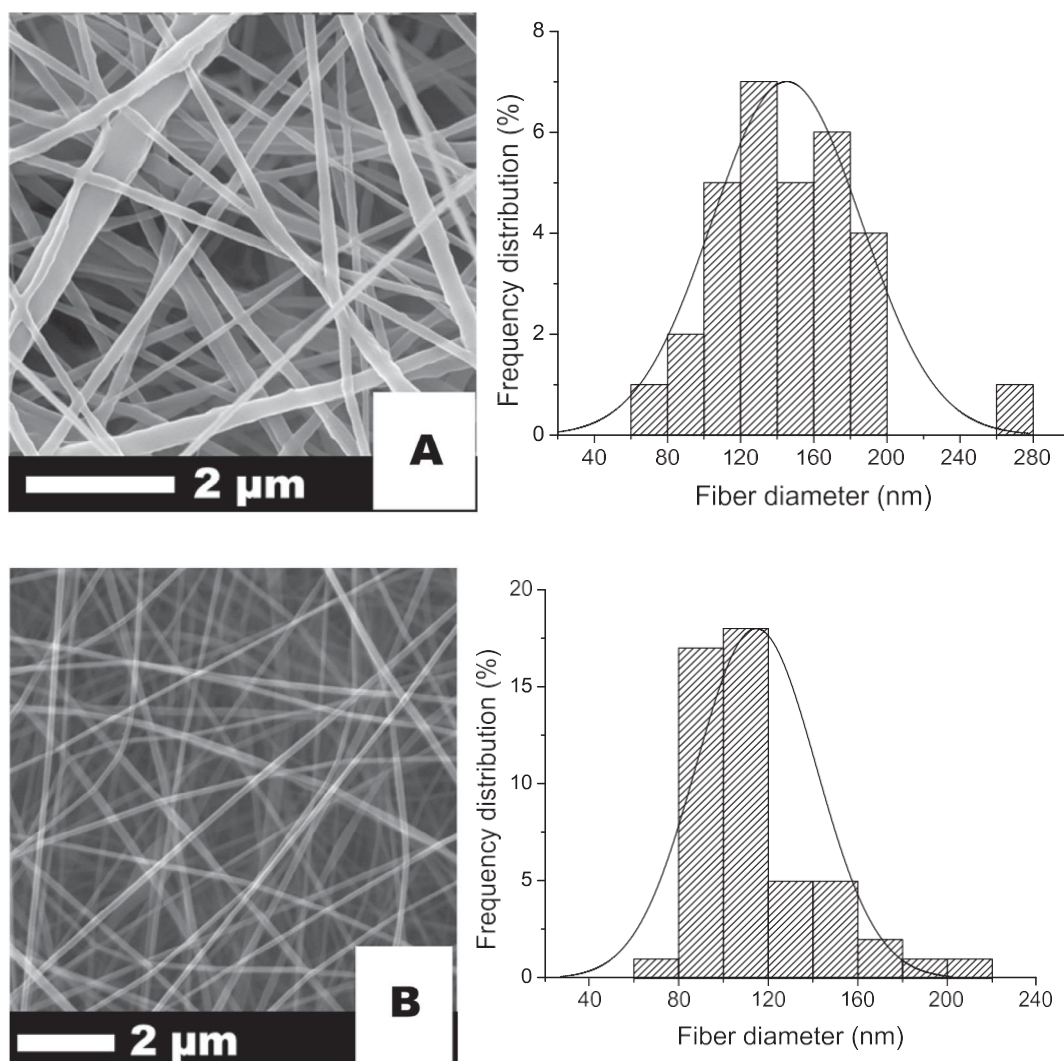
45

Figure 8   SEM images of (A) PSU + PU and (B) PVDF + PAN.

enzyme immobilization (Li et al., 2014; Maryskova et al., 2016) or human osteoblastic (HOB) cell culture applications (Nirmala et al., 2011).

Cellulose acetate nanofibers are biocompatible and have high hydrophilicity, which make them a good candidate for water treatment. It has been mentioned that spinning of CA solutions is not easy to control (Liu et al., 2016). Despite changing process parameters, beads form easily. As shown in Fig. 4(A), we also observed many beads on the surface of the web. The easy way to eliminate the bead structure is mixing with other polymer. In this way, not only are the beads eliminated, but it is also possible to enhance the advantages of nanofibers.

The idea of mixing CA with PA6 or PVB polymers is to reduce the bead structure and improve surface morphology (Fig. 4). CA + PVB nanofibers have almost 5 times higher fiber diameters than pristine CA nanofibers, while CA + PA6 nanofiber diameters are almost equal to pristine CA. The PVB nanofibers have an average nanofiber diameter of around 350–370 nm, PA6 of around 40–60 nm (Fig. 5), and their mixture of around 180–200 nm. The results indicate that

an additional polymer has a huge effect on the final polymer diameter and the bead structure as well. The mixture of CA with PA6 or PVB did not change the spinning performance of pristine CA nanofibers. Among all CA and mixtures, CA + PA6 nanofibers are an excellent candidate for air (Matulevicius et al., 2016; Nicosia et al., 2016) and water filtration (Carpenter et al., 2015; Zhou et al., 2016).

It was observed that during spinning PVB nanofibers have the ability to stick to all the surfaces of the spinning unit, take-up cylinders and the feed tank, which leads to difficulty in keeping nanofibers on the surface of backing materials. The mixing of PVB with PA6 nanofibers has the advantage of decreasing the average fiber diameter and leads to narrower fiber diameter distribution. Moreover, the adhesion problem of the PVB nanofibers was eliminated and the area weight was increased almost 2.3 times, which translates into lower energy costs.

Polycaprolactone is a low-cost, biodegradable polyester. Studies showed that the biocompatibility of PCL nanofibers has a promising future in biomedical applications (Mahjour et al., 2016; Venugopal et al. (2005); Thorvaldsson et al.,

46

2008; Pajoumshariati et al., 2016). It was found that the adhesion property of PCL nanofibers is much lower than that of protein nanofibers, which might be a disadvantage for the lamination process (Baker et al., 2016). To improve the adhesion properties of PCL nanofibers, the mixture of PCL + PA6 and PCL + PVB was prepared. PVB has excellent adhesion properties and is very cheap compared to PCL and PA6. The results of SEM are shown in Fig. 6.

Fig. 6 shows that the mixture of PCL and PA6 solutions increases the bead structure of nanofibers while the spinning performance decreases dramatically. On the other hand, mixing PVB with PCL decreases the formation of beads on the surface of the layer but increases the average fiber diameter 3 times. The area weight of PCL was increased by adding PVB. If the adhesion properties of PVB nanofibers are considered, it can be concluded that nanofibers from the mixture of PCL with PVB would have increased adhesion properties and also a decreased bead structure of nanofiber layers.

Polysulfone, polyurethane, polyvinylidene fluoride and polyacrylonitrile are good candidates for wastewater filtration, reverse and forward osmosis and membrane distillation. All the polymers were easily electrospun into nanofibers using the wire electrospinning system. The SEM results of the various polymers are shown in Fig. 7.

In our previous experiments, we found that PSU nanofibers are not good in terms of their mechanical and abrasion properties. PSU nanofibers are damaged and removed from the backing material very easily under slight tension. PU nanofibers have good tensile properties and elasticity, and are insoluble in water. A mixture of PU with PSU improved the mechanical and abrasion properties of nanofibers. When external tension was applied, the PU/PSU nanofibers were not damaged or removed from the backing material (Fig. 8).

PAN has highly polar groups in the backbone that improve the hydrophilicity of the materials and are advantageous for wastewater treatment as they decreased the fouling effect. PVDF nanofibers are quite strong but highly hydrophobic. Combining PVDF with PAN can improve the hydrophilicity and mechanical properties of nanofibers. The mixture of nanofiber layers is shown in Fig. 8.

Pristine PU and PVDF nanofibers have a larger fiber diameter and diameter distribution in comparison with PSU and PAN. Both PSU and PAN nanofibers have a diameter of less than 100 nm, which is promising for air and water filtration. On the other hand, the mechanical properties and hydrophobicity of PSU and PVDF are disadvantages and can be easily eliminated by mixing with PU and PAN respectively. The mixture of PSU + PU nanofibers has an average fiber diameter of around 120–140 nm while that of the PAN + PVDF mixture is around 120 nm. Both results of the mixture showed significant surface morphology and small fiber diameters, which make them a good candidate for water and air filtration. The mixing of PSU/PU increased the area weight of PSU and PU 1.68 and 2.5 times respectively, while the mixture of PAN/PVDF increased PAN and PVDF to 1.99 and 1.02 respectively.

The main results of the work can be summarized as follows:

Mixing a chitosan polymer with PA6 can form nanofibers while a mixture of CH + PVB and CH + PCL did not form nanofibers.

Bead-free cellulose acetate nanofibers were produced by mixing with PA6 and PVB polymers. The CA + PA6 nanofi-

bers have a small fiber diameter of around 60 nm, which suggests a potential application area for high-efficiency air filtration.

The PA6 and PVB nanofibers were electrospun with average fiber diameters of around 50 and 400 nm respectively. PVB is quite a cheap polymer compared to other polymers and is easy to process and handle. There are not many studies about the application of PVB nanofibers. Based on the application area, the fiber diameter of PVB nanofibers can be reduced and the spinning performance can be increased by mixing with PA6.

PCL was mixed with PA6 and PVB. The resulting electrospun fibers showed that a mixture of PCL + PA6 creates beads on the surface of the nanofiber. On the other hand, a mixture of PCL + PVB nanofibers has good surface morphology and very high productivity. Using the adhesion properties of PVB, the adhesion properties of PCL nanofibers can be improved.

PSU, PU, PVDF and PAN all have special properties for various application areas. The mechanical properties and the area weight of PSU and PAN nanofibers were improved by mixing with PU and PVDF respectively.
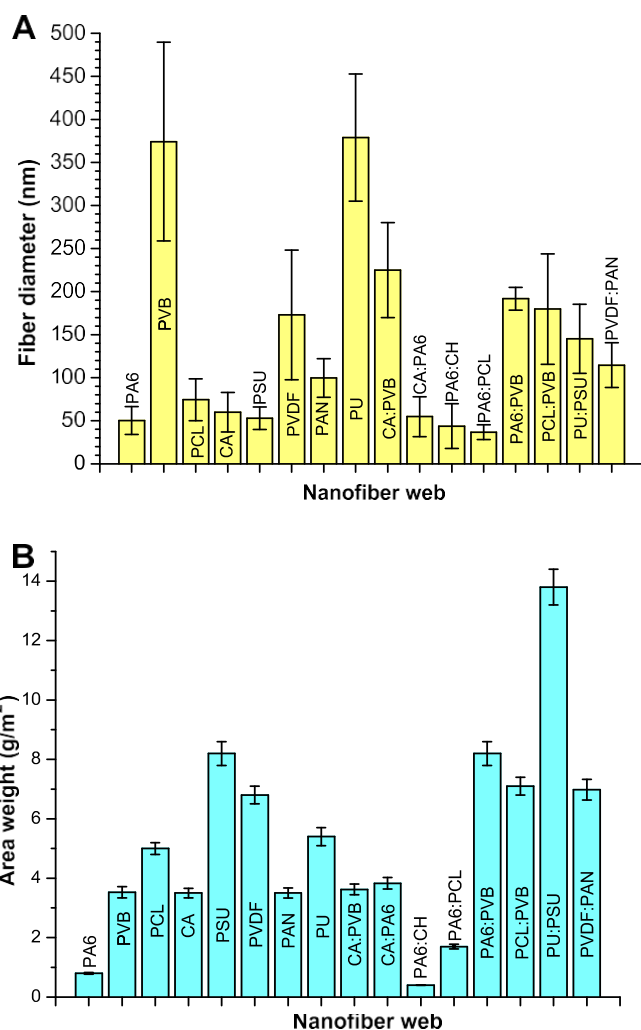

Figure 9 Comparison of various nanofiber webs according to their (A) fiber diameter and (B) area weight.

Hereby, Fig. 9 shows the area weight and the fiber diameter of all polymers and polymer mixtures. The idea of mixing polymers mainly showed advantages with respect to fiber diameter, diameter distribution and area weight.

1. Conclusion

The production of nanofibers using wire electrospinning has not been yet investigated in detail, although this technology has been utilized on an industrial scale. Wire electrospinning systems are superior to many production methods in the market due to their high productivity and ease of setting up and cleaning. Almost all polymers that form nanofibers in the needle electrospinning system can be electrospun using needle-free wire electrospinning at higher production efficiency rates.

It can be concluded that most common polymers in the market could be easily electrospun to produce nanofibers using the wire electrospinning system. The results of this work provide an insight into the industrial application of nanofibers. The optimization of nanofiber layers is time consuming and costly. The optimization process was almost completed by mixing of various spinnable polymers and the disadvantages and productivity of each nanofiber layer were improved by mixing of polymers.

References

Baker, S.R., Banerjee, S., Bonin, K., Guthold, M., 2016. Mater. Sci. Eng. C. 59, 203.

Bella, F., 2015. Electrochim. Acta 175, 151.

Bella, F., Sacco, A., Massaglia, G., Chiodoni, A., Pirri, C.F., Quaglio, M., 2015. Nanoscale 7 (28), 12010.

Carpenter, A.W., de Lannoy, C.F., Wiesner, M.R., 2015. Environ. Sci. Technol. 49, 5277.

Cengiz, F., Dao, T.A., Jirsak, O., 2010. Polym. Eng. Sci. 50, 936.

Fabbricante, A.S., Ward, G.F., Fabbricante, T.J., 2000. US Patents, 6114017.

Huang, T., Marshall, L.R., Armantrout, J.E., Yembrick, S., Dunn, H., Oconnor, J.M., Mueller, T., Avgousti, M., Wetzel, M.D., 2012. U. S. Patent, 8277271.

Huang, T., 2009. US Patents, 20090160099.

Iqbal, J., Wattoo, F.H., Wattoo, M.H.S., Malik, R., Tirmizi, S.A., Imran, M., Ghangro, A.B., 2011. Arab. J. Chem. 4 (4), 389.

Jirsak, O., Sanetrnik, F., Lukas, D., Kotek, V., Martinova, L., Chaloupek, J., 2004. US Patent, 7585437.

Jirsak, O., Sysel, P., Sanetrnik, F., Hruza, J., Chaloupek, J., 2010. J. Nanomater., 6 Article ID 842831

Kenawy, E.R.S., Azaam, M.M., Saad-Allah, K.M., 2015. Arab. J. Chem. 8 (3), 427.

LeCorre-Bordes, D., Tucker, N., Huber, T., Buunk, N., Staiger, M.P., 2016. J. Mater. Sci. 51 (14), 6686.

Li, C.J., Zhang, S.S., Wang, J.N., Liu, T.Y., 2014. Catal. Today 224, 94.

Liu, C., Li, X., Liu, T., Liu, Z., Li, N., Zhang, Y., Xiao, C., Feng, X., 2016. J. Membrane Sci. 512, 1.

Mahjour, S.B., Sefat, F., Polunin, Y., Wang, L., Wang, H., 2016. J. Biomed. Mater. Res. A. 104, 1479.

Maryskova, M., Ardao, I., Garcia-Gonzalez, C.A., Martinova, L., Rotkova, J., Sevcu, A., 2016. Enzyme Microb. Tech. 89, 31.

Matulevicius, J., Kliucininkas, L., Prasauskas, T., Buivydiene, D., Martuzevicius, D., 2016. J. Aerosol. Sci. 92, 27.

Nain, A.S., Wong, J.C., Amon, C., Sitti, M., 2006. Appl. Phys. Lett. 89 (18), 183105.

Nicosia, A., Keppler, T., Mü ller, F.A., Vazquez, B., Ravegnani, F., Monticelli, P., Belosi, F., 2016. Chem. Eng. Sci. 153, 284.

Nirmala, R., Navamathavan, R., Kang, H.S., El-Newehy, M.H., Kim, H.Y., 2011. Colloid. Surface. B 83, 173.

Pajoumshariati, S., Yavari, S.K., Shokrgozar, M.A., 2016. Ann. Biomed. Eng. 44, 1808.

Petras, D., Maly, M., Kovac, M., Stromsky, V., Pozner, J., Trdlicka, J., Mares, L., Cmelik, J., Jakubek, F., 2009. WO Patents, 2009010020.

Petras, D., Mares, L., Cmelik, J., Fiala, K., 2009. WO Patents, 2007137530.

Petras, D., Maly, M., Pozner, J., Trdlicka, J., Kovac, M., 2010. US Patents, 20100034914.

Sasithorn, N., Martinova, L., 2014. J. Nanomater., 9 Article ID 947315

Sobahi, T.R.A., Abdelaal, M.Y., Makki, M.S.I., 2014. Arab. J. Chem. 7 (5), 741.

Thorvaldsson, A., Stenhamre, H., Gatenholm, P., Walkenströ m, P., 2008. Biomacromolecules 9, 1044.

Torobin, L., Findlow, R.C., 2001. US Patents, 6183670.

Venugopal, J., Ma, L.L., Yong, T., Ramakrishna, S., 2005. Cell Biol. Int. 29, 861.

Wen, H.F., Yang, C., Yu, D.G., Li, X.Y., Zhang, D.F., 2016. Chem. Eng. J. 290, 263.

Yalcin Enis, I., Gok Sadikoglu, T., 2016. J. Ind. Text. http://dx.doi. org/10.1177/1528083716654470.

Yalcinkaya, B., Cengiz-Callioglu, F., Yener, F., 2014. Text. Res. J. 84 (16), 1720.

Yalcinkaya, F., Yalcinkaya, B., Jirsak, O., 2015. J. Nanomater., 12 Article ID 134251

Yalcinkaya, B., Yalcinkaya, F., Chaloupek, J., 2016a. Nanomaterials, 12 Article ID 2694373.

Yalcinkaya, F., Komarek, M., Lubasova, D., Sanetrnik, F., Maryska, J., 2016b. J. Nanomater., 7 Article ID 7565972

Yang, C., Yu, D.G., Pan, D., Liu, X.K., Wang, X., Bligh, S.W.A., Williams, G.R., 2016a. Acta Biomater. 35, 77.

Yang, T., Chen, Z., Zhang, H., Zhang, M., Wang, T., 2016b. Electrochim. Acta 217, 55.

Yener, F., Jirsak, O., 2012. J. Nanomater., 6 Article ID 839317

Yener, F., Yalcinkaya, B., Jirsak, O., 2013. J. Nanosci. Nanotechnol. 13, 4672.

Yu, D.G., Yang, C., Jin, M., Williams, G.R., Zou, H., Wang, X., Annie Bligh, S.W., 2016. Colloid. Surface. B 138, 110.

Zhou, Z., Lin, W., Wu, X.-F., 2016. Colloid. Surface. A 494, 21.

4.2. Mechanical Enhancement of Nanofiber Webs and Their Application in Wastewater Treatment

Nanofiber membranes have been tested in laboratories for so many years and showed great interest in water treatment. However, preparation in large-scale and commercialization still varies widely. Some of the products are already on the market (very limited amount), and some products are still on the way of commercialization that requires deep research before they can be considered for large-scale production due to some technical obstacles (such as compatibility with the existed membranes, operating cost, and potential environmental and health risks). To overcome these temporary technical obstacles, a concerted effort and collaboration are needed between universities, research institutions, government, industry, and stakeholders. As a result of efforts and collaborations, nanofiber membranes will provide consolidated solutions to water treatment.

In the following papers, we attempt to deal with the problem rigorously, starting by enhancement of mechanical properties of nanofiber membranes using lamination onto a support layer. Different adhesion method with different support has been selected to see their effect on overall membrane flux and selectivity. We investigated that the supporting layer, type of adhesion method, type of polymeric nanofiber, and density of the nanofiber layer have an impact on the water permeability and the rejection. The polymer type, supporting layer, and adhesion methods are the key parameters for the nanofiber membrane preparation. Based on the first reprint, the adhesive web lamination method was selected for membrane preparation. In the second and third paper, we tried to optimize the lamination conditions (such as heat, applied pressure, and time) for different polymeric nanofiber webs (PVDF and PAN), which are highly used in water treatment. Lamination effect on membrane characterization and membrane permeability has been introduced to literature. These two reprints (2 and 3) include a comprehensive study on lamination optimization and conditions for nanofibers membrane technology.

The contribution of the papers to the scientific community is based on the following results:

Determination of polymer type, adhesion method and support layer effects on the nanofiber membranes' water permeability and particle rejection. This is a major step for membrane preparation to select the right material and preparation method.

Investigate the lamination condition on the membrane performance and optimization of the lamination method. The lamination process is important to use nanofiber webs in membrane applications. For this reason, it is crucial to understand the lamination effects and optimization process.

Reprint:

1. Yalcinkaya F, Yalcinkaya B, Hruza J, Hrabak P. Effect of nanofibrous membrane structures on the treatment of wastewater microfiltration. Science of Advanced Materials. 2017 May 1;9(5):747-57.
2. Yalcinkaya F, Hruza J. Effect of laminating pressure on polymeric multilayer nanofibrous membranes for liquid filtration. Nanomaterials. 2018 May;8(5):272.
3. Roche R, Yalcinkaya F. Electrospun Polyacrylonitrile Nanofibrous Membranes for Point-of-Use Water and Air Cleaning. ChemistryOpen. 2019 Jan;8(1):97-103.

Effect of Nanofibrous Membrane Structures on the Treatment of Wastewater Microfiltration

Fatma Yalcinkaya*, Baturalp Yalcinkaya, Jakub Hruza, and Pavel Hrabak

Centre for Nanomaterials, Advanced Technologies and Innovation, Technical University of Liberec, Studentska 2, 46117, Liberec, Czech Republic

ABSTRACT

An experimental study for industrial wastewater was carried out using a cross-flow microfiltration unit. The effect of various nanofibrous membrane structures on the membrane permeability was investigated. Analysis of variations in nanofiber area weight, supporting material, the hydrophilicity of membranes, and the polymeric structure of the nanofiber layer revealed considerable effects on membrane permeability, the total amount of filtrated permeate and the total amount of carbon in the permeate solution. The removal of total organic carbon (TOC) was gradually decreased with the increasing area weight of the nanofiber layer. Low area weight nanofiber composite membranes were superior over high area weight ones, as a higher membrane permeability was maintained during the 15 hour test. The results indicate that the selection of the area weight of the nanofiber layers as well as the supporting layer are a key factor for increasing the flux and permeability.

KEYWORDS: Nanofibrous, Microfiltration, Wastewater, Nanofiber, Polyamide, Polyacrylonitrile.

1. INTRODUCTION

Wastewater reclamation is important for several industries, e.g., textile dyeing and finishing, pharmaceutical, marine and food.[1–8] New materials for wastewater filtration are constantly being designed due to the insufficient water resources and imbalance between water supply and consumption. The development of membrane technologies has recently reified applications in the treatment of wastewater. Membrane technologies may help to solve characteristic problems with traditional water treatment methods.

The importance of microfiltration (MF) technologies in the recycling of municipal or industrial wastewater using membrane processes is increasing.[9–12] MF is an effective process used to remove finely dispersed particles from waters. Reportedly, this technology is particularly effective in separating small particles of differing size and dissolved organic matter.

The polymeric nanofiber structures produced by the electrospinning method can help design improved types of microfiltration materials.[13–15] The use of nanofiber membranes for microfiltration is beneficial in particular as they demonstrate high permeability, enormous filtration efficiency due to highly porous structure, small pore size ($0 ∟ 10$ m). They also effectively separate impurities without adding reagents and have no by-products effected

by chemical reactions.[16–18] Membranes with a pore-size of $0 1∟0 5$ m or less almost completely filter not only bacteria but also viruses from water.[19–22]

Membrane fouling is the most serious problem affecting performance.[23–25] Characteristics, such as hydrophobicity, component materials, surface charge and roughness, operating conditions, pore sizes, the relationships between the size of solute and membrane pore size and the solute-membrane material affinity are the main reasons for membrane fouling.[26–29] It has been suggested that a membrane with a medium polysulfide pore should be used to obtain good membrane performance as well as to maintain the high rejection of colorant substances.[30] The nanofiber structure might be a solution to providing a high contact surface for the flocculant to interact with the particles and to be held inside the bioreactor by a membrane. Moreover, nanofibers may enhance the rigidity of the cake layer formed on the membrane surface by entangling with the bioflocs and make the cake layer less compressible under filtration pressure.

There are various types of membrane filtration units such as bundled hollow or parallel flat fiber units.[31] These units may be applied in wastewater treatment either in a submerged[32] or cross-flow mode.[33 34] In this work, a parallel flat cross-flow system was used, whereby water is circulated through the module using an external pump. A circulation pump can be used to achieve high cross-flow velocity. As a result, higher permeation flux can be obtained with a longer operation time. The advantage of using a cross-flow system is a reduction in the amount

of solid suspended particles on the membrane surface. Several studies have reported that cross-flow membrane microfiltration is an effective processes in wastewater reclamation.[35][36]

This paper presents the results of research investigations on the application of polymeric microfiltration membranes of various nanofibrous membrane structures for the removal of impurities from industrial wastewater using the cross-flow system. The filtration performance of various nanofibrous microfiltration membranes was compared according to their polymeric structure, area weight, hydrophilicity, and supporting layers. Microfiltration polymeric nanofibrous membranes were made from polyacrylonitrile (PAN) and polyamide 6 (PA6), whereas a lab-scale capillary MF module was built in our laboratory. PA6 was selected as the polymer due to the fact that the amide groups in PA6 provide high hydrogen bonding, which improves the thermal stability and mechanical strength. Polyacrylonitrile (PAN) has good characteristics including thermal stability (up to 130 C), tolerance to most solvents, and commercial availability. Both PA6 and PAN have superior fiber forming ability.

The greatest disadvantages of using nanofiber layer is its poor mechanical properties, which is a problem of application and long term usage. Nanofibrous membranes have not found any real applications due to the weakening high pressure commonly used in water treatment.[37] To address the weakening problem, the mechanical properties of nanofibrous material were improved using various types of lamination on various supporting layers. In this work, the effect of nanofiber area weight on the membrane permeability has been studied for the first time.

Another novelty of this paper is, that nanofiber layers were produced by using the Nanospider[38] industrial equipment, and that the layers strongly adhered on the supporting layer without any damage using various lamination technology to improve application in wastewater treatment. This study explored the feasibility of applying the nanofiber technology during industrial usage.

1. EXPERIMENTAL DETAILS

1.1. Materials

Polyacrylonitrile (PAN) with an average molecular weight (Mw) of 150 kDa was purchased from Dimachema Pigment Corporation; N N -dimethylformamide (DMF), 99.8% acetic acid (AA) and 98% formic acid (FA) were purchased from Penta s.r.o; polyamide 6 (PA6) was purchased from BASF-Ultramid B24 N 02. The supporting layers; 20 g/m^2 polyethylene terephthalate (PET) spun bond nonwoven and 45 g/m^2 PET woven webs were obtained from Hänsel and Co., GmbH (Germany) and the polyethylene/polypropylene (20/80) spun bond nonwoven bicomponents were obtained from Pegas Nonwovens.

The wastewater was obtained from an industrial company in the Czech Republic which produces pitch and tar oils.

1.2. Preparation of Nanofibrous Membranes for Microfiltration

The preparation procedures to fabricate nanofibrous membranes are as follows.

PAN solutions of 8 wt.% were prepared by dissolving polymer powder in DMF and stirring the solution at room temperature for 24 h until the solutions were homogeneous.

PA6 solutions of 12 wt.% were prepared by dissolving polymer pellet in an AA/FA (2/1) mixture and stirring the solution at 50 C for 24 h until the solutions were homogeneous.

The solutions were electrospun directly onto a silicon paper substrate using a NS 1S500U Nanospider unit. All of the process conditions were kept stable.

The electrospun nanofibers were laminated on
(a) 20 g/m^2 spunbond nonwoven polyethylene terephthalate (PET),
(b) 45 g/m^2 woven PET,
(c) 20 g/m^2 bicomponent spunbond (PE/PP).

A Meyer RPS-L Mini fusing machine was used to laminate the nanofibers with the supporting layers under heat (125 C) and pressure (15 N/cm) at a specific contact time (1.7 m/min).

One of the PA6 nanofiber layers (1.11 g/m^2) was immersed into surfactant water mixture (sodium stearate) for 2 minutes to improve hydrophilicity, then dried and laminated with woven web. The results showed that the nanofibrous membrane is totally hydrophilic with a contact angle of "0" which can be regarded as being "super hydrophilic."[39]

1.3. Other Analytical Methods and Equipment

The zero-shear viscosity of the polymer solutions was measured using a Fungilab Expert viscometer at 23 C.

The following parameters of the electrospun layer in the nanofibrous membranes, such as average fiber diameter and surface pore size, were analysed using a scanning electron microscope (SEM, Tescan Vega3 SB). All of the samples were coated for 60 s with a 7 nm layer of gold before SEM imaging to reduce the effect of charging. Image-J software was used to measure surface porosity and the average fiber diameter from more than 50 randomly selected fibers.

The contact angle was measured at different places of the samples at room temperature using a Kruss Drop Shape Analyzer DS4. A total of 2 l of distilled water was placed on the surface of a clean and dry membrane surface, and the average values were calculated.

Porosity, also known as packing density, defined the ratio of void volume to bulk volume.[13] The porosity of the

nanofibers was estimated using the following expression Eq. (1):

$$Porosity = \frac{1 - }{_0} \times 100 \qquad (1)$$

where is the density of the electrospun polymeric nanofiber and $_0$ is the density of bulk polymer.[14] The density of the electrospun layer was determined from the average of 5 samples.

An 1200-AEL capillary flow porometer (Porous Media Inc., Ithaca, NY) was used in this study to measure the pore size and distribution. The thickness of nanofibrous membrane layers was measured using a micrometer. Galden HT 230 with a defined surface tension of 19 dynes/cm was used as the wetting agent for mean pore size measurements.

The permeate flux (F) and the permeability (k) of the membrane were calculated by (Eq. (2) and (3)):

$$F = \frac{1}{A} \frac{dV}{dt} \ L/hm^2$$
$$k = \frac{F}{P} \ L/hm^2 bar \qquad (2)$$

where A is the effective membrane area (m^2), V is the total volume of permeate (F), P is trans membrane pressure (bar), and t is the filtration time (h).

The sum of organically bound carbon in the sludge was measured using the Total Organic Carbon (TOC) direct measurement method on an Analytik Jena Multi N/C 2100S (Germany) apparatus.

Tensile tests of the nanofibers and nanofibrous membranes were performed using a universal testing machine (Labor-Tech s.r.o., CR) with the extension rate of 10 mm/min at room temperature. The samples were 100 mm long, 25 mm wide, and the distance between the two clamps was 50 mm. Two directions were tested. The first was along the machine direction (MD), and the

other the cross direction (CD). The membranes were tested under wet conditions i.e., they were immersed in distilled water for 4 days before testing, and the nanofiber layers were measured under dry condition due to their low mechanical properties.

1.1. Microfiltration Set-Up
A custom-made cross-flow laboratory module equipped with air pressure control and a constant water flow velocity through the cell (70 L/min) was used to filtrate the wastewater using the nanofibrous membranes (the tested samples had a rectangle shape with a surface area of $1\ 95 \times 10^{-3}$ m^2) as shown in Figure 1. Bubble cleaning was applied to the surface during the experiment. Different membrane structures were placed both sides of the module. The membranes were tested for 15 hours and the flux was measured occasionally. All of the tests were performed at room temperature. Industrial sludge was used for the filtration test.

2. RESULTS AND DISCUSSION
The viscosity of the polymer solutions, as a function of the share rate, shows almost the same values for both of the polymers. The results are shown in Table I. Electrospun nanofiber layers were produced with various area weights and were laminated with various supporting layers as shown in Table II.

The same area weight (1.11 g/m^2) of the PA6 nanofiber layer was laminated on 3 different supporting materials. This was used to determine the effect of the supporting layer on the membrane permeability. Moreover, the effect of the permeability was determined using various levels of hydrophilicity, polymers, and area weights.

The thickness of the membrane has an important effect on the flux. The thickness of the nanofibrous membrane was measured and tabulated in Table III.
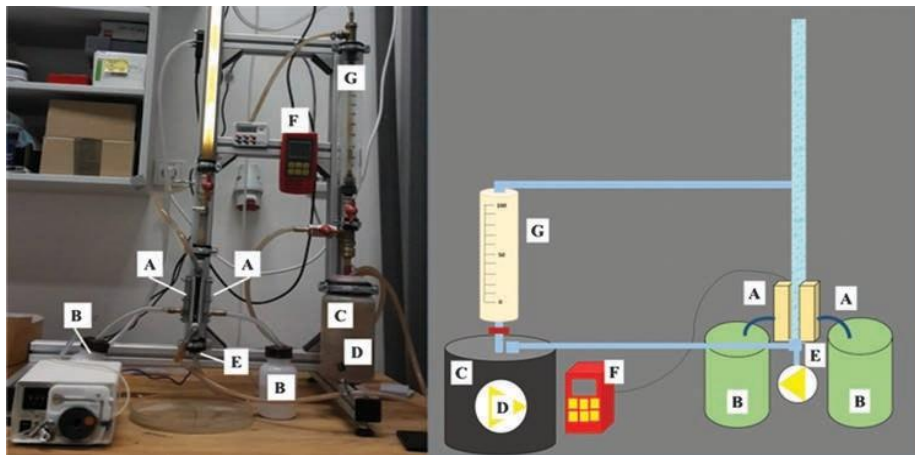

Fig. 1. The cross-flow unit: (A) membrane cells, (B) permeate, (C) feed, (D) pump, (E) surface bubble cleaning, (F) pressure controller, (G) feed
flow speed controller.

ARTICLE

Table I.	Viscosity of PAN and PA6 solutions.
Sample	Viscosity (Pa · s)
PAN	0 1909
PA6	0 1277

The results of Table III show that the difference in the thickness of the membrane increases slightly with the area weight of the nanofiber layer. All of the used supporting layers were thinner than 1 mm. The woven supporting layer has the greatest thickness of all the supporting layers. In general, it can be said that there is no considerable difference in the thickness and the values of the materials are very close to each other.

1.1. Tensile Strength

The mechanical properties of the nanofibrous membranes were strongly influenced by the mechanical properties of the supporting layers. The nanofiber layers were broken when the maximum tensile strength was applied to them. After lamination with strong supporting layers, the mechanical properties of the nanofibrous membranes were largely reinforced. Table IV shows the resulting tensile strength and elongation at the breaking point of the nanofiber layers and the nanofibrous membranes. The nanofiber layers showed much weaker mechanical properties compared with the nanofibrous membranes. The tensile strength of the nanofiber layers was increased from 3 to 24 times by the lamination of the supporting layers.

1.2. Membrane Characterization
1.2.1. Membrane Hydrophilicity

The contact angle is an important parameter in membrane sciences. Measurement of the contact angle (; [ ]) determines the hydrophilicity of the membrane. The contact angle values of the nanofibrous membranes are shown in Figure 2. It was found that the hydrophilicity of the membrane surface has an important influence on the membrane water flux and antifouling properties.[40][41] The lower the contact angle, the higher the membrane pure water

Table II. Prepared membranes and abbreviations.			
Nanofiber	Area weight (g/m^2)	Supporting layer	Abbreviation
PA6	1 11	–	PA6-1.11
		Bicomponent	PA6-1.11 bico
		PET nonwoven	PA6-1.11 aw
		PET woven	PA6-1.11 dot
	2 31	–	PA6-2.31
		Bicomponent	PA6-2.31 bico
PAN	3 21	–	PAN-3.21
		Bicomponent	PAN-3.21 bico
PA6-super hydrophilic	1 11	PET woven	PA6-1.11 SH dot

Table III.	Thickness of nanofibrous membranes.
Membran e	Thickness (mm)
PA6-SH d t	0 106
PA6-1.11 dot	0 118
PA6-1.11 aw	0 088
PA6-1.11 bico	0 068
PA6-2.31 bico	0 081
PAN-3.21 bico	0 086

flux. Nanoparticle-loaded hydrophilic polysulfone (PSf) increased the water flux by >600% in comparison to the plain PSf membrane, and also increased the oil rejection and antifouling against the formation of an oil layer on the surface of the membrane.[42] A cake model was studied to evaluate the drop in the PMMA membrane flux. The results showed that a higher hydrophilic character produces a lower rate of membrane fouling.[43]

Figure 2 indicates that two of the materials show a hydrophilic structure (contact angle < 90). Synthetic polymers with hydrophilic groups such as hydroxyl, carboxyl and carbonyl groups have either a strong or weak interaction with water. PA6 hydrophilic groups such as the hydroxyl group have a high affinity for moisture adsorption and are applied to the membrane technology, which increases the hydrophilicity of PA6 nanofibers.

PAN has a hydrophilic nature. PAN is a semi-crystalline polymer with high polarity. Its polar nitrile groups possess a high dipole moment around 3.9 D.[44] Polar compounds with a large dipole moment tend to be soluble in water, while those with a near zero dipole moment are called non–polar and tend to be insoluble in water. The high polarity of the PAN polymer increases the hydrophilicity of the nanofiber layer.

The dot-lamination of PA6 with the co-polyamide adhesive showed hydrophilic characteristics. It was found that hydrophilic membranes can be produced using co-polyamide polymers.[45] During the hot press in fusing equipment, the dot-shaped co-polyamide adhesives melted, passed through the pores of the nanofiber layer and covered the surface as shown in Figure 3. The co-polyamides
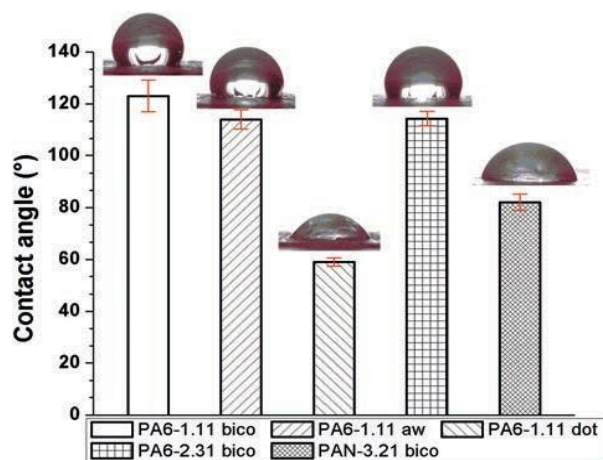
Fig. 2. Contact angle values of membranes.

Fig. 4. Fiber diameter of nanofiber layers before and after the lamination process.

on the surface increased the hydrophilicity of the membrane.

1.1.1. Membrane Surface Morphology Evaluation

Based on the SEM images, the membrane surface pore sizes, fiber diameter and distribution were analysed using Image J software. Image J porosity measurements are done in a 2D way (from SEM images) on the surface of membranes. To understand the effect of various polymeric nanofibers on the membrane morphological characteristics, the fiber diameter, fiber diameter distribution and surface porosity were determined as shown in Figures 4, 5 and Table IV. The porosity of the polymeric nanofiber layer was calculated using Eq. (1).

As shown in Figure 4 and 5 the fiber diameter of PA6 did not considerably change, whereas PAN increased after lamination. PAN nanofibers changed their round shape to a flattened shape after the heat and pressure of the lamination process, which may decrease the size of the pores.

Table V presents the results for the surface porosity, porosity and mean pore size of the nanofiber layers. The surface porosity indicated that the measurements were taken from the surface of the material.
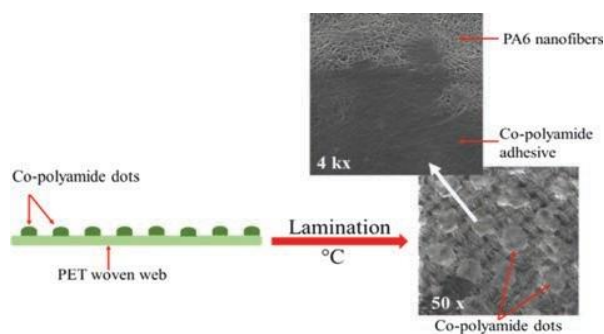

Fig. 3. Co-polyamide adhesive dots before and after the lamination process.
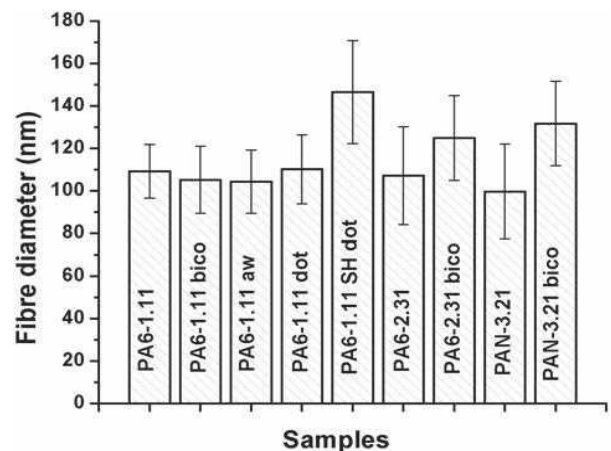
The nanofiber layers with lamination presented the lowest surface porosity and pore size, probably because of the hot press in the fusing equipment. It can be noted that the hot press lamination slightly affects both the fiber diameter, pore size, and the surface porosity. Moreover, immersing the PA6 nanofiber layer into a surfactant decreases the surface porosity of the membrane. There is no considerable difference in between pore size of the membranes.

This could be due to changes in the orientation and swelling of the fibers in the surfactant-water solution. It was not possible to measure the total membrane composite porosity due to the unknown density of the adhesives. Only the porosity of the nanofiber layers was measured. It can be concluded that the area weight plays an important role in the porosity of layers and slightly on mean pore size. A higher area weight yields a lower porous structure due to the compact packing density.

1.2. Microfiltration Process Results

1.2.1. Effect of Supporting Layer

Microfiltration experiments were carried out to study the permeability properties of the nanofibrous composite membranes. The flux and the permeability of permeate was calculated using Eqs. (2) and (3). The trans membrane pressure was almost the same for all the membranes whereas flux of permeate showed differences. Various supporting layers were used with their specific lamination technology. The supporting layers had almost the same thickness. The cross flow membrane filtration system was used during a 15-hour operating time as shown in Figure 1. Figure 6 shows the permeability of the membrane as a function of time for the various supporting layers.

The results showed that the supporting layer has an important role for the beginning of the process. Obviously, the permeability is initially high and falls off rapidly with filtration and permeability attenuation becomes more
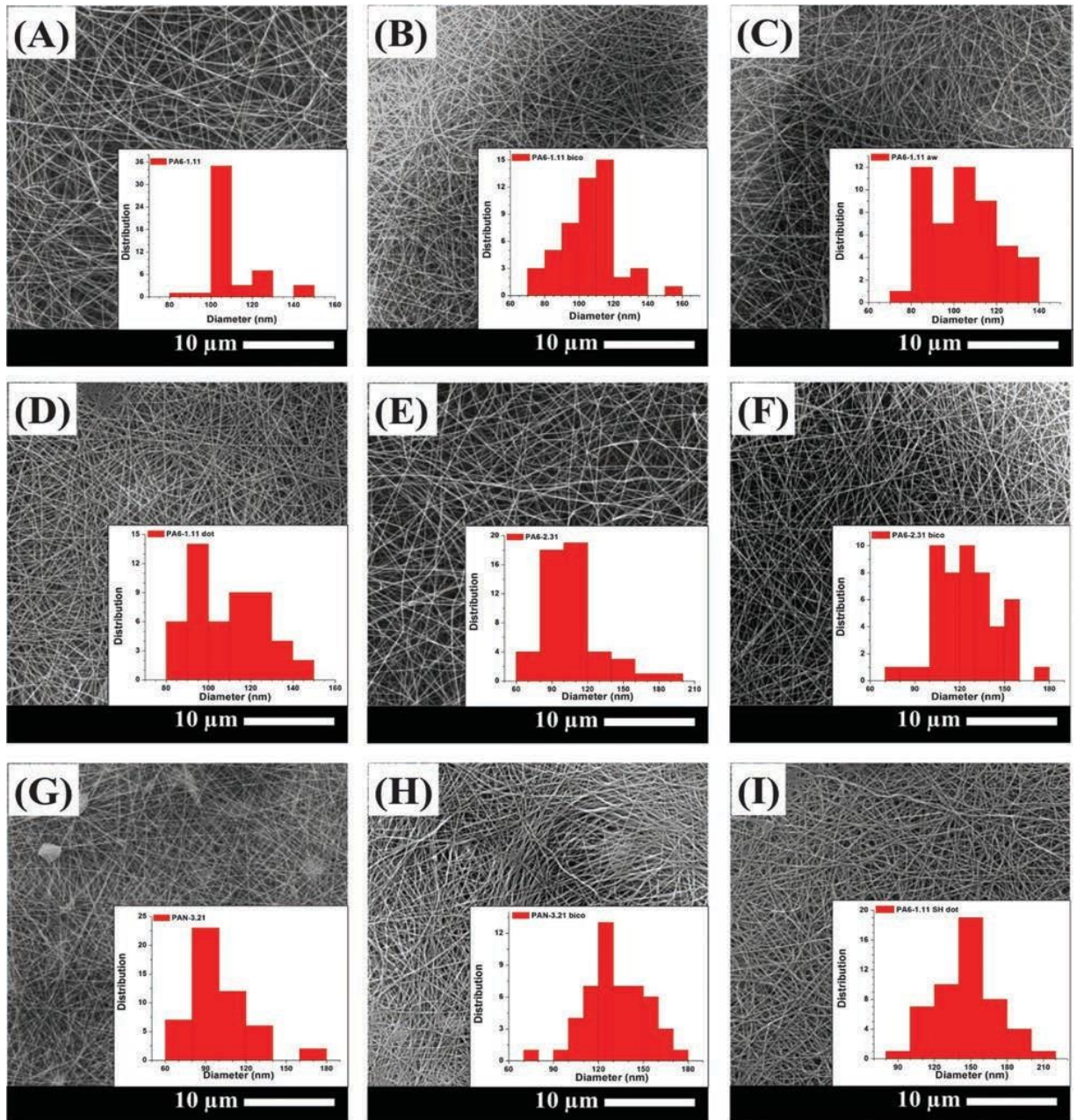
Fig. 5. SEM images and fiber diameter distribution of nanofiber layers before and after the lamination process, (A) PA6-1.11, (B) PA6-1.11 bico, (C) PA6-1.11 aw, (D) PA6-1.11 dot, (E) PA6-2.31, (F) PA6-2.31 bico, (G) PAN-3.21, (H) PAN-3.21 bico, (I) PA6-1.11 SH dot.

and more rapid over time. Many studies have shown that the flux decreases with operating time and reaches stable flux attenuation.[29 46–48] A similar permeability decline was observed for all of the membranes. The main reason is membrane fouling. Membrane fouling increases resistance to the flow of the continuous phase through the membrane due to blocking of the pores and deposition of a cake layer on the surface. Moreover, solid particle deposition within

the membrane pores can affect membrane fouling. The flux is affected by the formed cake layer that changes the pore size distribution and resistance to the permeate flow until it attains a steady state as the cake layer reaches the equilibrium thickness.

It can be seen from Figure 6 that the permeability of the membranes is almost steady after 11 hours of filtration. The PA6-1.11 bico and PA6-1.11 dot membranes reach

Table V. Porosity, surface porosity and pore size of nanofiber layers.

Membrane	Surface porosity (%)	Porosity of nanofiber (%)	Mean pore size (nm)
PA6-1.11	30 76	88 86	755 01 ± 350 60
PA6-1.11 bico	20 01	88 86	753 01 ± 350 32
PA6-1.11 aw	29 76	88 86	808 80 ± 348 10
PA6-1.11 dot	28 08	88 86	775 12 ± 351 05
PA6-1.11 SH dot	17 7	88 86	786 36 ± 349 75
PA6-2.31	29 97	87 02	762 35 ± 351 60
PA6-2.31 bico	25 61	87 02	727 01 ± 352 30
PAN-3.21	20 83	85 15	758 45 ± 345 80
PAN-3.21 bico	19 93	85 15	710 60 ± 343 70

Fig. 7. Supporting layers and surface porosity in %; (A) PET spunbond nonwoven, (B) bicomponent spunbond nonwoven, (C) PET woven web.

almost the same permeability value after 13 hours filtration whereas PA6-1.11 aw has higher than others.

The packing density of the material is very important for the permeate flux and the membrane permeability. The results showed that not only the nanofiber layer on the surface but also supporting layer plays a big role for flux efficiency.

Figure 7 shows the supporting layers and their surface porosity calculated by image J program. The PET spunbond has a very open structure, which helps to increase the permeate flux and permeability compared to the other supporting layers. It is evident that the supporting layer under the nanofiber layer is an important parameter for the membrane filtration process.

1.1.1. Effect of Nanofiber Area Weight

The effect of the nanofiber area weight on the permeate flux and the membrane permeability has not been studied
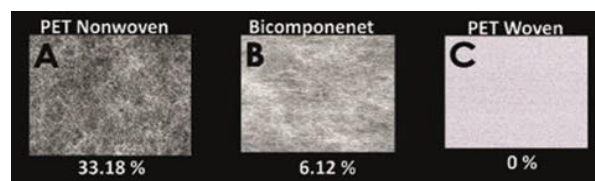
properly yet. Packing density, basis weight (area weight), fiber diameter and thickness of the nanofiber layer all effect permeate flux efficiency. It is well known that packing density plays an important role on the porosity and the bubble point of the nanofiber layer.[49–51] Packing is directly related to the area weight of the nanofibrous material. Figures 4 and 5 show that the diameters of the nanofiber layers are close to each other. Permeability was compared according to various area weights of the nanofibers as shown in Figure 8.

PA6-1.11 and PA6-2.31 are the same material. The area weight of the layers was arranged by changing the speed of the backing paper on the Nanospider equipment. A slower speed of the backing paper leads to more fibers being collected on the surface of the paper. Figure 8 shows that the area weight of the nanofibers is an important parameter for wastewater treatment. The permeability of PA6-1.11 bico was almost four times higher than PA6-2.31 at the end of the 15-hour operation time. The results show that low area weights of the nanofiber layers tend to have higher permeability, but the retention efficiency of the solid particles can be compromised.
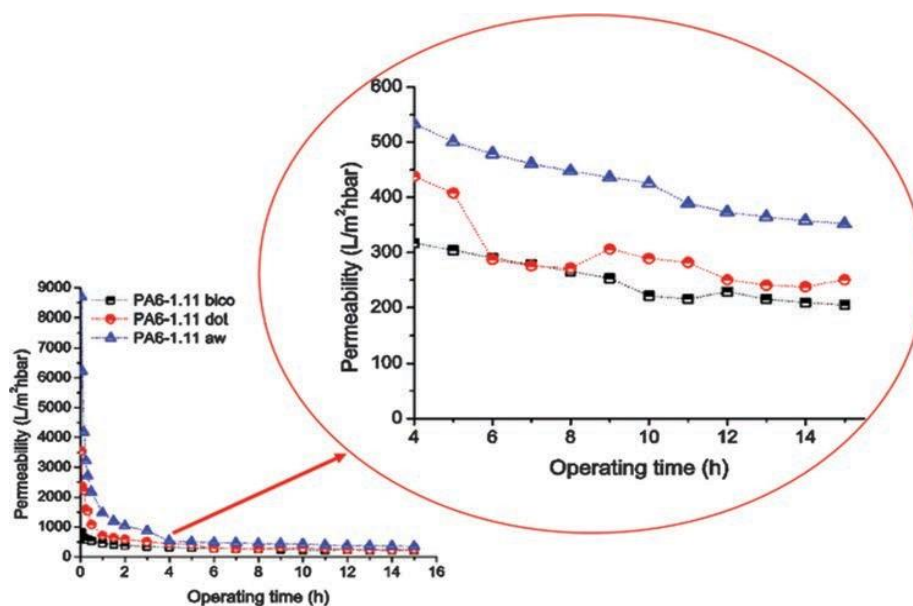
Fig. 6. Membrane permeability as a function of time for the various supporting layers.
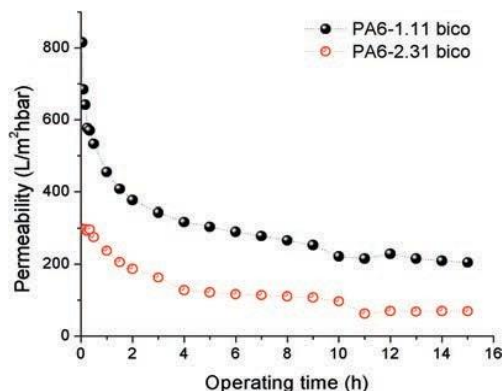
Fig. 8. Membrane permeability as a function of the time of the various area weight of nanofiber layers.

1.1.1. Effect of Polymer Type

Pore blockage, rejection of solid compounds and the permeate flux characteristics of the membrane strongly depend on the chemical structure of the active layer and the features of the surface where the primary separation of solutes occurs. Different membrane types can show different levels of permeability.[52][53] Lehman et al. showed that the use of a ceramic membrane can lead to a high flux due to less membrane fouling.[54] A comparison of the different polymers is shown in Figure 9.

PA6-2.31 bico and PAN-3.21 bico nanofiber layers had very similar profiles throughout the period of filtration. Figure 9 shows that the permeability of high area weight PA6-2.31 bico and PAN-3.21 bico membranes are almost the same after 4 hours of filtration. The low area weight PA6-1.11 bico membrane had a 4-times higher permeability than high area weight PA6-2.31 bico and PAN-3.21 bico membranes even after 14 hours of filtration. The result shows that area weight is much more important for permeability than the type of polymer.
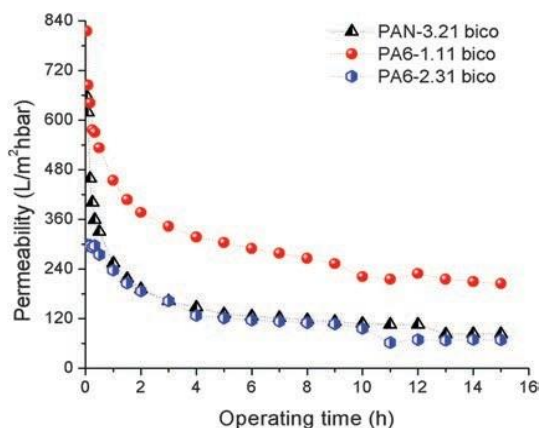
1.1.2. Effect of Hydrophilicity

In water treatment, hydrophilic membranes show resistance to fouling because of their affinity for water.[55][56] Figure 10, shows the permeability of the same material with different contact angles. PA6-1.11 SH dot is super hydrophilic, and PA6-11 dot is hydrophilic. The results of the test showed that super hydrophilic material has a slightly less permeability than hydrophilic material. Unlike the literature, increasing the hydrophilicity of the same membrane did not increase flux. It is evident that super hydrophilic membranes increase fouling due to blocking of the pores with solid compounds. Water is strongly bound to a highly hydrophilic membrane surface, and foulants penetrate through the pores.

To compare the permeability, PA6 (1.11 g/m^2) nanofiber composite membranes with various contact angles were studied as shown in Figure 11. The results show that hydrophilic membranes PA6-1.11 SH dot and PA6-1.11 dot have a lower permeability than hydrophobic PA6-1.11 aw (CA $\approx 110^0$). Increasing the hydrophilicity of same nanofiber layer with the same area weight did not increase the permeability of the membrane. The supporting layer has a greater influence on the membrane permeate flux and permeability than the hydrophilicity of the membrane under the same operating conditions.

The amounts of total filtrated permeate during a constant time according to membrane structure are given in Figure 12.

The results show that the supporting layer and a low area weight have an important impact on total separation in wastewater, which has a direct effect on the cost of operation.

1.2. TOC Test Results

The separation of wastewater can be easily observed. The difference between feed and permeate water is illustrated in Figure 13(A). The membrane before and after filtration is shown in Figure 13(B). Figure 13 shows that black

Fig. 9. Membrane permeability as a function of the time of the various polymeric nanofiber layers.
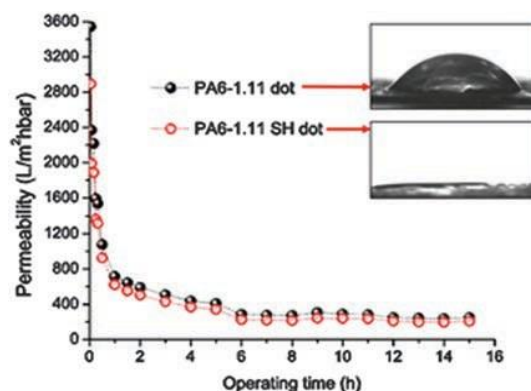

Fig. 10. Membrane permeability as a function of time (hydrophilic and super hydrophilic membrane).
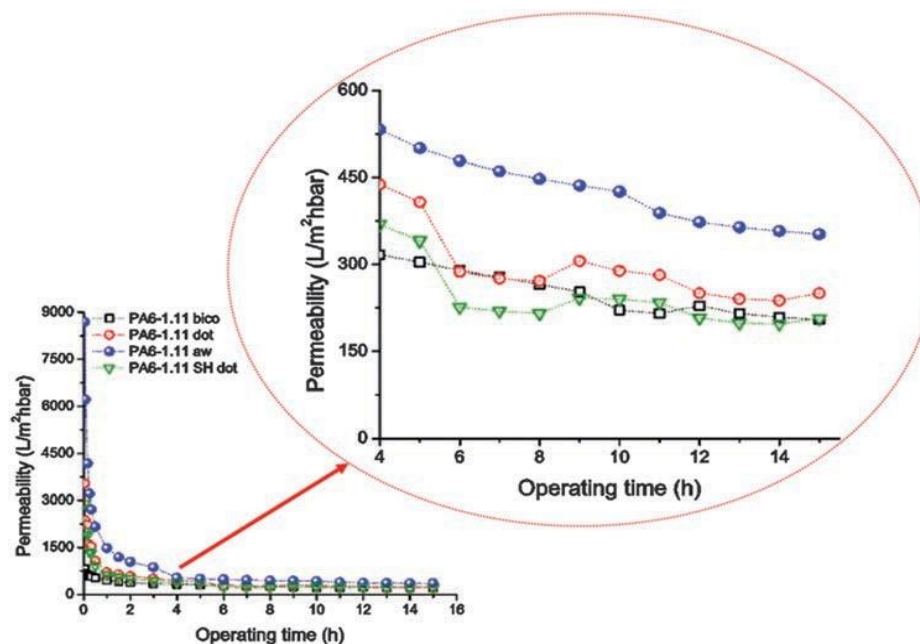
Fig. 11. Membrane permeability as a function of time (membranes with various contact angles (CA)).

solid compounds were caught by the nanofiber composite membrane and the sludge separated.

Qualitative measurement is not sufficient to determine the efficiency of separation. TOC tests were run for quantitative measurement (Fig. 14). The TOC was used to measure the sum of all organic carbons within the feed and permeate water, representing the concentration of mg/L. TOC analysis is a quick and reliable method for the measurement of dissolved organic pollution of industrial wastewater. Before measuring the TOC of wastewater (feed solution), a rough filtration (pore size of the filter is 0 45 m) was performed to eliminate any large particles. Figure 14 shows the TOC rejection of the membranes. The high area weight nanofibrous membranes had very

good TOC retention of more than 70%. However, the lowest area weight nanofiber membranes (PA6-1.11 dot and PA6-1.11 aw) had a lower retention of approximately 40%. When the TOC results are compared with the results of the total amount of filtrated permeate and surface porosity and the mean pore size, the relation is visible. The nanofibrous membranes with a more open and porous structure not only increase the amount of filtrated permeate and flux but also increase the amount of solid particles passing through the membrane. It should be taken into consideration that the feed solution was filtrated before TOC measurement due to the high amount of organic compounds.

It was found that the use of a nanofiber membrane decreases the TOC value from 5057 mg/L to 14.8 mg/L.[57] In another work using a ceramic membrane microfilter, a retention in TOC of 64% was achieved.[58] Surely, the TOC retention of all the samples higher than 40% which is compatible with literature.[57 58] Surprisingly, a comparison of the results of PA6-11 dot and PA6-1.11 SH dot showed that the hydrophilicity of the membranes increases the retention of total organic carbon from the feed solution.
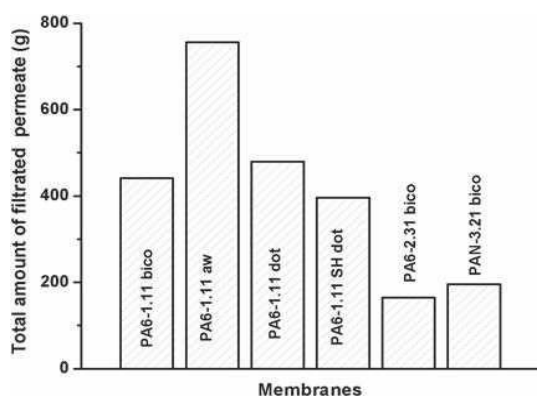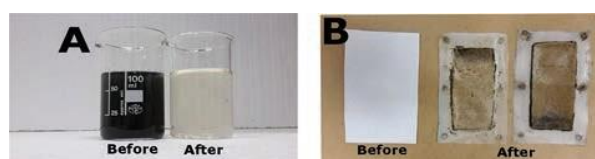

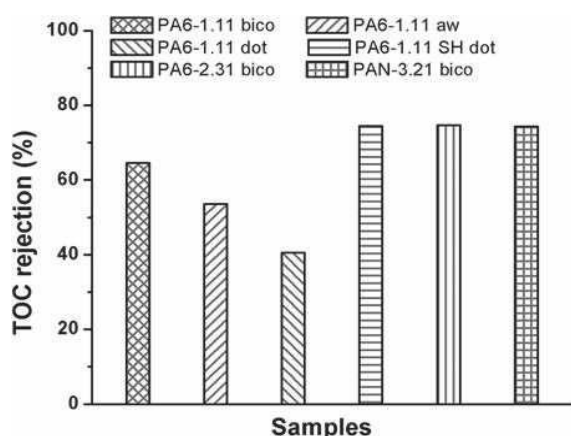Fig. 12. Amount of permeate after 15 hours of operating time.

Fig. 14. The TOC retention by membranes.

There can be two explanations; firstly, the highly absorbent PA6-1.11 SH dot membrane allows the feed solution to pass through the membrane very quickly and solid particles in the feed solution stick to the membrane surface and block the pores. Secondly, due to swelling of the PA6-1.11 SH dot nanofiber layer in chemical treatment, the diameter of the pores is reduced after lamination.

1. CONCLUSION

In this study, the influence of the structure of nanofibrous membranes on microfiltration was studied. The fiber diameter of membranes was changed to between 90–150 nm without altering the porosity. The operating conditions were kept stable during the process. Based on the results of the evaluation tests we can state that:

— The same nanofiber layer on various supporting layers was laminated, and the membrane permeability was measured. It was observed that an open structure supporting layer slightly increases the membrane permeability while the total amount of filtrated permeate increases dramatically.

— Nanofiber layers with various area weights reflected the fact that it is very important to arrange the area weight of the nanofiber layer. A more compact nanofiber composite membrane means low flux of permeate. The results indicate that the area weight of the nanofiber layer has the most important effect on the permeate flux performance and membrane permeability.

— Both PA6 and PAN nanofiber layers have almost the same permeability when the area weight is above 2 g/m^2. It was found that area weight has a bigger impact on membrane permeability.

— Unlike the literature, it was found that increasing hydrophilicity of the same type of membrane did not increase the flux. Furthermore, permeate flux and permeability decrease slightly due to blocking the pores from the beginning of the filtration process. Hydrophilicity is not responsible for improvements in performance.

— For all the membrane types, the permeability decreased sharply at the start, presumably due to pore blockage by a cake layer on the surface. Nevertheless, the permeability reached a steady state after a while, indicating that a stable dynamic layer was formed.

— TOC results showed that the nanofibrous membranes are able to retain organic compounds well. It was found that not only the higher area weight nanofiber layer but also the hydrophilicity of the membrane increases the retention of organic compounds.

Solid particles of a small size easily penetrated the pores of the nanofibrous membrane and then block them by adsorption on the membrane surface. Because of fouling, the flux of the membranes declines and reaches stable flux attenuation after a while, which results in increases in the cost of the operation of the membrane. The best results were obtained for a PA6-1.11 g/m^2 laminated with PET non-woven membrane (PA6-1.11 aw). By changing the operational conditions and using additives, the fouling effect can be minimized. A PA6 nanofiber composite membrane with low area weight shows good potential for microfiltration processes in industrial application.

References and Notes

1. V. Jegatheesan, B. K. Pramanik, J. Chen, D. Navaratna, C. Y. Chang, and L. Shu, *Bioresour. Technol.* 204, 202 (2016).
2. D. S. Patil, S. M. Chavan, and J. U. K. Oubagaranadin, *Journal of Environmental Chemical Engineering* 4, 468 (2016).
3. A. Majouli, S. Tahiri, S. Alami Younssi, H. Loukili, and A. Albizane, *Ceram. Int.* 38, 4295 (2012).
4. N. Tahri, G. Masmoudi, E. Ellouze, A. Jrad, P. Drogui, and R. Ben Amar, *Journal of Cleaner Production* 33, 226 (2012).
5. N. A. Weerasekara, K.-H. Choo, and S.-J. Choi, *J. Membrane Sci.* 447, 87 (2013).
6. V. V. Ranade and V. M. Bhandari, Chapter 1-Industrial wastewater treatment, Recycling, and Reuse: An Overview: Industrial Wastewater Treatment, Recycling and Reuse, Butterworth-Heinemann, Oxford (2014), pp. 1–80.
7. S. O. Ganiyu, E. D. van Hullebusch, M. Cretin, G. Esposito, and M. A. Oturan, *Sep. Purif. Technol.* 156, 891 (2015).
8. S. Chen, J. Yu, H. Wang, H. Yu, and X. Quan, *Desalination* 363, 37 (2015).
9. A. Gallego-Molina, J. A. Mendoza-Roca, D. Aguado, and M. V. Galiana-Aleixandre, *Chem. Eng. Res. Des.* 91, 369 (2013).
10. A. G. Fane, C. Y. Tang, and R. Wang, 4.11—Membrane technology for water: Microfiltration, Ultrafiltration, Nanofiltration, and Reverse Osmosis A2, Treatise on Water Science, edited by Wilderer, Peter, Elsevier, Oxford (2011), pp. 301–335.
11. X. Shang, H. C. Kim, J. H. Huang, and B. A. Dempsey, *Sep. Purif. Technol.* 147, 44 (2015).
12. B. K. Pramanik, F. A. Roddick, and L. Fan, *J. Membrane Sci.* 475, 147 (2015).

1. R. S. Barhate, C. K. Loong, and S. Ramakrishna, *J. Membrane Sci.* 283, 209 (2006).
2. R. Wang, Y. Liu, B. Li, B. S. Hsiao, and B. Chu, *J. Membrane Sci.* 392–393, 167 (2012).
3. P. Gibson, H. Schreuder-Gibson, and D. Rivin, *Colloids and Surfaces A: Physicochemical and Engineering Aspects* 187–188, 469 (2001).
4. H. Ma, B. Chu, and B. S. Hsiao, 15-Functional nanofibers for water purification A2-Wei, Qufu, Functional Nanofibers and their Applications, Woodhead Publishing (2012), pp. 331–370.
5. A. Dasari, J. Quirós, B. Herrero, K. Boltes, E. García-Calvo, and R. Rosal, *J. Membrane Sci.* 405–406, 134 (2012).
6. H. M. Li, Q. G. Zhang, N. N. Guo, A. M. Zhu, and Q. L. Liu, *Chem. Eng. J.* 264, 329 (2015).
7. S. M. Lemma, A. Esposito, M. Mason, L. Brusetti, S. Cesco, and M. Scampicchio, *J. Food Eng.* 157, 1 (2015).
8. D. Bjorge, N. Daels, S. De Vrieze, P. Dejans, T. Van Camp, W. Audenaert, J. Hogie, P. Westbroek, K. De Clerck, and S. W. H. Van Hulle, *Desalination* 249, 942 (2009) .
9. X. Mi, K. S. Vijayaragavan, and C. L. Heldt, *Carbohyd. Res.* 387, 24 (2014).
10. W. Huang, Y. Wang, C. Chen, J. L. M. Law, M. Houghton, and L. Chen, *Carbohyd. Polym.* 143, 9 (2016).
11. K. J. Howe and M. M. Clark, *Environ. Sci. Technol.* 36, 3571 (2002).
12. A. W. Zularisam, A. F. Ismail, and R. Salim, *Desalination* 194, 211 (2006).
13. I. Rosas, S. Collado, A. Gutiérrez, and M. Díaz, *J. Membrane Sci.* 465, 27 (2014).
14. I. S. Chang, P. Le Clech, B. Jefferson, and S. Judd, *J. Environ. Eng-Asce* 128, 1018 (2002).
15. B. Lesjean, S. Rosenberger, C. Laabs, M. Jekel, R. Gnirss, and G. Amy, *Water Sci. Technol.* 51, 1 (2005).
16. V. M. Monsalvo, J. Lopez, M. M. Somer, A. F. Mohedano, and J. J. Rodriguez, *Desalin. Water Treat* 56, 3599 (2015).
17. R. W. Field, D. Wu, J. A. Howell, and B. B. Gupta, *J. Membrane Sci.* 100, 259 (1995).
18. M. R. Bilad, P. Declerck, A. Piasecka, L. Vanysacker, X. Yan, and I. F. J. Vankelecom, *Sep. Purif. Technol.* 78, 105 (2011).
19. S. Judd, *Trends Biotechnol.* 26, 109 (2008).
20. W. Lee, S. Kang, and H. Shin, *J. Membrane Sci.* 216, 217 (2003).
21. S. Guo, H. Kiefer, D. Zhou, Y. H. Guan, S. Wang, H. Wang, Y. Lu, and Y. Zhuang, *J. Biotechnol.* 221, 25 (2016).
22. K. J. Hwang and P. Y. Sz, *J. Membrane Sci.* 347, 75 (2010).
23. R. L. Goldsmith, Cross-flow filtration device with filtrate flow conduits and method of forming same, in, Google Patents (1988).
24. N. Rossignol, L. Vandanjon, P. Jaouen, and F. Quéméneur, *Aquacultural Engineering* 20, 191 (1999).
25. S. Homaeigohar and M. Elbahri, *Nanocomposite Electrospun Nanofiber Membranes for Environmental Remediation, Materials* 7, 1017 (2014).
26. O. Jirsak, F. Sanetrnik, D. Lukas, V. Kotek, L. Martinova, and J. Chaloupek, A Method of Nanofibres Production From a Polymer Solution Using Electrostatic Spinning and a Device for Carrying Out the Method, in, US Patent 20060290031 (2005).
27. J. Drelich and E. Chibowski, *Langmuir* 26, 18621 (2010).
28. L. Na, L. Zhongzhou, and X. Shuguang, *J. Membrane Sci.* 169, 17 (2000).
29. M. Ulbricht, H. Matuschewski, A. Oechel, and H. G. Hicke, *J. Membrane Sci.* 115, 31 (1996).
30. R. Jamshidi Gohari, F. Korminouri, W. J. Lau, A. F. Ismail, T. Matsuura, M. N. K. Chowdhury, E. Halakoo, and M. S. Jamshidi Gohari, *Sep. Purif. Technol.* 150, 13 (2015).
31. N. A. Ochoa, M. Masuelli, and J. Marchese, *J. Membrane Sci.* 226, 203 (2003).
32. Q. Y. Wu, X. N. Chen, L. S. Wan, and Z. K. Xu, *The Journal of Physical Chemistry B* 116, 8321 (2012).
33. R. Wagener, J. Schneider, U. Delius, F. Herold, G. E. Miess, and U. Meyer-Blumenroth, Hydrophilic, asymmetric, chemically-resistant polyaramide membrane, in, US Patent 5536408 A (1996).
34. K. Scott, R. J. Jachuck, and D. Hall, *Sep. Purif. Technol.* 22–23, 431 (2001).
47. L. Song, *J. Membrane Sci.* 139, 183 (1998).
48. M. Zhang and L. Song, *Environ. Sci. Technol.* 34, 3767 (2000).
49. S. Soliman, S. Sant, J. W. Nichol, M. Khabiry, E. Traversa, and A. Khademhosseini, *J. Biomed. Mater Res. A* 96, 566 (2011).
50. J. Matulevicius, L. Kliucininkas, D. Martuzevicius, E. Krugly, M. Tichonovas, and J. Baltrusaitis, *J. Nanomater.* 2014, 13 (2014).
51. J. Sirc, R. Hobzova, N. Kostina, M. Munzarova, M. Juklickova, M. Lhotka, S. Kubinova, A. Zajicova, and J. Michalek, *J. Nanomater.* 2012, 14 (2012).
52. A. Świerczynska and J. Bohedziewicz, *Membranes and Membrane Processes in Environmental Protection* 119, 209 (2014).
53. M. Bodzek and K. Konieczny, *Sep. Purif. Technol.* 14, 69 (1998).
54. S. G. Lehman, S. Adham, and L. Liu, *J. Environ. Eng. Manage.* 18, 257 (2008).
55. J. S. Louie, I. Pinnau, I. Ciobanu, K. P. Ishida, A. Ng, and M. Reinhard, *J. Membrane Sci.* 280, 762 (2006).
56. A. L. Ahmad, B. S. Ooi, A. W. Mohammad, and J. P. Choudhury, *Desalination* 168, 215 (2004).
57. B. Chen, X. Xiong, Z. Yao, N. Yin, Z.-X. Low, and Z. Zhong, *Desalination* 355, 147 (2015).
58. A. Bottino, G. Capannelli, A. Del Borghi, M. Colombino, and O. Conio, *Desalination* 141, 75 (2001).

Effect of Laminating Pressure on Polymeric Multilayer Nanofibrous Membranes for Liquid Filtration

Fatma Yalcinkaya [1,2],* and **Jakub Hruza [1,2]**

[1] Department of Nanotechnology and Informatics, Institute of Nanomaterials, Advanced Technologies and Innovation, Technical University of Liberec, Studentska 1402/2, 46117 Liberec, Czech Republic; jakub.hruza@tul.cz

[2] Institute for New Technologies and Applied Informatics, Faculty of Mechatronics, Studentska 1402/2, 46117 Liberec, Czech Republic

* Correspondence: yenertex@hotmail.com; Tel.: +420-485-353-389

Abstract: In the new century, electrospun nanofibrous webs are widely employed in various applications due to their specific surface area and porous structure with narrow pore size. The mechanical properties have a major influence on the applications of nanofiber webs. Lamination technology is an important method for improving the mechanical strength of nanofiber webs. In this study, the influence of laminating pressure on the properties of polyacrylonitrile (PAN) and polyvinylidene fluoride (PVDF) nanofibers/laminate was investigated. Heat-press lamination was carried out at three different pressures, and the surface morphologies of the multilayer nanofibrous membranes were observed under an optical microscope. In addition, air permeability, water filtration, and contact angle experiments were performed to examine the effect of laminating pressure on the breathability, water permeability and surface wettability of multilayer nanofibrous membranes. A bursting strength test was developed and applied to measure the maximum bursting pressure of the nanofibers from the laminated surface. A water filtration test was performed using a cross-flow unit. Based on the results of the tests, the optimum laminating pressure was determined for both PAN and PVDF multilayer nanofibrous membranes to prepare suitable microfilters for liquid filtration.

Keywords: nanofiber; lamination; water filtration

1. Introduction

Electrospun polymeric nanofiber web has gained increasing importance in the production of engineered surfaces with sub-micron to nano-scale fibers. The widely employed areas of electrospun nanofibers are tissue engineering [1,2], wound healing [3], drug delivery systems [4], composites [5], solar cells [6], protective clothing [7], lithium-ion batteries [8,9], sensors [10–12], gas sensors and separators [13,14], and air and water filtration [15–19], owing to their high surface-area-to-volume ratio, highly porous structure and extremely narrow pore size. The main factor influencing the application of nanofibers is their mechanical properties. An electrospun nanofiber has very poor mechanical strength due to low contact and adhesion between the fibers.

Several methods have been developed to provide suitable mechanical strength to electrospun nanofibers. One of the most common methods is to blend several polymers, the advantage of which is that it is easy and low-cost. However, it is necessary to use polymers which can dissolve in the same solvent system, of which there are only a few [20,21]. In another method, lamination was achieved using an epoxy composite. In this method, an electrospun layer was laid on the

epoxy/curing agent in a mold and then the curing process was performed for a period of 16 h [22]. Nanofiber reinforced nanomaterials such as carbon nanotubes and graphene represent another route for improving the mechanical strength of nanofibers. However, this method is costly and in some cases has a low efficiency [23,24]. Charles et al. [25] used a dip coating method to improve the mechanical strength of nanofibers. They described the mechanical properties of a composite system comprising hydroxyapatite (HA)-coated poly (L-lactic acid) (PLLA) fibers in a poly (ε-caprolactone) (PCL) matrix. A biomimetic method was used to coat the fibers with HA, and a dip-coating procedure served for the application of PCL to the coated fibers. The composite was formed into a bar using compression molding at low temperatures. The disadvantage of this method is that it is a time- and chemical-consuming procedure. Xu et al. [26] developed a self-reinforcing method to enhance the strength of polycarbonate (PC) membranes. In this method, the PC nanofibers were immersed into a solvent (30%) and non-solvent (70%) mixture, which resulted in enhancement in the strength (128%) owing to the fusion of junction points. The entire porous structure on the PC nanofibers was destroyed, which greatly impaired the application of the membranes. The thermal lamination method is one of the most reliable, repeatable, time-saving, environmentally friendly and cost-effective methods used to adhere two surfaces. In this method, an adhesive polymer or web is usually applied between two surfaces. Using heat and pressure, the surfaces adhere to each other. There is a large amount of research related to improving the strength of nanofibers; however, the number of reports is still limited compared to those dealing with lamination technology. Jiricek [27,28] and Yalcinkaya et al. [29,30] used a bi-component polyethylene (PE)/polypropylene (PP) spunbond as a supporting layer for nanofiber layers. A fusing machine was used for the lamination process. A nanofiber layer was adhered on the outer surface of the bi-component due to the low melting point of PE. The resultant multilayer nanofibrous membranes were used for micro and nanofilters. The supporting material and the density of the nanofibers have an influence on the water and air permeability of the multilayer materials. Yoon et al. [7] laminated nanofibers with various densities of polyurethane (PUR) fiber onto different textile surfaces using an adhesive web. The results showed that the various multilayer nanofibrous membrane structure designs had a considerable influence on the degrees of breathability and waterproofness of the textile surfaces. In our previous work [31], it was observed that both the supporting material and the density of the nanofiber web have an influence on the water permeability of the multilayer nanofibrous membranes. The lower area weight with open structure supporting materials has higher water flux and permeability. Kanafchian et al. [32] used a heat-press technique to laminate the polyacrylonitrile (PAN) nanofiber on a polypropylene spunbond at various laminating temperatures. It was observed that, when the applied temperature is lower than the melting point of polypropylene spunbond, the nanofiber web remains unchanged. Moreover, the increase in temperature increased the adhesion between nanofiber while decreasing the air permeability.

Although the system and parameters of the electrospinning process have been well analyzed, there is still a lack of information about a proper lamination technique for nanofiber webs. So far, mainly the effect of temperature on the lamination of electrospun nanofiber webs has been investigated using heat-press methods [32–34]. Yao et al. [33] studied the effect of the heat-press temperature, pressure, and duration on the morphological and mechanical characteristics of an electrospun membrane for membrane distillation. The results showed that the temperature and duration of the heat-press play more important roles than the pressure in the heat-press treatment. However, the pressure varied between 0.7 and 9.8 kPa at 150 °C during a 2-h period, which is time- and energy-consuming and therefore a more comprehensive parametric study is required. The aim of this study is to consider the influence of laminating pressure on the properties of multilayer nanofibrous membranes. Polyvinylidene (PVDF) and polyacrylonitrile (PAN) are the most commonly used nanofiber layers owing to their chemical and thermal stability. Herein, both polymers were electrospun using a semi-industrial scale nanofiber production method. The nanofiber layers were laminated onto a nonwoven surface to improve their mechanical strength via the heat-press method, which is easy to scale and is an energy-saving method at various applied pressures. Other conditions, such as

temperature and the duration of lamination, were kept stable. The effect of the laminating pressure on the nanofiber web has not yet been well reported. To investigate the effect of the pressure on the nanofiber/laminate process, surface morphology under an optical microscope, the minimum bursting pressure, air permeability, water permeability and contact angle tests were applied. Our objective was to optimize the lamination technology and produce multilayer nanofibrous membranes for suitable application in liquid filtration. Another novelty of this paper is that nanofiber layers were produced by using the industrial equipment, and that the layers strongly adhered on the supporting layer without any damage using various lamination pressures to improve their application in liquid filtration.

1. Materials and Methods

1.1. Preparation of Nanofibre Webs

13 wt. % PVDF (Solef 1015, Bruxelles, Belgium) was prepared in *N,N*-dimethylacetamide (DMAC) and 8 wt. % PAN (150 kDa H-polymer, Elmarco, Liberec, Czech Republic) was prepared in *N,N*-dimethylformamide. The solvents were purchased from Penta s.r.o. (Prague, Czech Republic). The solutions were stirred overnight using a magnetic stirrer. Nanofiber webs were prepared using the semi-industrial Nanospider electrospinning device (Elmarco, Liberec, Czech Republic) as shown in Figure 1.
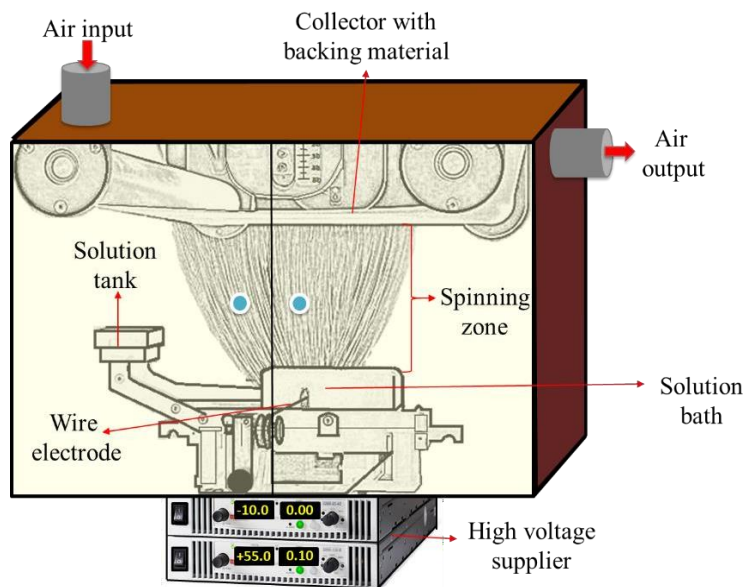
Figure 1. Schematic diagram of an electrospinning unit.

The solution is placed in a solution tank, which is a closed system and connected to a solution bath. The wire electrode passes along a metal orifice in the middle of the solution bath. The solution bath is moved back and forward to feed the surface of the wire electrode. The solution bath feeds the polymer solution on a moving stainless steel wire. The speed of the bath is 240 mm/s. A high voltage supplier is connected to a positively charged wire electrode (55 kV). A second wire electrode, which is connected to a negatively charged voltage supplier (-15 kV), is placed on the top of the spinning unit. A conveyor backing material is placed between the two electrodes. The spinning takes place between the two electrodes. The nanofiber web is collected on baking paper moving in front of the collector electrode. The distance between the electrodes is 188 mm. The distance between the second electrode and the supporting backing material is 2 mm. The speed of the backing material for PAN and PVDF is 15 mm/min and 20 mm/min, respectively. The amount of solution on the wire is controlled with the speed of the solution bath, the diameter of the wire (0.2 mm) and the diameter of

the metal orifice (0.6 mm) in the middle of the solution bath. No solution dipping was observed. An air conditioning unit is used to control the humidity and temperature of the spinning in a closed chamber. The temperature and humidity of the input air are set to 23 °C and 20% by the air-conditioning system. The volumes of air input and output are 100 and 115 m^3/h, respectively. The area weight of the PVDF and PAN nanofibers was set at 3 g/m^2.

1.1. Lamination of Nanofibre Webs

The prepared nanofiber webs were cut into A4 size (210 ×297 mm^2). As a supporting layer, 120 g/m^2 of polyethylene terephthalate spunbond nonwoven and 12 g/m^2 of adhesive web were used (the supplier information is not given). Heat-press equipment (Pracovni Stroje, Teplice, Czech Republic) was used for the lamination process (Figure 2). In this equipment there are two metallic hot plates (upper and lower) used under pressure. The nanofibers, a copolyamide adhesive web and a polyethylene terephthalate spunbond supporting layer were placed between the two hot plates. Two silicon layers were used to block direct contact between the multilayer nanofibrous membranes and the hot plates. The heat was applied (130 °C) for a duration of 3 min. Pressures of 50, 75 and 100 kN were applied between the upper and lower plates. For each pressure, PVDF and PAN nanofiber webs were used. The resultant multilayer nanofibrous membranes were termed PAN50, PAN75, PAN100, PVDF50, PVDF75, and PVDF100 according to the pressure value.
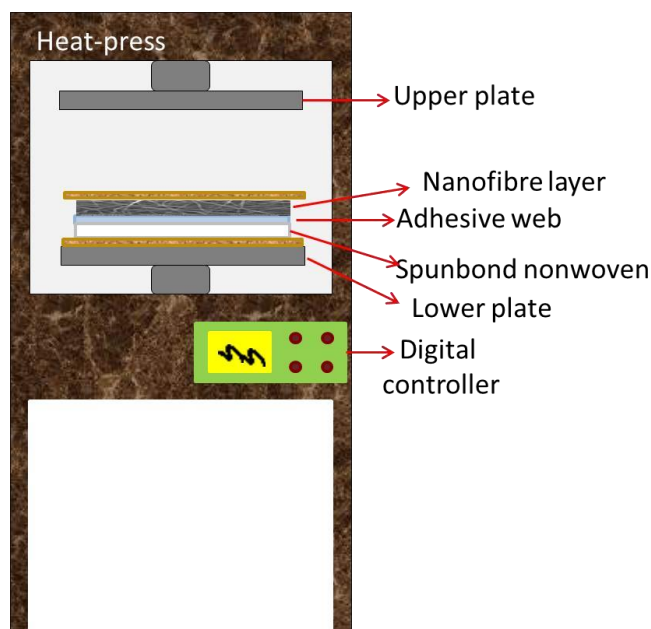
Figure 2. Schematic design of the heat-press equipment and replacement of the multilayer nanofibrous membranes.

1.2. Characterization of the Multilayer Nanofibrous Membranes

The surface morphology of the electrospun fibers and laminated multilayer nanofibrous membranes was observed using a scanning electron microscope (SEM, Vega 3SB, Brno, Czech Republic). From each sample, at least 50 fibers were measured. The fiber diameter was analyzed using the Image-J program (free online program). The Origin-Lab program was used to evaluate the diameter distribution. The surface contact angle of the samples was measured using a Krüss Drop Shape Analyzer DS4 (Krüss GmbH, Hamburg, Germany), at five different points, using distilled water (surface tension 72.0 mN m^{-1}) and ethylene glycol (surface tension 47.3 mN m^{-1}) on the clean and dry samples at room temperature. The air permeability of the multilayer nanofibrous membranes was tested using an SDL

ATLAS Air Permeability Tester (@200 Pa and 20 cm^2, Rock Hill, SC, USA). At least three measurements were taken for each sample.

The maximum, average and minimum pore sizes were determined by a bubble point measurement device, which was developed in our laboratory. The bubble point test allowed the size of the pores of the porous material to be measured. The pore flow means a set of continuous hole channels connecting the opposite sides of the porous material (see Figure 3). At least three measurements were taken.
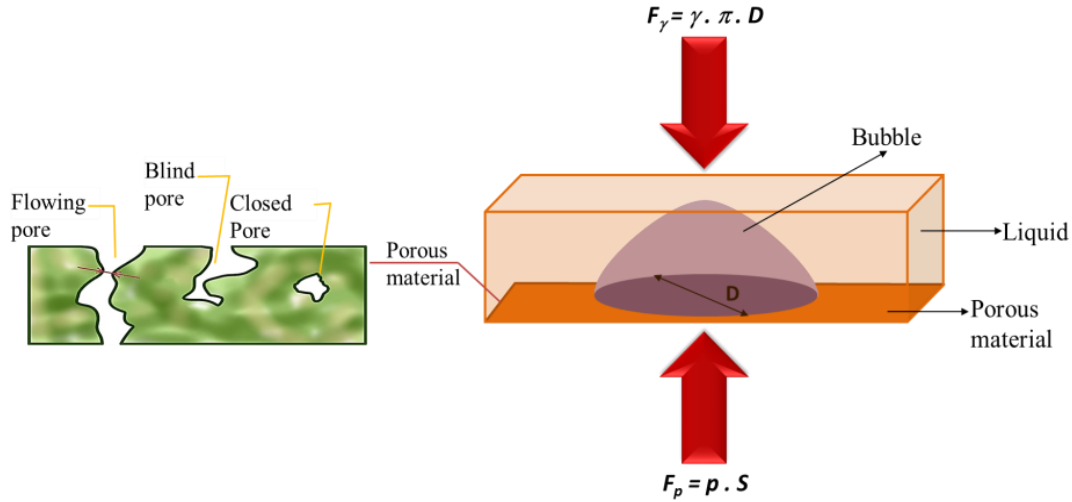

Figure 3. Schematic diagram of pore flow and forces acting on a pore.

The main part of the method was to control the pressure needed to pass a liquid through the tested porous material and for wetting the sample. This is because the wetting force (and hence the opposite force required to extrude the liquid) depends on the pore circumference. The principle for calculating the pore size is shown in Figure 3 and Equations (1) and (2).

$$F_\gamma = \gamma \pi D \qquad\qquad (1)$$

$$Fp = pS \qquad\qquad (2)$$

where F_γ is the force given by surface tension γ of the liquid around the perimeter of πD. The force Fp is given by external pressure p displacing the liquid from the pores and acting on the surface of pore S. It is possible to calculate the magnitude of the force given by the surface tension and the force given by the pore pressurizing fluid. By increasing the air pressure and measuring its flow through the sample, the size of the average and minimum pores can also be determined. In this case, it is necessary to compare the pressure curve of the wet sample with the pressure curve of the dry sample (see Figure 4). The dry sample pressure curve required to determine the mean and minimum pores is also applicable for determining the air permeability coefficient (K) of the sample calculated according to the relation (Equation (3)):

$$K = Q/(\Delta p\ A) \qquad\qquad (3)$$

where Q is the air flow rate (m^2/s), Δp is the pressure drop of the sample, and A is the area of air flow (m^2).

When the pressure increases in the dry sample, the flow rate also increases. Conversely, in the wet sample, at the beginning, there is no flow because all the pores are filled with the liquid. At a certain pressure, the gas empties the largest pore, which determines the minimum pore size, and gas begins to flow through the wet sample. The intersection between the calculated half-dry and the wet sample gives the mean flow pore size. When all the pores are emptied, an intersection between the wet and dry curve will be observed. This means the relation between the applied pressure and the detected

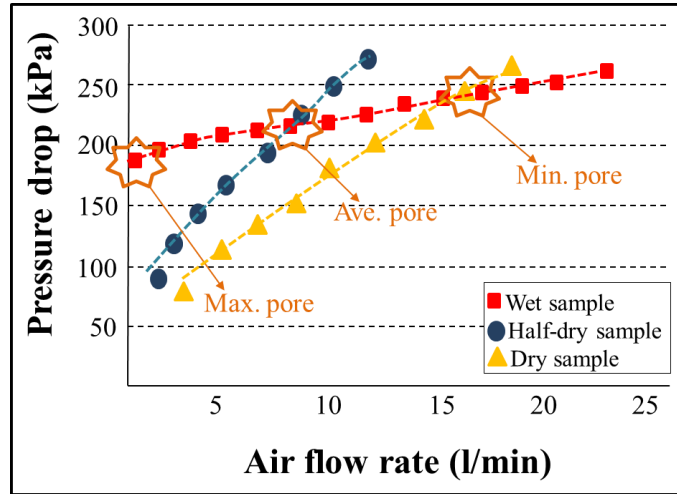flow becomes linear and the intersection of the wet and dry curve represents the detected minimum pore size.

Figure 4. Example of a pressure drop determination to calculate the pore size.

The bursting strength of the multilayer nanofibrous membrane was tested, and the maximum delamination pressure was recorded. The testing device was developed in our laboratory as shown in Figure 5. In this test, the samples were placed between two rings, and the nanofiber side of the samples was placed on the upper side. The sample size was 47 mm in diameter. Pressurized water was sent to the membrane, and the hydrostatic pressure was measured using a pressure controller, which was placed in front of the membrane and connected to a computer. The hydrostatic pressure was increased gradually, and as soon as the nanofiber layer burst, the pressure value on the screen decreased sharply. The maximum pressure value was recorded as the bursting strength of the membrane. The testing samples are shown in Figure 5. After bursting, the nanofiber layer delaminated from the surface of the multilayer membrane. At least three measurements were taken for each membrane.
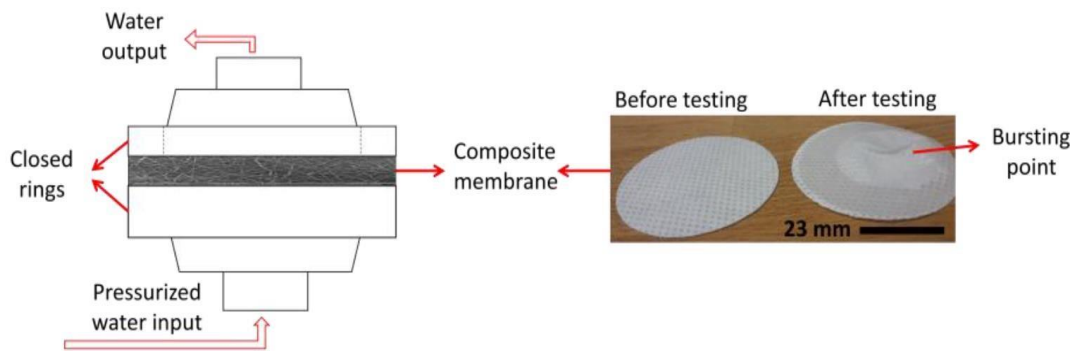

Figure 5. Bursting strength testing unit.

A lab-scale cross-flow filtration unit was developed as shown in Figure 6. Tap water was used as the feed solution. The maximum amount of feed solution was 1500 mL. The flux (F) and the permeability (k) of the membranes were calculated according to Equations (4) and (5) [31,35]:

$$F = \frac{1}{A}\frac{dV}{dt} \tag{4}$$

$$k = F/p \qquad (5)$$

where A is the effective membrane area (m^2), V is the total volume of the permeate (L), p is the transmembrane pressure (bar), and t is the filtration time.
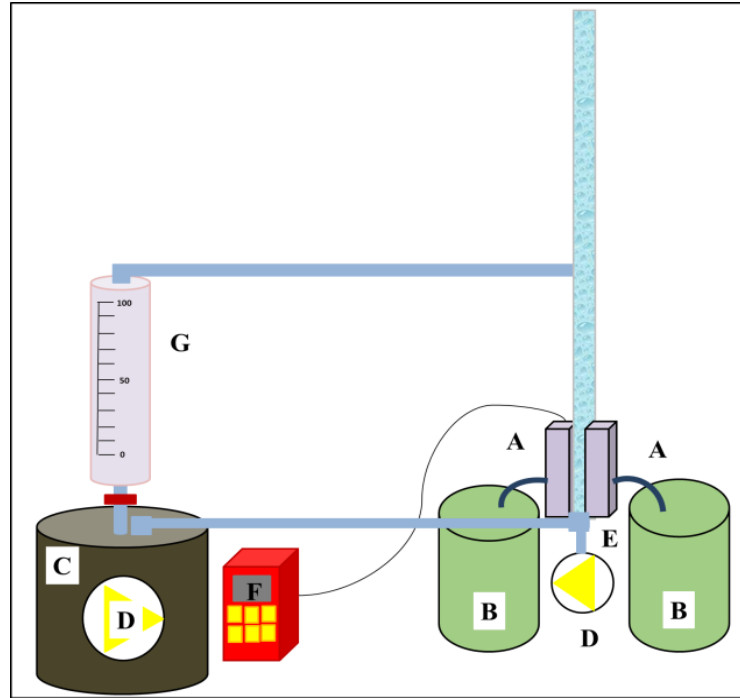

Figure 6. A cross-flow unit: (A) membrane cells; (B) permeate; (C) feed; (D) pump; (E) surface bubble cleaning; (F) pressure controller; (G) feed flow speed controller.

1. Results and Discussion

1.1. Characterization of Nanofibre Webs and Laminated Multilayer Nanofibrous Membranes

To characterize the nanofiber webs into the format of multilayer nanofibrous membranes, various aspects of their material properties were carefully considered. These properties include the fiber diameter, diameter distribution, mean pore size, wetting property, air permeability, and bursting strength.

The surface morphology of the nanofiber webs before and after lamination was imaged using a scanning electron microscope as shown in Figure 7. The average fiber diameter of the PAN and PVDF nanofibers before lamination was determined to be 171 nm and 221 nm, respectively. The diameter of the PVDF nanofibers was greater than that of the PAN nanofibers. The main reason was the difference in viscosity. In previous work [36], it was determined that a 14 wt. %. PVDF solution has a viscosity of 969 mPa.s, while 8 wt. %. PAN has 191 mPa.s. Based on the viscosity results, one can expect that a polymeric solution with a lower viscosity will have a lower fiber diameter. After the lamination process, neither the PVDF nor the PAN nanofiber diameters significantly changed at a pressure of 50 kN (Figure 8). However, significant changes were observed at laminating pressures of 75 kN and 100 kN. When the highest laminating pressure was applied (i.e., 100 kN), the diameter of the PAN and PVDF nanofibers increased by 14% and 25%, respectively. The fibers were flattened under heat and pressure, and the fiber diameter increased gradually. The highest fiber diameter changes were observed in the case of the PVDF nanofiber layer due to its lower glass transition and melting temperature compared to PAN [37,38].
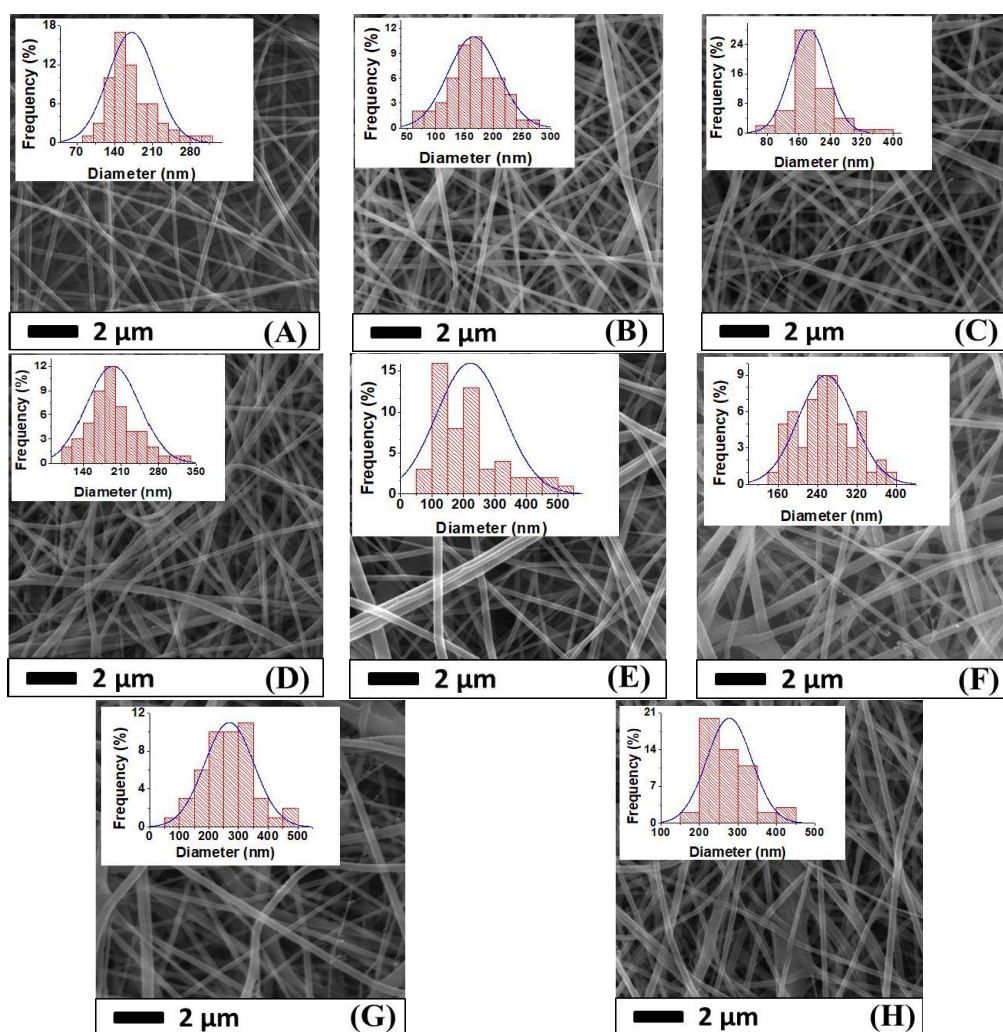
Figure 7. SEM images and fiber diameter distribution of (**A**) PAN nanofiber web before lamination; (**B**) PAN50; (**C**) PAN75; (**D**) PAN100; (**E**) PVDF nanofiber web before lamination; (**F**) PVDF50; (**G**) PVDF75; and (**H**) PVDF100.
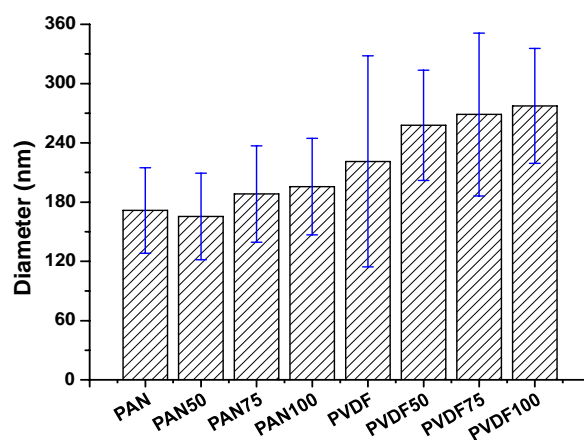

Figure 8. Fiber diameter of various multilayer nanofibrous membranes under different laminating pressures.

It was verified that there is a strong correlation between the electrospun fiber diameters and the polymer concentration, which has been well documented in the literature [39–41]. From the SEM images, the PAN and PVDF multilayer nanofibrous membranes exhibited bead-free surface morphology.

The average pore size of the membranes is given in Figure 9. Electrospun materials readily deform at low pressures. Since the tensile strength of PVDF and PAN nanofibers before lamination is quite low to withstand air pressure, their pore size was not measured.
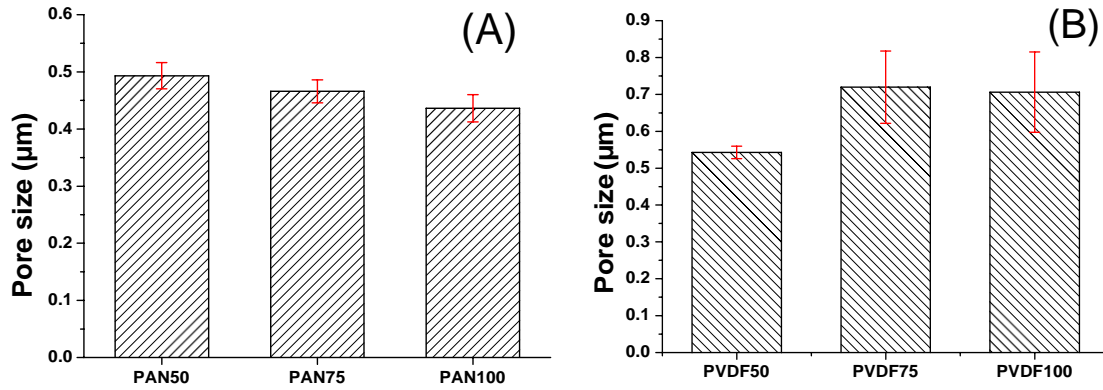

Figure 9. The relationship between the mean pore size and the laminating pressure of (**A**) PAN and (**B**) PVDF multilayer nanofibrous membranes.

In general, there is a correlation between the fiber diameter and the average pore size of the nanofibers. Reducing the fiber diameter increases the surface area and compact web structure, which results in a small pore size [42]. Bagherzadeh et al. [43] demonstrated a theoretical analysis to predict the pore size of electrospun nanofibers. According to their theory, at a given web porosity, increasing the fiber diameter and thickness of the web reduces the dimensions of the pores. This theory was validated experimentally, and the results were compared with the existing theory to predict the pore size distribution of nanofiber mats. Their results showed that the pore size significantly increased with an increase in fiber diameter, web porosity and density of the layers. In this work, the correlation between the diameter of the PVDF nanofibers and the mean pore size was compatible with the literature, while PAN showed an opposite correlation. The laminating pressure effect must be taken into consideration. The nanofiber layer did not change; only the fibers flattened after lamination due to the pressure. It was expected that a higher pressure would cause a lower pore size since the fibers flattened and melting adhesive filled more of the pores and covered the surface of the nanofibers as shown in Figure 10. The PAN multilayer nanofibrous membranes fulfilled this expectation while the PVDF did not. Figure 9B shows that the average pore size and the standard deviation of the pore size measurements increased with pressure, which could be due to possible damage of the PVDF nanofibers under high pressure. Gockeln et al. [44] investigated the influence of laminating pressures on the microstructure and electrochemical performance of the lithium-ion battery electrodes. The results indicated that all the laminated samples showed highly porous and homogeneous networks, while the pore size slightly decreased with an increase in laminating pressure. At higher pressures, the intrinsic electrical conductivity was improved due to more compression.

The water and ethylene glycol wettability of the PAN and PVDF multilayer nanofibrous membranes were examined by a contact angle measurement as shown in Figure 11. The surface energy and surface roughness are the dominant factors for the wettability. As can be seen from Figure 11, an increase in laminating pressure decreased the water and ethylene glycol contact angle of both PAN and PVDF multilayer nanofibrous membranes. Hence, ethylene glycol has a lower surface energy compared to water, with the differences in contact angle value being 20° for PAN and 30° for PVDF. Similar behavior was observed in the literature [45,46]. It is well known that when the surface

energy is lowered, and surface roughness is raised, the hydrophobicity is enhanced [47–49]. With the help of heat, the higher laminating pressure on the surface may cause changes to the surface shape and make the surface flatter, which results in an increase in the surface wettability (Figure 11). The PVDF membranes showed hydrophobic characteristics at the lowest laminating pressure (i.e., 50 kN), while at higher laminating pressures they showed hydrophilic properties. By setting the lamination process parameters, one can prepare hydrophilic PVDF multilayer nanofibrous membranes without any surface modification.
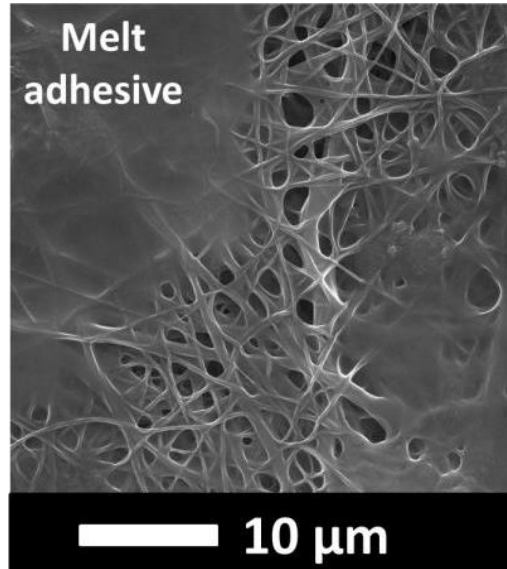
Figure 10. An illustration of adhesive melting over the surface of a nanofiber web, forming a non-porous film.
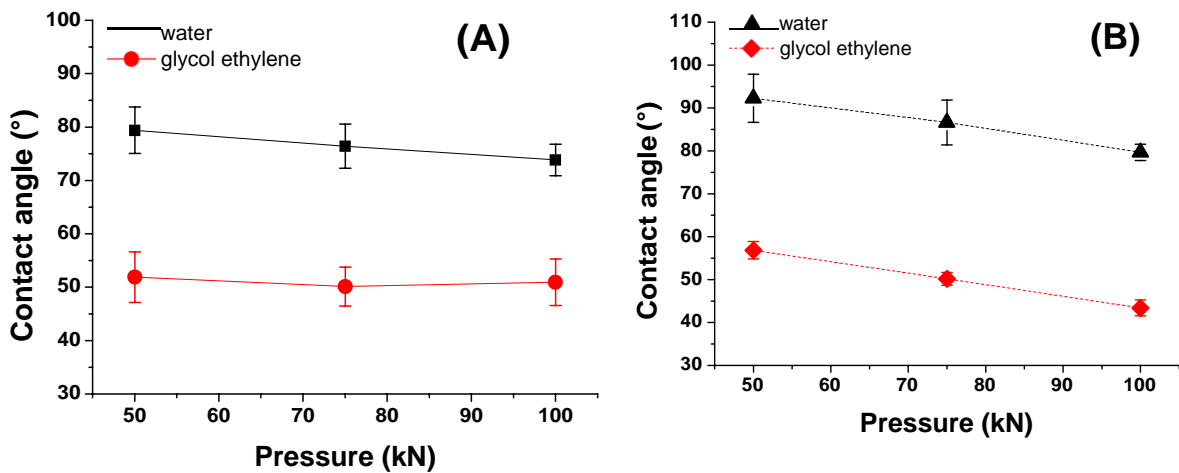
Figure 11. Contact angle vs. laminating pressure of (**A**) PAN; (**B**) PVDF multilayer nanofibrous membranes.

The morphology of the nanofiber webs, including their pore size, shape, size distribution and porosity, has a significant influence on the air permeability of the multilayer membrane. To investigate the effect of laminating pressure on the air permeability of the multilayer nanofibrous membranes, the samples were placed on a circular sample holder, and the air flow rates through the samples were measured (Figure 12A). Like the air flows, the areas of the sample and pressure drop remained constant

during the measurement. Due to the weakness of neat nanofiber layers, the air permeability test was not performed. In a previous study [31], the tensile strength of the nanofiber layers was found to be between 3 and 4.33 (N/25 mm), which is extremely low to withstand any external force.
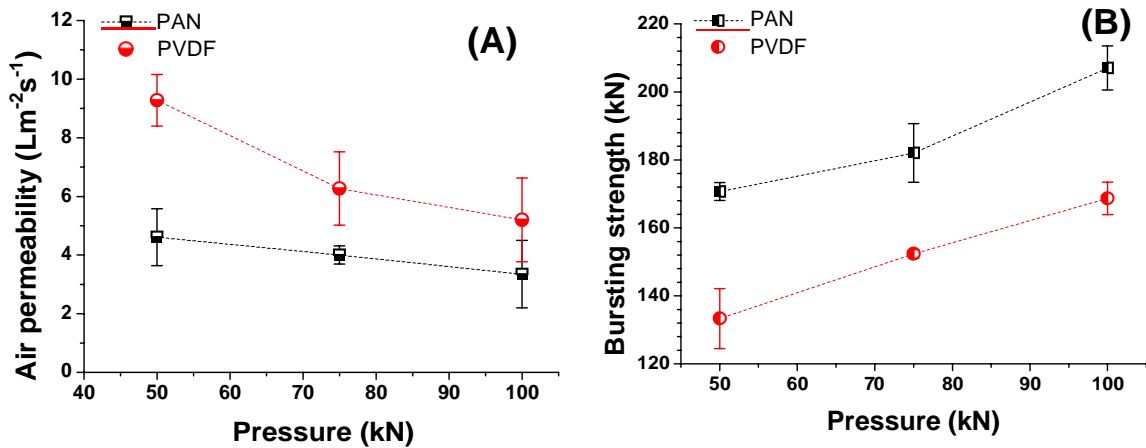
Figure 12. Influence of laminating pressure on (**A**) air permeability; and (**B**) bursting strength of multilayer nanofibrous membranes.

Abuzade et al. [50] studied the effects of the process parameters (e.g., concentration of solution, applied voltage) on the porosity and air permeability of an electrospun nanoweb. The results showed that the nanofiber diameter and size distribution are dominant parameters in controlling the pore sizes formed by the nanofiber intersections and air permeability of the electrospun web. Figure 12A showed that increasing the laminating pressure lowered the air permeability of the multilayer membranes. Compression of the melting adhesive, filling the pores of the nanofiber and nonwoven web, covered the surface of the thin nanofiber layer and created a non-porous film (Figure 10). As a result, the breathability of the membranes was decreased. Similarly, Kanafchian et al. [32] claimed that during the lamination, the melt adhesive penetrates through the nanofiber/fabric structure, which leads to filling of the pores of nanofibers and a decrease in air permeability. The PAN multilayer nanofibrous membrane has a lower air permeability than PVDF, mainly due to the lower fiber diameter of the PAN nanofibers compared to the PVDF nanofibers. Rajak et al. [51] prepared PAN nanofiber webs from various concentrations. The results indicated that changes in concentration affect the fiber diameter. At a higher concentration and fiber diameter, the air permeability has a higher value.

A bursting test was performed to determine the mechanical strength of the laminated layers, and the results are shown in Figure 12B. The test method has been developed in our laboratory. The maximum delamination point of the multilayer nanofibrous membranes was measured using hydrostatic pressure. The results showed that PAN nanofibers have a better adhesion to the supporting layer and a better bursting strength compared to PVDF. The adhesion between the layers is related to the material surface chemistry and its influence on adhesion, together with the properties of adhesive materials and interactions at the adhesive-substrate surface interface. Materials that can wet each other tend to have a better adhesion, and the wettability of the material is related to its surface energy. For instance, low surface energy materials such as poly(tetrafluoroethylene), ceramics, and silicon, are resistant to wetting and adhesive bonding [52]. Lee et al. [53] found that the surface energy of PAN is around 44 mJ/m^2, while this value was calculated as 54.1 mJ/m^2 by Pritykin et al. [54]. On the other hand, PVDF has a very low surface energy value of around 26 mJ/m^2 [55]. Due to the lower surface energy of PVDF compared to PAN, the adhesion between the layers is weaker, which results in low lamination strength. The results show that laminating pressure plays an important role in the bursting strength. By increasing the laminating pressure under heat, the melted adhesive fills the pores of the nanofibers and nonwovens and penetrates through the layers. A better mechanical strength is

achieved due to the entanglement of the adhesive web and the layers. The results showed that the bursting strength of a material can be improved by adjusting the lamination conditions.

1.1. Evaluation of Liquid Filtration by Cross-Flow Filtration

Taking their practical applications into consideration, laminated multilayer nanofibrous membranes were used to further investigate their water permeability performance due to their hydrophilic, porous, small pore size and predominant mechanical properties for liquid filtration. A cross-flow filtration unit was prepared in our laboratory. Using Equation (5), the water permeability of the PAN and PVDF multilayer nanofibrous membranes was calculated (Figures 13 and 14).
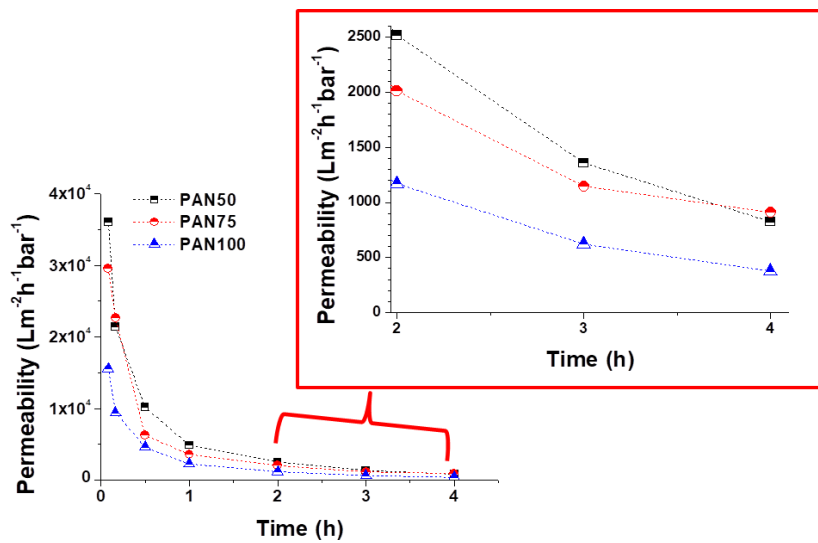

Figure 13. Permeability of PAN multilayer nanofibrous membranes at various laminating pressures over time.
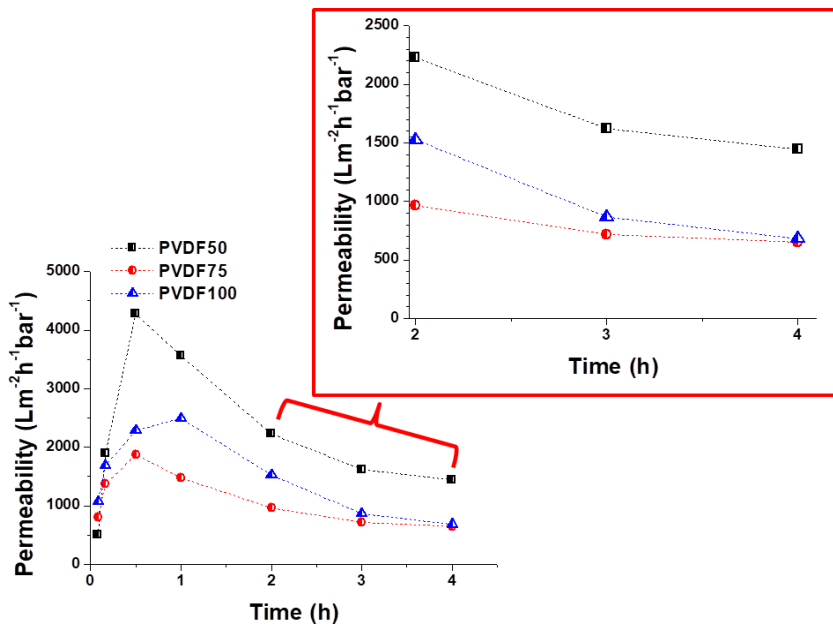

Figure 14. Permeability of PVDF multilayer nanofibrous membranes at various laminating pressures over time.

A decrease in permeability was observed for both the PAN and PVDF multilayer nanofibrous membranes depending on the operation time as shown in Figures 13 and 14. There are a few possible reasons for the decrease in permeability during liquid filtration. The first reason is concentration polarization, which is a consequence of the selectivity of the membrane. When the liquid passes through the membrane, the solute is retained by the membrane surface with a relatively high concentration. Moreover, the hydrophilicity of the membrane decreases over time during filtration due to membrane fouling and concentration polarization. Since tap water is not pure, dissolved molecules, suspended solids, and organics may be contained in the water, which can cause a decrease in the water flux due to fouling. The second reason is that close to the membrane surface, the effective transmembrane pressure (TMP) driving force reduces due to an osmotic pressure difference between the filtrate and the feed solution. TPM is generally observed in the case of ultra-filtration (UF) membranes. Another reason may be related to the compression/collapse of membrane pores, thereby causing a reduction in water permeability. The operating conditions (feed pressure, temperature, pH, flow rate, etc.) are also effective factors in membrane permeability. In general, the flux decline is caused by a decreased driving force and/or an increased resistance of the membrane, raw water characteristics, and particulate matter levels [56–58].

At the beginning, all the PAN membranes had the highest permeability (Figure 13). After a 4-h filtration test, the flux declined to 824, 909, and 375 $Lm^{-2}h^{-1}bar^{-1}$ in the case of PAN50, PAN75, and PAN100, respectively. The results indicated that laminating pressure has a huge impact on the water permeability of the multilayer membranes. The laminating pressure and the permeability of the membranes showed a non-linear relationship in the case of the PAN membranes. PAN50 and PAN75 multilayer nanofibrous membranes showed the best water permeability. On the other hand, all the PVDF membranes showed very low initial permeability at the beginning due to the hydrophobic nature of the PVDF nanofibers, and the melted adhesive web partially occupied the membrane

pores, increasing the hydraulic resistance to filtration (Figure 14). The results of 4 h of filtration of PVDF membranes showed that the highest permeability (1444 $Lm^{-2}h^{-1}bar^{-1}$) was only achieved at the lowest laminating pressure (50 kN). PVDF75 and PVDF100 had almost the same permeability value (650 and 681 $Lm^{-2}h^{-1}bar^{-1}$, respectively) after the 4-h filtration test. Li et al. [59] reported a simple strategy to improve the waterproof/breathable performance and mechanical properties of electrospun PVDF fibrous membranes using a thermo-pressing system. It was found that the effect of temperature and pressure on PVDF has a synergistic effect on the fiber morphology and crystal structure. By properly adjusting the temperature and pressure, robust mechanical properties and excellent waterproof/breathable performance of PVDF membranes were achieved.

In terms of water permeability, PAN75 has the best results from the PAN membranes. PVDF50 showed the best permeability results after the 4-h filtration test from all the PAN and PVDF membranes. The results showed that after proper lamination multilayer nanofibrous membranes are suitable for future application in liquid filtration.

1. Conclusions

There is a huge demand for the filtration application of nanofiber layers due to their specific surface, low pore size and high porosity. In this study, the effect of laminating pressure on PAN and PVDF multilayer nanofibrous membranes was investigated to prepare suitable microfilters for liquid filtration. The surface morphology, average pore size, air permeability, water permeability, bursting strength, and the contact angle of the membranes were compared. Different performance levels were achieved by varying the laminating pressure of the multilayer nanofibrous membranes. The pressure effect had a considerable influence on air permeability, average pore size, contact angle, bursting strength, and water permeability. The surface morphology results showed that the fiber diameter slightly increased with an increase in laminating pressure, while the water and ethylene glycol contact angles decreased. The main effect of laminating pressure was observed on the average pore size, air permeability, bursting strength and water permeability of the membranes. PVDF50 showed the

best water filtration of all the membranes. However, the bursting strength of PVDF50 is the lowest, may cause possible damage and delamination of the layers under pressure over time. PAN nanofibers a better adhesion to the surface of the multilayer. PAN75 was selected as the best candidate for filtration due to its high water permeability and mechanical strength. PVDF multilayer nanofi membranes showed better air permeability than PAN, which may be better for the possible applicat air filtration. These findings imply that to achieve the best permeable membrane results, the lamin process should be carefully optimized.

Author Contributions: Fatma Yalcinkaya conceived and designed the experiments; Fatma Yalcinkaya perform experiments; Fatma Yalcinkaya analyzed the data; Jakub Hruza contributed reagents/materials/analysis too preparation of tools; Fatma Yalcinkaya wrote the paper.

Conflicts of Interest: The authors declare that there is no conflict of interest.

References

1. Gao, J.; Zhu, J.; Luo, J.; Xiong, J. Investigation of microporous composite scaffolds fabricated by embedding sacrificial polyethylene glycol microspheres in nanofibrous membrane. *Compos. Part A Appl. Sci. Manuf.* **2016**, *91*, 20–29. [CrossRef]

2. Tang, Y.; Chen, L.; Zhao, K.; Wu, Z.; Wang, Y.; Tan, Q. Fabrication of PLGA/HA (core)-collagen/amoxicillin (shell) nanofiber membranes through coaxial electrospinning for guided tissue regeneration. *Compos. Sci. Technol.* **2016**, *125*, 100–107. [CrossRef]

3. Zhang, W.; Ronca, S.; Mele, E. Electrospun nanofibres containing antimicrobial plant extracts. *Nanomaterials* **2017**, *7*, 42. [CrossRef] [PubMed]

4. Sill, T.J.; von Recum, H.A. Electrospinning: Applications in drug delivery and tissue engineering. *Biomaterials* **2008**, *29*, 1989–2006. [CrossRef] [PubMed]

5. Tan, L.; Gan, L.; Hu, J.; Zhu, Y.; Han, J. Functional shape memory composite nanofibers with graphene oxide filler. *Compos. Part A Appl. Sci. Manuf.* **2015**, *76*, 115–123. [CrossRef]

6. Zhao, X.G.; Jin, E.M.; Park, J.Y.; Gu, H.B. Hybrid polymer electrolyte composite with SiO_2 nanofiber filler for solid-state dye-sensitized solar cells. *Compos. Sci. Technol.* **2014**, *103*, 100–105. [CrossRef]

7. Yoon, B.; Lee, S. Designing waterproof breathable materials based on electrospun nanofibers and assessing the performance characteristics. *Fibers Polym.* **2011**, *12*, 57–64. [CrossRef]

8. Fehse, M.; Cavaliere, S.; Lippens, P.E.; Savych, I.; Iadecola, A.; Monconduit, L.; Jones, D.J.; Rozière, J.; Fischer, F.; Tessier, C.; et al. Nb-doped TiO_2 nanofibers for lithium ion batteries. *J. Phys. Chem. C* **2013**, *117*, 13827–13835. [CrossRef]

9. Aydın, H.; Çelik, S.Ü.; Bozkurt, A. Electrolyte loaded hexagonal boron nitride/polyacrylonitrile nanofibers for lithium ion battery application. *Solid State Ionics* **2017**, *309*, 71–76. [CrossRef]

10. Wang, X.; Drew, C.; Lee, S.H.; Senecal, K.J.; Kumar, J.; Samuelson, L.A. Electrospun nanofibrous membranes for highly sensitive optical sensors. *Nano Lett.* **2002**, *2*, 1273–1275. [CrossRef]

11. Liu, P.; Wu, S.; Zhang, Y.; Zhang, H.; Qin, X. A fast response ammonia sensor based on coaxial PPy–PAN nanofiber yarn. *Nanomaterials* **2016**, *6*, 121. [CrossRef] [PubMed]

12. Macagnano, A.; Perri, V.; Zampetti, E.; Bearzotti, A.; De Cesare, F.; Sprovieri, F.; Pirrone, N. A smart nanofibrous material for adsorbing and detecting elemental mercury in air. *Atmos. Chem. Phys.* **2017**, *17*, 6883–6893. [CrossRef]

13. Zhang, X.F.; Feng, Y.; Huang, C.; Pan, Y.; Yao, J. Temperature-induced formation of cellulose nanofiber film with remarkably high gas separation performance. *Cellulose* **2017**, *24*, 5649–5656. [CrossRef]

14. Zampetti, E.; Pantalei, S.; Bearzotti, A.; Bongiorno, C.; De Cesare, F.; Spinella, C.; Macagnano, A. TiO$_2$ nanofibrous chemoresistors coated with PEDOT and PANi blends for high performance gas sensors. In *Procedia Engineering*; Elsevier: Amsterdam, The Netherlands, 2012; Volume 47, pp. 937–940.

15. Ge, J.; Choi, N. Fabrication of functional polyurethane/rare earth nanocomposite membranes by electrospinning and its VOCs absorption capacity from air. *Nanomaterials* **2017**, *7*, 60. [CrossRef] [PubMed]

16. Desai, K.; Kit, K.; Li, J.; Michael Davidson, P.; Zivanovic, S.; Meyer, H. Nanofibrous chitosan non-wovens for filtration applications. *Polymer* **2009**, *50*, 3661–3669. [CrossRef]

17. Liao, Y.; Tian, M.; Wang, R. A high-performance and robust membrane with switchable super-wettability for oil/water separation under ultralow pressure. *J. Memb. Sci.* **2017**, *543*, 123–132. [CrossRef]

18. Li, Z.; Kang, W.; Zhao, H.; Hu, M.; Wei, N.; Qiu, J.; Cheng, B. A novel polyvinylidene fluoride tree-like nanofiber membrane for microfiltration. *Nanomaterials* **2016**, *6*, 152. [CrossRef] [PubMed]

19. Sood, R.; Cavaliere, S.; Jones, D.J.; Rozière, J. Electrospun nanofibre composite polymer electrolyte fuel cell and electrolysis membranes. *Nano Energy* **2016**, *26*, 729–745. [CrossRef]

20. Yalcinkaya, F. Preparation of various nanofiber layers using wire electrospinning system. *Arab. J. Chem.* **2016**. [CrossRef]

21. Ding, Y.; Zhang, P.; Long, Z.; Jiang, Y.; Xu, F.; Di, W. The ionic conductivity and mechanical property of electrospun P(VdF-HFP)/PMMA membranes for lithium ion batteries. *J. Memb. Sci.* **2009**, *329*, 56–59. [CrossRef]

22. Jahanbaani, A.R.; Behzad, T.; Borhani, S.; Darvanjooghi, M.H.K. Electrospinning of cellulose nanofibers mat for laminated epoxy composite production. *Fibers Polym.* **2016**, *17*, 1438–1448. [CrossRef]

23. Charles, L.E.; Kramer, E.R.; Shaw, M.T.; Olson, J.R.; Wei, M. Self-reinforced composites of hydroxyapatite-coated PLLA fibers: Fabrication and mechanical characterization. *J. Mech. Behav. Biomed. Mater.* **2012**, *17*, 269–277. [CrossRef] [PubMed]

24. Iqbal, Q.; Bernstein, P.; Zhu, Y.; Rahamim, J.; Cebe, P.; Staii, C. Quantitative analysis of mechanical and electrostatic properties of poly(lactic) acid fibers and poly(lactic) acid-carbon nanotube composites using atomic force microscopy. *Nanotechnology* **2015**, *26*, 105702. [CrossRef] [PubMed]

25. Charles, L.F.; Shaw, M.T.; Olson, J.R.; Wei, M. Fabrication and mechanical properties of PLLA/PCL/HA composites via a biomimetic, dip coating, and hot compression procedure. *J. Mater. Sci. Mater. Med.* **2010**, *21*, 1845–1854. [CrossRef] [PubMed]

26. Xu, Y.; Zhang, X.; Wang, X.; Wang, X.; Li, X.; Shen, C.; Li, Q. Simultaneous enhancements in the strength, modulus and toughness of electrospun polymeric membranes. *RSC Adv.* **2017**, *7*. [CrossRef]

27. Jiříček, T.; Komárek, M.; Chaloupek, J.; Lederer, T. Maximising flux in direct contact membrane distillation using nanofibre membranes. *Desalin. Water Treat.* **2017**, *73*, 249–255. [CrossRef]

28. Jiříček, T.; Komárek, M.; Chaloupek, J.; Lederer, T. Flux enhancement in membrane distillation using nanofiber membranes. *J. Nanomater.* **2016**, *2016*, 1–7. [CrossRef]

29. Yalcinkaya, B.; Yalcinkaya, F.; Chaloupek, J. Thin film nanofibrous composite membrane for dead-end seawater desalination. *J. Nanomater.* **2016**, *2016*, 1–12. [CrossRef]

30. Yalcinkaya, B.; Yalcinkaya, F.; Chaloupek, J. Optimisation of thin film composite nanofiltration membranes based on laminated nanofibrous and nonwoven supporting material. *Desalin. Water Treat.* **2017**, *59*, 19–30. [CrossRef]

31. Yalcinkaya, F.; Yalcinkaya, B.; Hruza, J.; Hrabak, P. Effect of nanofibrous membrane structures on the treatment of wastewater microfiltration. *Sci. Adv. Mater.* **2016**, *9*, 747–757. [CrossRef]

32. Kanafchian, M.; Valizadeh, M.; Haghi, A.K. A study on the effects of laminating temperature on the polymeric nanofiber web. *Korean J. Chem. Eng.* **2011**, *28*, 445–448. [CrossRef]

33. Yao, M.; Woo, Y.C.; Tijing, L.D.; Shim, W.-G.; Choi, J.-S.; Kim, S.-H.; Shon, H.K. Effect of heat-press conditions on electrospun membranes for desalination by direct contact membrane distillation. *Desalination* **2016**, *378*, 80–91. [CrossRef]

34. Mohammadian, M.; Haghi, A.K. Study on the production of a new generation of electrospun nanofiber webs. *Bulg. Chem. Commun.* **2014**, *46*, 530–534.

35. Yalcinkaya, F.; Siekierka, A.; Bryjak, M. Preparation of fouling-resistant nanofibrous composite membranes for separation of oily wastewater. *Polymers* **2017**, *9*, 679. [CrossRef]

36. Yalcinkaya, F.; Yalcinkaya, B.; Pazourek, A.; Mullerova, J.; Stuchlik, M.; Maryska, J. Surface modification of electrospun PVDF/PAN nanofibrous layers by low vacuum plasma treatment. *Int. J. Polym. Sci.* **2016**, *2016*, 1–9. [CrossRef]

37. Gopalan, A.I.; Santhosh, P.; Manesh, K.M.; Nho, J.H.; Kim, S.H.; Hwang, C.G.; Lee, K.P. Development of electrospun PVdF-PAN membrane-based polymer electrolytes for lithium batteries. *J. Memb. Sci.* **2008**, *325*, 683–690. [CrossRef]

38. Liu, T.-Y.; Lin, W.-C.; Huang, L.-Y.; Chen, S.-Y.; Yang, M.-C. Surface characteristics and hemocompatibility of PAN/PVDF blend membranes. *Polym. Adv. Technol.* **2005**, *16*, 413–419. [CrossRef]

39. Hammami, M.A.; Krifa, M.; Harzallah, O. Centrifugal force spinning of PA6 nanofibers—Processability and morphology of solution-spun fibers. *J. Text. Inst.* **2014**, *105*, 637–647. [CrossRef]

40. Essalhi, M.; Khayet, M. Self-sustained webs of polyvinylidene fluoride electrospun nano-fibers: Effects of polymer concentration and desalination by direct contact membrane distillation. *J. Memb. Sci.* **2014**, *454*, 133–143. [CrossRef]

41. Beachley, V.; Wen, X. Effect of electrospinning parameters on the nanofiber diameter and length. *Mater. Sci. Eng. C Mater. Biol. Appl.* **2009**, *29*, 663–668. [CrossRef] [PubMed]

42. Lowery, J.L.; Datta, N.; Rutledge, G.C. Effect of fiber diameter, pore size and seeding method on growth of human dermal fibroblasts in electrospun poly(ε-caprolactone) fibrous mats. *Biomaterials* **2010**, *31*, 491–504. [CrossRef] [PubMed]

43. Bagherzadeh, R.; Najar, S.S.; Latifi, M.; Tehran, M.A.; Kong, L. A theoretical analysis and prediction of pore size and pore size distribution in electrospun multilayer nanofibrous materials. *J. Biomed. Mater. Res. Part A* **2013**, *101*, 2107–2117. [CrossRef] [PubMed]

44. Gockeln, M.; Pokhrel, S.; Meierhofer, F.; Glenneberg, J.; Schowalter, M.; Rosenauer, A.; Fritsching, U.; Busse, M.; Mädler, L.; Kun, R. Fabrication and performance of $Li_4Ti_5O_{12}$/C Li-ion battery electrodes using combined double flame spray pyrolysis and pressure-based lamination technique. *J. Power Sources* **2018**, *374*, 97–106. [CrossRef]

45. Stiubianu, G.; Nicolescu, A.; Nistor, A.; Cazacu, M.; Varganici, C.; Simionescu, B.C. Chemical modification of cellulose acetate by allylation and crosslinking with siloxane derivatives. *Polym. Int.* **2012**, *61*, 1115–1126. [CrossRef]

46. Law, K.-Y.; Zhao, H. Wetting on rough surfaces. In *Surface Wetting*; Springer International Publishing: Cham, Switzerland, 2016; pp. 55–98.

47. Youngblood, J.P.; McCarthy, T.J. Ultrahydrophobic polymer surfaces prepared by simultaneous ablation of polypropylene and sputtering of poly(tetrafluoroethylene) using radio frequency plasma. *Am. Chem. Soc. Polym. Prepr. Div. Polym. Chem.* **1999**, *40*, 563–564. [CrossRef]

48. Chen, W.; Fadeev, A.Y.; Hsieh, M.C.; Öner, D.; Youngblood, J.; McCarthy, T.J. Ultrahydrophobic and ultralyophobic surfaces: Some comments and examples. *Langmuir* **1999**, *15*, 3395–3399. [CrossRef]

49. Wenzel, R.N. Surface roughness and contact angle. *J. Phys. Colloid Chem.* **1949**, *53*, 1466–1467. [CrossRef]

50. Abuzade, R.A.; Zadhoush, A.; Gharehaghaji, A.A. Air permeability of electrospun polyacrylonitrile nanoweb. *J. Appl. Polym. Sci.* **2012**, *126*, 232–243. [CrossRef]

51. Rajak, A. Synthesis of electrospun nanofibers membrane and its optimization for aerosol filter application. *KnE Eng.* **2016**, *1*. [CrossRef]

52. Von Fraunhofer, J.A. Adhesion and cohesion. *Int. J. Dent.* **2012**, *2012*, 1–8. [CrossRef] [PubMed]

53. Lee, L.-H. Relationships between surface wettability and glass temperatures of high polymers. *J. Appl. Polym. Sci.* **1968**, *12*, 719–730. [CrossRef]

54. Pritykin, L.M. Calculation of the surface energy of homo- and copolymers from the cohesion parameters and refractometric characterisics of the respective monomers. *J. Colloid Interface Sci.* **1986**, *112*, 539–543. [CrossRef]

55. Chen, N.; Hong, L. Surface phase morphology and composition of the casting films of PVDF-PVP blend. *Polymer* **2001**, *43*, 1429–1436. [CrossRef]

56. Kim, K.-M.; Woo, S.; Lee, J.; Park, H.; Park, J.; Min, B. Improved permeate flux of PVDF ultrafiltration membrane containing PVDF-g-PHEA synthesized via ATRP. *Appl. Sci.* **2015**, *5*, 1992–2008. [CrossRef]

57. Van den Berg, G.B.; Smolders, C.A. Flux decline in ultrafiltration processes. *Desalination* **1990**, *77*, 101–133. [CrossRef]

58. Meier-Haack, J.; Booker, N.A.; Carroll, T. A permeability-controlled microfiltration membrane for reduced fouling in drinking water treatment. *Water Res.* **2003**, *37*, 585–588. [CrossRef]

59. Li, X.; Lin, J.; Bian, F.; Zeng, Y. Improving waterproof/breathable performance of electrospun poly(vinylidene fluoride) fibrous membranes by thermo-Pressing. *J. Polym. Sci. Part B Polym. Phys.* **2017**, *56*, 1–10. [CrossRef]

Electrospun Polyacrylonitrile Nanofibrous Membranes for Point-of-Use Water and Air Cleaning

Remi Roche[b] and Fatma Yalcinkaya*[a]

ctrospun polyacrylonitrile (PAN) nanofibrous mem- ere prepared by using heat-press lamination under nditions. The air permeability and the burst-pressure run to select the membranes for point-of-use air and aning. Membrane characterization was performed by ning electron microscopy, contact angle, and average measurements. Selected membranes were used for ust filtration and cross-flow water filtration tests. Air dust filter results indicated that electrospun PAN nanofibrous membranes showed very high air-dust filtration efficiency of more than 99.99 % in between PM$_{0.3}$ and PM$_{2.5}$, whereas cross-flow filtration test showed very high water permeability over 600 L/(m^{2}hbar) after 6 h of operation. Combining their excellent efficiency and water permeability, these membranes offer an ideal solution to filter both air and water pollutants.

1. Introduction

Water and air pollution are increasing concern all over the world as a risk of human health.[1–3] Air pollution can cause asthma, skin irritation, nausea, cancer, brain damage, birth defects, respiratory and heart problems due to gaseous pollutants and particulate matter (PM).[4–8] Based on inhalable particle size, PM is classified into coarse (2.5–10 μm), fine (0.1–2.5 μm) and ultrafine (< 0.1 μm).[9] Exposure to elevated PM levels over the long term can reduce life expectancy by a few years while short-term exposure contributes to acute cardiovas- cular morbidity and mortality.[8] Under this condition, an efficient air filter is demanded to capture of air pollutants in different sizes. Textile based high-efficiency particulate air (HEPA) and ultra-low particulate air (ULPA) filters can capture very small PM with a filtration efficiency over than 99.90 %.[9] Fibrous materials that have fiber diameter about a few micro- meters with porosity around 80–90 % can easily remove sub-micrometer and micrometer particles from air and water with a high efficiency. Beside the air pollution, water pollution is another issue that needs an emergency solution for the current and future life. The availability of freshwater resources has been reduced due to a growing population. As a result of population growth, the amount of water consumption and the number of manufacturing and industrial production have been increased.

The industries, such as chemical, paper, beverage, automotive, food, agriculture, power generation, textiles, and garments consume tons of water daily. By 2030, it is expected that the demand for water supply will exceed about 40 % of current supply.[10] Before reuse or releasing the used water directly to nature, it is necessary to clean the water from contaminations. Membrane technology is one of the effective and successful methods to compete with conventional separation process for the treatment of wastewater due to their low cost, energy- efficiency, compactness, high permeability, and high selectivity and easy-to-operate properties. In principle, the membrane acts as a semi-permeable barrier that separates two distinct phases usually under a driving force. For an effective separation and high throughput, the membrane should have a proper pore size with a highly porous structure.

Nanofibrous webs have a large surface area to volume, high porosity, tight pore size and high permeability that make them an appropriate candidate for filtration applications. Therefore, nanofibers have received increased attention in water and air domain applications. The first commercialized application of electrospun nanofibers was in air filters.[11] Despite the high permeability and tight pore size, the application of nanofiber webs in the water domain area is limited. The main reason is the mechanical weakness of single layer nanofiber web. In the application of membranes, the nanofiber webs require addi- tional supporting layer or additives to provide strength. Several methods have been reported to develop mechanical strength of the nanofiber webs. Blending of polymers,[12] dip-coating,[13] or polymer and an additive such as epoxy[14] or inorganics[15,16] were suggested as solutions for the improvement of the strength. However, these methods require time and chemicals which is costly. Recently, Wirth et al.[17] reported ultrasonic welding of polyacrylonitrile (PAN) nanofiber mats without destruction of the mat morphology. Various welding patterns were used and their effects on adhesion forces between both joined nanofiber mats and different failure mechanisms have been investigated. The results indicated that some welding patterns enabled bonding stronger than the mats themselves.

[a] Dr. F. Yalcinkaya
Department of Nanotechnology and Informatics
Institute of Nanomaterials, Advanced Technologies and Innovation
Technical University of Liberec
Studentska 1402/2, 46117, Liberec, Czech Republic
E-mail: fatma.yalcinkaya@tul.cz
[b] R. Roche
National Polytechnic Institute of Chemical Engineering and Technology (INP-ENSIACET)
4, allée Emile Monso – CS 44362, 31030 Toulouse Cedex 4, France

However, this method still needs to optimize based on materials and the pattern of welding equipment. Other attempts to prevent damage of nanofiber webs have been done as nanofiber-coated yarn.[18–21] A macroscopic size random yarn has been used as core and nanofiber layer was covered around. To form a textile structure, it is necessary to use knitting or weaving technology. An external yarn is necessary to cover for the protection of the open surface of the nanofiber layer before knitting or weaving which makes the process costly. In the various study, the nanofibers webs are combined to a support either like layer to layer or sandwiched structure between different layers.[22–30] Jiricek[31,32] and Yalcinkaya et al.[24,33] used a bi-component polyethylene (PE) /polypropylene (PP) spun bond as a supporting layer for nanofiber layers. Heat-press technique was applied using a fusing machine for the lamination process. The polyvinylidene fluoride (PVDF) and polyamide-6 (PA-6) nanofiber layers were adhered on the outer surface of the bi-component due to the low melting point of PE. The resultant multilayer nanofibrous membranes were used for water distillation and desalination. In the previous work,[26,30] the PVDF nanofibrous membranes have been prepared using heat-press technique under various conditions. Results indicated that PVDF nanofibers are suitable as water and air filters. In this work, polyacrylonitrile (PAN) nanofiber web was prepared using needle-free wire electrospinning industrial production method. PAN is easy to electrospun into nanofiber and has thermal stability, tolerance to most solvents, and commercial availability.[34,35] The mechanical strength of the prepared electrospun web was improved by lamination with a supporting layer and adhesive web. The lamination conditions, such as temperature, duration of heat-press and force of the press have been investigated. The air permeability and burst pressure tests were run to determine membranes for air and water filtration test. The ultimate goal of this work is to introduce electrospun PAN nanofibrous membranes that prepared by industrial production method as air and water filter. So far, there has been no deep work reported for the lamination of PAN nanofibers using heat press under various lamination condition and then apply for both air and water filtration.

1. Results and Discussion

1.1. Selection of the Membranes

PAN nanofiber layer was laminated under various conditions and 18 types of membranes were prepared. The selection of the filter membranes has been done based on their air permeability and bursting pressure as shown in Figure 1. Figure 1 is divided into 6 pieces according to the temperature and duration of lamination. In each piece, there are three values which show the lamination force in the order of 40, 50, and 100 kN, respectively. Membranes were selected according to high bursting pressure and the air permeability. Hence, there is no previous work dealing with optimum air permeability and the bursting pressure of membranes, we decided to select the membranes which had higher air permeability and bursting
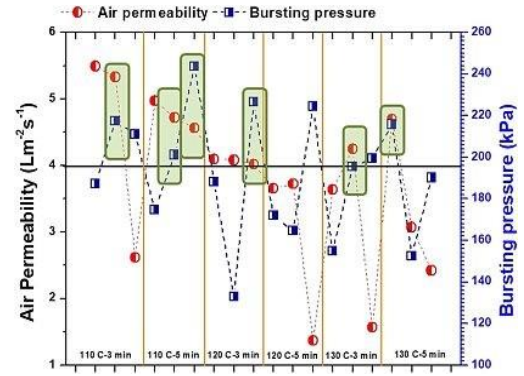

Figure 1. Effect of lamination conditions on air permeability and the delamination strength of various PAN membranes.

pressure. In this case, a line was drawn in Figure 1, on 4 $Lm^{-2}s^{-1}$ air permeability and 195 kN bursting pressure. The selective membranes were marked with a green square.

Based on the Figure 1, (a) the air permeability of the membranes decreased with increased temperature, applied lamination force, and lamination duration, (b) since, bursting pressure depends on both adhesion properties of the hybrid materials and the conditions of lamination, it is difficult to explain the relationship between bursting pressure and the lamination condition.

It is possible to say that, lamination force had an effect on bursting pressure, such as when the applied pressure increased the bursting pressure was increased. However, under high heat (130 °C) and long lamination period (5 min), the adhesive web and nanofiber layer lost its strength and resulted in low resistance to delamination. Results also suggested that the air permeability of the membrane was in direct proportion to the applied force of the lamination process. Higher applied force means, melted adhesive can penetrate through the pores of the nanofiber layer and reduce the porosity of the membrane. The melted adhesive covered the surface of the nanofiber layer. As a result, a non-fibrous, film structure can form on the surface as shown in Figure 2. The region of film adhesive on the surface of the membrane blocked the pores. Even though these regions
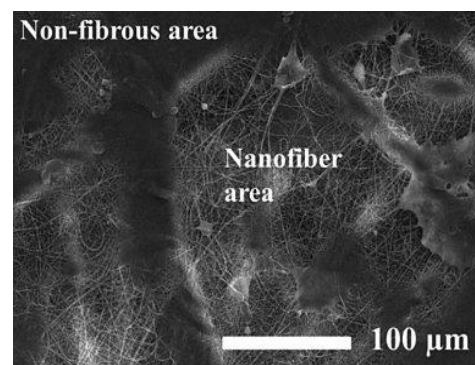

Figure 2. The surface of the PAN nanofibrous membrane after the lamination process.

are not demanded, these regions provide better adhesion between the support and nanofiber layer. To prepare an optimal material, it should be considered both permeability and the bursting resistance of the membranes.

The air permeability is an important criterion for the membrane permittivity, especially for the air filters. On the other hand, bursting pressure shows the necessary minimum pressure to destroy or to separate nanofiber layer from the supporting materials. In this case, selection high air permeability and the bursting pressure are demanded. Based on the results in Figure 1, only 5 membranes showed higher air permeability and at the same time higher bursting pressure. These membranes are; PAN_110_50_3, PAN_110_50_5, PAN_110_100_5, PAN_120_100_3, PAN_130_50_3, PAN_130_40_5.

1.1. Surface Characterization

The SEM images of the samples are taken and shown as in Figure 3. Comparing the diameter of the fiber, SEM images showed that after the lamination process, the fiber diameter increased almost 75 % more due to the structural change of PAN under heat and pressure. Unlike the literature finding,[36] hot press process affected the fiber diameter of PAN nanofibers. Sabantina et al.[37] observed that the diameter of the PAN nanofiber on the polypropylene substrate increased while the PAN nanofiber diameter stayed constant on aluminum foil after stabilization under 280 °C.

Under the force and applied temperature of the lamination, the fibers were getting flattened. Increasing applied temperature and the force caused fusion and bending. As a result, fiber diameter increased. Figure 3 (g) was taken to observe the fiber diameter under the highest force (100 kN), temperature (130 °C) and duration (5 min) of the lamination. Apparently, PAN_130_100_5 had the highest fiber diameter among the others. In the literature, it was found that applying heat treatment increased the fusion at interfiber contact points which increased the mechanical strength of the electrospun membranes.[38,39] The mechanical strength of the PAN nanofiber increased 760 times after hot-press process.[36] However, excessive lamination temperature, force, and duration may cause low mechanical strength and deterioration of the mechanical property.

Water contact angle of the membranes was measured and shown in Figure 4. The contact angle results indicate that membranes are hydrophobic which is not an advantage for liquid separation. Membranes which has a water contact angle greater than or equal to 90° is counted as hydrophobic membranes.[22] It was found that the hydrophobic PVDF became hydrophilic after the lamination process.[30] Unlike the PVDF membranes, the lamination conditions at given range did not change the wettability of the membranes. The previous work showed that neat PAN nanofiber has a contact angle around 70° under the lamination condition at a temperature of 135 °C and 50 kN pressure for 3 min.[40] That might be the melted effect of adhesive web and the changing of the PAN structure under high temperature. In general, it is known that hydrophobic membranes tend to foul easier than hydrophilic ones. For this
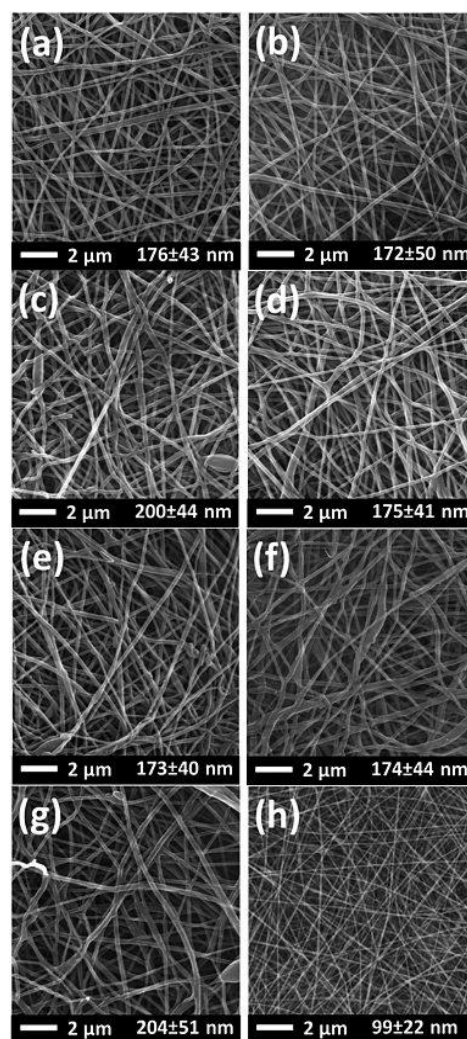

Figure 3. SEM images of a) PAN_110_50_3, b) PAN_110_50_5, c) PAN_110_100_5, d) PAN_120_100_3, e) PAN_130_50_3, f) PAN_130_40_5, g) PAN_130_100_5, and h) PAN nanofiber before lamination process.
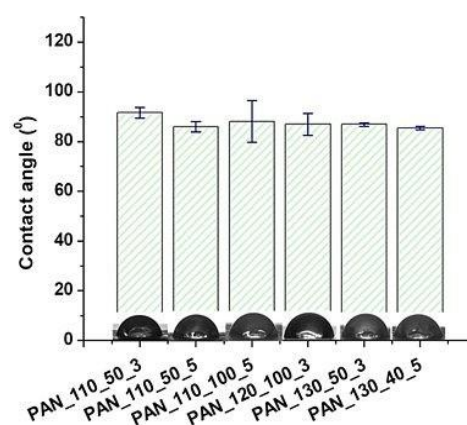

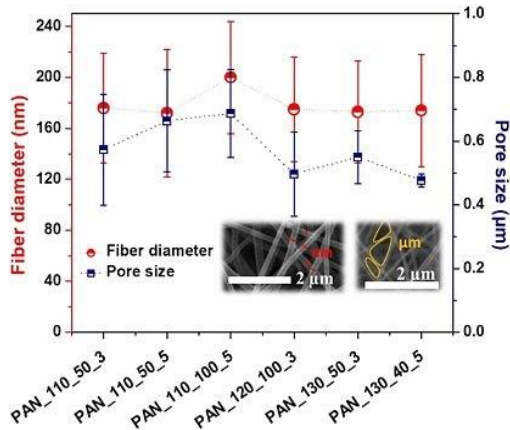**Figure 4.** Water contact angle of the electrospun PAN membranes.

Figure 5. Pore size vs. fiber diameter of the electrospun PAN membranes.

reason, a surface modification is required for the increase of the electrospun PAN membrane wettability. Previous works showed that the hydrophilic surface modification of electrospun PAN membrane with plasma treatment was not long lasting while additional chemical modification provided permeant wettability.[40,41]

Membrane pore size is an important criterion for the selectivity and the permeability of the membrane. Pore size, size distribution, and porosity are parameters that directly influence the air permeability of the nanofiber web. Fiber diameter plays a major role in the pore size of the nanofiber layers.[42–44] The average pore size according to the fiber diameter of the membranes is shown in Figure 5. The pore size and the fiber diameter of the membranes showed almost the same behavior. Pore size increased with fiber diameter. Li et al. showed that the pore size and pore size distribution of the polylactic acid (PLA) nanofiber membranes directly related to fiber diameter and area weight of the membrane.[45] Herein, the area weight of the membranes was kept the same while fiber diameter slightly changed depends on the lamination condition. In that case, it can be assumed that only fiber diameter and the lamination conditions are strongly associated with the pore size of the membranes. The adhesive during lamination process is melting and can fill pores of the membranes which might cause a reduction in pore size and porosity of the membranes. A proper lamination condition has to be determined without losing the performance of the membranes.

1.1. Filtration Results

Air filtration test was run and the removal of the particles in between $PM_{0.1}$ and $PM_{2.5}$ has been measured. Non-slip flow is the dominant mechanism for the high-efficiency particulate air (HEPA) and ultra-low particulate air (ULPA) filters. The problem of commercial HEPA and ULPA filters are that they can clog very easily due to the limited specific surface area.[9,46] Since the fiber size of the nanofibers is small in the nm range, the slip-flow mechanism becomes more important to disturb the

airflow.[47] As a result, the dust particles are collected to the surface not inside of the nanofiber layer which could improve the cleaning of the membranes.

The efficiency of the particle removal of the nanofibrous membranes is given in Figure 6. In all experiments, the superficial air velocity was 5 cm/s with a filter area 100 cm^2.
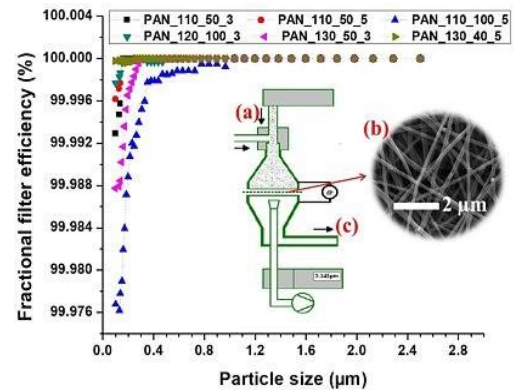

Figure 6. Filtration efficiency of the membranes against to various particle sizes and the schematic diagram of the filtration unit: a) dust particles, b) nanofibrous membrane, and c) filtered air.

Air filtration results indicated that all the membranes have superior filtration efficiency over than 99.97 % at various particle sizes. Among all membranes, PAN_130_40_5 showed highest filter efficiency (> 99.999 %) for the $PM_{0.1}$.

Zhao et al.[48] prepared PAN nanofibers in various fiber diameters using lithium chloride salt (LiCl) at various concentrations. The air transmission resistance of the PAN membranes was measured to verify slip flow of air molecules from the surface of the nanofibers. The slip-effect could be controlled by the fiber diameter at standard atmospheric condition. They found that the slip-effect was gradually weakening with the reduction of fiber diameter. Their results indicated that PAN fibrous membranes with the optimized parameters showed very high $PM_{2.5}$ purification efficiency of 99.09 %, low air resistance of 29.5 Pa, and long service life. In this work, since the fiber diameter of the membranes are almost equal after the lamination process, the lamination condition was the only effective parameter on the permeability of the membranes. To characterize the filter performance, quality factor (*QF*) was calculated. The *QF* of the membranes was calculated using the Eq. 1:[48,49]

$$QF = \ln(1-n)/\Delta P \qquad (1)$$

where *P* is the pressure drop, and *n* is the filtration efficiency. The quality factor has been calculated for the $PM_{0.1}$. The *QF* of PAN membranes are given in Figure 7. *QF* is directly proportional to filtration efficiency while was negatively proportional to the pressure drop. The higher the *QF* means the better the filter performance. Herein, both PAN 110_50_3 and PAN_130_40_5 showed the highest *QF* among the other membranes. The
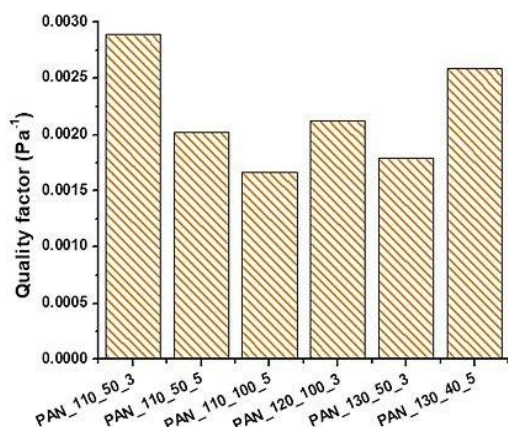
Figure 7. *QF* of various PAN nanofibrous membranes.

PAN_130_40_5 showed not only the better dust filtration efficiency, but also *QF* compared to other PAN membranes.

The results indicated that PAN nanofibrous membranes had high particle separation efficiency for coarse and fine particles. However, the air permeability of the PAN membranes was extremely low (lower than 6 $Lm^{-2}s^{-1}$) which increase the pressure drop and low energy saving for long-term use. In general, nanofiber webs itself have a very low-pressure drop. After the lamination process, most probably the melted adhesive web filled to pores of nanofiber web and decreased the porosity of the membranes. As a result, the air permeability decreased. However, PAN membranes can be potentially employed as HEPA filter with high efficiency in clean air applications such as in airplanes, hospitals, and clean rooms.

The water permeability test was run using tap water. The tap water is not pure; it contains several minerals, inorganics, hormones, fluorine compounds, etc. that can cause membrane fouling. The water permeability test was run to proof whether the membranes were suitable for water treatment or not. The results are given in Figure 8. The results indicated that the
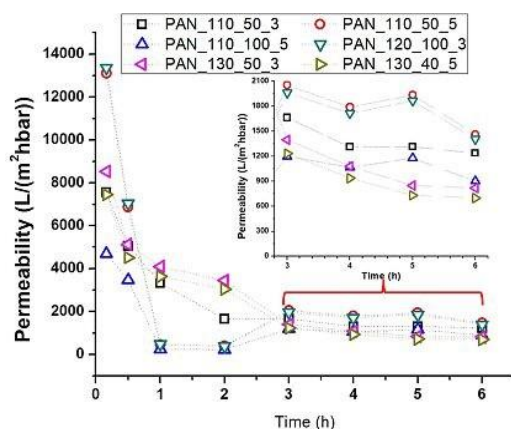

Figure 8. Water permeability of the various PAN nanofibrous membranes during 6 h.

permeability of the membranes was over than 4000 L/(m^2 hbar). However, the permeability reduced gradually through the membrane in time due to several possible reasons such as concentration polarization and membrane fouling.[26,50,51] After 3 h of operation, the membrane permeability reached to steady-state. Among the all membranes, PAN_110_50_3, PAN_110_50_5 and PAN_120_100_3 showed the highest permeabil- ity (> 1200 L/(m^2 h bar)) after 6 h of operation. On the other hand, membranes that laminated at the highest temperature (130 °C) showed the lowest permeability which is almost half of other membranes (> 600 L/(m^2 h bar)). The results indicated lamination temperature had an influence on the water perme- ability of PAN nanofibrous membranes. It was found that heated PAN nanofibers over their glass temperature, the segmental mobility of the molecular chains and dipole-dipole interaction of the nitrile groups increased. The nitrile groups started to release from their bound state. As a result, crystallization of the fiber improved.[52–54] Herein, the temper- ature most probably affects the crystalline structure and pore size (Figure 5) of the PAN membranes which may reduce the water permeability. It was found that water absorption rate decreased with an increased crystallinity of the polymer.[55–57]

It can be generalized that PAN nanofibrous membranes that laminated using heat-press showed extremely high permeabil- ity compared to that literature[58,59] which showed less than 400 L/(m^2 hbar) for pure water permeation.

Hwang et al.[60] compared three types of commercial membranes for crossflow microfiltration. The membranes were MF-Millipore® (made of mixed cellulose esters), Durapore® (made of modified polyvinylidene difluoride) and Isopore® (made of bisphenol polycarbonate) membrane with the same mean pore size of 0.1 µm. The results indicated that Isopore membrane showed the highest flux rate ($\approx 5\times 10^5$ L/(m^2s)) compared to MF-Millipore ($\approx 4\times 10^5$ L/(m^2s)) and Durapore ($\approx 2\times 10^5$ L/(m^2 s)) membranes after 3000 second of operation time. The flux rates of the membranes in this work were changed in between 1×10^5 L/(m^2 s) (PAN_110_100_5) and 2×10^5 L/(m^2 s) (PAN_130_50_3) after 3600 seconds of operation time. The filtration test results indicated that PAN membranes are comparable with the commercial membranes without any post-treatment.

The results indicate, PAN nanofibrous membranes that laminated under various condition showed enormous water permeability. Electrospun PAN nanofibrous membrane seems a good candidate for the treatment of wastewater. Comparable results were obtained in the literature using PVDF nanofibrous membranes.[30] The PVDF nanofibrous membranes that were laminated under different condition using the same heat-press system showed very high water permeability. It can be concluded that the heat-press lamination system is suitable for the preparation of nanofibrous membranes for water treatment.

1. Conclusions

PAN nanofibers were laminated under various conditions and tested as air and liquid filtration in order to assay whether these

laminated membranes are suitable for end use or not. The air permeability and the burst pressure tests determined the selective membranes according to their permeable structure and resistance to delamination. Selected membranes used for air and water filtration. The air filtration results showed the membranes had very high filtration efficiency ($\geq$ 99.97) for $PM_{0.1}$. However, the membranes showed very low air permeability due to adhesion method. The adhesive between the membrane and support melted and reduced the porosity of the membrane. The low air permeable membranes require more energy and which is costly. The air permeability problem can be overcome using different lamination technique. Conversely, PAN membranes showed very high water permeability (> 600 L/(m^2 h bar)) after 6 h of operation. Results indicate that electrospun PAN nanofibrous membranes laminated by heat-press are more suitable for water domain application compared to air filtration. Hence, the aim of this work is the investigation of the lamination process and effect on air and water filtration, the self-cleaning property and the surface modification of PAN membranes will be studied as future work.

Experimental Section

Preparation of Membranes

8% wt. of PAN (150 kDa H-polymer, Elmarco, Liberec, Czech Republic) was prepared in N, N-dimethylacetamide (DMAc) and mixed over the night. The solvent was purchased from Penta s.r.o. (Prague, Czech Republic). The prepared solution was electrospun using needle-free electrospinning equipment (Nanospider NS 8S1600U, Elmarco, Liberec, Czech Republic). The spinning conditions were determined as; + 55kV/-15 kV voltage with a distance between the electrodes was 188 mm. The humidity and the temperature were set as unchanged by using an air controlling unit as 20 % RH and 23 °C. A backing paper was used as collecting material for the nanofiber with a speed of 15 mm/min. The final density of the nanofiber web was 3 g/m^2. The details of the electrospinning system and the spinning conditions were given in somewhere else.[26]

Prepared nanofiber webs were undergone to a lamination process to combine nanofibers onto a suitable substrate for filtration application. A co-polyamide adhesive web (Protechnic, Cernay, France) was used between 100 g/m^2 polyethylene terephthalate spun bond nonwoven supporting layer (Mogul Co. Ltd., Gaziantep, Turkey) and the PAN nanofiber to adhere layers. For this aim, heat-press (hot-press) equipment is used (Pracovni Stroje, Teplice, Czech Republic). Lamination condition was optimized by changing of applied heat, force and the duration of lamination time. Table 1 shows the lamination condition and the abbreviation of each sample. 18 samples were prepared and tested. The abbreviation of the samples was given according to the name of nanofiber_lamination temperature_lamination force_duration of lamination.

Characterization of the Membranes

Scanning electron microscope (SEM, Vega 3SB, Brno, Czech Republic) and Krüss Drop Shape Analyzer DS4 (Krüss GmbH, Hamburg, Germany) were used to determine both surface shape and contact angle of the samples. At least 50 measurements for fiber diameter and 5 measurements for the contact angle were

Table 1. Preparation of nanofibrous membranes under various lamination conditions.

Nanofiber	Temperature [°C]	Applied force [kN]	Time [min]	Abbreviation
PAN	110	40	3	PAN_110_40_3
		50		PAN_110_50_3
		100		PAN_110_100_3
		40	5	PAN_110_40_5
		50		PAN_110_50_5
		100		PAN_110_100_5
	120	40	3	PAN_120_40_3
		50		PAN_120_50_3
		100		PAN_120_100_3
		40	5	PAN_120_40_5
		50		PAN_120_50_5
		100		PAN_120_100_5
	130	40	3	PAN_130_40_3
		50		PAN_130_50_3
		100		PAN_130_100_3
		40	5	PAN_130_40_5
		50		PAN_130_50_5
		100		PAN_130_100_5

done. The pore size of the samples was measured according to capillary flow porosimetry theory using a custom-made device in our laboratory.

Burst-pressure of the nanofiber layer from the supporting layer was measured by the device built in our laboratory.[26] Using burst-pressure, the minimum strength to burst nanofibrous membranes was measured.

Filtration tests

The air permeability of all multilayer nanofibrous membranes was tested using an SDL ATLAS Air Permeability Tester (@200 Pa and 20 cm^2, South Carolina, US). At least three measurements were taken for each sample.

For air filtration, the particle filtration test for the selected membranes done was by MPF 1000 HEPA filtration device (PALAS GmbH, Karlsruhe, Germany) in between $PM_{0.1}$ and $PM_{2.5}$.

A cross-flow filtration unit was built in our laboratory for the water filtration test as shown in Figure 9. The flux (F) and the permeability
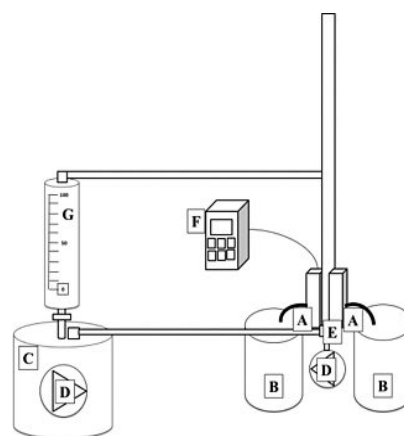

Figure 9. A cross-flow unit: A) membrane cells, B) permeate, C) feed, D) pump, E) surface bubble cleaning, F) pressure controller, G) feed flow speed controller.

(k) of the selected membranes were calculated according to Eq. (2) and (3):

$$F = (1/A)(dV/dt) \tag{2}$$

$$k = (F/p) \tag{3}$$

where A is the effective membrane area (m^2), V is the total volume of the permeate (L), p is the transmembrane pressure (bar), and t is the filtration time (h).

Acknowledgements

Conflict of Interest

The authors declare no conflict of interest.

[1] M. J. H. Worthington, R. L. Kucera, I. S. Albuquerque, C. T. Gibson, A. Sibley, A. D. Slattery, J. A. Campbell, S. F. K. Alboaiji, K. A. Muller, J. Young, *Chem. Eur. J.* **2017**, *23*, 16219–16230.

[2] A. Nomura, C. W. Jones, *Chem. Eur. J.* **2014**, *20*, 6381–6390.

[3] R. Zhang, Z. Yu, L. Wang, Q. Shen, X. Hou, X. Guo, J. Wang, X. Zhu, Y. Yao, *Chem. Eur. J.* **2017**, *23*, 13696–13703.

[4] A. F. W. Ho, W. Wah, A. Earnest, Y. Y. Ng, Z. Xie, N. Shahidah, S. Yap, P. P. Pek, N. Liu, S. S. W. Lam, *Int. J. Cardiol.* **2018**, *271*, 352–358.

[5] W. H. Organization, "Ambient (outdoor) air quality and health," can be found under http://www.who.int/en/news-room/fact-sheets/detail/ambient-(outdoor)-air-quality-and-health, **n.d.**

[6] R. D. Brook, S. Rajagopalan, C. A. Pope, J. R. Brook, A. Bhatnagar, A. V. Diez-Roux, F. Holguin, Y. Hong, R. V. Luepker, M. A. Mittleman, *Circulation* **2010**, *121*, 2331–2378.

[7] C. A. Pope, R. T. Burnett, G. D. Thurston, M. J. Thun, E. E. Calle, D. Krewski, J. J. Godleski, *Circulation* **2004**, *109*, 71–77.

[8] I. Markevych, F. Tesch, T. Datzmann, M. Romanos, J. Schmitt, J. Heinrich, *Sci. Total Environ.* **2018**, *642*, 1362–1368.

[9] V. V Kadam, L. Wang, R. Padhye, *J. Ind. Text.* **2018**, *47*, 2253–2280.

[10] M. Mahdi, A. Shirazi, A. Kargari, S. Ramakrishna, J. Doyle, M. Rajendrian, P. Ramesh Babu, *J. Membr. Sci. Res.* **2017**, *3*, 209–227.

[11] D. Groitzsch, E. Fahrbach, *Microporous Multilayer Nonwoven Material for Medical Applications*, **1985**, US4618524A.

[12] F. Yalcinkaya, *Arab. J. Chem.* **2016**, DOI 10.1016/j.arabjc.2016.12.012.

[13] L. F. Charles, M. T. Shaw, J. R. Olson, M. Wei, *J. Mater. Sci. Mater. Med.* **2010**, *21*, 1845–1854.

[14] A. R. Jahanbaani, T. Behzad, S. Borhani, M. H. K. Darvanjooghi, *Fibers Polym.* **2016**, *17*, 1438–1448.

[15] L. E. Charles, E. R. Kramer, M. T. Shaw, J. R. Olson, M. Wei, *J. Mech. Behav. Biomed. Mater.* **2012**, *17*, 269–277.

[16] R. Liu, L. Ma, J. Mei, S. Huang, S. Yang, E. Li, G. Yuan, *Chem. Eur. J.* **2017**, *23*, 2610–2618.

[17] E. Wirth, L. Sabantina, M. Weber, K. Finsterbusch, A. Ehrmann, *Nanomaterials* **2018**, *8*, 746.

[18] F. Yalcinkaya, M. Komarek, D. Lubasova, F. Sanetrnik, J. Maryska, *Nanocon 2014, 6th Int. Conf.* **2015**.

[19] J. Malašauskienė, R. Milašius, *J. Nanomater.* **2013**, *2013*, 1–6.

[20] F. Yalcinkaya, M. Komarek, D. Lubasova, F. Sanetrnik, J. Maryska, *J. Nanomater.* **2016**, *2016*, 1–7.

[21] C. K. Liu, H. J. He, R. J. Sun, Y. Feng, Q. shi Wang, *Mater. Des.* **2016**, *112*, 456–461.

[22] F. Yalcinkaya, B. Yalcinkaya, J. Hruza, P. Hrabak, *Sci. Adv. Mater.* **2016**, *9*, 747–757.

[23] M. Kanafchian, M. Valizadeh, A. K. Haghi, *Korean J. Chem. Eng.* **2011**, *28*, 445–448.

[24] B. Yalcinkaya, F. Yalcinkaya, J. Chaloupek, *J. Nanomater.* **2016**, *2016*, 1–12.

[25] B. Yoon, S. Lee, *Fibers Polym.* **2011**, *12*, 57–64.

[26] F. Yalcinkaya, J. Hruza, *Nanomaterials* **2018**, *8*, 272.

[27] W. Liu, S. Wang, M. Xiao, D. Han, Y. Meng, *Chem. Commun.* **2012**, *48*, 3415–3417.

[28] F. Yalcinkaya, B. Yalcinkaya, J. Hruza, P. Hrabak, J. Maryska, in *NANOCON 2016 - Conf. Proceedings, 8th Int. Conf. Nanomater. - Res. Appl.*, TANGER, Brno, **2016**.

[29] P. Valipour, V. Babaahmadi, K. Nasouri, *Adv. Polym. Technol.* **2014**, *33*, DOI 10.1002/adv.21440.

[30] R. Roche, F. Yalcinkaya, *Nanomaterials* **2018**, *8*, 771.

[31] T. Jiříček, M. Komárek, J. Chaloupek, T. Lederer, *Desalin. Water Treat.* **2017**, *73*, 249–255.

[32] T. Jiříček, M. Komárek, J. Chaloupek, T. Lederer, Komá, M. Rek, J. Chaloupek, T. Lederer, *J. Nanomater.* **2016**, *2016*, 1–7.

[33] B. Yalcinkaya, F. Yalcinkaya, J. Chaloupek, *Desalin. Water Treat.* **2017**, *59*, 19–30.

[34] Y. Mei, C. Yao, K. Fan, X. Li, *J. Membr. Sci.* **2012**, *417–418*, 20–27.

[35] F. Yalcinkaya, A. Siekierka, M. Bryjak, *Polymers (Basel).* **2017**, *9*, 679.

[36] A. A. Ali, G. C. Rutledge, *J. Mater. Process. Technol.* **2009**, *209*, 4617–4620.

[37] L. Sabantina, M. Á. Rodríguez-Cano, M. Klöcker, F. J. García-Mateos, J. J. Ternero-Hidalgo, Al Mamun, F. Beermann, M. Schwakenberg, A. L. Voigt, J. Rodríguez-Mirasol, *Polymers (Basel).* **2018**, *10*, 735.

[38] Z. Ma, M. Kotaki, S. Ramakrishna, *J. Membr. Sci.* **2005**, *265*, 115–123.

[39] L. Zhang, L.-G. Liu, F.-L. Pan, D.-F. Wang, Z.-J. Pan, *J. Eng. Fibers Fabr.* **2012**, *7*, 7–16.

[40] F. Yalcinkaya, *J. Appl. Polym. Sci.* **2018**, *135*, 46751.

[41] F. Yalcinkaya, A. Siekierka, M. Bryjak, *RSC Adv.* **2017**, *7*, 56704–56712.

[42] R. A. Abuzade, A. Zadhoush, A. A. Gharehaghaji, *J. Appl. Polym. Sci.* **2012**, *126*, 232–243.

[43] S. J. Eichhorn, W. W. Sampson, *J. R. Soc. Interface* **2010**, *7*, 641–649.

[44] M. Krifa, W. Yuan, *Text. Res. J.* **2016**, *86*, 1294–1306.

[45] D. Li, M. W. Frey, Y. L. Joo, *J. Membr. Sci.* **2006**, *286*, 104–114.

[46] A. Podgórski, A. Bałazy, L. Gradoń, *Chem. Eng. Sci.* **2006**, *61*, 6804–6815.

[47] S. Sundarrajan, K. Luck Tan, S. Huat Lim, S. Ramakrishna, *Procedia Eng.* **2014**, *75*, 159–163.

[48] X. Zhao, S. Wang, X. Yin, J. Yu, B. Ding, *Sci. Rep.* **2016**, *6*, 35472.

[49] Z. Jiang, H. Zhang, M. Zhu, D. Lv, J. Yao, R. Xiong, C. Huang, *J. Appl. Polym. Sci.* **2018**, *135*, 45766.

[50] P. Aimar, M. Meireles, P. Bacchin, V. Sanchez, in *Membr. Process. Sep. Purif.*, Springer Netherlands, Dordrecht, **1994**, pp. 27–57.

[51] H. Rezaei, F. Z. Ashtiani, A. Fouladitajar, *Braz. J. Chem. Eng.* **2014**, *31*, 503–518.

[52] M. Sadrjahani, S. A. Hosseini Ravandi, *Fibers Polym.* **2013**, *14*, 1276–1282.

[53] J. C. Masson, *Acrylic Fiber Technology and Applications*, M. Dekker, **1995**.

[54] A. K. Gupta, A. K. Maiti, *J. Appl. Polym. Sci.* **1982**, *27*, 2409–2416.

[55] Y. Lin, W. Zhong, L. Shen, P. Xu, Q. Du, *J. Macromol. Sci. Phys.* **2005**, *44 B*, 161–175.

[56] T. Negoro, W. Thodsaratpreeyakul, Y. Takada, S. Thumsorn, H. Inoya, H. Hamada, in *Energy Procedia*, Elsevier, **2016**, pp. 323–327.

[57] D. W. Auckland, R. Cooper, in *Conf. Electr. Insul. Dielectr. Phenom. - Annu. Rep. 1974*, IEEE, **1974**, pp. 71–79.

[58] N. Scharnagl, H. Buschatz, *Desalination* **2001**, *139*, 191–198.

[59] Y. Xu, Q. Wei, *Functional Nanofibers and Their Applications*, Woodhead Publishing, **2012**.

[60] K. J. Hwang, T. T. Lin, *J. Membr. Sci.* **2002**, *199*, 41–52.

4.3. Surface Modification and Application of Nanofiber Membranes in Water Treatment

The application of nanofibers in membrane technology is quite problematic due to various technical obstacles mentioned in "*Chapter 1-Main problems*". During our research, we tried to focus on introducing nanofiber webs into liquid separation applications and tried to solve problems one by one in the frame of our limits and efforts. Besides the preparation of nanofiber membranes, we focused on the possible applications. Moreover, to improve nanofiber permeability, selectivity, rejection, and fouling resistance property, surface modification has been introduced to nanofiber membranes. In the following reprints, we represent results for the how-to modify nanofiber membrane surfaces, application of nanofiber layers for the separation of oily wastewater from a different source, application of nanofiber membrane as thin film support layer for the separation of seawater and chiral component. The main results of the reprints include;

Application of polyamide nanofiber membrane (prepared by different adhesion method) for the separation of pitch and tar oils, engine oil/water mixture, and kitchen oil/water mixture: Based on the results, it can be suggested that polyamide nanofiber membrane is suitable for the separation of wastewater from industry and engine oil/water mixture but not for the kitchen oil (first reprint)

Surface modified nanofiber membranes for separation of kitchen oil: Two different approaches are followed. In the first, the membrane surface is activated by plasma, and then chemical modification is followed. In the second approach, nanoparticles (NPs) have been incorporated on the nanofiber surface. In both cases, the membrane showed too high flux and selectivity for the water in the oil/water mixture. Incorporation of NPs improved membrane fouling resistance. In all research, the mixture of oil/water prepared half to half and in emulsion form, which caused membranes to foul easily. However, modified nanofiber membranes showed outstanding performance with fouling resistance properties promising for the domestic wastewater separation process (reprints 2-5).

Thin film composite nanofiltration membranes (TFCN) based on laminated nanofibrous and nonwoven supporting material: Nanofiber membranes as support layer offer advantages on classical nonwoven material for the thin film composite (TFC) membranes. The nanofibers provide an increased surface area, intrinsically high porosity with an interconnected pore structure and high surface porosity, which increases the effective membrane area by reducing the amount of thin film layer masked by the support layer. In the last two reprints, the nanofiber membrane has been used as a supporting layer for the thin film composite nanofiltration (reprints 6-7). In the one attempt, seawater desalination has been done, and our membranes had high flux and ion rejection for real seawater with a high amount of salt ions. In the second attempt, it is the first time a unique combination of nonporous composite membranes with the microfibrous structures together with the chiral active substance used at the same time for the separation of chiral drugs. The separation has been done from liquid phases by pertraction that uses an adsorption-enantioselective membrane.

All the work submitted in this habilitation thesis suggests that nanofibers are a good candidate for membrane technology.

Reprint:

1. Yalcinkaya F, Yalcinkaya B, Hruza J. Electrospun Polyamide-6 Nanofiber Hybrid Membranes for Wastewater Treatment. Fibers and Polymers. 2019 Jan;20(1):93-9.
2. Yalcinkaya F, Siekierka A, Bryjak M. Surface modification of electrospun nanofibrous membranes for oily wastewater separation. RSC advances. 2017;7(89):56704-12.
3. Yalcinkaya F, Siekierka A, Bryjak M. Preparation of fouling-resistant nanofibrous composite membranes for separation of oily wastewater. Polymers. 2017 Dec;9(12):679.
4. Boyraz E, Yalcinkaya F, Hruza J, Maryska J. Surface-modified nanofibrous PVDF membranes for liquid separation technology. Materials. 2019 Jan;12(17):2702.
5. Torres-Mendieta R, Yalcinkaya F, Boyraz E, Havelka O, Wacławek S, Maryška J, Černik M, Bryjak M. PVDF nanofibrous membranes modified via laser-synthesized Ag nanoparticles for a cleaner oily water separation. Applied Surface Science. 2020 May 15:146575.
6. Yalcinkaya B, Yalcinkaya F, Chaloupek J. Thin film nanofibrous composite membrane for dead-end seawater desalination. Journal of Nanomaterials. 2016 Aug 1;2016.
7. Gaálová J, Yalcinkaya F, Cuřínová P, Kohout M, Yalcinkaya B, Koštejn M, Jirsák J, Stibor I, Bara JE, Van der Bruggen B, Izák P. Separation of racemic compound by nanofibrous composite membranes with chiral selector. Journal of Membrane Science. 2020 Feb 15;596:117728.

Electrospun Polyamide-6 Nanofiber Hybrid Membranes for Wastewater Treatment

Fatma Yalcinkaya[1,2]*, Baturalp Yalcinkaya[1], and Jakub Hruza[1,2]

[1]*Department of Nanotechnology and Informatics, Institute of Nanomaterials, Advanced Technologies and Innovation, Technical University of Liberec, Studentska 1402/2, Liberec 46117, Czech Republic*
[2]*Institute for New Technologies and Applied Informatics, Faculty of Mechatronics, Technical University of Liberec, Studentska 1402/2, Liberec 46117, Czech Republic*

Abstract: Electrospun nanofiber hybrid membranes have superior membrane performance due to their high specific surface area, narrow pore size, high porosity, and uniform pore size. Recently, increasing attention has been given to hydrophilic membranes such as polyamide 6 (PA6) in applications microfiltration and reverse osmosis. Electrospun PA6 nanofiber hybrid membranes have not found any real application due to their poor mechanical strength under high pressure. In this study, PA6 nanofiber layer was prepared using wire electrospinning method. Three supporting material with different adhesion method has been used to improve the mechanical properties of the membranes. Membranes were characterized with Scanning Electron Microscope images, pore size, and contact angle measurements. Tensile strength and the delamination tests were run to measure the mechanical properties of the membranes. Three types of wastewater were carried out during filtration; using real wastewater supplied from a company which consists of pitch and tar oils, engine oil/water mixture and kitchen oil/water mixture. Results indicated that the adhesion method and the supporting layer played a big role in the permeability of the membranes. The PA6 nanofiber hybrid membranes exhibited high water fluxes in even at low pressures which indicate that electrospun nanofiber membranes might be highly promising for microfiltration applications.

Keywords: Wastewater, Nanofiber, Membrane selectivity, Microfilter, Polyamide

Introduction

Membrane technology as an easy, efficient, versatile, chemical-free and low-cost method has been extensively used in many separation processes, such as water purification, desalination, distillation, and oily wastewater treatment. Despite these advantages of the membranes, the widespread application of the membranes for oily wastewater remains limited due to membrane fouling. The surfactant adsorption and/or pore sealing by oil droplets cause a severe decline of the flux and rejection rate. Several attempts have been done to improve the flux and rejection rate of the membranes. For instance, the mixing of inorganic nanoparticles has been found to be helpful for membrane permeability and fouling resistance by increasing the hydrophilicity or changing the pore structure of the membranes [1-6]. Genne *et al.* found that membrane permeability increased for growing amounts of inorganic zirconium oxide (ZrO_2) grains added to the casting solution which resulted in the formation of a highly porous surface layer [7]. Yan *et al.* prepared organic-inorganic composite membranes that were formed by nano-sized alumina particles in the poly(vinylidene fluoride) solution. The additional nano-sized Al_2O_3 particles improved the surface hydrophilicity of the membrane which increased the flux and antifouling performance of the membrane [2]. Ebert *et al.* investigated the influence of titanium dioxide (TiO_2) in poly (vinylidene fluoride) (PVDF) and polyamide-

imide (PAI) membranes. The membranes with the TiO_2 support showed significantly better permeate quality even at high-temperature range [5].

The demand for high performance and the efficient membrane has led to increasing attention in advanced functional nanofiber materials. Electrospun nanofiber hybrid membranes have superior membrane performance due to their high specific surface area, narrow pore size, high porosity, and uniform pore size while maintaining a very good permeation flux. These advantages can directly contribute to both high permeation flux and solute rejection ratio for microfiltration (MF) applications [8,9]. Moreover, the production cost of nanofiber hybrid membranes is estimated almost half compared to commercial membranes [10].

In this study, we demonstrate a novel microfiltration polyamide 6 (PA6) nanofibrous hybrid membrane, having an average fiber diameter of about 90 nm, laminated on various support with the various adhesive method. The aim of the lamination process is to enhance the mechanical strength of the membranes which can withstand external forces during liquid separation. The vast majority of all reported nanofibrous membrane research involves permeability and the selectivity of the membranes while there is not enough research has been done to improve the mechanical strength of the membranes. In our previous work, we focus on to improve the mechanical strength of the poly(vinylidene fluoride) and polyacrylonitrile nanofiber web [11]. Herein, PA6 nanofibers are used for liquid separation. The PA6 polymer has excellent mechanical properties including high tensile strength, high

---

*Corresponding author: fatma.yalcinkaya@tul.cz

flexibility, low creep, good resilience, and high impact strength (toughness). Moreover, it is very simple to produce PA6 nanofibers using electrospinning system. Although significant scientific activity has occurred with regards the use of polyamides as nanofibrous membranes, there is no previous work dealing with the improvement of mechanical strength of the PA6 nanofibrous hybrid membranes. The primary objective of this study is to prepare highly permeable and mechanically strong PA6 nanofibrous hybrid membrane prepared for the various wastewater treatments. For this aim, three types of feed solution were carried out for wastewater filtration; using real wastewater supplied from a company which consists of pitch and tar oils, engine oil/water mixture, and kitchen oil/water mixture and membrane performance has been evaluated.

Experimental

Preparation of Electrospun Membrane

12 % wt. of PA6 (BASF-Ultramid B24, Germany) solution were prepared by dissolving the polymer pellets in acetic acid/formic acid (2/1 % wt.) solvent mixture over the night. All the solvents were purchased from Penta s.r.o. (Prague, Czech Republic). The PA6 nanofiber layers were prepared using a lab-scale wire electrospinning system (Figure 1). The principle of wire electrospinning system has been introduced to literature several times [11-13]. In brief, the solution is placed in a solution tank, which is a closed system and connected to a solution bath. The positively charged wire electrode (60 kV) passes along a metal orifice in the middle of the solution bath. There is a solution bath with a speed of 240 mm/s which is moved back and forward to feed the surface of the wire electrode with a polymeric solution. Behind a mobile supporting backing paper (55 mm/min), a second wire electrode, which is connected to a negatively charged voltage supplier (-40 kV). The distance between the electrodes is 180 mm. While the spinning takes
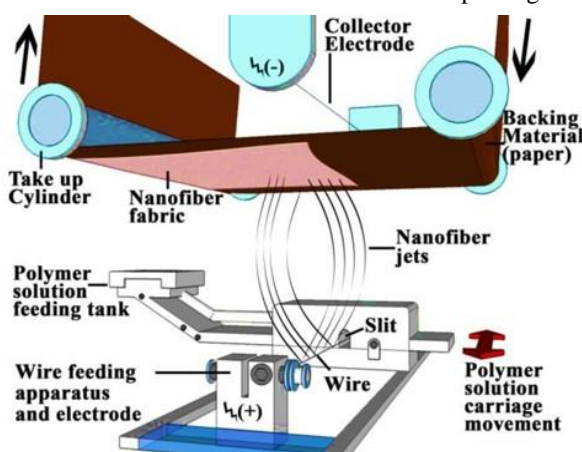

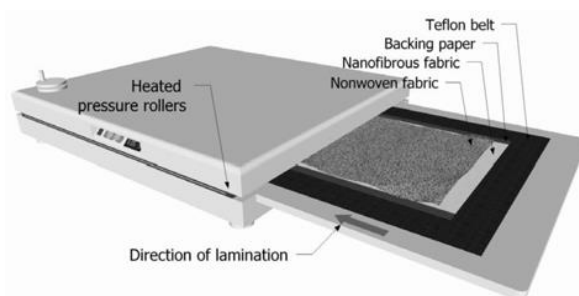Figure 1. Schematic diagram of wire electrospinning unit.

Figure 2. Schematic diagram of the lamination process.

place between the two electrodes, the polymeric nanofiber web is collected on baking paper. No solution dipping was observed. An air conditioning unit is used to control the relative humidity (31 %) and temperature (22 $^\circ$C) of the spinning in a closed chamber. The area weight of the PA6 nanofiber was set around 2 g/m^2.

The prepared nanofiber layers adhered onto various surfaces to enhance their mechanical properties. 17 g/m^2 polyethylene terephthalate (PET) woven web (plain weave structure), 20 g/m^2 bicomponent spunbond and 100 g/m^2 (PET) spunbond nonwoven webs were used as supporting material. Since it was not possible to get the same density of supporting layer from different suppliers, different density of supporting materials was used. Each supporting layer had a different adhesion method. For instance, 17 g/m^2 supporting layer had its own adhesive on the surface while it was purchased. The co-polyamide dot adhesive glue was used to adhere 17 g/m^2 woven web and PA6 nanofibers. The bi-component spunbond material was composed of polypropylene (inner) and polyethylene (outer) surface which showed an adhesion role for the PA6 nanofiber layers under heat and pressure. Since 100 g/m^2 nonwoven did not have any adhesive on the surface, a 3 g/m^2 co-polyamide net was used between the nonwoven and PA6 nanofiber layer. A mini fusing machine (Meyer, Germany) was used for the lamination process as shown in Figure 2 [14]. For lamination, the conditions are arranged as; speed of belt was 1.7 m/min, the temperature was 130 $^\circ$C and the pressure was 15 N/cm^2. The nanofiber layer was placed to the top of the adhesive surface which was connected to the supporting layer. Due to heat, pressure and the contact time of lamination, the adhesives were melted and adhered the nanofibers to the surface of the supporting layers. Abbreviations for the samples are given according to the density of the supporting material, such as PA6-17, PA6-20, and PA6-100.

Characterization of the Membrane

The surface characterizations of the membranes were done using a scanning electron microscope (SEM, Vega 3SB, Brno, Czech Republic). From each sample, at least 50 fibers were measured. The fiber diameter was analyzed and the

diameter distribution was evaluated. The surface contact angle of the samples was measured using a Krüss Drop Shape Analyzer DS4 (Krüss GmbH, Hamburg, Germany), at five different points, using distilled water (surface tension 72.0 mN m^{-1}) on the clean and dry samples at room temperature. A device was built in our laboratory to determine the maximum, average and minimum pore sizes. The bubble point test allowed the size of the pores of the porous material to be measured. The principle of the measurement was explained in previous work [11].

Mechanical Properties of the Membrane

The tensile strength of the membranes was measured using the universal testing machine (Labor-Tech s.r.o., CR) with the extension rate of 10 mm/min at room temperature. The samples were 100 mm long, 25 mm wide, and the distance between the two clamps was 50 mm. Both machine direction (MD), and the other the cross direction (CD) was measured. Another device was built in our laboratory for the measurement of the maximum resistance of the nanofiber layers for delaminating from the supporting layer [11]. The samples were placed between two rings. The sample size was 47 mm in diameter. Pressurized water was applied to the membrane, and the hydrostatic pressure was measured using a pressure controller. The hydrostatic pressure was increased gradually, and as soon as the nanofiber layer delaminated, the pressure value on the screen decreased sharply. The maximum pressure value was recorded as the bursting strength of the membrane. At least 3 measurements were done for each sample.

Filtration Test

Filtration test was done using a cross-flow filtration unit which was developed in our laboratory. Three types of feed solutions were prepared and tested during filtration. In the first test, a wastewater was supplied from an industrial company which has pitch and tar oil in the feed. In the second and the third tests, engine and kitchen (sunflower) oils in water were used as feed solutions. The amount of engine oil and the kitchen oil in 1 liter of water was 200 ml. The fraction of oil in feed solution was 20 % v/v. The velocity of the feed solution was 20 l/min.

The permeability (k) of the membranes was calculated using equation (1):

$$[k] = F/T_p \ (l/(\text{m}^2\text{hbar})) \tag{1}$$

where F is the flux of membranes in $l/(\text{m}^2\text{h})$ and T_p is the transmembrane pressure in bar.

Results and Discussion

Characterization of the Membrane

The SEM images of the membranes were taken after the lamination process to observe any possible damages (Figure 3). Fiber diameter distribution was evaluated. The results indicated that there was no visible damage observed on the surface of the nanofibers. The diameter of the nanofiber web is around 90 nm after the lamination process.

Despite no damage, it was observed that in some points the adhesive web was over the surface of the nanofibers and created blind points with zero pores as shown in Figure 4. It was not possible to get rid of these blind points for a proper lamination. From these blind points, fibers adhered to the substrate very strongly in a mechanical way.

Surface wettability of the membranes was investigated by using contact angle measurement. The results are shown in Figure 5.
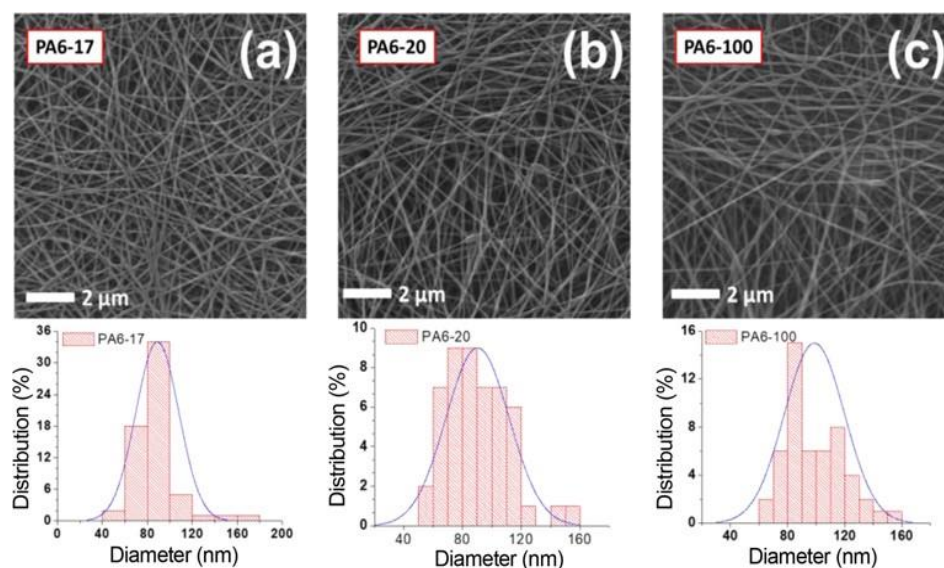

Figure 3. SEM images of the (a) PA6-17, (b) PA6-20, and (c) PA6-100 nanofibrous membranes.
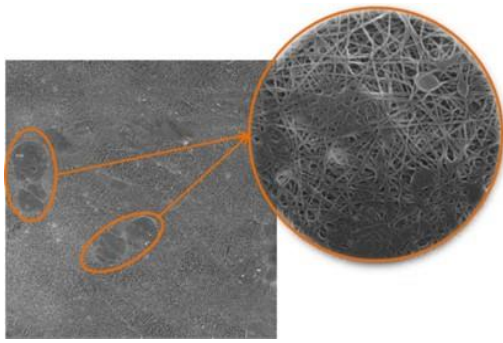
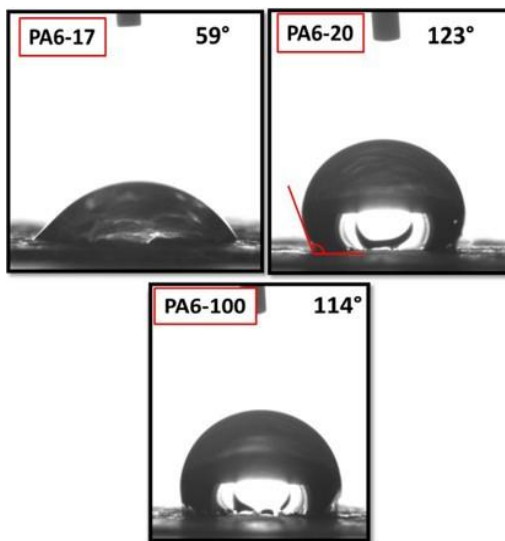Figure 4. Adhesives cover the surface of the nanofiber layer.

Figure 5. The contact angle of the various PA6 nanofibrous hybrid membranes.

The results of contact angle showed that even though the surface has the same polymeric nanofiber, each substrate showed different hydrophilicity. The main reason is due to adhesive glues. Since the adhesives covered the surface of nanofibers place to place, the material showed the characteristics of the adhesive web. For instance, the PA6-17 has co-polyamide dot glues which were distributed to the surface of the supporting material evenly. It seems that the co-polyamide used in PA6-17 had the hydrophilic characteristic. Aiba *et al*. found that N-methylated aromatic random co-polyamides of the amide linkages increased the chain mobility at the membrane surfaces and consequently enhanced the water-induced surface reorganization [15]. Konagaya *et al*. prepared flat asymmetric membranes of the co-polyamides which were hydrophilic characteristics [16]. In another work, the hydrophilicity of the polyolefin membranes was improved by preparing polyolefin-polyamide mixture [17].

The membrane PA6-20 showed the highest hydrophobicity due to polyolefin adhesive. One of the most known characteristics of polyolefin is their hydrophobicity.

In the case of PA6-100, a co-polyamide net was used as adhesive. The density of the web was 3 g/m^2 and with a very open structure which means, the contact area of the co-polyamide adhesive net with nanofibers are lower than that contact area of co-polyamide dots with nanofiber. Even though the hydrophilicity of the PA6-17 is superior compared to other membranes due to more adhesive glue on the nanofiber surface, we can expect that more pores of the nanofibers were filled with adhesive glue. As a result, the permeability of PA6-17 could be lower than other membranes. The information for the dot co-polyamide glue and the co-polyamide adhesive net has not been given by the supplier. There is also a possibility that both co-polyamide had different characteristics which would result in differences in wettability. Compared to contact angle results, we can say that the lamination method has a very huge effect on the hydrophilicity of the nanofibrous membranes. The hydrophilicity of the membranes can be change with adhesion method.

The mean pore size, tensile strength and the delamination strength of the membranes are given in Table 1.

The pore size of the membranes was determined by the PA6 nanofiber layer on the top. Since the same nanofiber layer was used, any change in the mean pore size has been observed. On the other hand, there was a huge difference in the mechanical properties of the membranes. The supporting layers under the nanofiber webs were determined the mechanical properties of the membranes. Since PA6-100 has the highest density, the tensile strength on both MD and CD was the highest compared to other membranes.

The PA6-100 showed the highest delamination resistance compared to other membranes. The reason could be due to the interaction between adhesive with nanofiber and adhesive with supporting layer. The adhesion between the layers was physically due to the van der Waals forces. The surface tension of each material plays a key role for intermolecular forces which determine the attraction of the materials. The strength of adhesion between the layers depends not only on the intermolecular interactions at the interface but also on the mechanical response of each material. There have been several proposed theory to explain the mechanism of the adhesion such as adhesion based on the surface properties (adsorption and wetting) [18], on

Table 1. Mechanical properties of the PA6 nanofibrous membranes

Sample	Mean pore size (µm)	Tensile strength (25 mm/N)		Max. delamination strength (kPa)
		MD	CD	
PA6-17	0.755±0.09	20.34±10.56	16.34±4.12	55±5.73
PA6-20	0.753±0.14	36.35±1.71	37.88±2.33	47±17.90
PA6-100	0.710±0.08	91.99±12.50	81.40±5.00	84±8.65

chemical interactions [19], on fracture mechanics, on diffusion [20] or on electrostatic interaction [21,22]. The adsorption theory has the widest applicability while the other theories may be appropriate in certain circumstances. In literature, it is proposed that one of the most important factors influencing adhesive strength is the ability of the adhesive to spread spontaneously on the substrate when the joint is initially formed [23]. Herein, the adhesion strength between the PA6-100 layers had the highest value.

Filtration Tests

In the first test, a wastewater from the industrial company has been used. The exact source of the water was not given by the company. The feed solution included pitch and tar oil. The permeability of the PA6 nanofibrous hybrid membranes has been evaluated and shown in Figure 6.

The permeability measurement was done during 15 hours. Obviously, the permeate flux rate is initially high and falls off rapidly with a time of filtration and flux attenuation becomes more and more rapid in time. There are some reasons for the decrease in permeability. The first reason is that membrane fouling. Membrane fouling is to increase the resistance to the flow of liquid through the membrane due to blocking the pores and deposition of a cake layer on the surface. The second reason is concentration polymerization. Moreover, the hydrophilicity of the membrane decreased over time during filtration due to membrane fouling and concentration polarization. After 6 hours of filtration, steady-state permeability has been observed for all the membranes. The main reason is that the cake layer reached the equilibrium thickness.

After 15 h of filtration test, the PA6-100 membrane showed much higher permeability than compared to others (over 400 l/m^2 hbar). There could be a few reasons. 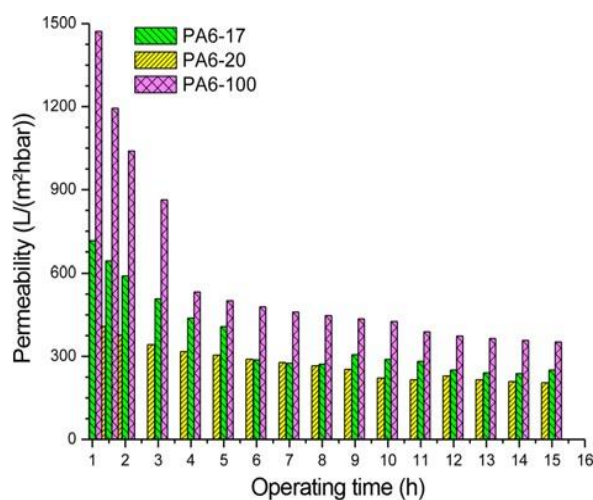In general, hydrophilic membranes could improve the membrane permeability. However, in some cases, hydrophilicity plays a disadvantage for membrane permeability. The microvoids could be generated as defects in the hydrophilic membranes, which may cause negative effects on membrane permeability and even causes the collapse of membranes under trans-membrane pressure [24]. Even though the PA617 had the highest hydrophilicity, the membrane performance was lower compared to PA6-100. Another reason could be the adhesive material filling the pores of the nanofibers. Since PA6-100 has less contact with adhesive web compared to PA6-17, the porosity is higher. Higher porosity results in higher permeability. Moreover, co-polyamide adhesive net was used for adhesion of PA6-100 while hydrophobic polyolefin surface was used for PA6-20. Since there was no way to get rid of adhesives from the top of the nanofiber layer, the hydrophobic structure of PA6-20 decreased the permeability and increased the membrane fouling. It was observed in the literature that hydrophobic membranes tend to foul easily due to the hydrophobic interaction between solutes, the membrane surface and pores [25,26].

The feed and the permeate solutions are given in Figure 7.

In the second step of the filtration test, the PA6-100 membrane was selected as an optimum membrane for engine oil/water separation due to high membrane permeability and mechanical strength. The results of permeability are given in Figure 8. Because of the high porosity of the PA6-100 nanofibrous membrane, the membrane exhibited outstanding performance including high permeability (around 524 $l/(m^2$ hbar)) and selectivity.

It was found that the engine oil separation test results were showing the same permeability decline as in the case of wastewater treatment. The membrane fouling is the main reason. PA6 is highly polar and has an affinity to water molecules which selectively allows the water molecules to pass through the membrane while restricting the passing for oil molecules. Apparently, PA6-100 is a hydrophilic/oleophobic membrane. The wetting behavior of the PA6-100 membrane

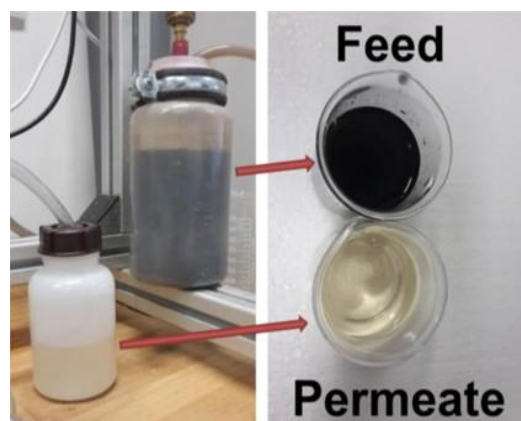Figure 6. Wastewater separation: Permeability of PA6 nanofibrous membranes after wastewater treatment.

Figure 7. Feed and permeate solution for the PA6-100 nanofibrous membrane for wastewater separation.

Figure 8. Engine oil/water separation: permeability of the PA6-100 nanofibrous membrane.
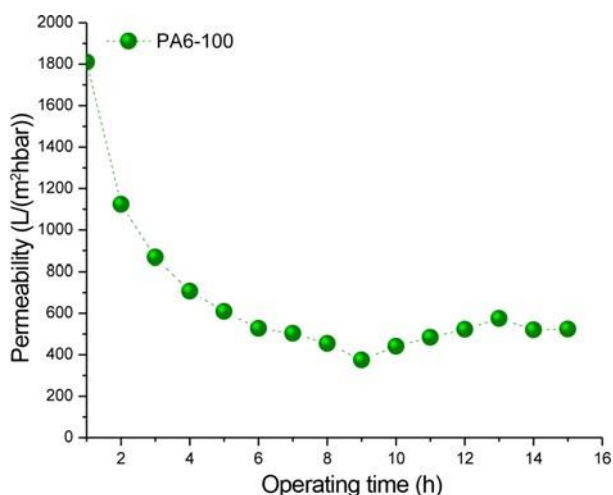

Figure 10. Kitchen oil/water separation: permeability of the PA6-100 nanofibrous membrane.

Figure 9. Feed and permeate solution for the PA6-100 nanofibrous membrane for engine oil/water separation.

allowed only water molecules to penetrate through the membrane and rejected oil molecules. The wetting behavior may be due to the small water molecules can penetration the polymer coating immediately while the large oil molecules cannot penetrate or penetrate much more slowly. There is another mechanism to explain the wetting behavior of the membranes. This mechanism proposed that the polymer coatings may take different conformations on top of the surface when faced with water and oil: more hydrophilic segments will be attracted with water, resulting in a hydrophilic property.

The feed and the permeate solutions are given in Figure 9.

In the third filtration test, kitchen oil/water mixture was used as feed solution. The water was colored to green with food colorant to better determination of selectivity. The permeability result of PA6-100 membrane is given in Figure 10.

The Figure 10 shows that unlike the wastewater or engine oil/water treatment, the permeability results of kitchen oil/ water separation is quite low. The reasons could be the size of different oils or the organic compounds of different oils. Oil droplets blocked the membrane surface by pore sealing. Moreover, the colorant effect should be considered. It is well known that PA membranes have an affinity for colorants. The food colorant could block the PA6 membrane pores and

Figure 11. Feed and permeate solution for the PA6-100 nanofibrous membrane for kitchen oil/water separation.

cause to fouling. The feed and the permeate solutions are given in Figure 11.

Oil droplets were clearly visible in the feed, whereas no droplets were observed in the permeate solution. Even though selectivity of the PA6-100 nanofibrous membrane for kitchen oil/water separation was very good, the permeability result was not sufficient. The results showed us that for oil separation; only selected oils can be successfully separated using a PA6 nanofibrous membrane. All the membranes suffered from the fouling. A post surface treatment is necessary to improve resistant to fouling.

Conclusion

In this work, a novel PA6 nanofiber hybrid membrane been successfully prepared for liquid filtration. To improve the mechanical strength of the nanofiber layers, various supporting layers with different adhesion method has been applied. The tensile strength and the delamination tests

showed that only PA6-100 membrane has the best performance. The permeability performance of PA6-100 membrane was superior in the separation of wastewater from industry and the oil from the engine oil/water mixture. The performance of PA6-100 membrane was extremely low for the separation of kitchen oil/water mixture. The PA6-100 nanofiber hybrid membrane seems promising for the wastewater treatment and only selected oily water separation. But prior to industrial operation, it seemed necessary to adjust an antifouling property of the membrane. In summary, this work could assist in obtaining a better understanding of the nanofiber hybrid membranes for liquid separation.

Acknowledgments

References

1. W. C. Chong, E. Mahmoudi, Y. T. Chung, M. M. BaAbbad, C. H. Koo, and A. W. Mohammad, *Desalin. Water Treat.*, 96, 12 (2017).

2. L. Yan, Y. S. Li, and C. B. Xiang, *Polymer (Guildf),* 46, 7701 (2005).

3. A. Bottino, G. Capannelli, V. D'Asti, and P. Piaggio, *Sep. Purif. Technol.*, 22-23, 269 (2001).

4. W. Chen, Y. Su, L. Zhang, Q. Shi, J. Peng, and Z. J. Jiang, *Memb. Sci.*, 348, 75 (2010).

5. K. Ebert, D. Fritsch, J. Koll, and C. J. Tjahjawiguna, *Memb. Sci.*, 233, 71 (2004).

6. G. Arthanareeswaran, T. Sriyamunadevi, and M. Raajenthiren, *Sep. Purif. Technol.*, 64, 38 (2008).

7. Genné, S. Kuypers, and R. Leysen, *J. Membr. Sci.*, 113, 343 (1996).

8. Y. Ko, Y. Choi, Y. Jang, J. Choi, and S. Lee, *Desalin. Water Treat.*, 97, 87 (2017).

9. M. J. A. Shirazi, S. Bazgir, M. M. A. Shirazi, and S. Ramakrishna, *Desalin. Water Treat.*, 51, 5974 (2013).

10. D. Bjorge, N. Daels, S. De Vrieze, P. Dejans, T. Van Camp, W. Audenaert, J. Hogie, P. Westbroek, K. De Clerck, and S. W. H. Van Hulle, *Desalination*, 249, 942 (2009).

11. F. Yalcinkaya and J. Hruza, *J. Nanomaterials*, 8, 272 (2018).

12. B. Yalcinkaya, F. Yalcinkaya, and J. Chaloupek, *J. Nanomater.,* Article No. 2694373, 2016 (2016).

13. F. Yalcinkaya, *Arab. J. Chem.,* doi:10.1016/j.arabjc.2016.12.012 (2016).

14. B. Yalcinkaya, F. Yalcinkaya, and J. Chaloupek, *Desalin. Water Treat.*, 59, 19 (2017).

15. M. Aiba, K. Ito, T. Tokuyama, H. Tomioka, T. Higashihara, M. Ueda, and H. Matsumoto, *Macromol. Chem. Phys.,* 219, 1 (2018).

16. S. Konagaya and M. Tokai, *J. Appl. Polym. Sci.*, 76, 913 (2000).

17. J. Meier-Haack, M. Valko, K. Lunkwitz, and M. Bleha, *Desalination*, 163, 215 (2004).

18. S. Wu, *J. Adhes.*, 5, 39 (1973).

19. A. Ahagon and A. N. Gent, *J. Polym. Sci. Polym. Phys. Ed.*, 7, 1285 (1975).

20. E. Helfand and Y. J. Tagami, *Chem. Phys.*, 56, 3592 (1971).

21. B. V. Derjaguin, N. A. Krotova, V. V. Karassev, Y. M. Kirillova, and I. N. Aleinikova, *Prog. Surf. Sci.*, 45, 95 (1994).

22. H. W. Kammer, *Acta Polym.*, 34, 112 (1983).

23. A. Kinloch, "Adhesion and Adhesives: Science and Technology", p.18, Springer Netherlands: Dordrecht, 1987.

24. Y. Zhu, D. Wang, L. Jiang, and J. Jin, *NPG Asia Mater.*, Article No. e101, 6 (2014).

25. K.-H. Choo and C.-H. Lee, *J. Colloid Interface Sci.*, 226, 367 (2000).

26. F. Y. Guo, P. C. Sun, and J. F. Wei, *Environ. Technol. (United Kingdom)*, 39, 3159 (2018).

RSC Advances

Surface modification of electrospun nanofibrous membranes for oily wastewater separation

Fatma Yalcinkaya, [iD] *[a] Anna Siekierka[b] and Marek Bryjak[b]

This paper presents a method for producing nanofibrous composite membranes for the separation of a vegetable oil–water mixture. Neat polyvinylidene fluoride (PVDF), polyacrylonitrile (PAN) nanofibres and PVDF/PAN mixtures were used to prepare the membranes. Argon plasma treatment, followed by a chemical surface modification, was applied to alter the hydrophilicity and oleophobicity of the membranes. The obtained results showed that the membranes change their surface character (hydrophilicity and oleophilicity) in relation to the mixing ratio of the PVDF/PAN nanofibres and the surface modification parameters. These results can extend the application of PVDF, PAN and PVDF/PAN nanofibrous membranes to the treatment of oily water.

1. Introduction

Oil–water emulsions emitted into the soil or water from domestic and industrial wastewater are one of the most severe issues that threaten human life and ecological systems, with a significant amount of oily wastewater generated every day. Thus, there is a growing demand to produce an oil–water separation system that has high selectivity, high efficiency, low fouling properties and is easy to apply and manage.

Microfiltration membranes are applied for oil–water separation treatment, along with other methods, such as bioremediation and chemical methods.[1–3] The production of high-performance membranes with anti-fouling properties still remains challenging. Surface absorption, surface grafting and blending are some of the methods used for the surface modification of membranes[4–10] to improve their anti-fouling properties. A hydrophilic membrane surface helps to reduce biofouling and protein adhesion in microfiltration. Blending materials is considered the simplest and most inexpensive approach for surface modification. Recently, the plasma modification method has attracted interest due to its extremely short modification time and non-destructive action. However, the modification is usually not permanent on most polymer surfaces, often disappearing within hours or days of treatment.[11–13] To counteract this phenomenon, a post-treatment method should be applied to provide a permanent surface modification.

Polyvinylidene fluoride (PVDF) is one of the most frequently used polymers in membrane technology due to its outstanding chemical, thermal and oxidation resistance properties,[14–16] while polyacrylonitrile (PAN) is a common polymer that is characterised by its thermal stability, tolerance to most solvents, strong antioxidant capacity and commercial availability.[17,18] PVDF has better mechanical properties than PAN.[19] PAN is a hydrophilic polymer, whereas PVDF is a hydrophobic polymer. The versatility of both polymers thus makes them suitable for manufacturing membranes for liquid/liquid and liquid/solid separations.

The objective of this paper is to evaluate the properties of modified nanofibrous composite membranes obtained from PVDF, PAN and PVDF/PAN mixtures. Mixing the polymers should increase the hydrophilicity of the nanofibre web while also increasing the strength of the web by binding its fibres together. However, the main disadvantage regarding the use of nanofibres in filtration is their lack of mechanical integrity. Two of the novelties of this paper are that the nanofibre layers were produced with the Nanospider industrial equipment,[20] and that the layers strongly adhered to a nonwoven supporting layer without any damage, using hot-press lamination technology to improve their performance in liquid filtration applications. The microwave plasma technique, followed by a chemical post-treatment, was used to hydrophilise the membrane surfaces. While similar papers dealing with the plasma modification of polymer membranes have been published,[21–26] none have considered the use of a nanofibre web surface modification with both plasma and chemical treatments for liquid/liquid and liquid/solid separations. This study may thus provide a better understanding of the effects of surface modifications on the permeability and liquid selectivity of the membranes as a function of chemical modification time.

[a]Technical University of Liberec, Institute for Nanomaterials, Advanced Technology and Innovation, Studentska 1402/2, 46117 Liberec, Czech Republic. E-mail: yenertex@hotmail.com

[b]Wroclaw University of Science and Technology, Faculty of Chemistry, 27 Wybrzeze Stanislawa, Wyspianskiego, 50-370 Wroclaw, Poland

93

PAN (Elmarco s.r.o., Czech Republic) was dissolved in dimethylformamide (DMF) to produce an 8% wt. PAN solution, and PVDF (Solef 1015, Belgium) was dissolved in dimethylacetamide (DMAc) to produce a 13% wt. PVDF solution. The DMF and DMAc solvents were purchased from Penta s.r.o., Czech Republic. The solutions were stirred overnight. Five different samples were prepared, defined by their PVDF/PAN nanofibre blend ratios (Table 1). A Nanospider electrospinning device (Elmarco s.r.o., Czech Republic) was used to produce the nanofibres under controlled and stable processing conditions, following previous studies (Fig. 1).[27] A solution carriage feeds the polymer solution on a 0.2 mm moving stainless steel wire. The speed of the carriage is 245 mm s[1]. High voltage suppliers are connected to the wire electrode (60 kV) and the collector electrode (15 kV). When the applied voltage exceeds a critical value, the polymer solution jets move towards the collector, the solvent evaporates, and the nanofibre web is collected on baking paper moving in front of the collector electrode. The speed of the movement of the baking paper is 10 cm min[1]. The distance between the electrodes is 18 cm. The temperature and humidity of input air are set to 23 C and 20% by the air-conditioning system. The intake and outlet airflows are 100 and 115 m[3] h[1], respectively.

The zero-shear viscosity of the polymer solutions was measured using a Fungilab Expert viscometer at 23 C.

Pressure-driven liquid filtration applications require that the membranes possess sufficient mechanical strength to withstand the operational conditions. The nanofibres were thus laminated onto a nonwoven spunbond supporting material to improve the mechanical strength of the membranes. The surface of the membranes was characterised by Scanning Electron Microscope (SEM, Vega 3SB) and the fibre diameters were analysed using the Image-J image processing software. The surface contact angle of the samples was measured at room temperature using a Kruss Drop Shape Analyzer DS4 with distilled water on the clean and dry samples. The PVDF/PAN mixture of polymeric nanofibres was evaluated using Fourier transform infrared spectroscopy (FTIR, Nicolet iZ10 by Thermo Scientific). A 1200-AEL capillary flow porometer (Porous Media Inc., Ithaca, NY) was used in this study to measure the pore size of the samples.

The prepared nanofibrous composite membranes were cut into 5 cm 5 cm squares and subjected to the standard plasma treatment.[10] Microwave-induced low vacuum argon (Ar) plasma
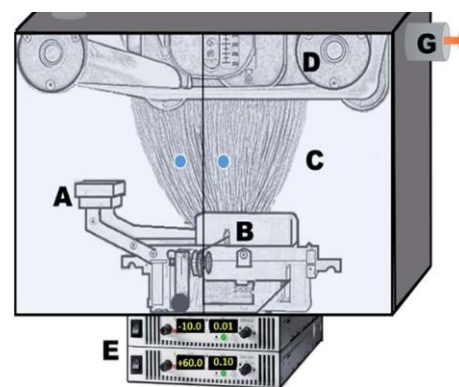

Fig. 1 Schematic illustration of the electrospinning device, with key components labelled. (A) Solution tank (feeds the solution towards the wire); (B) wire electrode; (C) spinning area; (D) collecting electrode, connected to a silicon paper as supporting material; (E) high voltage supply; (F) air intake; and (G) air outlet.

was used to modify the surface for 5 min. The scheme of the plasma reactor is shown in Fig. 2. After the plasma treatment, the samples were exposed to the atmosphere for 20 min and then immersed in 1 M sodium hydroxide (NaOH) aqueous solution. The times of sample immersion were 0, 2, 4, 6 and 24 h. The samples were then rinsed and kept in distilled water.

A Millipore Amicon 50 mL stirred filtration cell (Millipore Corporation Billerica, Massachusetts, USA), with an active filtration area of 13.4 cm[2], was used to evaluate membrane
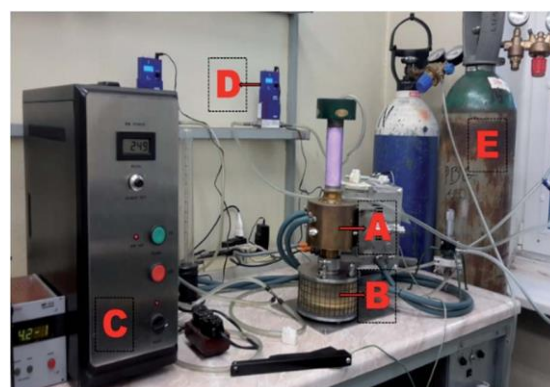
Fig. 2 Remote microwave plasma device, with key components labelled. (A) Low vacuum microwave plasma head; (B) reaction chamber; (C) MW generator; (D) Ar gas flowmeter; and (E) Ar gas tank.

Table 1 Key physical parameters of the PVDF/FAN samples analysed in this study

Sample code	PVDF/PAN wt ratio	Viscosity (mPa)	Area weight (g m[2])	Pore size (nm)
S1	1/0	969.3	3.52 0.5	2030 562
S2	0/1	190.9	1.29 0.5	710 344
S3	2/1	718.0	1.99 0.5	790 516
S4	1/1	499.3	4.35 0.5	910 245
S5	1/2	348.5	0.72 0.5	820 324
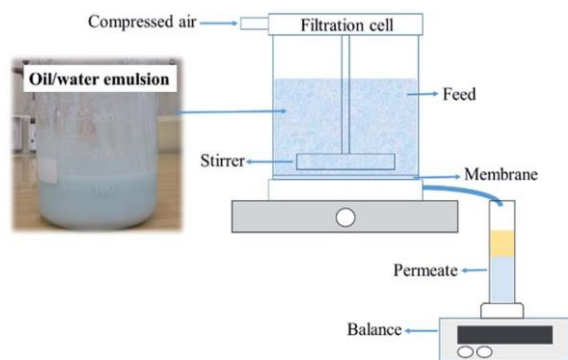
Fig. 3 Schematic diagram of dead-end filtration.

performance (Fig. 3). The feed solution was prepared by mixing blue-coloured distilled water with vegetable (kitchen) oil in a 1 : 1 volume ratio. Water was coloured using methylene blue to properly observe the separation process. The feed solution was mixed with a hand mixer for a few minutes until a uniform mixture was obtained. The tested dry membrane was placed in the filtration cell, which was then filled with 20 mL of filtrated distilled water. The separation conditions were created under 0.02 bar pressure. A 50 mL oil–water mixture was used for each test. The oil–water mixture did not separate into two phases during filtration. A magnetic stirrer was used to mix the feed solution during filtration. After the separation test, the permeate solution was collected in a glass graduated cylinder tube and sealed tightly to avoid evaporation. The permeate was kept for 24 h to separate into two phases and then determine the resultant water and oil percentages in volume ratio. The oil and water contents were calculated according to eqn (1):

$$C_S = \frac{V_S}{V_P} \times 100\%; \tag{1}$$

where C_S is the content of selected liquid (oil or water), V_S is the volume of selected liquid and V_P is the total volume of the permeate.

The permeate flux (F) and permeability (k) of the membrane were calculated according to eqn (2) and (3), respectively:

$$F = \frac{dV}{A\,dt}; \tag{2}$$

$$k = \frac{F}{p}; \tag{3}$$

where A is the effective membrane area (m²), V is the total volume of F, p is transmembrane pressure (bar) and t is the filtration time.

1. Results and discussion

1.1. Surface analysis and characterisation of the unmodified membranes

The SEM images in Fig. 4 show that there is no damage to the fibres on the top surface of the substrate, which suggests that the lamination was done successfully.
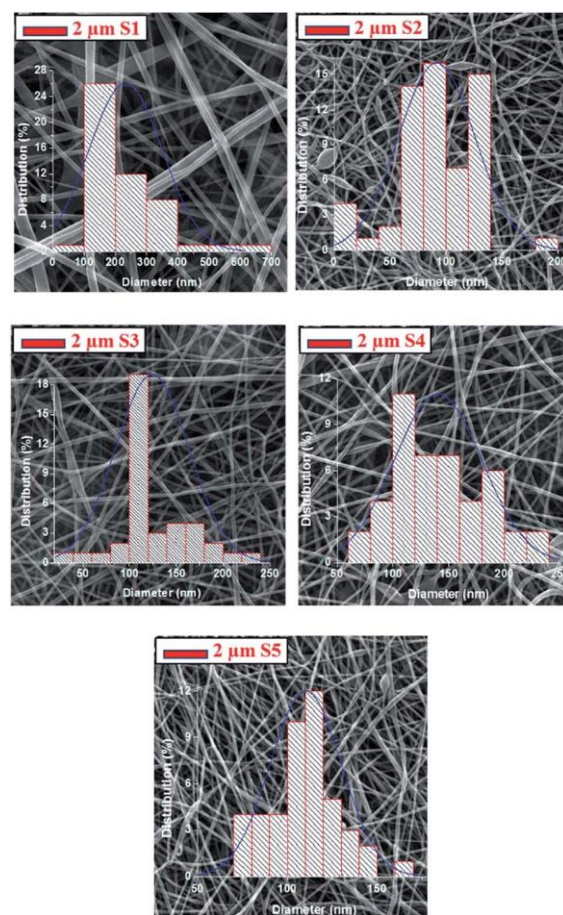

Fig. 4 SEM images of the unmodified samples after lamination.

It should be noted that the PVDF nanofibres possess a fibre diameter that is 2.5 times larger than that of the PAN nanofibres. Mixing the PVDF polymer with PAN yields a fibre diameter that is 1.6 times smaller than that of the neat PVDF sample nanofibres. It was observed that the neat PAN nanofibres have a beaded structure, which could be due to the low viscosity of the PAN solution (Table 1). Bead-free nanofibres were obtained after mixing PAN with PVDF. There were no visible changes in the observed fibre diameter after lamination.

Water contact angle measurements are one of the simplest and easiest methods for determining the hydrophilic or hydrophobic nature of chemical groups attached to the surface of the layers. Based on the water contact angle observations (Fig. 5), it was evident that the addition of PAN increased the hydrophilicity of the resultant PVDF/PAN membranes. The results showed that a neat PAN (S2) web, with a contact angle of less than 90, could be considered as a hydrophilic material.[28] Sample S5 had a contact angle close to 90, while samples S1, S3 and S4 each had angles larger than 90 and exhibited hydrophobic characteristics. The contact angles changed after surface modification. The plasma and chemical modifications resulted in fully wettable surfaces with a contact angle of 0. Only two modified images are shown in Fig. 5. Tran *et al.*[29] found that using non-polymer-forming plasma gas treatments, such as Ar,
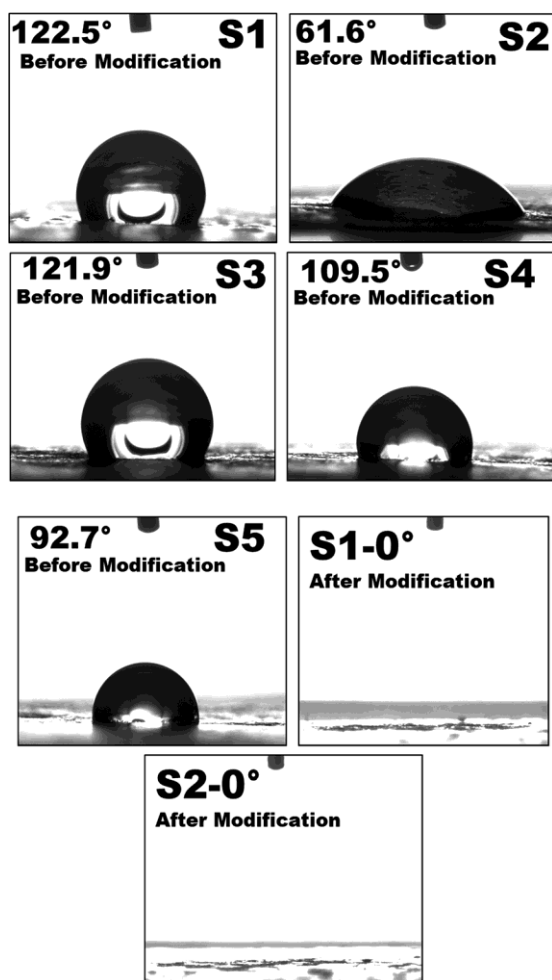
Fig. 5 Water contact angles of unmodified and modified nanofibrous membranes.

Fig. 6 FTIR spectra of the five PVDF/PAN samples.

He and O_2 plasma treatments, increase the membrane surface hydrophilicity and membrane permeability. Similarly, super-hydrophilic PVDF electrospun membranes have been obtained by oxygen plasma treatment. Moreover, the plasma treatment did not significantly influence the average size and morphology of the nanofibres.[30] Another study showed that both the surface modifications of PVDF and the surface wettability improved under plasma exposure.[31] The most significant result is the hydrophilic modification of the PVDF membrane.

The FTIR spectra were collected to investigate the chemical structure of the PVDF/PAN nanofibrous webs, shown in Fig. 6. The spectra confirmed the presence of both polymers in the blends, the absorption bands at 2240 cm[1] and 1664 cm[1] for the PAN nitrile groups and the stretching bands at 1173 cm[1] and 876 cm[1] for the $-CF_2$ and C–F groups of PVDF, respectively. The characteristic peaks for PVDF and PAN were modified according to the composition of the PVDF/PAN mixture.

1.1. Characterisation of the modified membranes

The mechanism of plasma deposition and chemical surface modification is shown in Fig. 7. Ar plasma treatment and
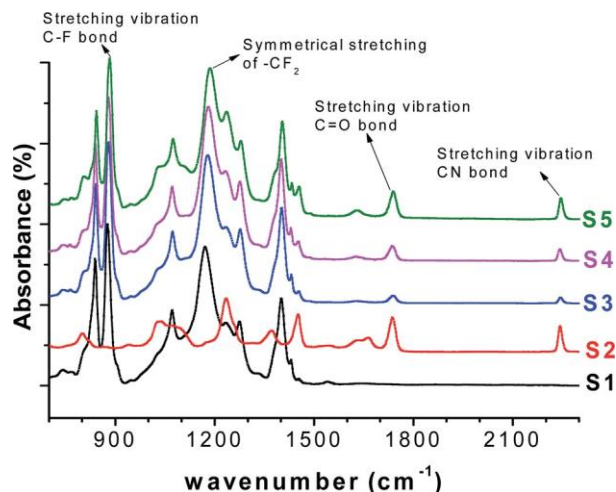
chemical operation with NaOH were used to modify the membrane surfaces. The Ar plasma treatment should crosslink the polymers on the surface fibres and introduce polar groups there, while the chemical operation with NaOH should turn the nitrile groups into more polar carboxylic functionalities. The exploitation of both methods of surface modification should provide more stable and highly hydrophilic properties for the long-lasting service of the membranes.

FTIR spectra were used to verify the effect of the plasma and chemical modifications on the composite membrane surfaces of S1, S2 and S4 (Fig. 8–10). Fig. 8–10 show that the modification caused a marked change in the surface functionality for the PVDF membranes, while only slight changes were observed for the PAN and PVDF/PAN (1/1) membranes. Tables 2 and 3 describe the key absorbance peaks of the evaluated membranes in greater detail.

Compared to unmodified PAN membranes, the peak at 1737 cm[1] shifted to 1733 cm[1] after surface modification (Fig. 8). A sharp increase in the peak at 1733 cm[1] was observed after the plasma treatment and NaOH surface modification, likely due to the presence of an extra carboxylic group on the modified surface.

Significant differences were observed after surface modification of the PVDF membranes (Fig. 9). The very broad and less intense peak between 2500 and 3500 cm[1] was due to O–H functionalities that improve the hydrophilicity of the membranes. The change in peak shape was due to of the extent of hydrogen bond stretching among the alcohol or carboxylic acid groups. These peaks change significantly with the surface
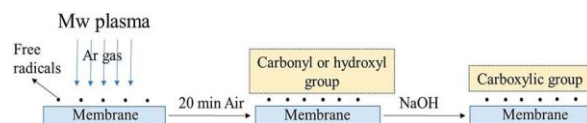

Fig. 7 Schematic diagram of membrane surface modification using a plasma and NaOH solution.
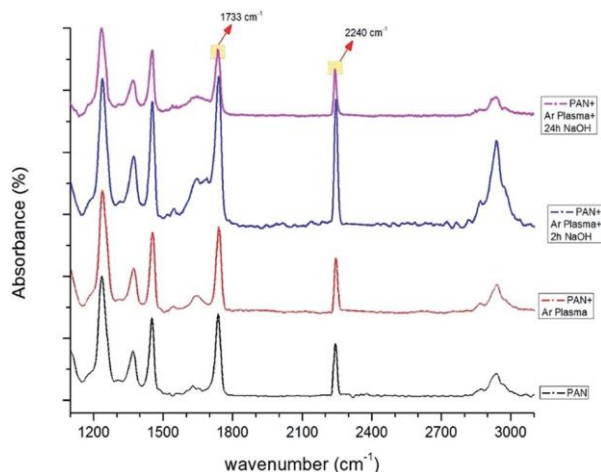
96

Fig. 8 FTIR spectra of PAN membranes before and after surface treatment (only Ar plasma, Ar plasma + 2 h NaOH, Ar plasma + 24 h NaOH).

modification and length of NaOH treatment. The peak at 2928 cm^1 indicated the C–H stretching frequency due to the parent hydrocarbon chain of the compound.

There were no significant changes in the PVDF/PAN 1/1 mixture after surface modification (Fig. 10). The FTIR results indicate that the surface of the PVDF membrane was successfully modified, following the modification mechanism shown in Fig. 7. Given the presence of carboxylic groups on the membrane surface, one can expect the highly permeable and anti-fouling reaction of such materials.

1.1. Oil–water separation

Surface treatment allows for the creation of specific surface chemistries that increase membrane permeability and reduce membrane fouling. However, separation of the oil–water mixture is always difficult, so several microfilters are used for this purpose.

The filtration results for the unmodified membranes, as well as the membranes modified by the Ar plasma and NaOH treatments, are shown in Fig. 11. The permeability of the membranes was compared before and after surface modification. The time "0" refers to the membranes without any treatment. The distilled water permeability values increased tremendously for the modified membranes.

The permeability of all of the composite membranes depends on both the surface modification and modification time. It was found that the immersion of the samples in NaOH for 6 h resulted in the highest permeability result for each membrane type (Fig. 11). The highest permeability was achieved for the S5 sample, which was 20 times higher than the permeability of the untreated S5 sample.

It was observed that the permeabilities of S2, S4 and S5 decreased after increasing the NaOH immersion to 24 h (Fig. 11). A commercially available ultrafiltration membrane of PAN was pre-treated in NaOH solution.[47] The NaOH-induced hydrolysis of nitrile groups on the membrane surface led to a decrease in both the pore diameter and permeability of the membrane. The average pore diameter underwent a 4.3-fold decrease during the hydrolysis. The results showed that modification of the membrane surface by anchoring carboxylic groups made the surface less prone to protein deposition. The hydrolysis of PAN and PAN/PVDF membranes resulted in the
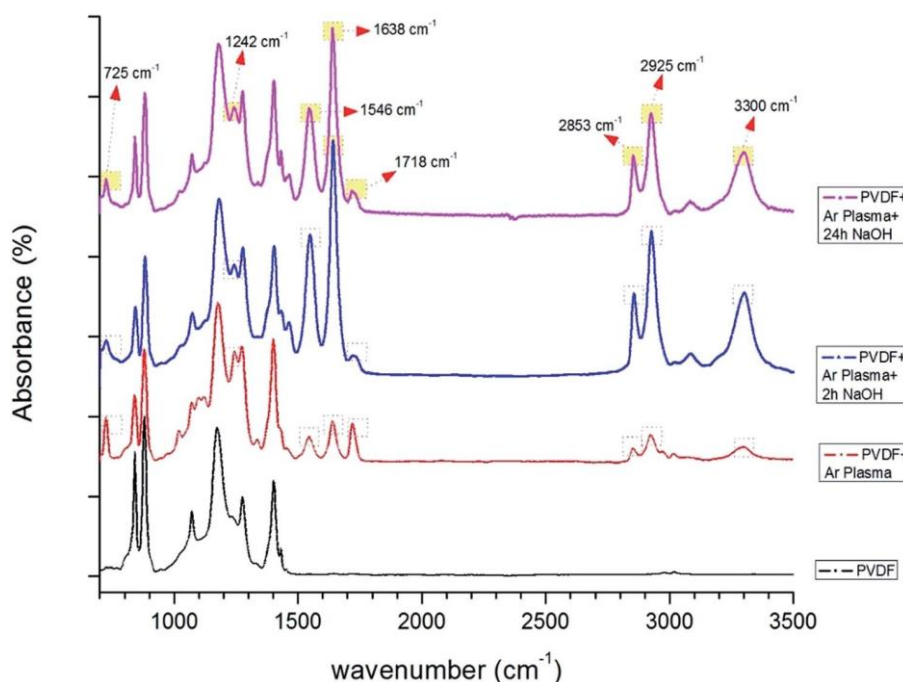

Fig. 9 FTIR spectra of PVDF membranes before and after surface treatment (only Ar plasma, Ar plasma + 2 h NaOH, Ar plasma + 24 h NaOH).
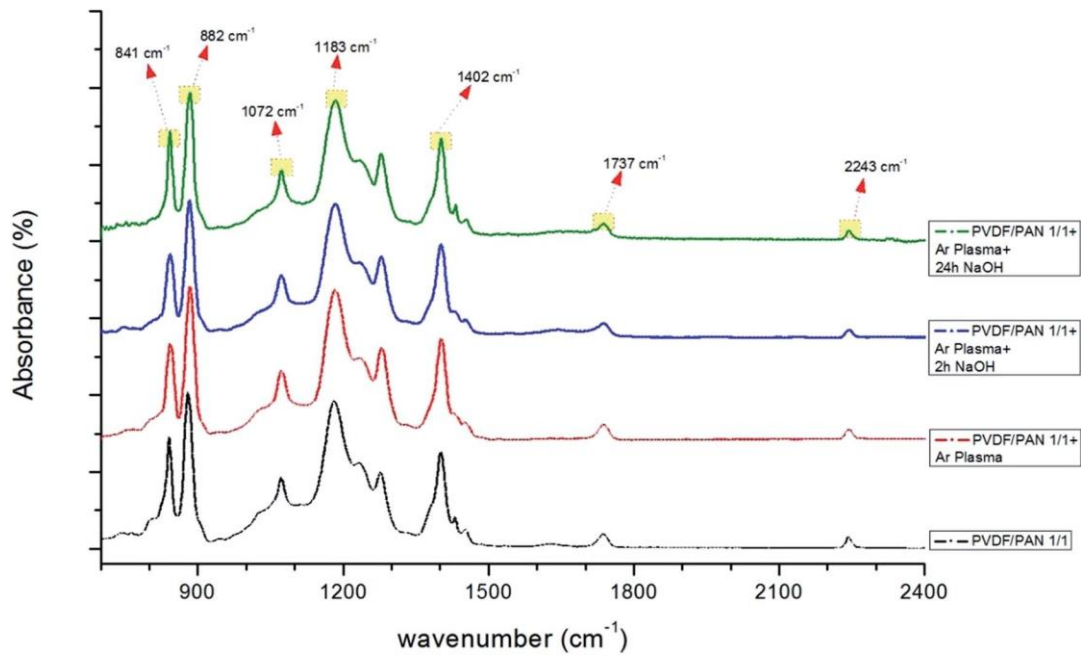
Fig. 10 FTIR spectra of PVDF/PAN (1/1) membranes before and after surface treatment (only Ar plasma, Ar plasma +

2 h NaOH, Ar plasma + 24 h NaOH).

swelling of the PAN polymers and a decrease in pore diameter. The pore sizes of the membranes were not measured after surface modification. The swollen pores apparently reduced the permeability of the membranes. A 6 h NaOH treatment seems optimum for all membranes.

An example filtration procedure for an oil–water mixture through the prepared membranes is shown in Fig. 12, with the results of the separation included in Table 4.

The results in Table 4 show that the modification of the nanofibrous membranes had a great effect on the selectivity of the membranes. The membranes in the first row, with a zero immersion time, had no surface treatment. Opposite to unmodified PAN, the unmodified PVDF shows hydrophobic/oleophilic properties. Similar results were recorded in the literature, where the neat PVDF membranes showed hydrophobic/oleophilic characteristics either in surfactant-free

Table 2 FTIR spectroscopy absorption bands for modified and unmodified PAN

Wavelength (cm^{-1})	Explanation
1240, 1369, 1453, 2938	Vibration of aliphatic CH groups (CH, CH$_2$, CH$_3$)[32]
1733, 1737	Stretching vibration of the C$=$O bond. The presence of this C$=$O peak could be due to residual DMF in the PAN fibers.[32] Moreover, additional surface treatment changes the intensity of the peak due to the carboxylic group on the surface
2240, 2242	Stretching vibration of the nitrile groups (CN) in acrylonitrile structure[33]

water-in-oil emulsion or a surfactant-stabilised water-in-oil emulsion.[48–50] The hydrophilicity and oleophilicity of the unmodified membranes change based on the ratio of PVDF/PAN. In the sample of PAN composite membranes, the hydrophilic/oleophobic characteristics of the PAN did not change after surface modification. However, the water permeability of the PAN composite membranes underwent a 4-fold improvement after 6 h of immersion in the NaOH solution. It was observed that surface modification of neat PVDF allowed the material to exhibit hydrophilic properties. The literature showed that treated PVDF membranes can convert the membrane from being highly hydrophobic to being super-hydrophilic when wetted with water and with a high permeability.[51,52] When the porous hydrophobic material is immersed in water, the water cannot penetrate the pores. However, the reduction of the surface tension of the solution (by the addition of salt or NaOH) made the membranes 'permeable' for water. The effects of both the surface modification and the increase in pore permeability improve the membrane hydrophilicity. Zhang *et al.*[53] prepared a superhydrophilic/superoleophobic PAN ultrafiltration membrane by an alkaline-induced phase inver- sion process by the addition of NaOH into coagulation bath.

This induced the *in situ* hydrolysis of –CN groups in the PAN chain to –COOH groups, which resulted in the superwetting of

the PAN membranes. The membrane showed ultralow oil adhesion, thus endowing the membrane with superior oil–water separation properties and a high water permeability.

The mixture of polymers showed that it was possible to control the oil or water uptake by altering the time of modifi-cation. In general, it is possible to conclude that the surface modification of the membranes improves their hydrophilicity

Table 3 FTIR spectroscopy absorption bands for modified and unmodified PVDF

Wavelength (cm[1])	Explanation
725	Methylene swing in-plane vibration due to C–C rocking vibrations in –(CH$_2$)$_n$. The absorbance is originating from exposure of the polymer + plasma bond to air for 20 min[34,35]
841	C–F stretching vibration of PVDF[36]
881	C–C–C asymmetrical stretching vibration of PVDF[36]
1175	Band for –CF$_2$ symmetrical stretching and a phase of PVDF[37–39]
1242	Enhanced carbonyl absorption peak –C–O– stretching band[40,41]
401	–C–F– stretching[39]
1546	Carboxylate peak asymmetric –O–C–O–[42]
1638–1718	Carbonyl (C =O) stretching vibrations. Primarily centred around 1710–1720 cm[1] (ref. 43)
2853	Symmetric stretching of CH$_2$
2925	Asymmetric stretching of C–H[44]
3020	Asymmetric starching vibration of the CH$_2$ groups[45]
2500–3300	O–H stretching absorption[46]

while decreasing their oleophilicity. PVDF nanofibres had a better mechanical and abrasion resistance compared to the PAN nanofibres. Surface-modified PVDF nanofibres seem to be suitable for the separation of water from water–oil mixtures. Moreover, it was found that a mixture of PVDF with PAN can be hydrophilic/oleophobic and gain a higher permeability compared to neat PVDF and neat PAN membranes.

The study presents the first industrial nanofibre production method to fabricate nanofibres for the separation of oily wastewater. Moreover, easy spinnable polymers and an inexpensive surface modification method were used to change surface hydrophilicity and oleophobicity. Compared to similar
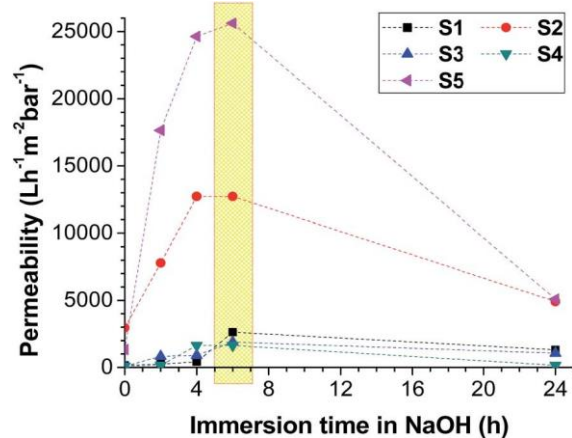

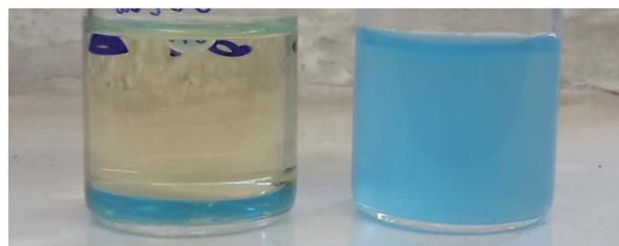Fig. 11 The permeability of the samples after various modification times in the NaOH solution.

Fig. 12 Permeates after oil–water filtration. Sample S1 (left) and S2 (right) after 4 h in NaOH solution.

studies in the literature, the membranes tested here showed very high permeability after separation.[54–58]

Based on the permeability and selectivity results, S5 was selected as the best candidate for the filtration of oily wastewater. The surface morphology of S5 was investigated by SEM image after surface modification and separation test, as shown in Fig. 13.

The SEM results showed that the diameter of the nanofibres increased with increasing immersion time, while the size distribution of the nanofibres improved. This is due to the swelling of PAN nanofibres in the NaOH aqueous solution. Similar results were obtained in the literature.[47] Yang *et al.*[59] found that after immersing the PAN membranes in NaOH, the hydraulic permeability decreased, and an increase in the rejection of dextran was observed due to the swelling of the hydrolysed layer. Kim *et al.*[60] found that the annealed PAN membrane underwent a decrease in pore size after it was treated with 2 M NaOH or CH$_3$ONa for over 2 h. The reason for this is that NaOH-induced hydrolysis of the nitrile groups on the membrane surface results in membranes with decreasing pore diameters. The pore diameters of the samples were not measured after modification, because the pore size measure- ments were done on dry membranes. Drying the wet nanofibre web would cause cracking on the surface of the nanofibres, which highlights that it is better to keep the membrane in a wet condition once it has been wetted. After surface modification, the membranes were kept in distilled water until the separation test was run. The SEM results indicate that fibres grew and became flattened, likely due to the decrease in pore size. After separation, the membranes were dried in the oven without any cleaning, and the SEM images were taken. The images showed that after oil separation, all membrane surfaces were contami- nated with oil (Fig. 13). The fibres are barely visible under a cake

Table 4 The water and oil contents in the permeates

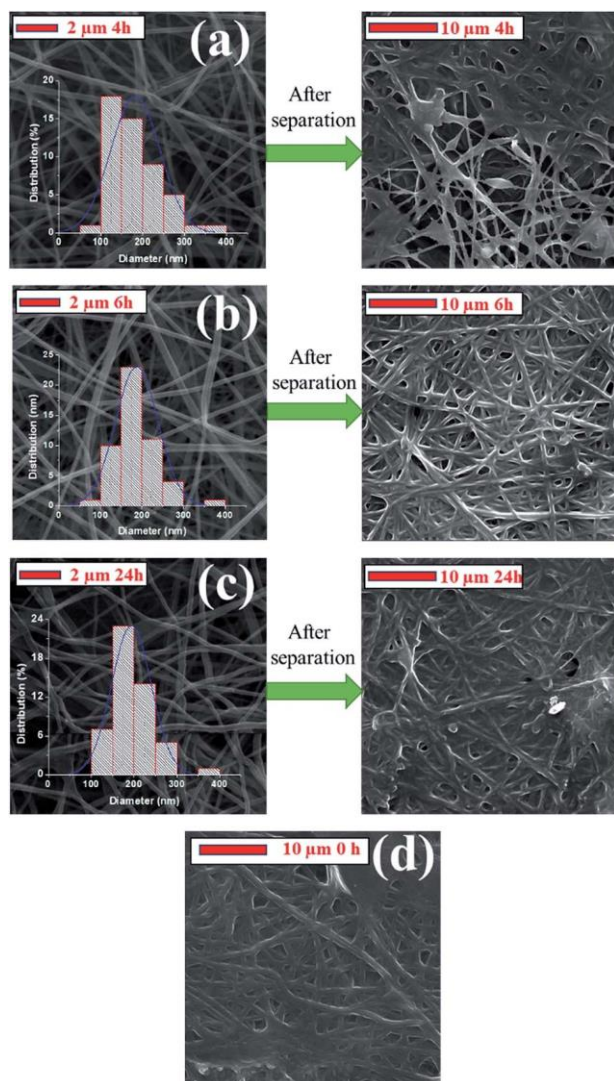| Time in NaOH (h)	Water content (%)					Oil content (%)				
	S1	S2	S3	S4	S5	S1	S2	S3	S4	S5
0	0	100	0	50	73	100	0	100	50	27
2	10	100	26	100	81	90	0	74	0	19
4	18	100	50	100	86	82	0	50	0	14
6	74	100	100	100	100	26	0	0	0	0
24	78	100	100	100	100	22	0	0	0	0

Fig. 13 SEM images of sample S5 after: (a) 4 h, (b) 6 h and (c) 24 h surface modification and their SEM images after the separation test, (d) unmodified membrane after the separation test.

The membrane permeability can also be altered based on the chemical treatment parameters. In the case of membranes with modified PAN, water permeability increases dramatically. Depending on modification parameter, a permeability of 25 000 L m^2 h bar^1 was achieved with Ar plasma exposure followed by NaOH modification. The FTIR results confirm the polymer mixture and surface modification. Contact angle measurements showed that after surface treatment, membranes become highly hydrophilic, with the water drop immediately disappearing. SEM studies revealed no physical damage to the polymer surface lamination.

The distilled water flux for the modified membranes increased dramatically because of its high hydrophilicity. The oily wastewater fouling was considerably reduced by the membrane flux for modified membranes.

Improved strength and, in the instance of PVDF, the improved wettability of the membranes, make them more suitable for aqueous filtration. These prepared membranes could thus be used for the practical microfiltration of oily wastewater.

Conflicts of interest

There are no conflicts to declare.

Acknowledgements

layer. The permeability results of the 24 h modification were quite low compared to the 2, 4 and 6 h separation tests. It is visible from the SEM image that the total surface of the 24 h modified membrane was totally covered with an oil film, which led to a marked decrease in its permeability.

1. Conclusions

Functional PVDF, PAN and PVDF/PAN nanofibrous composite membranes were successfully fabricated for the separation of an oily wastewater. It was found that both the polymer blending method and modification of the membranes can change the surface hydrophilicity and oleophilicity. These changes can be attributed to structural changes in the membranes to decrease surface energy and increase in pore permeability.

Notes and references

1 M. A. Zahed, H. A. Aziz, M. H. Isa, L. Mohajeri and S. Mohajeri, *Bioresour. Technol.*, 2010, 101, 9455–9460.
2 A. Vidyasagar, K. Handore and K. M. Sureshan, *Angew. Chem., Int. Ed.*, 2011, 50, 8021–8024.
3 R. R. Fouad, H. A. Aljohani and K. R. Shoueir, *Mar. Pollut. Bull.*, 2016, 112, 46–52.
4 J. Kim and B. Van der Bruggen, *Environ. Pollut.*, 2010, 158, 2335–2349.
5 X. Zhao, Y. Su, W. Chen, J. Peng and Z. Jiang, *J. Memb. Sci.*, 2012, 415–416, 824–834.
6 S. Kang, A. Asatekin, A. M. Mayes and M. Elimelech, *J. Memb. Sci.*, 2007, 296, 42–50.
7 X. X. Xu, C. L. Zhou, B. R. Zeng, H. P. Xia, W. G. Lan and X. M. He, *Sep. Purif. Technol.*, 2012, 96, 229–236.
8 S.-H. Oh, J.-W. Ma, J. M. Bae, Y. Kang, J.-P. Ahn, H.-K. Kang, J. Chae, D. Suh, W. Song, S. Kim and M.-H. Cho, *Appl. Surf. Sci.*, 2017, 419, 1–8.
9 Z. Xu, K. Miyazaki and T. Hori, *Appl. Surf. Sci.*, 2016, 370, 243–251.

10   I. Gancarz, M. Bryjak, J. Wolska, A. Siekierka and   W. Kujawski, Chem. Pap., 2016, 70, 350–355.

11 M. Tsuchida and Z. Osawa, Colloid Polym. Sci., 1994, 272, 770–776.

12 I. Punga and G. Borcia, J. Adv. Res. Phys., 2013, 4, 1–5.

13 J. G. A. Terlingen, H. F. C. Gerritsen, A. S. Hoffman and J. Feijen, J. Appl. Polym. Sci., 1995, 57, 969–982.

14 K. Y. Wang, S. W. Foo and T. S. Chung, Ind. Eng. Chem. Res., 2009, 48, 4474–4483.

15   W. Chen, Y. Su, J. Peng, X. Zhao, Z. Jiang, Y. Dong, Y. Zhang, Y. Liang and J. Liu, Environ. Sci. Technol., 2011, 45, 6545– 6552.

16 A. K. Manna, M. Sen, A. R. Martin and P. Pal, Environ. Pollut., 2010, 158, 805–811.

17 M. Amirilargani, A. Sabetghadam and T. Mohammadi, Polym. Adv. Technol., 2012, 23, 398–407.

18 B. P. Tripathi, N. C. Dubey, R. Subair, S. Choudhury, M. Stamm, K. T. Gause, J. J. Richardson, F. Caruso and V. Abetz, RSC Adv., 2016, 6, 4448–4457.

19 R. M. Elkhaldi, S. Guclu and I. Koyuncu, Desalin. Water Treat., 2016, 57, 26003–26013.

20 O. Jirsak, F. Sanetrnik, D. Lukas, V. Kotek, L. Martinova and J. Chaloupek, WO Pat., WO/2005/024101, 2005.

21 K. Smolinska, M. Bryjak, J. Wolska and W. Kujawski, Mater. Chem. Phys., 2014, 148, 548–553.

22 K. Smolinska and M. Bryjak, Desalination, 2012, 300, 64–69.

23   M. Ulbricht and G. Belfort, J. Memb. Sci., 1996, 111, 193–215. 24 D. S. Wavhal and E. R. Fisher, J. Memb. Sci., 2002, 209, 255–269.

25 M. Suzuki, A. Kishida, H. Iwata and Y. Ikada, Macromolecules, 1986, 19, 1804–1808.

26   M. Gorjanc, M. Mozetič, G. Primc, A. Vesel, K. Spasič, N. Puač, Z. L. Petrovič and M. Kert, Appl. Surf. Sci., 2017, 419, 224–234.

27 Y. Fatma, A. Siekierka, M. Bryjak and J. Maryska, IOP Conf. Ser.: Mater. Sci. Eng., 2017, 254, 102011.

28 F. Yalcinkaya, B. Yalcinkaya, J. Hruza and P. Hrabak, Sci. Adv. Mater., 2017, 9, 747–757.

29 T. D. Tran, S. Mori and M. Suzuki, Thin Solid Films, 2007, 515, 4148–4152.

30 D. M. Correia, C. Ribeiro, V. Sencadas, G. Botelho, S. A. C. Carabineiro, J. L. G. Ribelles and S. Lanceros- Méndez, Prog. Org. Coatings, 2015, 85, 151–158.

31 M. D. Duca, C. L. Plosceanu and T. Pop, Polym. Degrad. Stab., 1998, 61, 65–72.

32   J. Li, S. Su, L. Zhou, V. Kundrát, A. M. Abbot, F. Mushtaq, D. Ouyang, D. James, D. Roberts and H. Ye, J. Appl. Phys., 2013, 113, 24313.

33 S. N. M. Salleh, M. Z. Abdullah and A. A. Wahab, MATEC Web Conf., 2014, 13, 4014.

34 E.-G. Schlosser, Angew. Chemie, 1987, 99, 284.

35 N. Naresh Kumar, S. Yap, F. bt Samsudin, M. Khan and R. Pattela Srinivasa, Polymers, 2016, 8, 295.

36 H. Bai, X. Wang, Y. Zhou and L. Zhang, Prog. Nat. Sci.: Mater. Int., 2012, 22, 250–257.

37 R. Li, C. Chen, J. Li, L. Xu, G. Xiao, D. Yan, B. Liu, G. M. Veith, S. Dai, Q. H. Yang, H. M. Ning, J. H. Li, Y. Li and Y. H. Zhao, J. Mater. Chem. A, 2014, 2, 3057.

38 D. Mandal, K. Henkel and D. Schmeisser, J. Phys. Chem. B, 2011, 115, 10567–10569.

39 F. Yalcinkaya, B. Yalcinkaya, A. Pazourek, J. Mullerova, M. Stuchlik and J. Maryska, Int. J. Polym. Sci., 2016, 2016, 4671658.

40 B. Yan and B. Zhang, Analytical methods in combinatorial chemistry, CRC Press, 2011.

41 R. Bodîrlˇau, R. Bodîrlˇau and C. A. Teacˇa, Rom. J. Phys., 2008, 93–104.

42 G. E. Dunn and R. S. McDonald, Can. J. Chem., 1969, 47, 4577–4588.

43 V. N. Rai, C. Mukherjee and B. Jain, Indian J. Pure Appl. Math., 2017, 55, 775–785.

44 G. C. Nille, V. K. Singh and K. R. C. Reddy, J. Ayurveda Holist. Med., 2016, 4, 1–11.

45 A. Bashir, S. K. Raghuvanshi, S. Hartha, N. P. Sharma, J. B. M. Krishna and M. A. Wahab, Prog. Nanotechnol. Nanomater., 2013, 2, 42–46.

46 B. S. Gupta, B. P. Jelle, T. Gao and T. Gao, Int. J. Spectrosc., 2015, 2015, 1–7.

47 M. Bryjak, H. Hodge and B. Dach, Appl. Macromol. Chem. Phys., 1998, 260, 25–29.

48 W. Zhang, Z. Shi, F. Zhang, X. Liu, J. Jin and L. Jiang, Adv. Mater., 2013, 25, 2071–2076.

49 J. Kong and K. Li, Sep. Purif. Technol., 1999, 16, 83–93.

50 Z. Zhou and X.-F. Wu, Mater. Lett., 2015, 160, 423–427.

51 M. Obaid, H. O. Mohamed, A. S. Yasin, M. A. Yassin, O. A. Fadali, H. Kim and N. A. M. Barakat, Water Res., 2017, 123, 524–535.

52 W. Zhang, Y. Zhu, X. Liu, D. Wang, J. Li, L. Jiang and J. Jin, Angew. Chem., Int. Ed., 2014, 53, 856–860.

53 F. Zhang, S. Gao, Y. Zhu and J. Jin, J. Memb. Sci., 2016, 513, 67–73.

54 C. Yang, G. Zhang, N. Xu and J. Shi, J. Memb. Sci., 1998, 142, 235–243.

55 X. Hu, Y. Yu, J. Zhou, Y. Wang, J. Liang, X. Zhang, Q. Chang and L. Song, J. Memb. Sci., 2015, 476, 200–204.

56 M. H. Tai, P. Gao, B. Y. L. Tan, D. D. Sun and J. O. Leckie, ACS Appl. Mater. Interfaces, 2014, 6, 9393–9401.

57 C.-T. Hsieh, J.-P. Hsu, H.-H. Hsu, W.-H. Lin and R.-S. Juang, Surf. Coat. Technol., 2016, 286, 148–154.

58 C. Li, C. Song, P. Tao, M. Sun, Z. Pan, T. Wang and M. Shao, Sep. Purif. Technol., 2016, 168, 47–56.

59 M.-C. Yang and J.-H. Tong, J. Memb. Sci., 1997, 132, 63–71.

60 I.-C. Kim, H.-G. Yun and K.-H. Lee, J. Memb. Sci., 2002, 199, 75–84.

Preparation of Fouling-Resistant Nanofibrous Composite Membranes for Separation of Oily Wastewater

Fatma Yalcinkaya [1,*], Anna Siekierka [2] and Marek Bryjak [2]

[1]   Department of Nanotechnology and Informatics, Technical University of Liberec, Institute for Nanomaterials, Advanced Technologies and Innovation, Studentska 1402/2, 46117 Liberec, Czech Republic

[2]   Faculty of Chemistry, Wroclaw University of Science and Technology, 27 Wybrzeze Stanislawa Wyspianskiego, 50-370 Wroclaw, Poland; anna.siekierka@pwr.edu.pl (A.S.); marek.bryjak@pwr.edu.pl (M.B.)

*   Correspondence: yenertex@hotmail.com; Tel.: +420-485-353-389

Abstract: A facile and low-cost method has been developed for separation of oily wastewater. Polyvinylidene fluoride/polyacrylonitrile (PVDF/PAN) nanofibers laminated on a supporting layer were tested. In order to create highly permeable and fouling-resistant membranes, surface modifications of both fibers were conducted. The results of oily wastewater separation showed that, after low vacuum microwave plasma treatment with Argon (Ar) and chemical modification with sodium hydroxide (NaOH), the membranes had excellent hydrophilicity, due to the formation of active carboxylic groups. However, the membrane performance failed during the cleaning procedures. Titanium dioxide (TiO_2) was grafted onto the surface of membranes to give them highly permeable and fouling-resistance properties. The results of the self-cleaning experiment indicated that grafting of TiO_2 on the surface of the membranes after their pre-treatment with Ar plasma and NaOH increased the permeability and the anti-fouling properties. A new surface modification method using a combination of plasma and chemical treatment was introduced.

Keywords: nanofiber; modified nanofiber; nanocomposite

1. Introduction

The increasing amount of industrial and domestic oily wastewater has become one of the most important problematic issues for the environment and human health. Oil–water emulsion separation has gained more importance in recent decades. A few methods have been developed for oil–water separation, such as oil containment booms [1], coagulation method [2], oil sorption materials [3–5], oil skimmers [1], air flotation [6], and combustion [7]. However, these methods have disadvantages, like secondary pollution, expensive operation, low efficiency, complicated operation, and they are time-consuming. Microfiltration is one of the simplest and widely used methods for separation of oily wastewater. Many researchers have developed various types of microfilters. Membranes are the most important part of the microfiltration process [8]. For instance, it was found that superhydrophilic in situ-crosslinked zwitterionic polyelectrolyte/polyvinylidene fluoride-blend membranes exhibit high water permeation flux and good antifouling properties for separating oil-in-water emulsions with high separation efficiency [9]. Cao et al. prepared hyperbranched polyethyleneimine (HPEI) glass fiber membranes for oil–water separation. The modified membrane showed high permeation and quantitative oil rejection with excellent thermal and chemical stability, compared with polymer-based membranes [10]. Cumming et al. [11] developed a method for characterizing the rejection efficiency, by using an asymmetric metal microfilter to separate oil in a water dispersion. Results showed that the rejection of oil drops depended on the size distribution of the emulsion, and the use of a surface

filter without any internal tortuosity excluded the possibility of internal fouling. However, fouling is a common problem that has to be faced during microfiltration. In fouling, the membrane is contaminated by a solution or particle, which results in a decrease in membrane performance. In general, fouling forms on hydrophobic surfaces as a result of aggregation, protein adsorption, and denaturation at the membrane–solution interface [12].

Fouling causes a decrease in the performance of the filters, and generates extra costs for repetitive cleaning procedures. For effective oily water treatment, antifouling membranes with very high selectivity are required. More often, the selectivity and the fouling resistant properties of the membranes are strongly dependent on their surface wettability. With this aim in mind, many researchers have employed various modifications to change the surface properties of the polymeric membranes, such as surface grafting, blending, surface coating, and surface absorption [13–19]. Zhang et al. [20] fabricated a Graphene oxide modified polyacrylonitrile hierarchical-structured membrane. It was found that this hierarchical-structured membrane exhibited a very high flux, feasible rejection ratio, and superior antifouling performance in separating an oil–water emulsion, due to its surface hydrophilicity. In another work [21], pancreatic enzyme was immobilized on polyethersulfone membranes by electron beam modification. The anti-fouling property of the membrane was obtained after switching on the catalytic activity of the enzyme by adjusting the pH and temperature. As a result, the membrane surface actively degraded a fouling layer, and regained its initial permeability. Yang et al. [22] fabricated a superhydrophilic and superoleophobic nanocomposite coating by spray casting nanoparticle–polymer suspensions on various substrates. They synthesized the polymer with hydrophilic and oleophobic properties by using the reaction of poly (diallyldimethylammonium chloride) (PDDA) with sodium perfluorooctanoate (PFO) in aqueous solution, in which PFO anions can coordinate to quaternary ammonium groups of PDDA. As a result of the high surface concentration of fluorinated groups, together with carboxyl and quaternary ammonium groups, oleophobic and hydrophilic material were fabricated. Water molecules are able to penetrate the surfaces, while oils cannot. An air plasma treatment was applied to enhance the hydrophilicity of the coating material and increase the water permeability, while there was no change in superoleophobic properties. Wei et al. [23] used maleic anhydride to graft onto a polyacrylonitrile (PAN) membrane surface via ultraviolet irradiation. Hyperbranched polyester grafting onto the PAN membrane surface, by the reaction of hydroxyl groups with anhydride groups of maleic anhydride, followed the grafting process. The filtration showed that modified membranes had a 4–6 times higher water flux and better antifouling properties than pristine PAN membranes, and their hydrophilicity was significantly improved. Zhang et al. [14] fabricated an ultralow oil-fouling amphiphilic copolymer incorporated poly(ether sulfone) (PES) heterogeneous membrane. First, the amphiphilic copolymer was prepared by semibatch reversible addition—where the fragmentation chain was transferred by poly (ethylene glycol) methyl ether methacrylate (PEGMA) and 3,3,4,4,5,5,6,6,7,7,8,8,8-tridecafluorooctyl acrylate (TFOA). The resultant amphiphilic fluorinated gradient copolymers were then incorporated into the PES. The resultant membrane showed effective oil–water emulsion separation due to the hydrophilicity of PEG and low surface energy of PTFOA. Wang et al. [24] prepared titanium dioxide (TiO_2) doped polyvinylidene fluoride (PVDF) nanofibers to prevent fouling of membranes in oil–water separation. TiO_2 gel was prepared and mixed with the PVDF solution before the spinning process. The membranes showed reversible separation of the oily water by UV (or sunlight) irradiation and heating treatment. Among various materials, TiO_2 has been widely used, due to its self-cleaning and photocatalytic properties [25,26].

In this work, nanofibers were produced as an active layer for microfiltration. The properties of the nanofibers, such as their ability to be embedded within other media, high surface-to-volume ratio, large porosity, narrow pore size, easiness to operate, and adjustable functionality, are much more effective than conventional polymeric membranes used in liquid filtration. Nanofibers have a porosity of over 80% in the structure, which improves the filtration efficiency of the membranes. The low mechanical strength of the nanofibers restricts their application in liquid filtration [27].

To overcome this problem, a special lamination technique was applied, and nanofibrous composite membranes were formed as microfilters. The principle of the lamination technique has been explained in our previous work [28–30]. The use of this lamination technique did not change the properties of the nanofibers on the surface of the membrane. A polyester nonwoven layer was selected as a supporting layer for the nanofibers. The lamination technology provides excellent adhesion of the nanofibers to the substrate, as well as durable structural stability, which provides a longer lifespan and greater effectiveness in the cleaning process. In this work, a mixture of PVDF and polyacrylonitrile (PAN) nanofibers were fabricated. PVDF has a high hydrophobicity and thermal stability, good chemical resistance and oleophilicity. Its good electrical properties result from the polarity of alternating groups on the polymer chain, and easiness to fabricate the nanofiber web [31,32]. PAN has good characteristics, including thermal stability, tolerance to most solvents, and commercial availability [33]. PAN nanofibers are more hydrophilic and better at plasma etching compared to PVDF [34,35]. However, PAN nanofibers have lower mechanical and abrasion resistance than PVDF. The aim of mixing both polymers is to improve the mechanical properties of the nanofiber web, while providing an effective plasma treatment. In addition, both of the polymers were selected due to their relative low cost and widespread commercial use.

The selectivity and permeability are two key factors in the membrane process. The selectivity of membranes is largely determined by the surface porosity and pore size of the substructure, and the chemical and physical properties of the membrane, while the permeability mainly depends on the hydrophilicity, porosity, and pore size of the membrane. Due to the lack of functional groups on the PVDF/PAN nanofibrous membrane surface, it is necessary to introduce some functional groups by surface modification. In this study, the nanofibrous composite membranes were covered by TiO_2 nanoparticles, due to their high stability, high photocatalytic activity, non-toxicity, low cost, chemical resistance, and antibacterial activity to certain microorganisms. TiO_2 nanoparticles can be used to successfully overcome the fouling problem. The nanoparticles were grafted on the surface of nanofibrous membranes using plasma and chemical pre-treatments. According to our knowledge, this method has not been reported so far. The ultimate goal of this work was to introduce a new surface modification method that could offer highly permeable and fouling resistant membranes.

1. Materials and Methods

1.1. Preparation of the Nanofiber Web

A total of 8 wt % polyacrylonitrile (PAN) (M_W = 150 kDa, purchased from Elmarcos.r.o., Liberec, Czech Republic) was dissolved in dimethylformamide (DMF), while 13 wt % polyvinylidene fluoride (PVDF) (form from Solef 1015, Bruxelles, Belgium) was dissolved in dimethylacetamide (DMAc). Solvents were purchased from Penta, s.r.o., Prague, Czech Republic. The solutions were stirred overnight. A nanofiber web blend was prepared. The blend ratio of PVDF/PAN nanofibers in the composite was 1/2 in wt %. This ratio was determined based on our previous experience [34,36]. A lab-scale Nanospider (Elmarco s.r.o., Liberec, Czech Republic) electrospinning device was used for the production of nanofibers under stable conditions (Figure 1). A solution tank fed the solution toward the wire electrode. If the electrical fields between the wire electrode and the collector overcome the surface tension, Taylor's cones were formed, and jets moved towards a take-up cylinder connected to a supporting material. The spinning conditions were kept stable by controlling the humidity, temperature and air input–output speed.
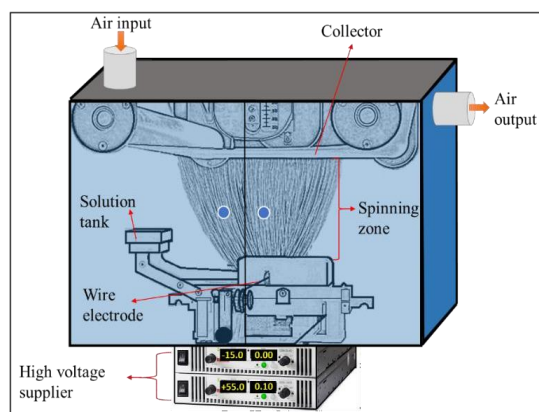
Figure 1. Schematic diagram of the Nanospider device.

1.1. Formation of a Nanofibrous Composite Membrane

The nanofiber web was gently laminated on a supporting layer using a Meyer RPS-L Mini lamination machine (Maschinenfabrik Herbert Meyer GmbH, Roetz, Germany) at room temperature (Figure 2).
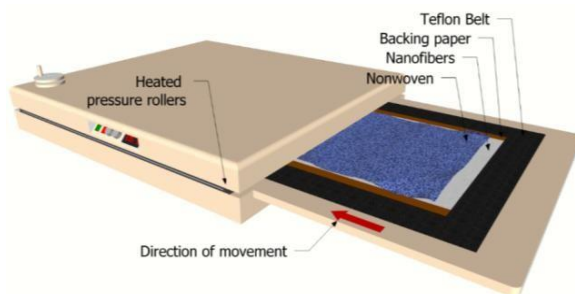

Figure 2. Lamination method and equipment [37].

The nanofiber web was collected on silicon paper. A 100 g/m^2 polyethylene terephthalate spunbond nonwoven fabric was used as supporting layer, and 3 g/m^2 of co-polyamide adhesive web were used to adhere the nanofibers and the nonwoven web. The lamination machine had a conveyer belt resistant to heat and damage. The maximum width of the samples was set as 400 mm, while there was no limitation on the length. The configuration of the substrate mainly depended on the application, and could be varied to reach the desired structural properties, including strength, stiffness, and durability, pliability and flexibility, and temperature resistance.

The zero-shear viscosity of the polymer solutions was obtained using a Fungilab Expert viscometer (Fungilab Leading Viscosity Technology, Barcelona, Spain) at 23 °C. The surface of the membranes was characterized using a Scanning Electron Microscope (SEM, Vega 3SB, Brno, Czech Republic) and fiber diameter, diameter distribution, and porosity were analyzed using the Image-J program (free online program). The surface contact angle of the samples was measured at room temperature using a Kruss Drop Shape Analyzer DS4 (Kruss GmbH, Hamburg, Germany), using distilled water on the clean and dry sample. An 1200-AEL capillary flow porometer (Porous Media Inc., Ithaca, NY, USA) was used in this study to measure the pore size. FTIR spectra were used to verify the effect of the plasma and chemical modifications on the composite membrane surface. The polymeric nanofiber membranes were evaluated using Fourier transform infrared spectroscopy (FTIR, Nicolet iZ10 by Thermo Fisher Scientific, Waltham, MA, USA).

1.1. Surface Treatment

The membranes were then subjected to the low vacuum plasma treatment described in the literature [38]. Microwave plasma treatment in argon was used to modify the surface for 5 min. After plasma activation, the sample was exposed to the atmosphere for 20 min, and then immersed in 1 M of a sodium hydroxide (NaOH) solution for 24 h.   The TiO$_2$ nanoparticles were prepared   as follows:

- Solution A: 5 wt % of titanium isopropoxide (Sigma-Aldrich, Sigma-Aldrich Sp. Z.o.o., Poznan, Poland) was mixed in a propanol solvent at 50 °C.
- Solution B: 5 wt % of diluted acetic acid was prepared.
- Solution C: Solution B was slowly poured into solution A at a ratio of 50:50 v/v.
- Solution D: Solution C was heated to remove any water.
- Solution E: Sodium hydroxide (NaOH) was used to neutralize the pH of solution D.

After the described procedure, the titanium dioxide with some amount of aliphatic chains was obtained. The presence of oxygen groups into the aliphatic chains was confirmed by FTIR analysis, shown in [39]. Hence, the crystallinity structure of TiO$_2$ can be classified as a polyamorous. Therefore, the average particle size of these materials will be larger than for pure anatase or rutile structure of TiO$_2$. However, application of acetic acid provided a decrease of average particle size of TiO$_2$ [40]. To show the photoactivity of the titanium dioxide layer, the photodegradation examination with BSA (bovine serum albumin) fouled layers were performed. These results are widely explained in our paper [38].

Finally, the membranes, after plasma and chemical treatments, were immersed into solution E for 2 days. The samples were rinsed and kept in distilled water.

PVDF/PAN 1/2 nanofibrous membranes were treated by plasma and chemical methods in four different configurations, as shown in Table 1.

Table 1. Preparation of nanofibrous composite membranes in various ways for different combinations of plasma and chemical methods.

Abbreviation of the Sample	Plasma Modification	Chemical Modification	UV Irradiation
P0*	-	-	-
P1	5 min Plasma + 20 min exposed to atmosphere	Immersed into NaOH for 24 h	-
P2	5 min Plasma + 20 min exposed to atmosphere	Immersed into solution E for 2 days	-
P3	5 min Plasma + 20 min exposed to atmosphere	Immersed into NaOH for 24 h and solution E for 2 days	-
P4	5 min Plasma + 20 min exposed to atmosphere	Immersed into NaOH for 24 h and solution E for 2 days	4 min under UV light

P0* is a neat PVDF/PAN membrane without any post-treatment.

It was proven that the TiO$_2$ surface becomes more hydrophilic after UV irradiation [41,42]. In this study, the effect of the UV irradiation on the fouling of TiO$_2$ covered nanofibrous membranes has been investigated.

1.2. Filtration and Self-Cleaning Experiments

The oil–water separation was carried out with a 50 mL Millipore Amicon stirred filtration cell (Millipore Corporation Billerica, MA, USA). A schematic diagram of the dead-end device is shown in Figure 3. The oil–water mixture (50%, v/v) was poured into the device. The water was coloured by

methylene blue to properly observe the separation process. The feed solution was mixed with a hand mixer for a few minutes, until a uniform mixture was obtained. Subsequently, 90 mL of distilled water was filtrated, followed by 45 mL of the oil–water mixture. This procedure was repeated a few times to determine the anti-fouling properties of the membrane. The membrane was not changed or replaced during each repeating step. The separation process was performed under a 0.02 bar pressure.
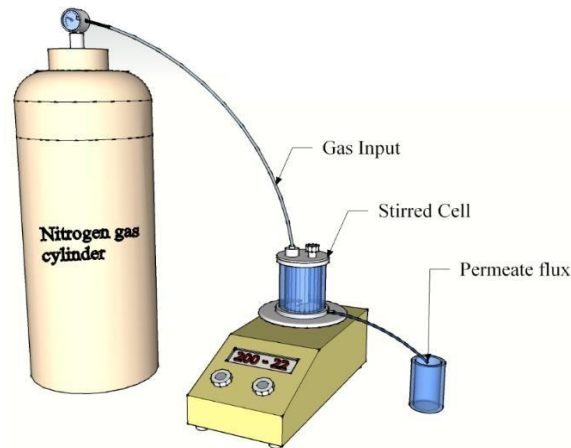

Figure 3. Schematic diagram of dead-end filtration.

The permeate flux (*F*) and the permeability (*k*) of the membrane were calculated (Equations (1) and (2)):

$$F = \frac{1}{A}\frac{dV}{dt} \tag{1}$$

$$k = \frac{F}{p} \tag{2}$$

where *A* is the effective membrane area (m^2), *V* is the total volume of the permeate (*F*), *p* is the transmembrane pressure (bar), and *t* is the filtration time [43].

1. Results

1.1. Membrane Characterization

The SEM images are given in Figure 4. The SEM images demonstrated that the lamination process did not damage the surface of the nanofiber layer. However, there were some blind spots, where the adhesive web covered the surface of the nanofibers and totally blocked the pores. In the resultant web, blind spots were rarely observed. It was not possible to remove these blind spots without delaminating the membranes, but it was possible to keep their number as low as possible. The fiber diameter of the nanofiber was around 110 nm, which was good for the filtration process, due to the small pore size. The pore size of the nanofiber was related to the diameter of the fiber. A lower fiber diameter yielded a lower mean pore size.

Table 2 shows the characterization of the nanofiber layer. The basis weight of the nanofiber web was less than 1 g/m^2, which was advantageous at high production speeds, and led to low production costs. The porosity of the membrane was quite important for the permeability of the membranes. In this study, the nanofiber layer had a porosity of more than 85% of its bulk volume. In theory, the low water contact angle indicates higher hydrophilicity and better wettability that increases the water permeability through the membrane. It is well know that hydrophilic membranes decrease the fouling due to the high affinity of the membrane to water molecules [44]. The pristine PVDF/PAN membrane without any surface treatment can be considered as being "hydrophobic" by definition [43].
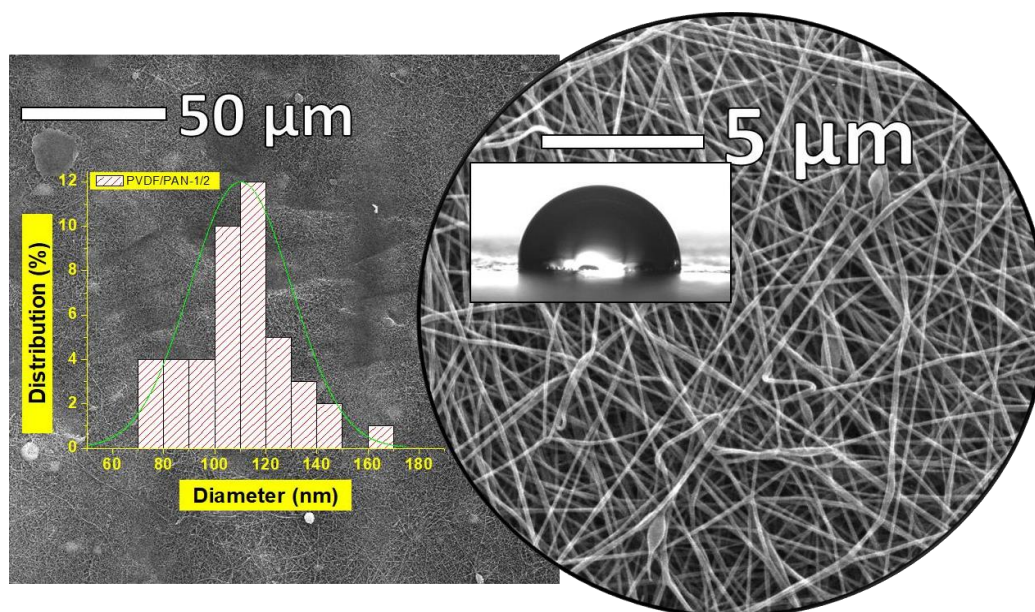
Figure 4. SEM images of PVDF/PAN nanofibers after the lamination process.

Table 2. Membrane characterization for PVDF/PAN nanofibers.

Polymer	Viscosity (Pa.s)	Basis Weight of Nanofiber (g/m^2)	Fiber Diameter (nm)	Porosity (%)	Avr. Pore Size (nm)	Contact Angle (°)
PVDF/PAN	0.35	0.76 ± 0.50	110.18 ± 19.90	>85	820 ± 32	92.7 ± 3

As shown in Table 2, the water contact angle of the pristine PVDF/PAN membranes was 92.7°. After surface modification with plasma, the water contact angle of the membranes decreased to 0°. These results indicate that the hydrophilicity of the membranes was improved by plasma and chemical modification.

All the surface modified membranes showed a "zero" water contact angle. The surface wettability of the membranes was improved by the plasma and plasma + chemical modification, due to the introduction of hydroxyl groups. Clouet et al. observed that argon plasma can be used to introduce oxygen functionality into the surface of the material [45]. For inert Ar gas plasma, functionalization of the surface is thought to take place on atmospheric exposure after the plasma treatment, as shown in Figure 5.

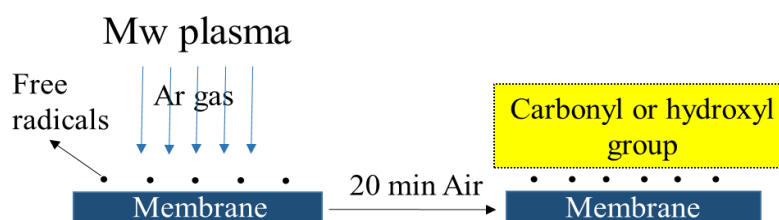**Figure 5.** Functionalization of membranes by atmospheric exposure subsequent to Ar plasma treatment.

The carboxyl/hydroxyl groups attached to the surface of the membrane increases the hydrophilicity of the membranes.

After incorporation, carboxyl or hydroxyl groups onto the fiber surface titanium dioxide deposition was performed. Particles of TiO$_2$ with aliphatic chains containing oxygen were obtained

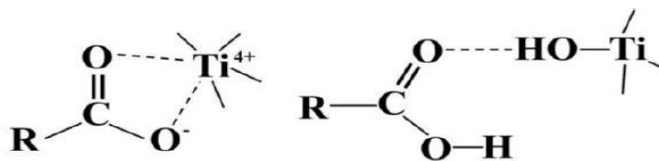via sol-gel method. The mechanism of self-assembly of TiO$_2$ on the polymer surface is described in Figure 6.

Figure 6. Mechanisms of self-assembly of TiO$_2$ with a polymer surface. Reproduction from [46].

In the first case, the titanium particles are connected to the surface by the ether coordination bonds, while in the second, the Ti is bonded by hydroxyl groups to the alkyl moieties. To verify the photoactivity of TiO$_2$ on the polymer surface, the photodegradation process was conducted. The results showed that the fouled layer of BSA could be removed from the membrane surface with 95% efficiency after UV irradiation in the presence of TiO$_2$ particles [38]. Unfortunately, the TiO$_2$ particles on the surface were not visible by means of our SEM instrument. We were only able to determine that they did not aggregate.

It was found that NaOH-induced hydrolysis of nitrile groups on the PAN surface resulted in increasing of membranes swelling with the time of treatment [47]. Yang et al. [48] hydrolyzed PAN hollow fiber in different concentrations of NaOH solution (0.5, 1 and 2 N). By increasing the concentration of NaOH, the concentration of carboxylic groups greatly increased. However, the highest concentration caused severe degradation of PAN fibers. In another paper dealing with chemical modification with NaOH, the decrease of water flux during the progress of hydrolysis with the increase of solute rejection was observed [49].

1.1. Filtration and Self-Cleaning Experiments

In this study, oil/water separation experiments were conducted by using a dead-end filtration device. The permeability of the each membrane was calculated according to Equation (2). Figure 7 shows the permeability of membranes for alternated filtration of water and the oily water. The process was repeated in each cycle. Between each cycle, the membranes were washed gently.

The performance of the membranes without post treatment is shown in Figure 7A. In each cycle, the filtration efficiency and the permeability of the membranes decreased drastically due to the fouling phenomenon. The permeability of the membranes with pure water decreased over 3000 times from the first to the fourth cycle. The same filtration protocol was repeated for the treated membranes.
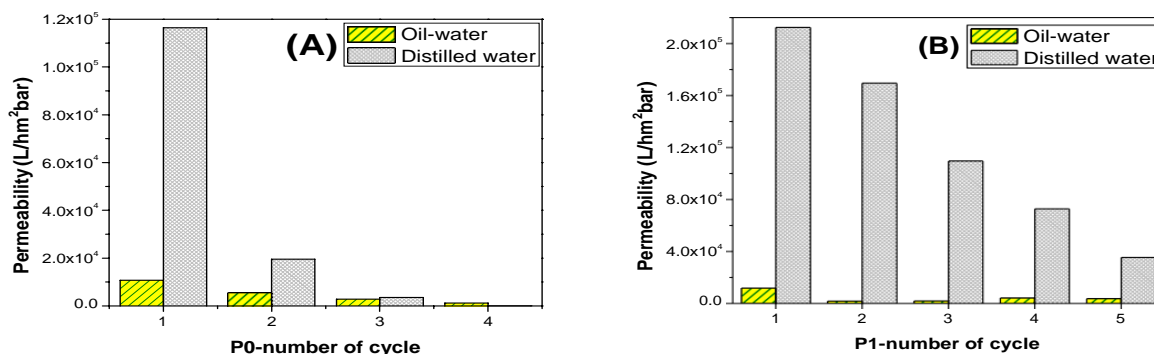

Figure 7.
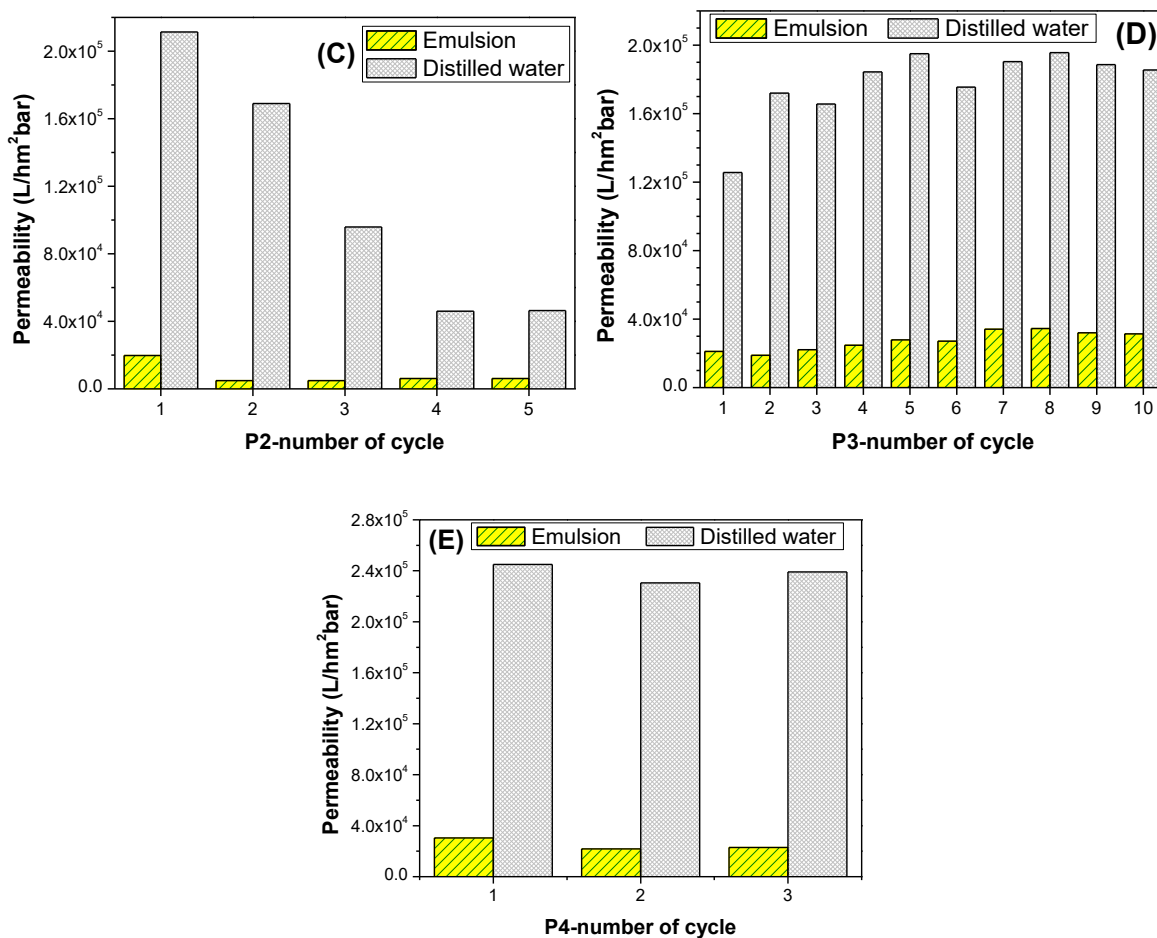*Cont.*

Figure 7. Repeated fouling and self-cleaning experiments of samples (**A**) P0, (**B**) P1, (**C**) P2, (**D**) P3, and (**E**) P4.

Membrane P1 showed better permeability than P0, due to the increase of hydrophilicity treatment. However, fouling was inevitable. At the end of the fifth cycle, the pure water permeability membranes decreased 6 times. A similar trend was observed for membrane P2. Immersing the men into the TiO$_2$ solution after plasma treatment did not improve the membrane performance. On the hand, membrane P3 showed excellent permeability with antifouling properties, even after the tenth cy mid-treatment between plasma and TiO$_2$ modification was necessary. Immersion in NaOH solutio effective method for grafting TiO$_2$ to the surface of the membrane, due to the creation of carboxylic g Once the sufficient surface grafting of TiO$_2$ had been obtained, the membrane fouling-resistan membrane permeability improved. A schematic diagram of the chemical modification process is sh Figure 8.

In the first stage, membranes treated with Ar microwave plasma were exposed to air for 2 Carbonyl/hydroxyl groups were formed on the surface of the membranes. Formation of carboxylic g on the surface occurred after NaOH treatment. Eventually, TiO$_2$ particles were grafted to the ac surface.

It is well known that UV radiation activates TiO$_2$ located on the surface. For this aim, membra was prepared and tested on a filtration unit. The results show that there is no high permeability diff between membranes P3 and P4. As UV treatment generates an extra cost, it can be concluded tha operation is not needed to improve membrane permeability.

110
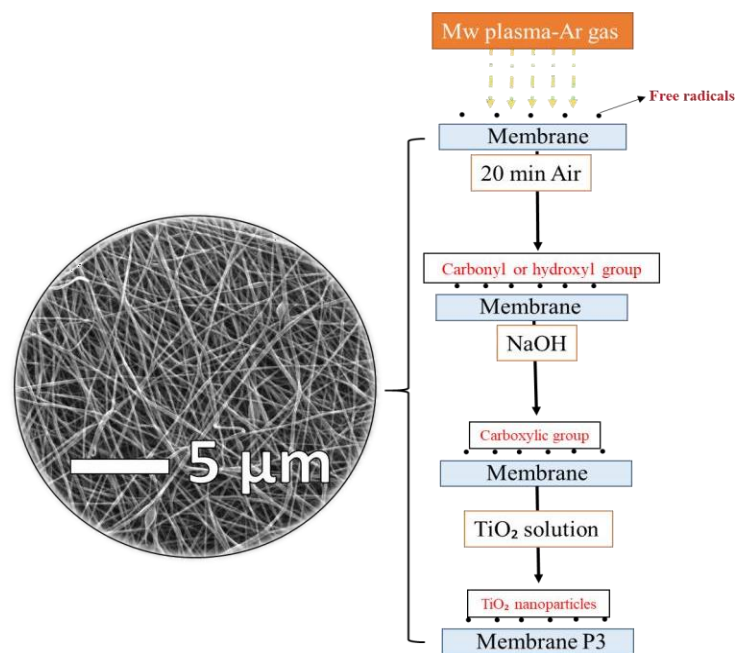
Figure 8. Schematic diagram of the surface modification of PVDF/PAN membranes.

The FTIR spectra were collected in order to investigate the chemical structure of the pristine membrane, and the membrane after plasma and chemical modification. Figure 9 confirms the presence of both polymers in the blend of PVDF/PAN. Stretching bands at 1175 cm^{-1}, 1412 cm^{-1}, and 876 cm^{-1} for the –CF$_2$ and C–F groups of PVDF, and absorption bands at 2239 cm^{-1} for the PAN nitrile groups, were observed. The TiO$_2$ sample had transmittance peaks in the range of 500–1000 cm^{-1}, which was assigned to the vibrations of Ti–O and Ti–O–Ti framework bonds. The bands around 1619 cm^{-1} corresponded to the bending modes of water Ti–OH [50–53].
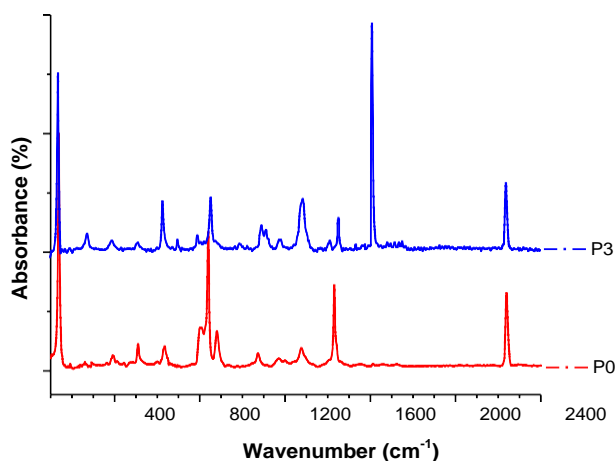
Figure 9. FTIR spectra of the neat sample and the sample after modification.

Figure 10 showed the permeability comparison of all of the membranes. The oily water and the pure water permeability was compared separately. All of the surface modified membranes exhibited higher pure water permeability than the pristine membrane. Moreover, membrane P3 has higher permeability and better anti-fouling properties compared to P0, P1, and P2, and its

fouling resistance property were remarkably improved. It can be concluded that the TiO$_2$ graf
hydrophilic membrane surface prevented direct adhesion of the oil droplets. Chen et al. [54] prepare
PVDF–MWCNT (multiwalled carbon nanotube) foam, which was characterized as a reusable and co
superhydrophobic–superoleophilic separator with good elasticity and low surface energy. The por
MWCNT foam exhibited high adsorption capacity to a variety of oils/organic solvents that made it a
candidate for large-scale industrial applications. Unlike our membranes, their foams worked on the
principle with a capacity 300–1200% of its own weight. Our membranes P0–P4 worked in the p
principle, and did not need any additional treatment.
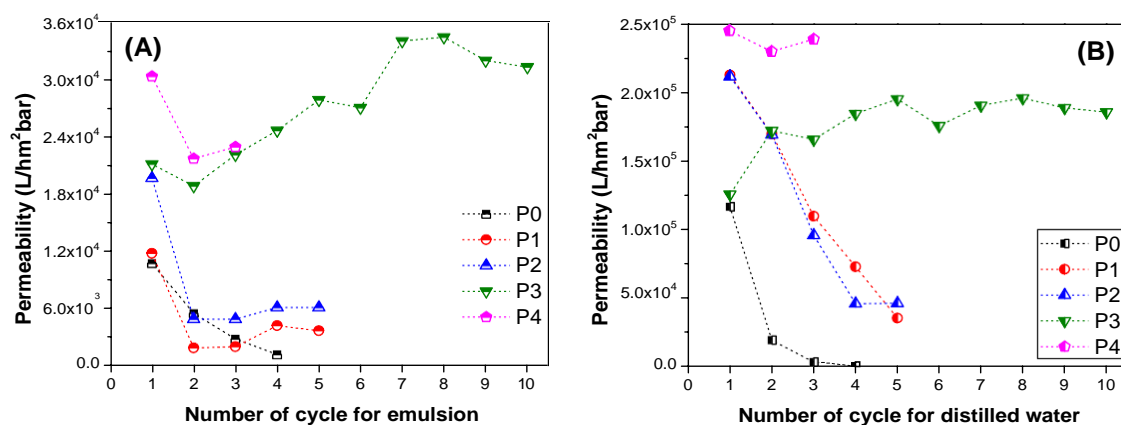
Figure 10. Permeability vs the number of cycles for (**A**) oil–water, and (**B**) distilled water.

The selectivity of the membranes is shown in Figure 11. The feed solution after separation wa
and the volume ratio of the oil and water was measured. The percentage of the selected liquid was ca
follows:

$$amount\ of\ selected\ liquid = \frac{V_{selected\ liquid}}{V_{total\ feed}} \times 100\ (\%) \qquad (3)$$

V is the volume in liters.
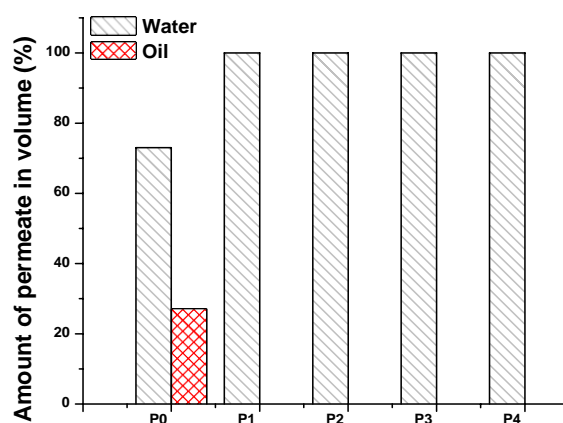
Figure 11. Selectivity of the membranes P0–P4.

Figure 11 shows that the neat PVDF/PAN membrane is both hydrophilic and oleophilic, while
treated membranes are more hydrophilic. The water selectivity of the pristine PVDF/PAN membran
from 73 to 100% as soon as the surface modification took place. The oleophobic

characteristics of the membranes made them attractive for the filtration of oily wastewater. Even thoug
membranes showed good hydrophilicity and oleophobicity, they were not sufficient enough to be ap
to the separation process. The sought membranes should be easily cleanable, and should not lose
performance over time. Only two of the investigated membranes, P3 and P4, fulfill the properties of
membranes for oil–water separation. On the other hand, the permeability of membranes P3 and P4
almost the same for the separation of oily wastewater. We determined that membrane P3 was the
membrane for separation, and that there was no need to expose it to UV light in order to activate the
particles on the membrane surface. The method used for the surface modification proved that h
permeable and highly selective membranes can be obtained for the separation of oily wastewater.

4. Conclusions

In summary, a PVDF/PAN nanofiber web was successfully fabricated and laminated. The resu
membranes showed both hydrophilic and oleophilic characteristics. A series of surface modifications
applied to the PVDF/PAN membranes to enhance the hydrophilicity and permeability of
membranes.

It was found that Ar-plasma surface treatment was not multifunctional; therefore, more than
chemical modification was required to accommodate the grafting of a functional TiO_2 group ont
membrane surface. Since the surface of the TiO_2-grafted membranes was able to build a h
hydrophilic and low surface energy barrier against the adhesion of oil droplets, the permeability an
antifouling properties were significantly enhanced. Undoubtedly, the most important part of the su
modification technique was grafting of TiO_2 onto the surface of the membrane.

In conclusion, we have reported a facile and low-cost method for the preparatio
hydrophilic/oleophobic membranes by using a new surface modification approach with a plasma
chemical method. Needless to say, surface treated polymeric PVDF/PAN membranes are a good cand
for use in separation technologies for water/oil emulsions.

Author Contributions: Marek Bryjak, Fatma Yalcinkaya and Anna Siekierka conceived and designed the experi
Fatma Yalcinkaya and Anna Siekierka performed the experiments; Fatma Yalcinkaya analyzed the data;
Bryjak, Fatma Yalcinkaya and Anna Siekierka contributed reagents/materials/analysis tools; Fatma Yalcinkaya
the paper.

Conflicts of Interest: The authors declare no conflict of interest. The founding sponsors had no role in the design
study; in the collection, analyses, or interpretation of data; in the writing of the manuscript, and in the decis

References

1. Cheng, M.; Gao, Y.; Guo, X.; Shi, Z.; Chen, J.; Shi, F. A functionally integrated device for effective and facile oil spill cleanup. *Langmuir* **2011**, *27*, 7371–7375. [CrossRef] [PubMed]
2. Ahmad, A.L.; Sumathi, S.; Hameed, B.H. Coagulation of residue oil and suspended solid in palm oil mill effluent by chitosan, alum and PAC. *Chem. Eng. J.* **2006**, *118*, 99–105. [CrossRef]
3. Paul, U.C.; Fragouli, D.; Bayer, I.S.; Athanassiou, A. Functionalized cellulose networks for efficient oil removal from oil–water emulsions. *Polymers* **2016**, *8*, 52. [CrossRef]
4. Liu, T.; Chen, S.; Liu, H. Oil adsorption and reuse performance of multi-walled carbon nanotubes. *Procedia Eng.* **2015**, *102*, 1896–1902. [CrossRef]
5. Okiel, K.; El-Sayed, M.; El-Kady, M.Y. Treatment of oil–water emulsions by adsorption onto activated carbon, bentonite and deposited carbon. *Egypt. J. Pet.* **2011**, *20*, 9–15. [CrossRef]
6. Al-Shamrani, A.A.; James, A.; Xiao, H. Destabilisation of oil–water emulsions and separation by dissolved air flotation. *Water Res.* **2002**, *36*, 1503–1512. [CrossRef]

7. Felizardo, P.; Joana Neiva Correia, M.; Raposo, I.; Mendes, J.F.; Berkemeier, R.; Bordado, J.M. Production of biodiesel from waste frying oils. *Waste Manag.* **2006**, *26*, 487–494. [CrossRef] [PubMed]

8. Mi, Y.; Li, J.; Zhou, W.; Zhang, R.; Ma, G.; Su, Z. Improved stability of emulsions in preparation of uniform small-sized konjac glucomanna (KGM) microspheres with epoxy-based polymer membrane by premix membrane emulsification. *Polymers* **2016**, *8*, 53. [CrossRef]

9. Zhu, Y.; Xie, W.; Zhang, F.; Xing, T.; Jin, J. Superhydrophilic in-situ-cross-linked zwitterionic polyelectrolyte/PVDF-blend membrane for highly efficient oil/water emulsion separation. *ACS Appl. Mater. Interfaces* **2017**, *9*, 9603–9613. [CrossRef] [PubMed]

10. Cao, Z.; Hao, T.; Wang, P.; Zhang, Y.; Cheng, B.; Yuan, T.; Meng, J. Surface modified glass fiber membranes with superior chemical and thermal resistance for O/W separation. *Chem. Eng. J.* **2017**, *309*, 30–40. [CrossRef]

11. Cumming, I.W.; Holdich, R.G.; Smith, I.D. The rejection of oil using an asymmetric metal microfilter to separate an oil in water dispersion. *Water Res.* **1999**, *33*, 3587–3594. [CrossRef]

12. Koehler, J.A.; Ulbricht, M.; Belfort, G. Intermolecular forces between proteins and polymer films with relevance to filtration. *Langmuir* **1997**, *13*, 4162–4171. [CrossRef]

13. Jiang, J.; Zhu, L.; Zhu, L.; Zhang, H.; Zhu, B.; Xu, Y. Antifouling and antimicrobial polymer membranes based on bioinspired polydopamine and strong hydrogen-bonded poly(*N*-vinyl pyrrolidone). *ACS Appl. Mater. Interfaces* **2013**, *5*, 12895–12904. [CrossRef] [PubMed]

14. Zhang, G.; Jiang, J.; Zhang, Q.; Gao, F.; Zhan, X.; Chen, F. Ultralow oil-Fouling heterogeneous poly(ether sulfone) ultrafiltration membrane via blending with novel amphiphilic fluorinated gradient copolymers. *Langmuir* **2016**, *32*, 1380–1388. [CrossRef] [PubMed]

15. Zhou, S.; Xue, A.; Zhao, Y.; Li, M.; Wang, H.; Xing, W. Grafting polyacrylic acid brushes onto zirconia membranes: Fouling reduction and easy-cleaning properties. *Sep. Purif. Technol.* **2013**, *114*, 53–63. [CrossRef]

16. Zhao, X.; Su, Y.; Chen, W.; Peng, J.; Jiang, Z. Grafting perfluoroalkyl groups onto polyacrylonitrile membrane surface for improved fouling release property. *J. Membr. Sci.* **2012**, *415–416*, 824–834. [CrossRef]

17. Ju, H.; McCloskey, B.D.; Sagle, A.C.; Wu, Y.H.; Kusuma, V.A.; Freeman, B.D. Crosslinked poly(ethylene oxide) fouling resistant coating materials for oil/water separation. *J. Membr. Sci.* **2008**, *307*, 260–267. [CrossRef]

18. Jing, B.; Wang, H.; Lin, K.Y.; McGinn, P.; Na, C.; Zhu, Y. A facile method to functionalize engineering solid membrane supports for rapid and efficient oil–water separation. *Polymer* **2013**, *54*, 5771–5778. [CrossRef]

19. Zhou, T.; Yang, J.; Zhu, D.; Zheng, J.; Handschuh-Wang, S.; Zhou, X.; Zhang, J.; Liu, Y.; Liu, Z.; He, C.; et al. Hydrophilic sponges for leaf-inspired continuous pumping of liquids. *Adv. Sci.* **2017**, *4*, 1700028. [CrossRef] [PubMed]

20. Zhang, J.; Xue, Q.; Pan, X.; Jin, Y.; Lu, W.; Ding, D.; Guo, Q. Graphene oxide/polyacrylonitrile fiber hierarchical-structured membrane for ultra-fast microfiltration of oil-water emulsion. *Chem. Eng. J.* **2017**, *307*, 643–649. [CrossRef]

21. Schulze, A.; Breite, D.; Kim, Y.; Schmidt, M.; Thomas, I.; Went, M.; Fischer, K.; Prager, A. bio-inspired polymer membrane surface cleaning. *Polymers* **2017**, *9*, 97. [CrossRef]

22. Yang, J.; Zhang, Z.; Xu, X.; Zhu, X.; Men, X.; Zhou, X. Superhydrophilic–superoleophobic coatings. *J. Mater. Chem.* **2012**, *22*, 2834–2837. [CrossRef]

23. Wei, X.; Fei, Y.; Shi, Y.; Chen, J.; Lv, B.; Chen, Y.; Xiang, H. Hemocompatibility and ultrafiltration performance of PAN membranes surface-modified by hyperbranched polyesters. *Polym. Adv. Technol.* **2016**, *27*, 1569–1576. [CrossRef]

24. Wang, Y.; Lai, C.; Wang, X.; Liu, Y.; Hu, H.; Guo, Y.; Ma, K.; Fei, B.; Xin, J. Beads-on-string structured nanofibers for smart and reversible oil/water separation with outstanding antifouling property. *ACS Appl. Mater. Interfaces* **2016**, *8*, 25612–25620. [CrossRef] [PubMed]

25. Daoud, W.A.; Leung, S.K.; Tung, W.S.; Xin, J.H.; Cheuk, K.; Qi, K. Self-cleaning keratins. *Chem. Mater.* **2008**, *20*, 1242–1244. [CrossRef]

26. Kaihong, Q.; Wang, X.; Xin, J.H. Photocatalytic self-cleaning textiles based on nanocrystalline titanium dioxide. *Text. Res. J.* **2011**, *81*, 101–110. [CrossRef]

27. Homaeigohar, S.; Elbahri, M. Nanocomposite electrospun nanofiber membranes for environmental remediation. *Materials* **2014**, *7*, 1017–1045. [CrossRef] [PubMed]

28. Yalcinkaya, F. Mechanically enhanced electrospun nanofibers for wastewater treatment. In Proceedings of the International Conference on Advances in Energy Systems and Environmental Engineering, Wroclaw, Poland, 2–5 July 2017; Volume 7

29. Yalcinkaya, F. Preparation of various nanofiber layers using wire electrospinning system. *Arab. J. Chem.* **2016**, *12*. [CrossRef]

30. Jiříček, T.; Komárek, M.; Chaloupek, J.; Lederer, T. Flux enhancement in membrane distillation sing nanofiber membranes. *J. Nanomater.* **2016**, *2016*, 9327431. [CrossRef]

31. Wang, Z.; Hou, D.; Lin, S. Composite membrane with underwater-oleophobic surface for anti-oil-fouling membrane distillation. *Environ. Sci. Technol.* **2016**, *50*, 3866–3874. [CrossRef] [PubMed]

32. Liao, Y.; Wang, R.; Tian, M.; Qiu, C.; Fane, A.G. Fabrication of polyvinylidene fluoride (PVDF) nanofiber membranes by electro-spinning for direct contact membrane distillation. *J. Membr. Sci.* **2013**, *425–426*, 30–39. [CrossRef]

33. Mei, Y.; Yao, C.; Fan, K.; Li, X. Surface modification of polyacrylonitrile nanofibrous membranes with superior antibacterial and easy-cleaning properties through hydrophilic flexible spacers. *J. Membr. Sci.* **2012**, *417–418*, 20–27. [CrossRef]

34. Yalcinkaya, F.; Yalcinkaya, B.; Pazourek, A.; Mullerova, J.; Stuchlik, M.; Maryska, J. Surface modification of electrospun PVDF/PAN nanofibrous layers by low vacuum plasma treatment. *Int. J. Polym. Sci.* **2016**, *2016*. [CrossRef]

35. Kang, Y.H.; Ahn, K.; Jeong, S.Y.; Bae, J.S.; Jin, J.S.; Kim, H.G.; Hong, S.W.; Cho, C.R. Effect of plasma treatment on surface chemical-bonding states and electrical properties of polyacrylonitrile nanofibers. *Thin Solid Films* **2011**, *519*, 7090–7094. [CrossRef]

36. Yalcinkaya, F.; Siekierka, A.; Bryjak, M.; Maryska, J. Preparation of various nanofibrous composite membranes using wire electrospinning for oil-water separation. In *IOP Conference Series: Materials Science and Engineering*; IOP Publishing Ltd.: Bristol, UK, 2017; Volume 254, p. 102011.

37. Yalcinkaya, B.; Yalcinkaya, F.; Chaloupek, J. Thin film nanofibrous composite membrane for dead-end seawater desalination. *J. Nanomater.* **2016**, *2016*, 2694373. [CrossRef]

38. Gancarz, I.; Bryjak, M.; Wolska, J.; Siekierka, A.; Kujawski, W. Membranes with a plasma deposited titanium isopropoxide layer. *Chem. Pap.* **2016**, *70*. [CrossRef]

39. Siekierka, A.; Kujawa, J.; Kujawski, W.; Bryjak, M. Lithium dedicated adsorbent for the preparation of electrodes useful in the ion pumping method. *Sep. Purif. Technol.* **2018**, *194*, 231–238. [CrossRef]

40. Bessekhouad, Y.; Robert, D.; Weber, J.V. Preparation of TiO$_2$ nanoparticles by Sol-Gel route. *Int. J. Photoenergy* **2003**, *5*, 153–158. [CrossRef]

41. Uosaki, K.; Yano, T.; Nihonyanagi, S. Interfacial water structure at as-prepared and UV-induced hydrophilic TiO$_2$ surfaces studied by sum frequency generation spectroscopy and quartz crystal microbalance. *J. Phys. Chem. B* **2004**, *108*, 19086–19088. [CrossRef]

42. Wang, R.; Hashimoto, K.; Fujishima, A.; Chikuni, M.; Kojima, E.; Kitamura, A.; Shimohigoshi, M.; Watanabe, T. Light-induced amphiphilic surfaces. *Nature* **1997**, *388*, 431–432. [CrossRef]

43. Yalcinkaya, F.; Yalcinkaya, B.; Hruza, J.; Hrabak, P. Effect of nanofibrous membrane structures on the treatment of wastewater microfiltration. *Sci. Adv. Mater.* **2017**, *9*, 747–757. [CrossRef]

44. Na, L.; Liu, Z.; Xu, S. Dynamically formed poly(vinyl alcohol) ultrafiltration membranes with good anti-fouling characteristics. *J. Membr. Sci.* **2000**, *169*, 17–28. [CrossRef]

45. Clouet, F.; Shi, M.K. Interactions of polymer model surfaces with cold plasmas: Hexatriacontane as a model molecule of high-density polyethylene and octadecyl octadecanoate as a model of polyester. I. Degradation rate versus time and power. *J. Appl. Polym. Sci.* **1992**, *46*, 1955–1966. [CrossRef]

46. Li, J.H.; Xu, Y.Y.; Zhu, L.P.; Wang, J.H.; Du, C.H. Fabrication and characterization of a novel TiO$_2$ nanoparticle self-assembly membrane with improved fouling resistance. *J. Membr. Sci.* **2009**, *326*, 659–666. [CrossRef]

47. Bryjak, M.; Hodge, H.; Dach, B. Modification of porous polyacrylonitrile membrane. *Die Angew. Makromol. Chem.* **1998**, *260*, 25–29. [CrossRef]

48. Yang, M.C.; Tong, J.H. Loose ultrafiltration of proteins using hydrolyzed polyacrylonitrile hollow fiber. *J. Membr. Sci.* **1997**, *132*, 63–71. [CrossRef]

49. Abedi, M.; Sadeghi, M.; Pourafshari Chenar, M. Improving antifouling performance of PAN hollow fiber membrane using surface modification method. *J. Taiwan Inst. Chem. Eng.* **2015**, *55*, 42–48. [CrossRef]

50. Grujic-Brojcin, M.; Scepanovic, M.; Dohcevic-Mitrovic, Z.; Popovic, Z.V. Infrared study of nonstoichiometric anatase TiO$_2$ nanopowders. *Sci. Sinter.* **2006**, *38*, 183–189. [CrossRef]

51. León, A.; Reuquen, P.; Garín, C.; Segura, R.; Vargas, P.; Zapata, P.; Orihuela, P.A. FTIR and Raman Characterization of TiO$_2$ Nanoparticles Coated with Polyethylene Glycol as Carrier for 2-Methoxyestradiol. *Appl. Sci.* **2017**, *7*, 49. [CrossRef]

52. Kumar, P.M.; Badrinarayanan, S.; Sastry, M. Nanocrystalline TiO$_2$ studied by optical, FTIR and X-ray photoelectron spectroscopy: Correlation to presence of surface states. *Thin Solid Films* **2000**, *358*, 122–130. [CrossRef]

53. Pan, H.; Wang, X.; Xiao, S.; Yu, L.; Zhang, Z. Preparation and characterization of TiO$_2$ nanoparticles

surface-modified by octadecyltrimethoxysilane. *Indian J. Eng. Mater. Sci.* **2013**, *20*, 561–567.

54. Chen, F.; Lu, Y.; Liu, X.; Song, J.; He, G.; Tiwari, M.K.; Carmalt, C.J.; Parkin, I.P. Table salt as a template to prepare reusable porous PVDF–MWCNT foam for separation of immiscible oils/organic solvents and corrosive aqueous solutions. *Adv. Funct. Mater.* **2017**, *27*, 1702926. [CrossRef]

Surface-Modified Nanofibrous PVDF Membranes for Liquid Separation Technology

Evren Boyraz [1], Fatma Yalcinkaya [1,2,*] Jakub Hruza [1,2] and Jiri Maryska [1,2]

[1] Center for nanomaterials, Advanced Technology and Innovation, Department of Nanomaterials and Informatics, Technical University of Liberec, Studentska 1402/2, 46117, Czech Republic
[2] Faculty of Mechatronics, Institute for New Technologies and Applied Informatics, Technical University of Liberec, Studentska 1402/2, 46117 Liberec, Czech Republic
* Correspondence: fatma.yalcinkaya@tul.cz; Tel.:+420-485-353-389

Abstract: Preparing easily scaled up, cost-effective, and recyclable membranes for separation technology is challenging. In the present study, a unique and new type of modified polyvinylidene fluoride (PVDF) nanofibrous membrane was prepared for the separation of oil–water emulsions. Surface modification was done in two steps. In the first step, dehydrofluorination of PVDF membranes was done using an alkaline solution. After the first step, oil removal and permeability of the membranes were dramatically improved. In the second step, TiO_2 nanoparticles were grafted onto the surface of the membranes. After adding TiO_2 nanoparticles, membranes exhibited outstanding anti-fouling and self-cleaning performance. The as-prepared membranes can be of great use in new green separation technology and have great potential to deal with the separation of oil–water emulsions in the near future.

Keywords: PVDF; membrane; surface modification; filtration; nanofiber; electrospinning

1. Introduction

Burgeoning industrial development unavoidably generates large volumes of wastewater that contain emulsified oil/water mixtures. Cost-effective and efficient separation processes for such mixtures are in high demand yet still challenging. Current separation techniques include centrifuges, magnetic separation, oil skimming, floating, and depth filters, which are more suitable for immiscible oil/water mixtures but not for emulsified ones [1]. Emulsified oil/water mixtures can contain droplet sizes less than a few microns, which require specific separation techniques.

Polymer-based microfiltration (MF) membranes were successfully used for the separation of oil/water emulsions. However, the permeability and flux of the membrane decline rapidly due to membrane fouling that reduces their performance over a short operation time. The main reason for the membrane fouling is that oil droplets plug the pore size of the membrane and/or adsorption of the surfactant. To address the membrane fouling problem, several attempts were made to improve the hydrophilicity of the membrane through blending of hydrophilic polymers, surface grafting, or surface modification. Zhang et al. [2] prepared an alkaline-induced phase inversion polyacrylonitrile (PAN) membrane, which showed superhydrophilic/underwater superoleophobic characteristics. During the phase inversion process, sodium hydroxide (NaOH) was added to the coagulation bath. In the NaOH coagulation bath, the –CN groups of PAN hydrolyzed to –COOH groups, which introduced hydrophilic components to the PAN. Moreover, adding NaOH led to the formation of a rough structure on the membrane surface. The resultant membrane showed very high flux with oil rejection of the oil residual. On the other hand, Fan et al. [3] prepared hydrophilic/oleophilic polystyrene (PS)/polyacrylonitrile (PAN) bicomponent membranes that exhibited extremely high oil flux. The bicomponent PS/PAN membrane was prepared using the electro-blowing method. Results indicated that the flux of the

membrane achieved up to 1800 L $m^{-2} \cdot h^{-1}$ (efficiency > 99.6%) with a flux recovery ratio of 94.09% after 10 cycle
the tensile strength of the membrane improved by increasing the ratio of PAN in the mixture. In another work
dioxide (TiO$_2$) nanoparticles were grafted onto the surface of polyvinylidene fluoride (PVDF)/polyacrylon
membranes using a two-step modification system. In the first step, hydroxyl and carbonyl groups were introdu
membrane surface using low-vacuum argon plasma treatment and a NaOH aqueous solution. In the secor
nanoparticles were grafted onto the surface of the membrane. Results indicated that the TiO$_2$ grafted membi
extremely high water permeability with a self-cleaning property. Nanofiber webs are a good candidate for use
applications due to their high surface   area, tight pore size, and highly porous structure. Even though th
filtration application on an industrial scale, water domain applications are still in progress. Mechanical str
nanofibers is not enough to withstand any pressure under water. There were a number of works submitted o
mechanical properties of nanofibers such as dip coating, addition of epoxy,
polymer or inorganics blending, tailoring, ultrasonic welding, heat pressing, etc. [5–14].

Herein, the mechanical problem of the nanofiber layer was solved using the heat-press lamination proces:
method, nanofiber webs were transported and adhered to a different surface without any damage [15]. A PVDF
membrane was used for the separation of oil/water emulsions. PVDF is commonly used in membrane technolo
outstanding mechanical, chemical, thermal, and oxidation resistance properties [16]. PVDF is an oleophilic/l
membrane due to its low surface energy (25 dynes cm^{-1}) [16,17]. The aim of this work was to prepare self-cle
nanofibrous hybrid membranes for the separation of oily wastewater.

For this reason, various nanofiber layers were used for the separation of oil–water emulsions. Firstly, pe
the membranes was measured and compared. Secondly, selected membranes were carried to the surface
process. Finally, the self-cleaning membrane was prepared for the separation of oil–water emulsions.

1. Materials and Methods

1.1. Membrane Preparation

PVDF nanofibers were obtained from Nanocenter (Laboratory of nanomaterial application, Technical U
Liberec, Liberec, Czech Republic). Nanofiber layers had densities of 1, 2, and 3 g/m^2. To increase mechanica
100-g/m^2 polyethylene terephthalate nonwoven (Mogul Nonwovens, Gaziantep, Turkey) was used as a supp
polyester adhesive was used to bind nanofibers to the nonwoven surface. The heat-press method was applied
previously [8,13,15]. The highest-density nanofiber web was taken for further surface modification. Sample abbr
given in Table 1.

Table 1. Abbreviations of the samples. PVDF—polyvinylidene fluoride.

Polymer	Density (g/m^2)	Modification	Abbreviation	Fiber Diameter (nm)
	1	-	PVDF 1	148.9 ± 23.1
	2	-	PVDF 2	148.5 ± 45.6
	3	-	PVDF 3	134.2 ±37.2
PVDF				
	3	NaOH	PVDF_N	164.9 ± 40.3
	1	NaOH + TiO$_2$	PVDF_NT	248.2 ± 47.8
	3	KOH	PVDF_K	174.9 ± 57.6
	3	KOH + TiO$_2$	PVDF_KT	197.0 ± 54.7

1.2. Surface Modification

The first step in the surface modification was done by dehydrofluorination of the PVDF membrane u
solutions. Two types of dehydrofluorinated PVDF were prepared with sodium hydroxide

(NaOH, Penta s.r.o., Prague, Czech Republic) and potassium hydroxide (KOH, Penta s.r.o., Prague, Czech Republic).

The reaction of the alkaline solution with PVDF is given as follows [18]:

$$-(CH_2-CF_2)- + xOH \rightarrow -(CH=CF)- + xF + H_2O,$$
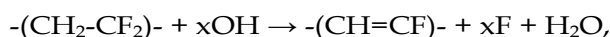
where x is Na or K.

After the lamination process, one of the membranes was immersed into 72 g of NaOH solution in 30 mL of distilled water (DI) for 48 h, while the other membrane was immersed into 2 g of KOH solution in 20 mL of isopropyl alcohol (IPA, Penta s.r.o., Prague, Czech Republic) for 1 h.

Subsequently, the membranes were taken from the alkaline solutions, washed several times with DI, and immersed into 0.5 g of titanium dioxide (TiO₂, 20 nm, Sigma-Aldrich spol. s.r.o, Prague, Czech Republic)/40 mL of DI mixture and kept for 24 h.

Immediately after TiO₂ treatment, the membranes were taken and washed several times using DI water via the immersion method and one-minute cleaning with the ultrasonic cleaner to remove excessive TiO₂ on the surface of the membrane.

Hydroxyl groups play an important role in the reaction chemistry of metal-oxide surfaces such as TiO₂. The reaction of the alkaline solution with PVDF and the interaction between the dehydrofluorinated PVDF and TiO₂ are shown in Figure 1.
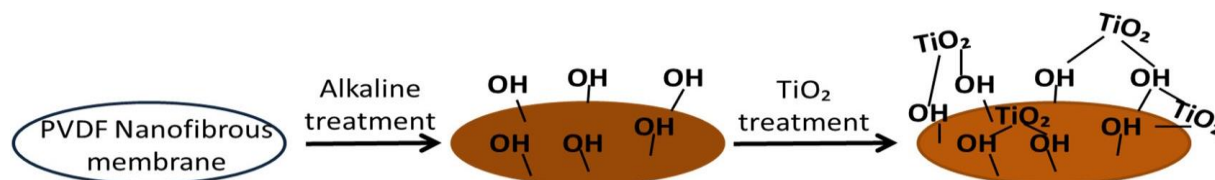

Figure 1. Surface modification of the polyvinylidene fluoride (PVDF) membrane.

The interaction between dehydrofluorinated PVDF and TiO₂ was studied in the literature [4,19,20].

1.1. Characterization

Surface morphology of the membranes was characterized using scanning electron microscopy (SEM, Vega 3SB, Brno, Czech Republic). The samples were mounted on a stub of metal with adhesive (double-sided adhesive), coated with 7 nm of gold, and then observed in the microscope under various magnifications at various places (accelerating voltage = 30 kV; beam intensity = 7). Fiber diameter was analyzed using the free online Image-J program. From each sample, at least 50 fibers were measured. Average, maximum, and minimum pore sizes of the membranes were measured using a custom-made porometer and the principle of bubble point measurement, as explained in the literature [15]. The bubble point test is used to determine the size of the pores of the porous material. In the bubble point test, sufficient gas pressure is applied to overcome the capillary forces of the wetted membrane pores to determine largest pore size. In this method, it is necessary to control the pressure needed to pass a liquid through the tested porous material and for wetting the sample. The size of the average and minimum pores can also be determined by increasing the air pressure and measuring its flow through the sample. In these circumstances, it is necessary to compare the pressure curve of the wet sample with the pressure curve of the dry sample. The flow rate increases when the pressure increases in the dry sample. On the other hand, in the wet sample, at the beginning, there is no flow because all the pores are filled with the liquid. At a certain pressure, the gas empties the largest pore, and gas begins to flow through the wet sample. The intersection between the calculated half-dry and the wet sample gives the mean flow pore size. When all the pores are emptied, an intersection between the wet and dry curve will be observed. This means that the relationship between the applied pressure and the detected flow becomes linear, and the intersection of the wet and dry curve represents

the detected minimum pore size. In this work, ethylene glycol (surface tension 47.3 mN$\cdot$m^{-1}) was used to wet the samples. Both wet and dry measurement were taken to determine maximum, minimum, and mean pore size. At least three measurements were taken.

Air permeability of the membranes was tested using an SDL ATLAS Air Permeability Tester (Rock Hill ATLAS Air Permeability Tester (at 200 Pa and 20 cm^2, Rock Hill, SC, USA). The air permeability test was used for determination of the air permeability of the flat membrane. A specimen was clamped over the test head opening by pressing down the clamping arm, which started the vacuum pump. Measurements were performed by application of 200 Pa of air pressure per 20 cm^2 of fabric surface. At least three measurements were taken at various places on the membrane. Results were expressed as L$\cdot$m$^{-2}\cdot$s^{-1}.

Bursting pressure of the membranes was tested, and the maximum delamination pressure was recorded using a custom-made device. The membrane (47 mm in diameter) was placed between two rings, and pressurized water was applied from one side until the nanofiber layer delaminated from the supporting layer. The hydrostatic pressure was measured using a pressure controller, which was placed in front of the membrane and connected to a computer. The hydrostatic pressure was increased gradually, and, as soon as the nanofiber layer burst, the pressure value on the screen decreased sharply. The maximum pressure value was recorded as the bursting/delamination strength of the membrane [15].

A Krüss Drop Shape Analyzer DS4 (Krüss GmbH, Hamburg, Germany) was used for the measurement of water contact angle using distilled water (surface tension 72.0 mN$\cdot$m^{-1}). Five measurements from each membrane were taken.

The hydroxyl groups on the PVDF nanofiber were observed using Fourier-transform infrared spectroscopy (FTIR, Nicolet iZ10 by Thermo Scientific, Prague, Czech Republic).

1.1. Emulsion Preparation

A 50 vol.%/50 vol.% oil/water emulsion was prepared. Water-soluble/oil-insoluble food colorant was used to detect permeate after separation. Nonionic Triton X-100 (Sigma-Aldrich spol. s.r.o, Prague, Czech Republic) was used as a surfactant for preparation of the emulsion. Generally, oil–water emulsions are prepared using nonionic surfactants [21]. The preparation method was as follows:

$-\rightarrow$ A few drops of pink color food colorant were mixed with 100 g of distilled water.
$-\rightarrow$ Then, 2 g of surfactant was added to the water and mixed with a magnetic stirrer for 10 min.
$-\rightarrow$ Next, 100 g of sunflower oil was added to the water/surfactant mixture.
$-\rightarrow$ Finally, the solution was mixed with a magnetic stirrer at 500 rpm for 24 h.

A digital microscope (Levenhuk Digital Microscope, Prague, Czech Republic) was used for the determination of oil droplet size (Figure 2). The emulsion was kept for one week without any stirring. Droplet size was then measured. There was no change in the size of the droplets. Average drop size was found to be 1.05 ± 0.34 μm.

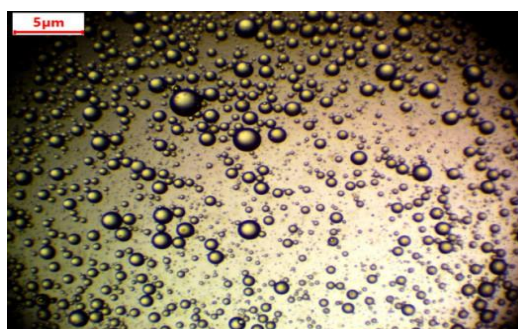**Figure 2.** Droplets of oil under a microscope.

An Amicon (50 mL stirred cell, Millipore Corporation, Billerica, MA, USA) dead-end filtration unit was used for the separation test. The flux and the permeability of the samples were calculated according to Equations (1) and (2).

$$F=G/At \hspace{4cm} (1)$$

$$P= F/T \hspace{4cm} (2)$$

where F is the flux ($L \cdot m^{-2} \cdot h^{-1}$), A is the area of the membrane (m^2), G is the amount of permeate (L), t is the time of the filtration process, T is the transmembrane pressure, and P is the permeability of the membrane ($L \cdot m^{-2} \cdot h^{-1} \cdot bar^{-1}$).

Selectivity of the membranes was observed according to permeate color, and the microscope was used to detect any oil droplets in the permeate. The separation test for one membrane was done a number of times. In the first step, only 15 mL of distilled water was used as feed; in the second step, 15 mL of emulsion was used. This process was repeated at least three times to observe membrane fouling or self-cleaning.

2. Results and Discussion

2.1. Characterization of the Membranes

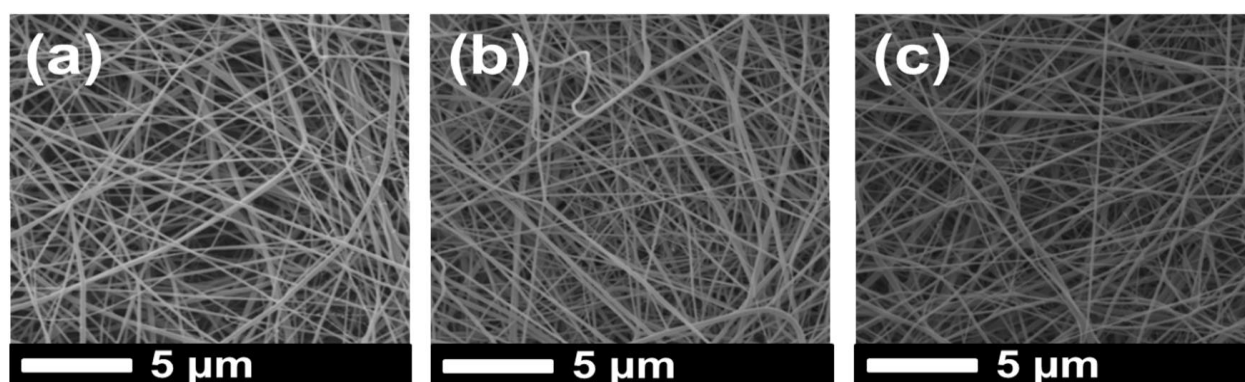SEM images of the samples were taken after lamination and the surface modification process (Figures 3 and 4).

Figure 3. SEM images of (**a**) PVDF 1, (**b**) PVDF 2, and (**c**) PVDF 3 after lamination.

It was observed that the fiber diameter did not change with increasing nanofiber web density (Figure 3, Table 1). Since spinning conditions remained the same, only the backing paper speed was changed to get various nanofiber web densities, which did not influence fiber diameter. On the other hand, treatment of the PVDF nanofiber with an alkaline solution yielded a slight increase in fiber diameter because of swelling of the fibers (Figure 4a,c). Figure 4b,d show that TiO_2 nanoparticles distributed very well on the surface of the nanofiber without any aggregation, showing that a regular dehydrofluorination took place. Hydrophilic OH groups on the membrane attached to the TiO_2 nanoparticles. The fibers became thicker after the TiO_2 nanoparticle attachment on the surface.

The FTIR spectra were collected in order to investigate the chemical structure of the PVDF nanofibrous webs. These are shown in Figure 5. The stretching bands at 1173 cm^{-1} and 876 cm^{-1} were attributed to the $-CF_2$ and C–F groups of PVDF. The spectra confirmed the presence of –OH groups
after surface modification, with absorption bands at 1600 cm^{-1} representing –OH group deformation vibrations. The very broad and less intense peak between 2500 cm^{-1} and 3500 cm^{-1} was due to O–H functionalities. It may be concluded that the bonded –OH groups played a major role in the hydrophilicity of the membranes.
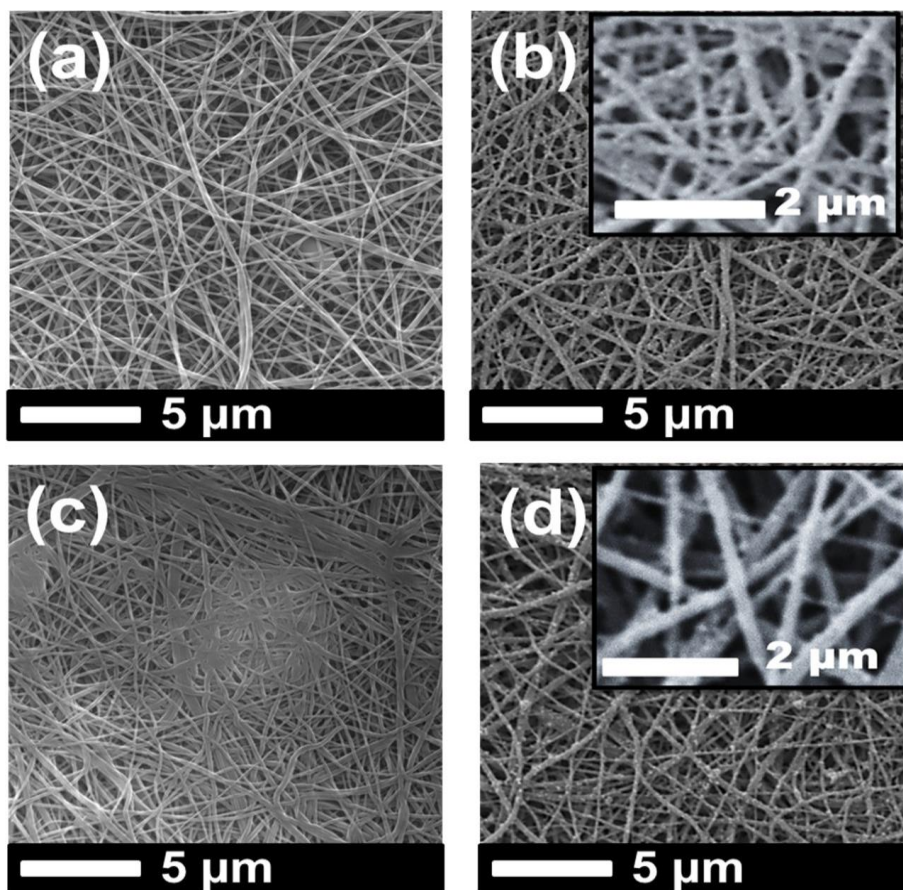
Figure 4. SEM images of (**a**) PVDF_N, (**b**) PVDF_NT, (**c**) PVDF_K, and (**d**) PVDF_KT.
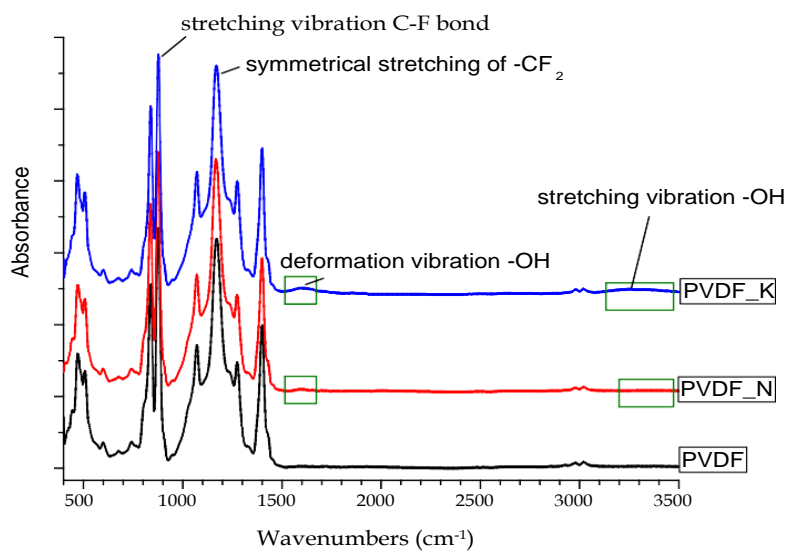

Figure 5. Fourier-transform infrared (FTIR) image of the PVDF membranes.

Pore size of the samples before modification was measured and is shown in Table 2. Membrane pore size for the modified samples was not measured. Once the samples were modified, they were kept wet in distilled water as recommended. It was found that drying of the modified and wetted

membrane could cause possible membrane cracks and damage. Unfortunately, pore size measurement only for the dry samples. Increased nanofiber web density caused a decrease in the average pore size compact structure. The role of pore size in the separation process was significant. Tight pore size incr selectivity of the membranes.

Table 2. Maximum and average pore size of the membranes.

Sample	Maximum Pore Size (μm)	Average Pore Size (μm)
PVDF 1	4.54 ± 0.14	2.50 ± 0.29
PVDF 2	4.20 ± 0.00	1.15 ± 0.08
PVDF 3	4.23 ± 0.05	0.72 ± 0.04

Air permeability of the membranes was measured after the lamination process. The main aim o was to observe whether the adhesive blocked the pore size of the nanofibers during lamination. The pressure test is another method of determining the quality of the lamination process. Using this strength of the lamination was measured. Figure 6 shows the relationship among density of the layer, air permeability, and bursting pressure.
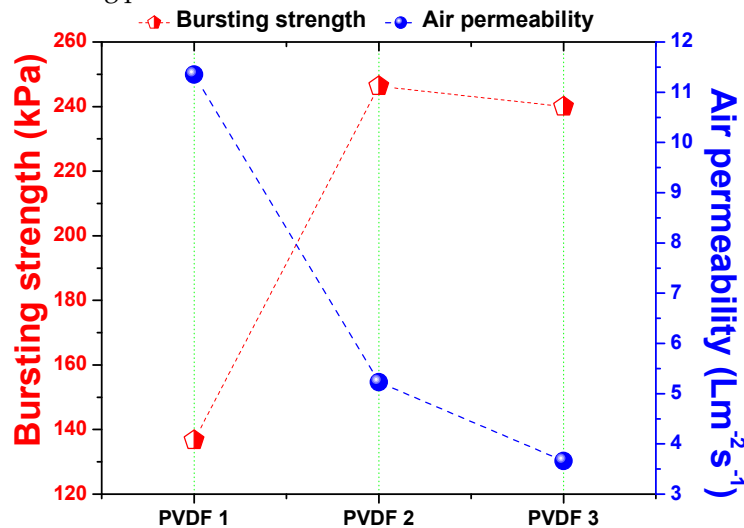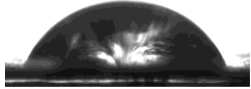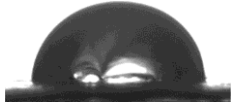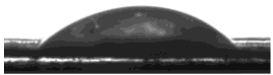

Figure 6. Bursting pressure and air permeability of the membrane according to nanofiber web

There was an inverse proportional relationship between the density of the nanofiber web permeability. Lower density meant fewer fiber bundles on the web, which resulted in a more open On the contrary, higher density meant more fiber bundles, which resulted in a compact structure. pressure results indicated that, at the lowest density (1 g/m^2), adhesion of the nanofibers to the sup not as strong as that at the higher nanofiber web density. The reason could have been the low m strength and high abrasion resistance of the low-density nanofiber fiber web. As soon as the fibe increased from 1 to 2 g/m^2, bursting pressure improved by 80%. Further improvements did not cha density significantly. Based on previous work [8,13], the minimum required bursting pressures for and polyacrylonitrile (PAN) nanofiber membranes were determined to be 175 kPa and 195 kPa, res When density exceeded 1 g/m^2, nanofibers showed a bursting pressure >175 kPa. It can be suggeste minimum required nanofiber web density is 2 g/m^2 for the preparation of membranes. Since the n with 3 g/m^2 showed excellent bursting pressure, and the possibility of modification of more fibe surface, this membrane was selected as the candidate for surface modification.

Water contact angle (CA) of the membranes was measured. Membrane behavior under emulsion changed due to additives such as surfactant. The CA of the membranes was measured after oil separation. Results are given in Table 3.

Table 3. Water contact angle (CA) of the membranes before and after separation.

Sample	CA before Separation (°)	CA after Separation (°)	Image (Before Separation)
PVDF 1	71.23 ± 1.31	62.40 ± 2.17	
PVDF 2	80.83 ± 1.53	47.46 ± 1.93	
PVDF 3	89.40 ± 4.67	35.32 ± 8.71	
PVDF_N	0	0	-
PVDF_NT	39.43 ± 3.01	0	
PVDF_K	0	0	-
PVDF_KT	0	0	-

The CA of the neat membranes without any modification had a contact angle <90°, which can be considered "hydrophilic". Typically, PVDF nanofibers have a hydrophobic nature. After lamination, the surface structure of the PVDF membranes most likely changed. Moreover, the adhesive web between the nanofiber and the supporting layer played a significant role. The adhesive web partly covered the surface of the nanofibers, which may have exhibited hydrophilic characteristics.

Results of the CA showed that increasing the density of the nanofiber web decreased the wettability of the samples. There was a proportional relationship between nanofiber web density and CA.

Research results indicated that increasing the hydrophilicity of the membrane prevented membrane fouling and improved membrane permeability [4,16,22].

1.1. Separation Test

A separation test was run using dead-end cell separation, and the permeability of the unmodified membranes was calculated according to Equation (2). Results are given in Figure 7, which compares unmodified membranes at various densities. Each membrane was used and circulated three times to measure fouling. Between each circulation, distilled water was filtrated. Results indicated that, at the beginning, PVDF 2 showed enormous permeability compared to the others. The lowest permeability was achieved using PVDF 3 at the first circulation. However, membranes PVDF 1 and PVDF 2 showed a sharp decrease in permeability with the second circulation; the reason for this was membrane fouling. The membrane with the highest nanofiber density (PVDF 3) showed a stable permeability after three circulations; this could have been due to the high specific surface area of PVDF 3. A higher density meant more nanofiber web was on the structure, resulting in a bigger surface area in total. On the contrary, Hobbs et al. [23] found that there is a proportional relationship between flux decline ratio and membrane surface area. A higher surface area showed a higher flux decline ratio.
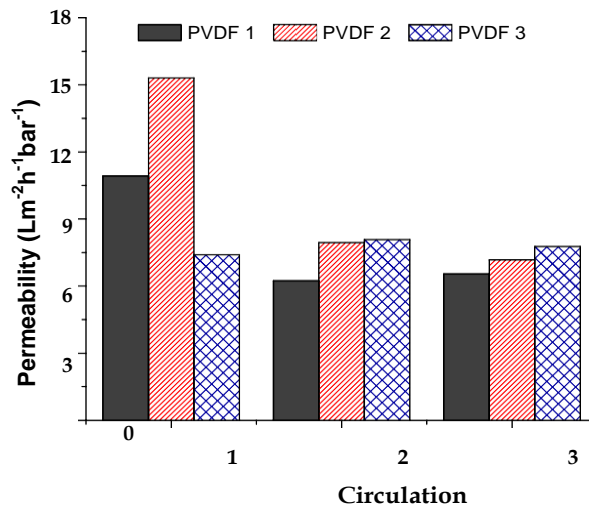
Figure 7. Permeability of the unmodified membranes.

Figure 8 shows the results of the modified membranes. Surface modification helped improve membrane surface cleaning. For long-term application, surface-modified membranes should be an excellent candidate for use in the separation process. Life span and performance of the membranes were improved using surface modification. Moreover, the added TiO_2 acted as an antibacterial on the membranes. The TiO_2 nanoparticles were activated under ultraviolet (UV) light during separation, which might have enhanced the performance, self-cleaning, and antibacterial properties of the membranes [24]. Montazer et al. [25] modified the surface of polyester/wool fabric using TiO_2 nanoparticles. Water adsorption increased, while the time of water droplet adsorption decreased.
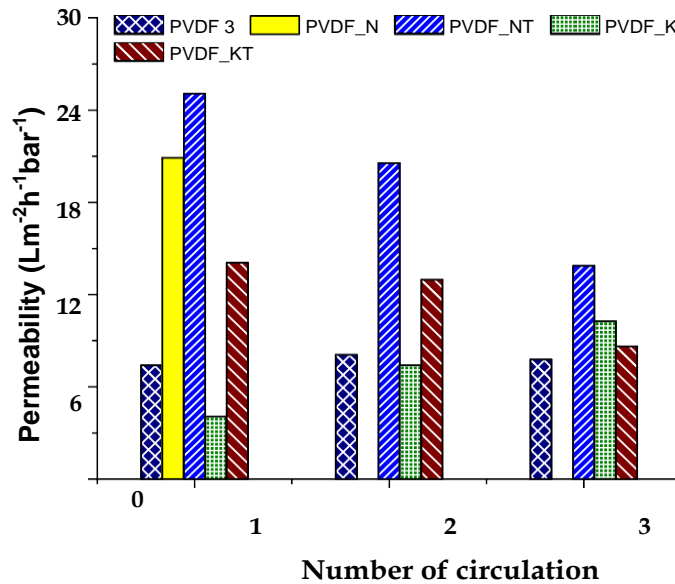
Figure 8. Permeability of the modified membranes.

Moreover, the antibacterial efficacy of the material against *Escherichia coli* was found to be 100%. In another study, it was reported that a polydimethylsiloxane (PDMS)/TiO_2 composite provided excellent photocatalytic properties and developed self-cleaning properties [26]. Xu et al. [27] prepared TiO_2–high-density polyethylene (HDPE) nanocomposite surfaces that exhibited superhydrophobicity. Exposure to UV light caused the surface of the composite to become hydrophilic. As a result, wettability and self-cleaning properties of the nanocomposite increased. More examples appeared in the literature. The effectiveness of TiO_2 nanoparticles on wettability and self-cleaning properties is indisputable.

125

The surface of the membranes after oil separation was detected using SEM images, as shown in Figure 9. We could understand from the SEM images that membranes with high permeability and surface cleaning attracted less oil. For instance, the permeability of the PVDF 3 decreased consistently in each circulation. PVDF_N was blocked after the first circulation. These two membranes showed, in the SEM images (Figure 9a,b), that an oily film covered the surface of the membranes. For the membranes PVDF_N and PVDF_NT, there was less oil contamination on the membrane surface. Based on this result, it can be concluded that surface modification improved membrane permeability and self-cleaning performance.
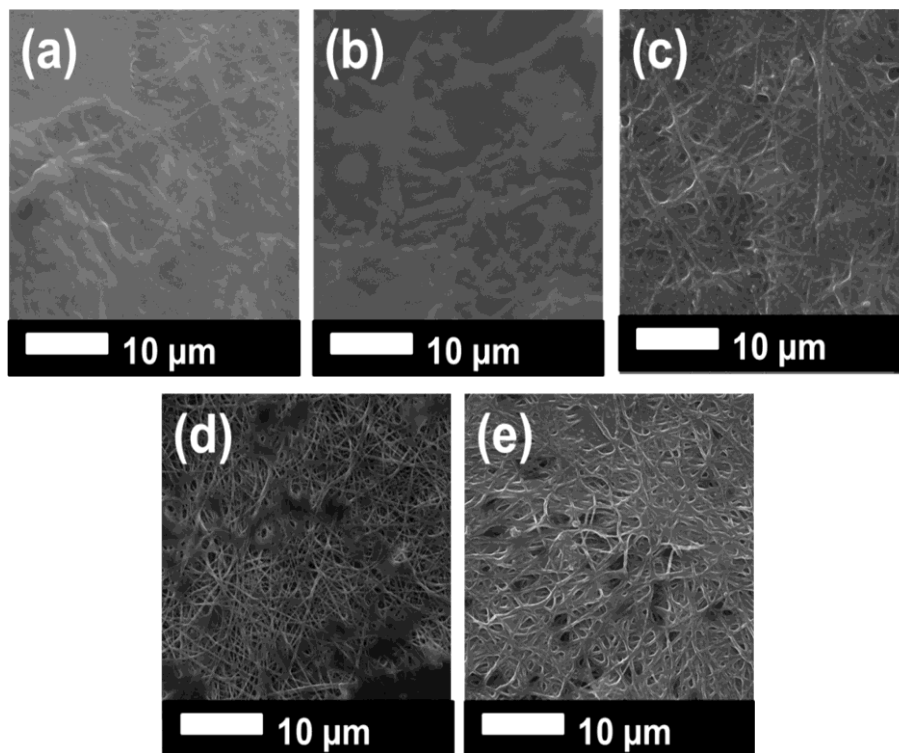
Figure 9. SEM images of the samples after oil separation: (**a**) PVDF 3, (**b**) PVDF_N, (**c**) PVDF_NT, (**d**) PVDF_K, (**e**) PVDF_KT.

Permeate solution was collected and checked under the microscope to detect any oil droplets. Moreover, coloring the water helped to detect oil content in the mixture. Unmodified membranes showed hydrophobic/oleophilic characteristics, while modified membranes were hydrophilic/oleophobic.

1. Conclusions

PVDF is one of the most frequently used polymers in the membrane filtration market due to its outstanding properties, such as chemical resistance, thermal stability, and high mechanical strength. Despite the superior properties of PVDF membranes, there is still plenty of room for improvement in membrane performance and life span. In this work, PVDF nanofibrous hybrid membranes were prepared for the separation of the oil–water emulsions. A two-step surface modification took place using alkaline solution and TiO_2 nanoparticle grafting. Water permeability of the membranes increased due to –OH groups and hydrophilic TiO_2 nanoparticles (NPs) on the membrane surface.

Moreover, membranes showed self-cleaning properties after the modification process. Photocatalytic activity can be improved through UV induction on the TiO_2-modified membranes. We believe that this method can be used in the separation of emulsified oil/water. Based on the result, it can be concluded that nanofiber webs are good candidates for water domain filtration applications.

References

1. Zhang, W.; Shi, Z.; Zhang, F.; Liu, X.; Jin, J.; Jiang, L. Superhydrophobic and superoleophilic PVDF membranes for effective separation of water-in-oil emulsions with high flux. *Adv. Mater.* **2013**, *25*, 2071–2076. [CrossRef]

2. Zhang, F.; Gao, S.; Zhu, Y.; Jin, J. Alkaline-induced superhydrophilic/underwater superoleophobic polyacrylonitrile membranes with ultralow oil-adhesion for high-efficient oil/water separation. *J. Memb. Sci.* **2016**, *513*, 67–73. [CrossRef]

3. Fan, L.; Yan, J.; He, H.; Deng, N.; Zhao, Y.; Kang, W.; Cheng, B. Electro-blown spun PS/PAN fibrous membrane for highly efficient oil/water separation. *Fibers Polym.* **2017**, *18*, 1988–1994. [CrossRef]

4. Yalcinkaya, F.; Siekierka, A.; Bryjak, M. Preparation of fouling-resistant nanofibrous composite membranes for separation of oily wastewater. *Polymers* **2017**, *9*, 679. [CrossRef]

5. Yalcinkaya, F. Preparation of various nanofiber layers using wire electrospinning system. *Arab. J. Chem.* **2016**. [CrossRef]

6. Grimmelsmann, N.; Grothe, T.; Homburg, S.V.; Ehrmann, A. Electrospinning and stabilization of chitosan nanofiber mats. In Proceedings of the IOP Conference Series: Materials Science and Engineering, Beijing, China, 24–27 October 2017; Volume 254, p. 102006.

7. Charles, L.F.; Shaw, M.T.; Olson, J.R.; Wei, M. Fabrication and mechanical properties of PLLA/PCL/HA composites via a biomimetic, dip coating, and hot compression procedure. *J. Mater. Sci. Mater. Med.* **2010**, *21*, 1845–1854. [CrossRef]

8. Roche, R.; Yalcinkaya, F. Incorporation of PVDF nanofibre multilayers into functional structure for filtration applications. *Nanomaterials* **2018**, *8*, 771. [CrossRef]

9. Jahanbaani, A.R.; Behzad, T.; Borhani, S.; Darvanjooghi, M.H.K. Electrospinning of cellulose nanofibers mat for laminated epoxy composite production. *Fibers Polym.* **2016**, *17*, 1438–1448. [CrossRef]

10. Liu, R.; Ma, L.; Mei, J.; Huang, S.; Yang, S.; Li, E.; Yuan, G. Large areal mass, mechanically tough and freestanding electrode based on heteroatom-doped carbon nanofibers for flexible supercapacitors. *Chem. A Eur. J.* **2017**, *23*, 2610–2618. [CrossRef]

11. Wirth, E.; Sabantina, L.; Weber, M.; Finsterbusch, K.; Ehrmann, A. Preliminary study of ultrasonic welding as a joining process for electrospun nanofiber mats. *Nanomaterials* **2018**, *8*, 746. [CrossRef]

12. Sabantina, L.; Hes, L.; Mirasol, J.R.; Cordero, T.; Ehrmann, A. Water vapor permeability through PAN nanofiber mat with varying membrane-like areas. *Fibres Text. East. Eur.* **2019**, *27*, 12–15. [CrossRef]

13. Roche, R.; Yalcinkaya, F. Electrospun polyacrylonitrile nanofibrous membranes for point-of-use water and air cleaning. *ChemistryOpen* **2019**, *8*, 97–103. [CrossRef] [PubMed]

14. Sabantina, L.; Kinzel, F.; Hauser, T.; Többer, A.; Klöcker, M.; Döpke, C.; Böttjer, R.; Wehlage, D.; Rattenholl, A.; Ehrmann, A. Comparative Study of Pleurotus ostreatus Mushroom Grown on Modified PAN Nanofiber Mats. *Nanomaterials* **2019**, *9*, 475. [CrossRef] [PubMed]

15. Yalcinkaya, F.; Hruza, J. Effect of laminating pressure on polymeric multilayer nanofibrous membranes for liquid filtration. *Nanomaterials* **2018**, *8*, 272. [CrossRef] [PubMed]

16. Yalcinkaya, F.; Siekierka, A.; Bryjak, M. Surface modification of electrospun nanofibrous membranes for oily wastewater separation. *RSC Adv.* **2017**, *7*, 56704–56712. [CrossRef]

17. Zhou, Z.; Wu, X.F. Electrospinning superhydrophobic-superoleophilic fibrous PVDF membranes for high-efficiency water-oil separation. *Mater. Lett.* **2015**, *160*, 423–427. [CrossRef]

18. Xiao, L.; Davenport, D.M.; Ormsbee, L.; Bhattacharyya, D. Polymerization and functionalization of membrane pores for water related applications. *Ind. Eng. Chem. Res.* **2015**, *54*, 4174–4182. [CrossRef]

19. Martakov, I.S.; Torlopov, M.A.; Mikhaylov, V.I.; Krivoshapkina, E.F.; Silant'ev, V.E.; Krivoshapkin, P.V. Interaction of cellulose nanocrystals with titanium dioxide and peculiarities of hybrid structures formation.
J. Sol-Gel Sci. Technol. **2018**, *88*, 13–21. [CrossRef]

20. Dong, L.; Liu, X.; Xiong, Z.; Sheng, D.; Lin, C.; Zhou, Y.; Yang, Y. Preparation of UV-blocking poly(vinylidene fluoride) films through SI-AGET ATRP using a colorless polydopamine initiator layer. *Ind. Eng. Chem. Res.* **2018**, *57*, 12662–12669. [CrossRef]

21. Shi, F.; Wu, J.; Zhao, B. Preparation and investigation of intelligent polymeric nanocapsule for enhanced oil recovery. *Materials* **2019**, *12*, 1093. [CrossRef]

22. Naseeb, N.; Mohammed, A.A.; Laoui, T.; Khan, Z. A novel PAN-GO-SiO$_2$ hybrid membrane for separating oil and water from emulsified mixture. *Materials* **2019**, *12*, 212. [CrossRef] [PubMed]

23. Hobbs, C.; Hong, S.; Taylor, J. Effect of surface roughness on fouling of RO and NF membranes during filtration of a high organic surficial groundwater. *J. Water Supply Res. Technol. AQUA* **2006**, *55*, 559–570. [CrossRef]

24. Martins, P.M.; Ribeiro, J.M.; Teixeira, S.; Petrovykh, D.Y.; Cuniberti, G.; Pereira, L.; Lanceros-Méndez, S. Photocatalytic microporous membrane against the increasing problem of water emerging pollutants. *Materials* **2019**, *12*, 1649. [CrossRef][PubMed]

25. Montazer, M.; Seifollahzadeh, S. Enhanced self-cleaning, antibacterial and UV protection properties of nano TiO$_2$ treated textile through enzymatic pretreatment. *Photochem. Photobiol.* **2011**, *87*, 877–883. [CrossRef] [PubMed]

26. Tavares, M.T.S.; Santos, A.S.F.; Santos, I.M.G.; Silva, M.R.S.; Bomio, M.R.D.; Longo, E.; Paskocimas, C.A.; Motta, F.V. TiO$_2$/PDMS nanocomposites for use on self-cleaning surfaces. *Surf. Coatings Technol.* **2014**, *239*, 16–19. [CrossRef]

27. Xu, Q.F.; Liu, Y.; Lin, F.J.; Mondal, B.; Lyons, A.M. Superhydrophobic TiO$_2$-polymer nanocomposite surface with UV-induced reversible wettability and self-cleaning properties. *ACS Appl. Mater. Interfaces* **2013**, *5*, 8915–8924. [CrossRef][PubMed]

ELSEVIER

PVDF nanofibrous membranes modified via laser-synthesized Ag nanoparticles for a cleaner oily water separation

R. Torres-Mendieta[a,*], F. Yalcinkaya[a], E. Boyraz[a], O. Havelka[a], S. Wacławek[a], J. Maryška[a], M. Černík[a], M. Bryjak[b]

[a] Institute for Nanomaterials, Advanced Technologies and Innovation, Technical University of Liberec, Studentská 1402/2, 461 17 Liberec, Czech Republic
[b] Department of Polymer and Carbon Materials, Wrocław University of Science and Technology, Wyb. St. Wyspianskiego 27, 50-370 Wrocław, Poland

A B S T R A C T

The relatively new exploitation of nanoassemblies used for the recovery of clean water from oily emulsions has received a great deal of attention recently. Among the different innovations, nanofibrous membranes decorated with nanoparticles seem to be the most promising option due to their versatility, recyclability, and high oil/water separation performance. In the current study, we introduce a laser-mediated strategy to produce poly-vinylidene fluoride nanofibrous membranes decorated with a low loading of Ag nanoparticles. The pristine membranes were firstly modified by an alkaline treatment to obtain hydroxyl groups on their surface, which then facilitated the nanoparticle decoration. The synthesis and decoration of the nanoparticles were achieved by the laser-mediated reduction of silver nitrate dissolved in water, while no hazardous reducing or stabilizing agents were employed in the process. In comparison with the unmodified membrane, the modified one displayed an outstanding hydrophilic behavior and a remarkable 3.9-fold improvement in the separation of water from oily emulsions with a nearly negligible permeability decline through the time. In sum, the introduced methodology not only enables the improvement over the oil/water separation performance in polymer-based membranes but also promises to reduce the environmental impact related to the design of nanotechnology-based solutions used in the sector.

1. Introduction

Over the last two centuries, the improper management of water has led to severe environmental issues. One of the most frequent is the oil wastewater contamination, which can be associated with health problems resulting from exposure to its toxic compounds [1]. The greatest challenge behind the treatment of oily polluted water lies in the complexity of removing tight emulsions or hydrate formations. The various solutions that the scientific community is currently exploring encompass the following alternatives: flotation, gravity separation, adsorption, electrocoagulation, flocculation, coagulation, and membrane filtration [2]. Among the different options, a combination of membrane filtration and contemporary nanotechnology advances appears to be one of the most promising. In addition to the inherent benefits of the membranes, such as their easiness of operation and smaller carbon footprint compared to other systems, the incorporation of nanomaterials like nanofibers provides a low flow resistance, bio-compatibility, and high porosity; properties that significantly improve the oil/water separation efficiency [3].

However, the technology still faces a major challenge; during the separation process, foulants such as colloids, microorganisms, organic matter, suspended solids, emulsified oils or macromolecules, accumulate on the membrane surface and block the membrane pores, resulting in an increase in the membrane mass transfer resistance and decrease in permeate flux [4]. To alleviate such drawbacks, chemical/mechanical cleaning, adjustment of operating conditions, pre-treatment of the feed water, and membrane surface modification have been tested [5], the latter being a solution with virtually unlimited alternatives. In this context, one of the most exciting forms of surface modification is the incorporation of metal and semiconductor nanoparticles (NPs) on the surface of nanofibrous membranes, which largely improves the long-term membrane permeability and antifouling properties [6], or provide them with additional purification features like the photocatalytic degradation of dissolved pollutants in the water [7]. In particular, the use of Ag NPs has been intensively explored due to its antibacterial performance, which prevents the biofouling of the membranes caused by settlement and growth of microorganisms, and its ability to turn hydrophobic surfaces into hydrophilic, which results in the increment of
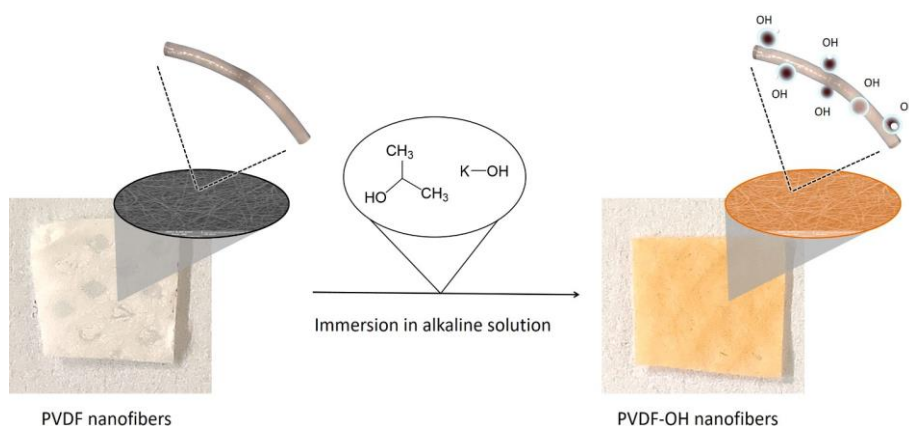
Fig. 1. Schematic diagram of the dehydrofluorination process.

the water flux, rejection of hydrophobic foulants like oil pollutants, and overall antifouling performance [8]. However, similar to the buildup case of most of the nanometric systems, their most common synthetic routes are associated with the use of hazardous reducing and stabilizing agents, which inevitably contributes to environmental pollution [9].

In the current work, we addressed this issue by exploring for the first time the employment of a laser-mediated synthesis strategy to generate ligand-free Ag NPs and decorate the surface of Polyvinylidene fluoride (PVDF) nanofibrous membranes in a single stage to improve their oil/water separation properties, while the usage of reducing or stabilizing agents was suppressed during the process.

The NPs synthesis strategy known as pulsed laser photoreduction/oxidation in liquids (LPL) is a technique driven by an extreme light-matter interaction; a pulsed laser source is used to promote the optical breakdown of a liquid that contains precursor metal salts. The extreme peak intensities required to reach the optical breakdown in various liquids ($>10^{10}$ W/cm^2) [10], usually lead to the photolysis of the solvent molecules and the formation of radicals, which prompt the reduction of the precursor metal salts. Subsequently, the reduced salts form the final NPs [11], which, if are in the vicinity of a nanofibrous material, can be physically adsorbed to its surface. As the process does not require the use of any stabilization agent, the surface of the decorating NPs remains free from any ligand; a highly desirable situation since the covering of NPs by ligands may result in the suppression of their physical and chemical properties or to crossed chemical effects [12].

Overall, the goal of the current work was to introduce in the oil/water separation literature, the use of a NPs laser-mediated synthesis strategy to improve the separation performance of nanofibrous membranes. Although the versatility of the proposed synthesis strategy has brought plenty of benefits to the eco-friendly design of complex nanometric systems, to our knowledge, it has never been applied in the fabrication of potent oil/water separation materials, where the preferred use of light over the commonly employed reducing chemical agents, may have not only a positive impact on the reduction of chemical waste generation but also the ligand-free surface of the laser-synthesized NPs may be of more significant benefit in terms of atom economy. Thus, the recovery of clean water from oily polluted sources is not overshadowed by the commonly employed polluting synthetic strategies behind the development of the materials used in the sector.

1. Experimental

1.1. Membrane preparation

PVDF nanofibers were prepared on a needleless electrospinning system (Nanospider NS 8S1600U, Elmarco, Liberec, Czech Republic). The nanofiber webs (density of 3.5 g/m^2) were collected on a silicon

paper, and further laminated to improve their mechanical strength by a heat-press equipment (Pracovni Stroje, Teplice, Czech Republic). For the hybrid membrane, a copolyester adhesive was used to adhere the nanofiber web to a polyethylene terephthalate spunbond nonwoven (100 g/m^2, Mogul Co. Ltd., Gaziantep, Turkey) under a thermal treatment of 130 C and a pressing force of 50 kN [13].

1.2. Surface modification

Even though PVDF is one of the most popular polymers used for building nanofibrous membranes, it is still a non-reactive material that may not allow the adsorption of NPs over its surface. To permit the NPs decoration, it was necessary to add hydroxyl groups over the surface of the nanofibers. For this, a 1.4 M solution of potassium hydroxide (KOH, Fluka, Czech Republic) in isopropanol (IPA, Fluka, Czech Republic) was prepared by magnetically stirring for 1 h at a temperature of 50 C. After the KOH was fully dissolved in the IPA, the solution was cooled at room temperature and stored for further use.

The dehydrofluorination of the PVDF membrane was performed by immersing the membrane in the alkaline solution and leaving it to react for 30 min at room temperature. Subsequently, the membrane's color changed from white to brown as it is graphically depicted in Fig. 1. Finally, the membrane was washed several times with deionized water (18.2 MΩcm) and further stored in clean deionized water.

1.3. Laser-mediated synthesis and decoration of Ag NPs

The Ag NPs synthesis and decoration of the membrane's surface took place at the same time. The synthesis setup was based on the one previously reported by our research team for the formation of Fe-Cu oxide nanocrystals [14]. In short, as it is graphically represented in Fig. 2, a laser beam was focused by a plano-convex lens in a glass vessel containing 5 mM liquid solution of silver nitrate (AgNO$_3$, Sigma–Aldrich, USA) in deionized water, and continuously mixed by a magnetic stirrer, where the concentration was selected according to previous reports [15]. During the process, a PVDF dehydrofluorinated membrane (PVDF-OH) was situated on the walls of the glass vessel, so the newly synthesized Ag NPs could be physically adsorbed onto the membrane's surface.

The laser source used for the experiments was a Nd:YLF (Litron Lasers; LDY300 PIV Series diode-pumped, dual cavity), delivering pulses with a duration of 150 nm full width at half maximum (FWHM) at a central wavelength of 527 nm, a repetition rate of 1 kHz each cavity, and a beam diameter of 5 mm at a width of 1/e^2. The average power used was 11 W, and the lens focal length was 35 mm. Therefore, the peak intensity used to irradiate the liquid solution was $7 \cdot 10^{10}$ W/cm^2, which according to the relevant literature, is enough to prompt the
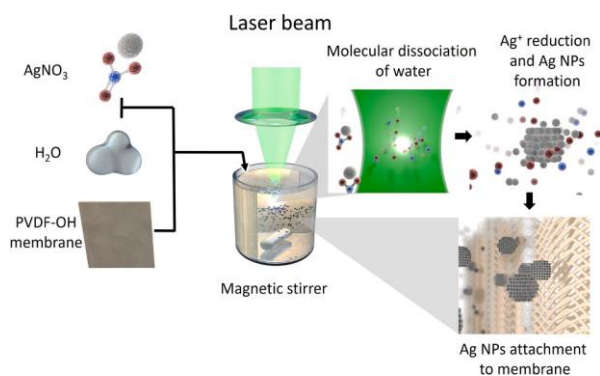
Fig. 2. Setup used for the laser-mediated synthesis and decoration of Ag NPs.

Fig. 3. Scheme of the dead-end filtration device.

optical breakdown in water that consequently leads to the creation of radicals that allow the reduction of the metal ions [10]. Once the NPs are synthesized, the magnetic stirrer permits their movement through the liquid medium taking them away from the laser focal point and approaching them to the membrane, where they are physically adsorbed through the OH- groups [16]. Note that the synthesis process was optimized to irradiate for 5 min every mL of the corresponding liquid solution; therefore, it may take a longer time the usage of larger liquid volumes. Besides, it is worth mentioning that the employment of a ns pulsed laser source with the laser parameters used in the current experiment, but with a shorter pulse duration than 150 nm, should lead to a more efficient reduction of metal ions since the peak intensity can be incremented.

Once the synthesis process finished, the magnetic stirrer kept working for another 2 h to increment the chances of fully decorating the whole of the membrane's surface. Afterward, the membrane decorated with the Ag NPs (Ag/PVDF-OH) was rinsed several times with deionized water to remove the Ag NPs that were not properly attached to the membrane. After, the used water was appropriately laid-off.

1.1. Membrane characterization

The OH- functionalization of the PVDF nanofibers was verified by Fourier transform infrared spectroscopy (FT-IR, NICOLET IZ10, Thermo Scientific, USA) performed in the dried samples. The corresponding spectra were taken at a wavenumber range of 4000–500 cm^{-1} with a resolution of 2 cm^{-1}. The surface roughness of the samples before and after the dehydrofluorination process was measured employing Atomic Force Microscopy (AFM, JPK nanowizard III, Bruker Corporation, USA). The scannings were always performed on a surface area of 10 × 10 μm using contact mode with a cantilever NANOSENSORS^{TM} PPP-CONTSCR.

The membrane's morphology was examined by field emission scanning electron microscopy (FE-SEM, UHR Carl Zeiss Ultra Plus, Jena, Germany). The instrument was operated at various accelerating voltages (EHT; 2–10 kV) and working distances (WD; 7.4–7.9 mm). The topography examination was performed by analyzing the secondary electrons (SEs), and the observation of the Ag NPs was assessed by analyzing the backscattered electrons (BSEs). Also, the elemental composition was verified with an energy-dispersive X-ray detector (EDX, Oxford X-Max 20, UK), which was attached to the FE-SEM and the corresponding quantification was performed using the software AZtec 2.4. The amount of Ag mass loading in the membrane's surface was roughly calculated by inspecting the FE-SEM micrographs, and their stability was assessed by the measurement of the Ag content in the resulting water after the separation tests through an inductively coupled plasma - mass spectrometer (ICP-MS; Perkin Elmer, NexION
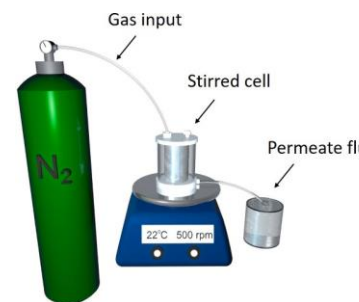
3000D, USA), which has a detection limit of 0.5 ng/L.

The pore size of the membranes was determined by the bubble point method using a Porometer 3G through a pore size analyzer (Quantachrome Instruments, Anton Paar GmbH, Germany). The tests were performed according to the ASTM F316-03(2011) standard. Finally, the water contact angle in air and underwater oil contact angle of the samples was determined using a Krüss Drop Shape Analyser DS4 (Krüss GmbH, Hamburg, Germany). For the water contact angle in air, the droplets consisted of deionized water (surface tension 72.0 mN/m, deionized by Aqual 27, Czech Republic), and the measurements were taken at six different points on the clean and dry samples at room temperature. For the underwater oil contact angle measurements, the droplets consisted of vegetable oil (Lukana sunflower oil, Czech Republic), and the measurements were taken by fixing the membranes at an altitude of 1 cm from the bottom of a water reservoir, which was covered with deionized water to a maximum height of 4 cm. The oil droplets were released from the bottom of the water reservoir so they could float and interact with the membrane's surface.

1.2. Separation test

A 50 mL Amicon dead-end filtration device (Millipore Corporation Billerica, MA, USA) was used for the filtration tests (Fig. 3). The feed solution for the filtration test was prepared by mixing a green-colored (Kovandvi, Czech Republic) distilled water with vegetable oil (Lukana sunflower oil, Czech Republic) in a 1:1 weight ratio and 0.1% wt. of the non-ionic Triton X100 surfactant (Sigma–Aldrich, USA) for making the emulsion. The feed was mixed by a magnetic stirrer (500 rpm) at room temperature for 5 h until a uniform emulsion was obtained. The stability of the emulsion was assessed by measuring the diameter of the oil droplets with an optical microscope (Levenhuk Digital Microscope, Czech Republic), just after the emulsion preparation and after two weeks while the emulsion kept stored at room temperature (Fig. S1 in the Supporting Material). The average diameter of the oil droplets in the recently prepared emulsion was (0.8 ± 0.2) μm, and the average size after two weeks was (1.1 ± 0.3) μm, which means that the agglomeration of oil droplets in the emulsion was minimal, and therefore the emulsion kept stable for two weeks, making it suitable for its usage in the separation tests.

The filtration tests consisted of 10 runs. For this, each membrane filtered a volume of 15 mL of distilled water before the runs. Later, the protocol for the runs was the following: filtration of 30 mL of the oil/water emulsion under a pressure condition of 0.02 bar, and in between each run the membrane was roughly cleaned by the filtration of 15 mL of distilled water. After the separation tests, the permeate solution was collected into a closed glass tube and kept for 24 h to analyze the residual water and oil under the optical microscope. Moreover, the amount of oil in the feed and permeate was determined by the Non-Purgeable Organic Carbon (NPOC) measurements by means of a total carbon analyzer (Jena MULTI N/C 2100S, Germany).

131

The permeate flux (F) and the permeability (k) of the membrane were calculated as follows:

$$F = V/(A.t) \tag{1}$$

$$k = F/p \tag{2}$$

where A is the effective membrane area (m^2), V is the total volume of permeate (L), p is the trans-membrane pressure (bar), and t is the filtration time (h). The decline of the membrane's permeability was determined from the differences between the permeability before (k_i) and after fouling (k_f) [17]:

$$Decline \quad in \quad permeability\,\textbf{(\%)} = \left(\frac{k_i - k_f}{k_i}\right) \times \textbf{100\%} \tag{3}$$

The flux recovery ratio (FRR **(%)**) was calculated according to:

$$FRR\,\textbf{(\%)} = (Jf/Ji) \times 100 \tag{4}$$

where J_i represents the pure water flux that can be filtrated by the clean membranes, and J_f represents the pure water flux that can be filtrated by the membranes after undergoing the final oil/water separation run. For PVDF, the measurement was taken after the 5th run because the membrane got fouled entirely after the 5th run. For PVDF-OH and Ag/PVDF-OH, the measurements were taken after the 10th run.

Finally, the rejection ratio (R **(%)**) was calculated according to:

$$(7)$$

$$R\,\textbf{(\%)} = \left(\textbf{1} - \frac{C_f}{C_i}\right) \times \textbf{100\%} \tag{5}$$

where $\textbf{C}_i$ (g/L) represents the carbon concentration in the feed and $\textbf{C}_f$ (g/

L) the carbon concentration in the final permeate liquid after completing the separation cycles. After the 5th run for PVDF and after the 10th run for PVDF-OH and Ag/PVDF-OH. Note that the NPOC analytical methodology measures the amount of carbon in the samples, therefore, as the feed was an emulsion composed by green-colored distilled water, vegetable oil, and the non-ionic Triton X100 surfactant, the $\textbf{C}_i$ and $\textbf{C}_f$ values not only reflect the amount of oil in the feed and permeate, respectively, but also the carbon coming from the colorant and the surfactant.

1. Results and discussion

1.1. Membrane characterization

PVDF is a dielectric polymer that displays a high thermal and chemical stability, conventionally attributed to the strong bonding CeF (485 kJ mol^{-1}) and an electronic shielding on the CeC bonds [18], which makes the polymer chemically inert and in general unable to be functionalized. However, as it has been extensively reported, when the polymer is exposed to a highly alkaline environment, as in the case of the current study (KOH/IPA), it is possible to promote its dehydrofluorination via the following process:

$$[-CH_2 - CF_2 -]_n + KOH \rightarrow [-CH = CF -]_n + KF + H_2O \tag{6}$$

As proposed by Ross et al. [19], an elimination reaction occurs, where the elements H and F remove from the polymer chain and a eC]Ce double bond is generated. Moreover, when the modified polymer chain is in contact with a hydroxide rich solution, it can experience the incorporation of hydroxyl groups through the following set of reactions:

In short, in the highly alkaline environment, the PVDF can undergo oxidative degradation, which leads to the presence of the hydroxyl groups on the material's surface [20].

As seen in Fig. 4 a), the FTIR spectra of both nanofibrous membranes, before and after being subject to the alkaline treatment, exhibit
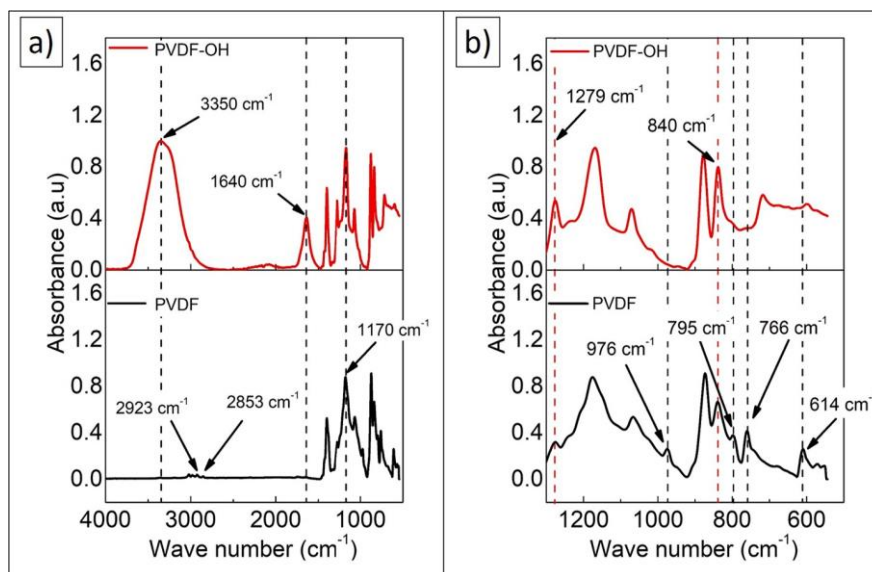
Fig. 4. FTIR spectra of pristine PVDF and PVDF-OH membranes, a) in the wavenumber range 500–4000 cm^{-1}, where the vertical dashed lines highlight the general differences between both spectra, b) in the wavenumber range 500–1300 cm^{-1}, where the vertical black dashed lines belong to peaks of the β phase of PVDF, and the vertical red dashed lines belong to peaks of the α phase of PVDF. (For interpretation of the references to colour in this figure legend, the reader is referred to the web version of this article.)

the typical band at 1170 cm^{-1} associated to the stretching vibrations of **CF$_2$** in the PVDF [20], and only the non-treated membrane clearly shows the peaks located at 2923, 2853 cm^{-1} usually associated to the stretching vibrations of CH$_2$. Besides, in both spectra displayed in Fig. 4 b), it is possible to identify the peaks located at 1279 and 840 cm^{-1}, that belong to the β phase of PVDF, but those belonging to the α phase of PVDF (976, 795, 766, and 614 cm^{-1}) are only observed in the non-treated membrane [21]. Moreover, the spectrum that belongs to the material after the alkaline treatment (PVDF-OH) exhibits two new peaks, a broad one centered at 3350 cm^{-1} that seems to overshadow the peaks corresponding to the CH$_2$ stretching vibrations and the other at 1640 cm^{-1}.

When the PVDF undergoes the current dehydrofluorination process, the peak located at 1640 cm^{-1} is usually associated to the conjugated

C=C the 3400 to 3200 cm^{-1} band is usually associated with the formation of a hydroxyl group in the material's surface [22]. Yet, it should be noted that even a minimal amount of H$_2$O from the air can get adsorbed in the material's surface resulting in the enhancement of the peak's intensity. In summary, the FTIR results suggest that the PVDF nanofi- brous membranes were successfully functionalized with OH- groups according to the relevant literature [23].

Besides, the alkaline treatment seems to suppress the peaks related to the α phase of the polymer and emphasize those belonging to its β phase. Since the β phase of the PVDF is more chemically active than the α one [24], its presence may contribute to the physisorption of the Ag NPs over the membrane's surface, and as Ribeiro et al. [25] suggest, it could be worth the optimization in the β phase generation towards a more efficient Ag NPs attachment.

The average surface roughness of the membranes was obtained from the AFM measurements (Fig. S2 in the Supporting Material), where the pristine PVDF and PVDF-OH membranes display a roughness **R**$_a$ of (240.9 ± 45.9) nm and (165.3 ± 1.3) nm, respectively. These results are in agreement with the common observation of the surface roughness decrease of PVDF-based membranes after being exposed to a KOH so-lution [26].

The FE-SEM micrographs in Fig. 5 show that there is no clear morphological change in the nanofibers before or after the alkaline treatment or even after the *in situ* synthesis of the Ag NPs. The only visible change is observed in the Fig. 5 c), exhibiting the appearance of small particles anchored to the surface of the nanofibers. In any case, the mean size of the nanofibers is (120 ± 25) nm.

Also, it is worth mentioning that the accelerating voltages and working distances were selected in order to observe the material without the necessity to use any further metal coating that may hide the presence of the Ag NPs when performing the chemical composition analysis.

In this context, Fig. 6 shows the comparison between the back-scattered electron (BSE) and secondary electron (SE) micrographs (Fig. 6 a) and b), respectively). Both pictures exhibit the presence of the NPs, but as the SE signal is rather surface-sensitive, the NPs are more visible in the BSE micrograph (Fig. 6 a)), which also confirms that the chemical composition of the NPs is of an Ag nature.

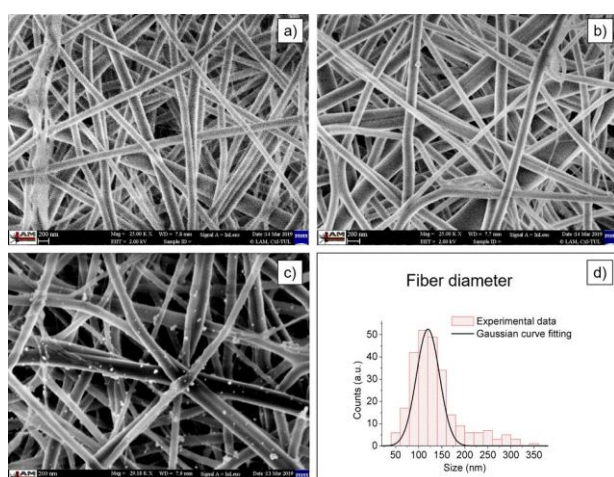**Fig. 5.** FE-SEM micrographs of a) the neat PVDF membrane (micrograph taken at EHT = 2.00 kV and WD = 7.8 mm), b) the PVDF-OH membrane before the laser synthesis of Ag NPs (EHT = 2.00 kV and WD = 7.7 mm), c) the membrane after the Ag NPs synthesis (EHT = 2.50 kV and WD = 7.9 mm) and d) the size histogram of the fiber diameter of the neat PVDF membrane, which also coincides with the PVDF-OH and Ag/PVDF-OH samples.
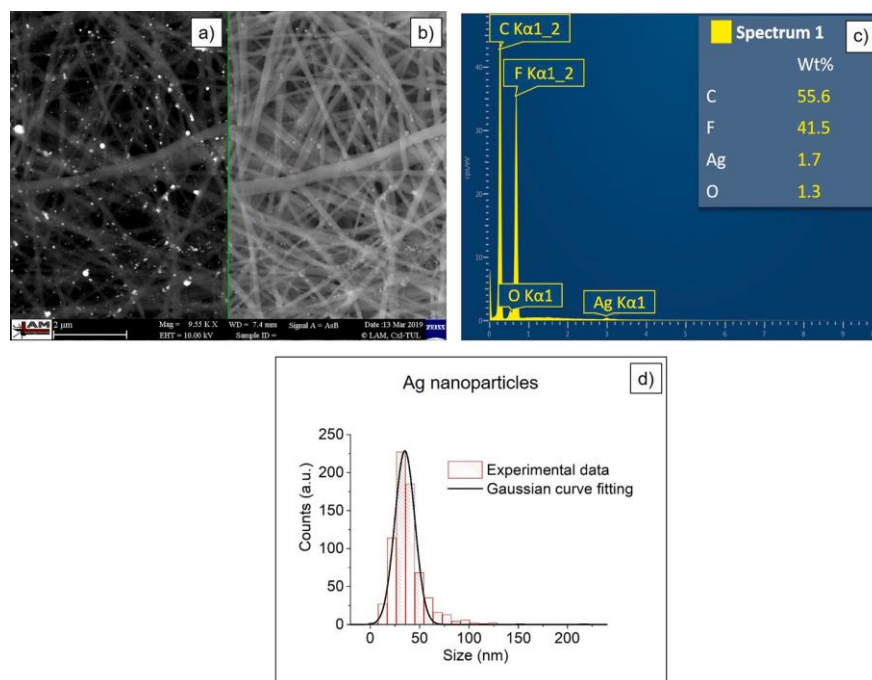
Fig. 6. a) BSE and b) SE micrographs of Ag/PVDF-OH, c) EDX spectrum of the specimen, and d) the size histogram of the Ag NPs considering 700 counts.

Conventionally, BSEs that re-emerge after interacting with the specimen under study are more strongly back-scattered when interacting with heavy elements than when interacting with the lighter elements. In our situation, this was verified by the EDX spectrum (Fig. 6 c)), whereby the only elements found in the sample were C, F, Ag and O, where Ag is the heaviest of them. Therefore, it is possible to infer that the NPs were made of Ag. Moreover, their distribution over the membrane and nanofibers surface is uniform (Fig. S3 in the Supporting Material), whereas the average size of the Ag NPs is (35 ± 10) nm. Considering that the atomic radius of Ag is 144 pm, and its atomic weight is 107.87 g/mol, the approximate Ag weight loading over a circular filter with a diameter of (4.45 ± 0.05) cm (dimensions used for the filtration tests) should be (8.58 ± 0.43)μg.

The current topographical distribution and size of the NPs is a highly desired situation because, as previously reported by different sources, the metal NPs improve the hydrophilicity and surface charge of the nanofibers resulting in the minimization of the fouling phenomenon [27].

The stability of Ag/PVDF-OH determined by the ICP-MS measurement of the water filtrated after various oil/water separation runs showed that after the first run the amount of Ag content in the filtrated water was only 0.013 mg/L, or ideally 0.19 μg in 15 mL of the filtrated water, after the second separation run, the Ag content decreased by one order of magnitude, and the subsequent runs kept presenting a decreasing Ag concentration (Table S1 in the Supporting Material). These results indicate that the most considerable Ag weight detached out of the nanofibers surface, which occurs at the first oil/water separation run, was a 2.2%. Therefore, it can be considered that the robustness of Ag/PVDF-OH permits the utilization of the material for the oil/water separation process without undergoing a significant loss of the Ag content. Moreover, according to the World Health Organization [28], and the United States Environmental Protection Agency [29], the maximum contamination level of silver in drinking water is set to 0.1 mg/L, which indicates that the low release of Ag from Ag/PVDF-OH, does not represent a risk for the human health.

Besides, the pore size measurements show that the untreated PVDF membrane has an average pore size of 0.34 μm. After the treatment

Table 1

Water contact angle measurements in air and underwater oil contact angle measurements. Note that since the oil droplet was not sticking to the surface of Ag/PVDF-OH by itself, it was necessary to rub the oil droplet to the membrane, so it could stay few seconds to take the picture.

Sample	Contact angle in air (°)	Contact angle underwater (°)	Image in air	Image underwater
PVDF	86.8 ± 8.4	70.4 ±4.5		
PVDF-OH	94.5 ± 5.8	101.6 ±3.0		
Ag/PVDF-OH	0.0	119.4 ± 2.5		

with the KOH solution (PVDF-OH), the average pore size slightly decreases to 0.27 μm, as previously reported [26], the pore size reduction might occur due to the microstructural shrinkage of the membrane by the surface treatment. After the NPs decoration process (Ag/PVDF-OH), the average pore size increased to 0.80 μm. The possible reason for this phenomenon is that when the laser mediated synthesis of the Ag NPs takes place, the optical breakdown of water is promoted, in which a resulting plasma is confined in the laser focal point that elevates the temperature in the solution [30]. While the process takes place, the thermal energy can be transmitted to the membranes and activate the movement of the fibers that are not densely packed. To clarify this fact, the PVDF-OH membrane was exposed to various temperatures in order to monitor the pore size change. The pore size of the membrane changed from 0.30, 0.31, 0.34, and 0.68 μm for the temperatures of 20, 36, 58, and 88 °C, respectively. Therefore, we consider that the combination of the heat transmitted from the optical breakdown spot while synthesizing the Ag NPs and the continuous stirring of the liquid resulted in the opening of the membrane's pores. That fact is visible in Fig. 5 where the Ag/PVDF-OH membrane has a more open structure

134

compared to the neat PVDF.

Finally, the water contact angle tests shown in Table 1 reveal that the addition of the hydroxyl groups (PVDF vs. PVDF-OH) does not lead to any significant effect on the wettability of the dry samples, when the tests are performed in air, which is in accordance with the relevant literature. Conventionally, the number of hydroxyl groups on the surface of the membranes is not the only factor that may lead to a change in wettability, e.g., differences in the surface structure may be more dominant [31]. Conversely, the Ag/PVDF-OH samples displayed outstanding hydrophilicity, which according to the literature, is due to the interaction between the Ag NPs and the liquid that gets in contact with the membrane (water in this case) [32]. Ideally, if no other oxidant is present, the O_2 dissolved in the water can promote the oxidation and consequent ion release of the Ag NPs through the following reaction.

$$2Ag_{(s)} + \frac{1}{2} O_{2(aq)} + 2H^+_{(aq)} \Leftrightarrow 2Ag^+_{(aq)} + H_2O_{(1)} \tag{8}$$
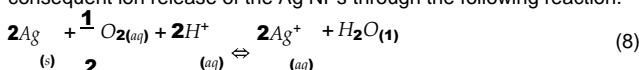
where $Ag_{(s)}$ refer to the solid Ag [33]. Further, the hydrated Ag^+ can get adsorbed onto the surface of the Ag NPs and the nanofibers, improving the adhesion and spread of the liquid by capillarity. Besides, it should be noted that despite the small amount of Ag weight loading, the larger hydrophilicity in Ag/PVDF-OH in comparison with the latest works in the field [34], can be attributed to the ligand-free nature of the Ag NPs produced in the current study. The lack of ligands covering the Ag NPs surface maximizes the number of possible elements able to undergo the oxidation and, consequently, Ag^+ release.

In addition, before the water contact angle tests, all of the samples were kept in a wet form. During this stage, the PVDF-OH and Ag/PVDF-OH specimens were immersed into deionized water, while the neat PVDF floated on the solvent. Once all of the membranes were dried and underwent the water contact angle test, the behaviour of the neat PVDF and Ag/PVDF-OH specimens remained hydrophobic and hydrophilic, respectively. In contrast, the behaviour of the PVDF-OH sample transitioned from hydrophilic to hydrophobic. In order to ratify this, spare portions of the samples that kept stored in the wet form (no contact with air) were used for underwater oil contact angle measurements, and the corresponding results confirmed the consistent behavior of pristine PVDF and Ag/PVDF-OH, and the transition for PVDF-OH depending on the storing conditions.

The PVDF-OH change from hydrophilic to hydrophobic might be explained by the flip-flop mechanism, which is commonly observed in surface functionalities attached to polymer-membranes [35]. After the eOH functionalization, the membrane exhibits hydrophilic behavior due to the affinity between the eOH groups on the surface of the fibers and the water molecules, but in the case of contact with air, the eOH groups may turn from the outside to the inside of the polymer surface because the air is hydrophobic. In the case of Ag/PVDF-OH, such a process is not viable since the NPs cannot be drawn under the polymer surface due to their big size compared to the eOH groups.

These results suggest that the simple addition of the OH- groups to the PVDF membrane does not lead to a long-lasting hydrophilic behavior, whereas the addition of Ag NPs do regardless the membranes are stored in a wet or dry form.

1.1. Membrane filtration properties

1.1.1. Emulsion permeability measurements

The results of the oil/water separation tests (Fig. 7 a)) show that the pristine PVDF membrane became fouled after the fifth run, while the PVDF-OH and Ag/PVDF-OH membranes did not become fouled even after 10 runs. The water permeability of the neat PVDF membrane increased 1.8-fold after the dehydrofluorination treatment and 3.9-fold after the addition of the Ag NPs; a substantial improvement in the oil/water separation performance when comparing with the latest membrane modification strategies for similar systems, which go from 2- to 4-fold [34,36–38].

The decline in permeability, which indicates the membrane's fouling, increased continuously for the PVDF membrane, while it remained constant and almost negligible for the treated membranes (Fig. 7 b)). In line with these results, the flux recovery ratio FRR(%) after the last oil/water separation run of the samples was 22.4% for PVDF, 43.5% for PVDF-OH, and 38.1% for Ag/PVDF-OH. These results indicate that the surface modification of PVDF clearly leads to an increment in its antifouling properties, even when the modified membranes underwent twice the number of oil/water separation runs than the unmodified one. Moreover, the water that was recovered after the 5th and 10th runs through PVDF, PVDF-OH and Ag/PVDF-OH membranes, respectively, was free of oil droplets (Fig. S4 in the Supporting Material), and the corresponding NPOC measurements revealed that the rejection rate R(%) of the membranes was 96.3% for PVDF, 96.1% for PVDF-OH, and 96.2% for Ag/PVDF-OH, which allows concluding that all the membranes greatly suppress the passage of oil droplets. Besides, beyond the scope of the current work, which explores the reduction of chemical-waste production by enforcing the usage of light sources to modify membranes, it is essential to keep in mind that the water flux and permeability of the membranes depend on the applied pressure [39]. Therefore, an increment in the applied pressure (0.02 bar in the current work) towards the industrial usage of the material should also reflect an increase in the water flux and permeability values.

As it is extensively reported, the roughness and hydrophobicity of the PVDF membrane are two significant factors that lead to its fouling and poor recyclability [40]. On the one hand, its rough surface allows the allocation of foulants. On the other hand, its hydrophobicity promotes the adhesion of hydrophobic organics to the membrane's surface resulting in its fouling. In the case of PVDF-OH, when the dehydrofluorination process takes place, the roughness in the surface of the nanofibers gets reduced as it is noticed from the AFM results, and the membrane becomes hydrophilic when stored in a wet form as the
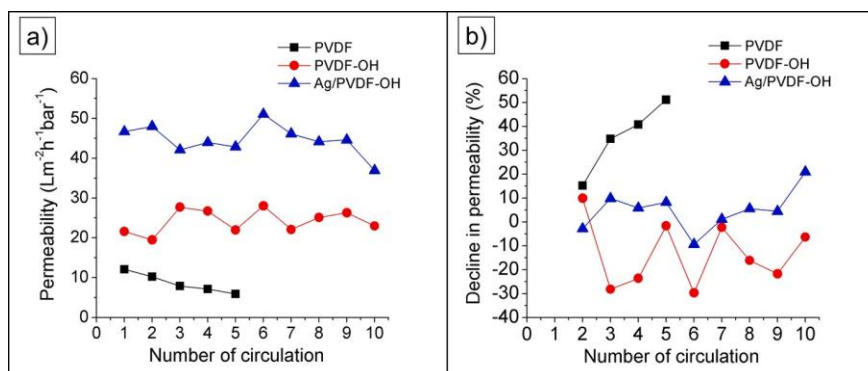

Fig. 7. Graphs showing the a) emulsion permeability and b) decline in permeability of the samples.
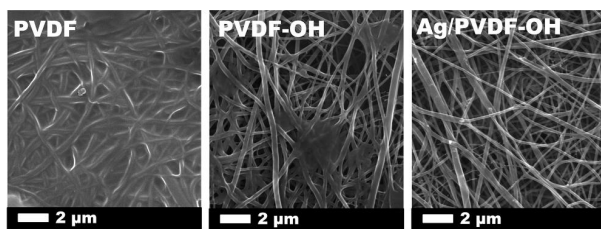
Fig. 8. Micrographs of the membranes after completing the emulsion run cycles.

underwater oil contact angle measurements exhibit it. These features make the membrane's surface, less favorable for the attachment of foulants leading to the observed increment in *FRR***(%)**, and even when its pore size is smaller than the untreated membrane, its hydrophilicity when stored in the wet form seems to have a dominant impact on the water permeability. However, as the water contact angle tests demonstrated, both the PVDF-OH and Ag/PVDF-OH membranes show a hydrophilic behavior when they are kept in a wet form, but when the membranes are dried, the PVDF-OH membrane becomes hydrophobic, which may consequently result in a negative impact on its permeability performance.

Differently, the superior permeability and recyclable performance of the Ag/PVDF-OH membrane can be mainly attributed to its larger pore size, Ag-induced hydrophilic behavior and resistance to the adhesion of oil droplets. On the one hand, larger pore sizes can be translated as empty spaces where a liquid can pass through; *ergo* the water permeability gets incremented. On the other hand, as it is exhibited in Fig. 8, which shows how the membranes look after completing the separation tests, the low load of (0.55 ± 0.03) **μ**g/cm^2 Ag NPs seem to not only increment the water permeability in the membrane but also reduce the adhesion of the oil droplets over its surface. As discussed above, when Ag NPs get in contact with a liquid medium that contains oxidant elements like dissolved O_2, the Ag NPs undergo an oxidation process that results in the release of Ag^+. As the liquid used in the oil/water separation tests is an emulsion composed of non-ionic oil droplets dispersed in water, it is possible to infer that despite other oxidants could be present, at least the O_2 dissolved in the emulsion could render the oxidation of the Ag NPs, and consequently, the Ag^+ release and adsorption over the membrane surface, which subsequently should lead to the preferential adhesion and spread of water rather than the non-ionic oil droplets due to a stronger electrostatic attraction of water (a polar solvent) to the membrane's surface covered by the Ag^+ [41], resulting in the possibility to re-use the material multiple times without experiencing a great blocking of the membrane pores, i.e., a reduction of the water permeability, as it is suggested by the increment in its *FRR* **(%)**. Therefore, the implementation of the current laser-based membrane modification methodology, not only contributes to reducing the use of chemicals and their consequent leftovers but in the framework of the latest advances in the field, also leads to a competitive improvement over the membrane's oil/water separation performance.

1. Conclusions

The main reason to conduct the current work was to explore the benefits of using light instead of hazardous reducing agents to generate NPs that decorate the surface of membranes used for the recovery of clean water from oily emulsions. For this, the LPL strategy was employed for the first time to synthesize Ag NPs in a medium free from reducing or stabilizing agents and decorate the surface of dehydrofluorinated PVDF nanofibrous membranes in a single-stage. The process incremented the membrane's pore size from 0.34 **μ**m to 0.80 **μ**m and allowed the uniform and stable incorporation of ligand-free Ag NPs with diameter of (35 ± 10) nm over the nanofibers, which rendered an outstanding hydrophilicity in the membranes while using an extremely

low NPs load of (0.55 ± 0.03) **μ**g/cm^2. These membrane modifications resulted in a 3.9-fold improvement of the oil/water separation performance over the unmodified PVDF membrane, the decline in permeability remained almost negligible after ten separation runs, and an increment in the flux recovery ratio, due to a minimization in the oil adherence over the membrane surface. Moreover, the pass of oil droplets through the membrane stayed suppressed despite the change in pore size, and the rejection rate kept > 96 **%**.

Overall, the current study revealed that the adoption of the laser-mediated membrane surface modification strategy leads to a comparable improvement over the oil/water separation performance to the one achieved by the latest polluting-linked and NPs-costly strategies. However, the replacement of chemicals by the light could be of paramount interest in the eco-friendly generation of efficient and recyclable materials for the oil/water separation sector.

Credit authorship contribution statement

R. Torres-Mendieta: Conceptualization, Methodology, Validation, Investigation, Writing - original draft, Resources, Writing - review & editing, Visualization, Supervision, Project administration. **F. Yalcinkaya:** Conceptualization, Methodology, Validation, Investigation, Writing - original draft, Resources, Writing - review & editing, Visualization, Supervision, Project administration. **E. Boyraz:** Methodology, Investigation. **O. Havelka:** Methodology, Investigation, Writing - review & editing. **S. Wacɫawek:** Investigation, Writing - review & editing. **J. Maryška:** Validation, Writing - review & editing, Supervision, Project administration. **M. Černik:** Validation, Writing - review & editing, Supervision, Project administration. **M. Bryjak:** Validation, Writing - review & editing, Supervision.

Declaration of Competing Interest

The authors declare that they have no known competing financial interests or personal relationships that could have appeared to influence the work reported in this paper.

Appendix A. Supplementary material

Supplementary data associated with this article can be found, in the online version, at https://doi.org/10.1016/j.apsusc.2020.146575.

References

[1] T. Birkhead, Stormy outlook for long-term ecology studies, Nature 514 (2014) 405, https://doi.org/10.1038/514405a.

[2] H.J. Tanudjaja, C.A. Hejase, V.V. Tarabara, A.G. Fane, J.W. Chew, Membrane-based separation for oily wastewater: A practical perspective, Water Res. 156 (2019) 347–365, https://doi.org/10.1016/j.watres.2019.03.021.

[3] F. Yalcinkaya, B. Yalcinkaya, J. Hruza, P. Hrabak, Effect of nanofibrous membrane structures on the treatment of wastewater microfiltration, Sci. Adv. Mater. 9 (2017) 747–757, https://doi.org/10.1166/sam.2017.3027.

[4] M.R. Esfahani, S.A. Aktij, Z. Dabaghian, M.D. Firouzjaei, A. Rahimpour, J. Eke, I.C. Escobar, M. Abolhassani, L.F. Greenlee, A.R. Esfahani, et al., Nanocomposite membranes for water separation and purification: Fabrication, modification, and applications, Sep. Purif. Technol. 213 (2019) 465–499, https://doi.org/10.1016/j.seppur.2018.12.050.

[5] S. Huang, R.H. Ras, X. Tian, Antifouling membranes for oily wastewater treatment: Interplay between wetting and membrane fouling, Curr. Opin. Colloid Interf. Sci. 36 (2018) 90–109, https://doi.org/10.1016/j.cocis.2018.02.002.

[6] N. Ismail, W. Salleh, A. Ismail, H. Hasbullah, N. Yusof, F. Aziz, J. Jaafar, Hydrophilic polymer-based membrane for oily wastewater treatment: A review, Sep. Purif. Technol. 233 (2019) 116007, https://doi.org/10.1016/j.seppur.2019.116007.

[7] D. Zioui, H. Salazar, L. Aoudjit, P.M. Martins, S. Lanceros-Méndez, Polymer-based membranes for oily wastewater remediation, Polymers 12 (1) (2020) 42, https://doi.org/10.3390/polym12010042.

[8] J.H. Jhaveri, Z. Murthy, A comprehensive review on anti-fouling nanocomposite membranes for pressure driven membrane separation processes, Desalination 379 (2016) 137–154, https://doi.org/10.1016/j.desal.2015.11.009.

[9] S.C. Abeyweera, K.D. Rasamani, Y. Sun, Ternary silver halide nanocrystals, Acc. Chem. Res. 50 (2017) 1754–1761, https://doi.org/10.1021/acs.accounts.7b00194.

[10] J. Noack, A. Vogel, Laser-induced plasma formation in water at nanosecond to femtosecond time scales: calculation of thresholds, absorption coefficients, and energy density, IEEE J. Quantum Electron. 35 (1999) 1156–1167, https://doi.org/10.1109/3.777215.

[11] M. Sakamoto, M. Fujistuka, T. Majima, Light as a construction tool of metal nanoparticles: synthesis and mechanism, J. Photochem. Photobiol., C 10 (2009) 33–56, https://doi.org/10.1016/j.jphotochemrev.2008.11.002.

[12] L. Kőrösi, M. Rodio, D. Dömötör, T. Kovács, S. Papp, A. Diaspro, R. Intartaglia, S. Beke, Ultrasmall, ligand-free ag nanoparticles with high antibacterial activity prepared by pulsed laser ablation in liquid, J. Chem. 2016 (4143560) (2016) 8, https://doi.org/10.1155/2016/4143560.

[13] R. Roche, F. Yalcinkaya, Incorporation of pvdf nanofibre multilayers into functional structure for filtration applications, Nanomaterials 8 (2018) 771, https://doi.org/10.3390/nano8100771.

[14] R. Torres-Mendieta, O. Havelka, M. Urbánek, M. Cvek, S. Wacławek, V.V.T. Padil, D. Jašíková, M. Kotek, M. Černík, Laser-assisted synthesis of fe-cu oxide nanocrystals, Appl. Surf. Sci. 469 (2019) 1007–1015, https://doi.org/10.1016/j.apsusc.2018.11.058.

[15] J.-P. Abid, A. Wark, P.-F. Brevet, H. Girault, Preparation of silver nanoparticles in solution from a silver salt by laser irradiation, Chem. Commun. (7) (2002) 792–793, https://doi.org/10.1039/B200272H.

[16] H. Chou, C. Wu, F. Lin, J. Rick, Interactions between silver nanoparticles and polyvinyl alcohol nanofibers, AIP Adv. 4 (2014) 087111, https://doi.org/10.1063/1.4890290.

[17] P. Kaner, D.J. Johnson, E. Seker, N. Hilal, S.A. Altinkaya, Layer-by-layer surface modification of polyethersulfone membranes using polyelectrolytes and agcl/tio2 xerogels, J. Membr. Sci. 493 (2015) 807–819, https://doi.org/10.1016/j.memsci.2015.05.048.

[18] B. Ameduri, B. Boutevin, G. Kostov, Fluoroelastomers: synthesis, properties and applications, Prog. Polym. Sci. 26 (2001) 105–187, https://doi.org/10.1016/S0079-6700(00)00044-7.

[19] G. Ross, J. Watts, M. Hill, P. Morrissey, Surface modification of poly (vinylidene fluoride) by alkaline treatment1. the degradation mechanism, Polymer 41 (2000) 1685–1696, https://doi.org/10.1016/S0032-3861(99)00343-2.

[20] D. Li, M. Liao, Study on the dehydrofluorination of vinylidene fluoride (vdf) and hexafluoropropylene (hfp) copolymer, Polym. Degrad. Stab. 152 (2018) 116–125, https://doi.org/10.1016/j.polymdegradstab.2018.04.008.

[21] P. Martins, A. Lopes, S. Lanceros-Mendez, Electroactive phases of poly (vinylidene fluoride): Determination, processing and applications, Progress Polym. Sci. 39 (4) (2014) 683–706, https://doi.org/10.1016/j.progpolymsci.2013.07.006.

[22] H. Wang, Z. Liu, E. Wang, R. Yuan, D. Gao, X. Zhang, Y. Zhu, A robust superhydrophobic pvdf composite coating with wear/corrosion-resistance properties, Appl. Surf. Sci. 332 (2015) 518–524, https://doi.org/10.1016/j.apsusc.2015.01.213.

[23] D. Li, M. Liao, Dehydrofluorination mechanism, structure and thermal stability of pure fluoroelastomer (poly (vdf-ter-hfp-ter-tfe) terpolymer) in alkaline environment, J. Fluorine Chem. 201 (2017) 55–67, https://doi.org/10.1016/j.jfluchem.2017.08.002.

[24] H. Pan, B. Na, R. Lv, C. Li, J. Zhu, Z. Yu, Polar phase formation in poly (vinylidene

[25] C. Ribeiro, C.M. Costa, D.M. Correia, J. Nunes-Pereira, J. Oliveira, P. Martins, R. Goncalves, V.F. Cardoso, S. Lanceros-Mendez, Electroactive poly (vinylidene fluoride)-based structures for advanced applications, Nature Protocols 13 (4) (2018) 681, https://doi.org/10.1038/nprot.2017.157.

[26] N.A. Samsure, N.A. Hashim, N.M.N. Sulaiman, C.Y. Chee, Alkaline etching treatment of pvdf membrane for water filtration, RSC Adv. 6 (2016) 22153–22160, https://doi.org/10.1039/c6ra00124f.

[27] E. Mahmoudi, L.Y. Ng, W.L. Ang, Y.T. Chung, R. Rohani, A.W. Mohammad, Enhancing morphology and separation performance of polyamide 6, 6 membranes by minimal incorporation of silver decorated graphene oxide nanoparticles, Sci. Rep. 9 (2019) 1216, https://doi.org/10.1038/s41598-018-38060-x.

[28] W.H.O. (WHO), W.H.O. Staff, Guidelines for drinking-water quality, vol. 1, World Health Organization, 2004.

[29] 2018 drinking water standards and advisory tables, https://www.epa.gov/sites/production/files/2018-03/documents/dwtable2018.pdf, accessed: 2020-02-03.

[30] P.K. Kennedy, A first-order model for computation of laser-induced breakdown thresholds in ocular and aqueous media. I. theory, IEEE J. Quantum Electron. 31 (1995) 2241–2249, https://doi.org/10.1109/3.477753.

[31] M. Fuji, M. Araki, T. Takei, T. Watanabe, M. Chikazawa, Structure and wettability of various silica surfaces: Evaluation on the nano and macro levels [translated], KONA Powder Particle J. 18 (2000) 236–241, https://doi.org/10.14356/kona.2000031.

[32] J.-H. Li, X.-S. Shao, Q. Zhou, M.-Z. Li, Q.-Q. Zhang, The double effects of silver nanoparticles on the pvdf membrane: Surface hydrophilicity and antifouling performance, Appl. Surf. Sci. 265 (2013) 663–670, https://doi.org/10.1016/j.apsusc.2012.11.072.

[33] J. Liu, R.H. Hurt, Ion release kinetics and particle persistence in aqueous nano-silver colloids, Environ. Sci. Technol. 44 (6) (2010) 2169–2175, https://doi.org/10.1021/es9035557.

[34] W. Xu, H. Zhuang, Z. Xu, M. Huang, S. Gao, Q. Li, G. Zhang, Design and construction of ag@ mofs immobilized pvdf ultrafiltration membranes with anti-bacterial and antifouling properties, Adv. Polym. Technol. (2020), https://doi.org/10.1155/2020/5456707.

[35] Y. Wang, X. Gong, Special oleophobic and hydrophilic surfaces: approaches, mechanisms, and applications, J. Mater. Chem. A 5 (8) (2017) 3759–3773, https://doi.org/10.1039/C6TA10474F.

[36] D. Sun, D. Yue, B. Li, Z. Zheng, X. Meng, Preparation and performance of the novel pvdf ultrafiltration membranes blending with pva modified sio2 hydrophilic nanoparticles, Polym. Eng. Sci. 59 (S1) (2019) E412–E421, https://doi.org/10.1002/pen.25002.

[37] Z. Xu, T. Wu, J. Shi, K. Teng, W. Wang, M. Ma, J. Li, X. Qian, C. Li, J. Fan, Photocatalytic antifouling pvdf ultrafiltration membranes based on synergy of graphene oxide and tio2 for water treatment, J. Membr. Sci. 520 (2016) 281–293, https://doi.org/10.1016/j.memsci.2016.07.060.

[38] X. Zhao, N. Jia, L. Cheng, R. Wang, C. Gao, Constructing antifouling hybrid membranes with hierarchical hybrid nanoparticles for oil-in-water emulsion separation, ACS Omega 4 (1) (2019) 2320–2330, https://doi.org/10.1021/acsomega.8b03408.

[39] X. Yi, S. Yu, W. Shi, N. Sun, L. Jin, S. Wang, B. Zhang, C. Ma, L. Sun, The influence of important factors on ultrafiltration of oil/water emulsion using pvdf membrane modified by nano-sized tio2/al2o3, Desalination 281 (2011) 179–184, https://doi.org/10.1016/j.desal.2011.07.056.

[40] M. Li, L. Wu, C. Zhang, W. Chen, C. Liu, Hydrophilic and antifouling modification of pvdf membranes by one-step assembly of tannic acid and polyvinylpyrrolidone, Appl. Surf. Sci. 483 (2019) 967–978, https://doi.org/10.1016/j.apsusc.2019.04.057.

[41] L. Huang, C. Maltesh, P. Somasundaran, Adsorption behavior of cationic and nonionic surfactant mixtures at the alumina–water interface, J. Colloid Interface Sci. 177 (1) (1996) 222–228, https://doi.org/10.1006/jcis.1996.0024.

PVDF nanofibrous membranes modified via laser-synthesized Ag nanoparticles for a cleaner oily water separation

R. Torres-Mendieta[*a], F. Yalcinkaya[a], E. Boyraz[a], O. Havelka[a], S. Wacławek[a], J. Maryška[a], M. Černik[a], M. Bryjak[b]

[a]Institute for Nanomaterials, Advanced Technologies and Innovation, Technical University of Liberec, Studentská 1402/2, 461 17 Liberec, Czech Republic.
[b]Department of Polymer and Carbon Materials, Wrocław University of Science and Technology, Wyb. St. Wyspianskiego 27, 50-370 Wrocław, Poland.

*Rafael.Torres@tul.cz
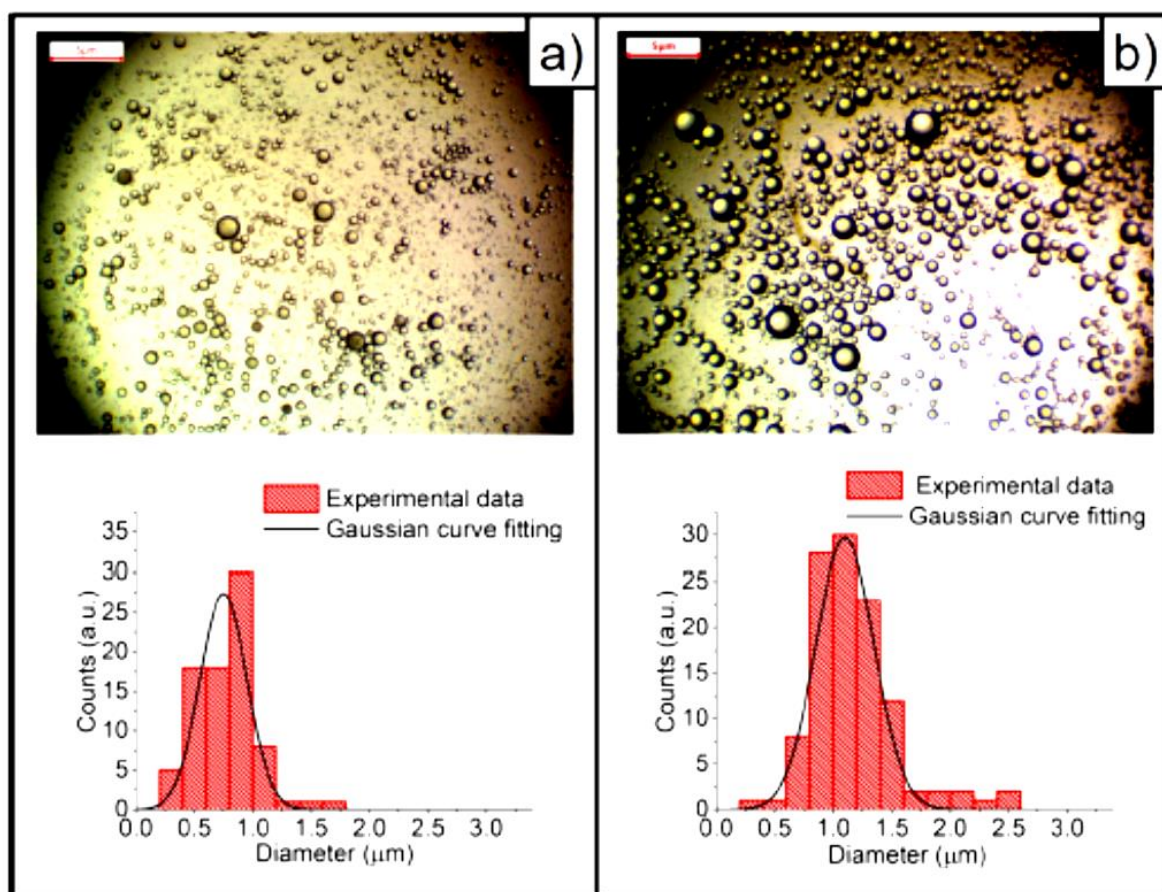
Figure S.1 Optical images of the emulsion (diluted in distilled water) and the corresponding histogram of oil droplets diameter of a) the freshly prepared emulsion and b) the emulsion after two weeks of preparation.
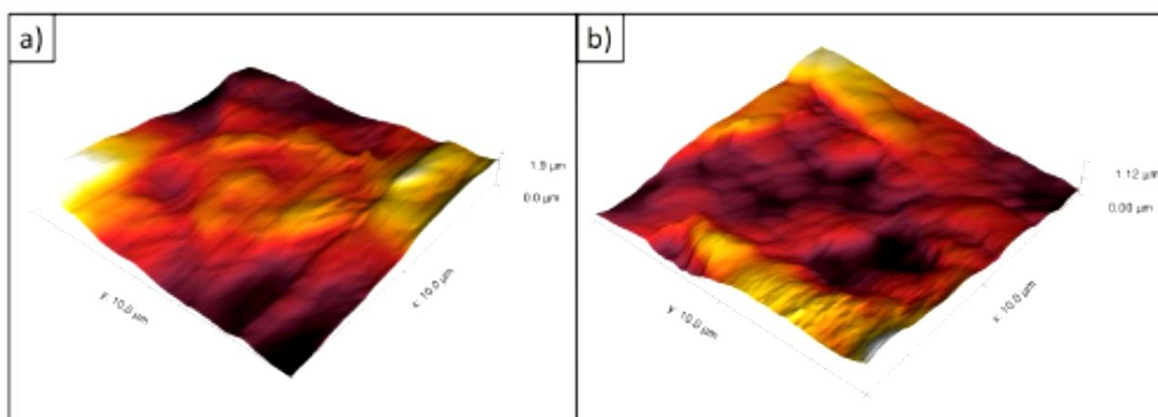
Figure S.2 AFM images of a) PVDF membranes and b) PVDF-OH membranes.

Figure S.3 FE-SEM micrograph of the Ag/PVDF-OH membrane (EHT = 2.50 kV and WD = 7.9 mm) and Mag= 50 K X, where it is possible to observe the uniform distribution of Ag NPs over the nanofibers.
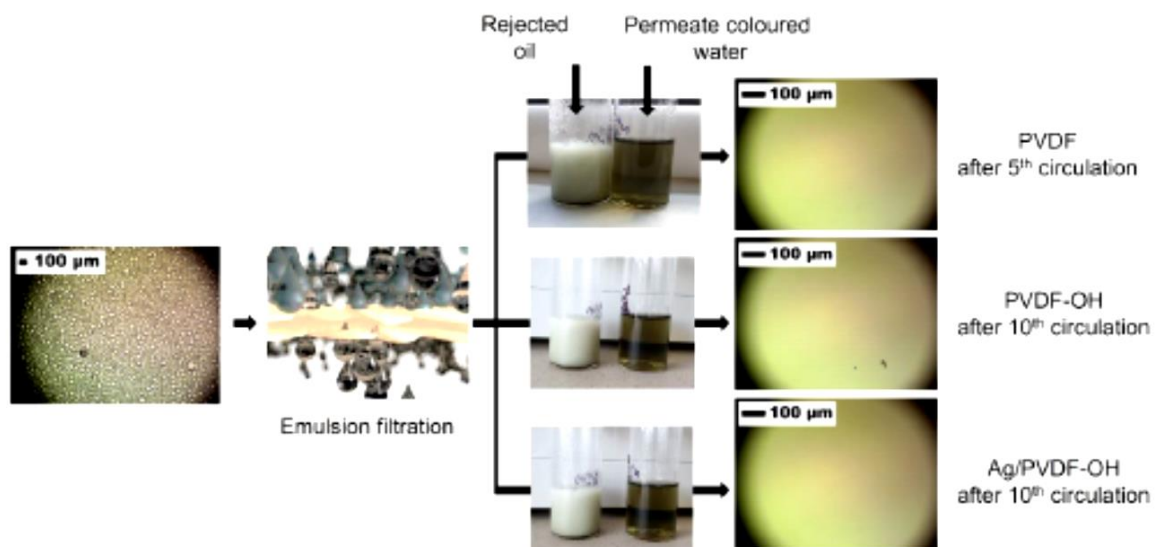
Figure S.4 Optical image of the emulsion (diluted in distilled water) and the water recovered after the filtration process.

No. of oil/water separation run	Ag concentration (mg/L)
1	0.012860
2	0.003970
3	0.002950
4	0.001383
5	0.001322
6	0.001902
7	0.001389
8	0.001315
9	0.001096
10	0.001605

Table S.1 Ag content in the filtered water after each oil/water separation runs.

Research Article

Thin Film Nanofibrous Composite Membrane for Dead-End Seawater Desalination

Baturalp Yalcinkaya,[1] Fatma Yalcinkaya,[1] and Jiri Chaloupek[2]

[1]Institute for Nanomaterials, Advanced Technologies and Innovation, Technical University of Liberec, Studentská 1402/2, 461
 17 Liberec, Czech Republic
[2]Department of Nonwoven and Nanofibrous Material, Faculty of Textile, Technical University of Liberec, Studentská 1402/2, 461
 17 Liberec, Czech Republic

Correspondence should be addressed to Baturalp Yalcinkaya; baturalpyalcinkaya@hotmail.com

The aim of the study was to prepare a thin film nanofibrous composite membrane utilized for nanofiltration technologies. The composite membrane consists of a three-layer system including a nonwoven part as the supporting material, a nanofibrous scaffold as the porous surface, and an active layer. The nonwoven part and the nanofibrous scaffold were laminated together to improve the mechanical properties of the complete membrane. Active layer formations were done successfully via interfacial polymerization. A filtration test was carried out using solutions of $MgSO_4$, NaCl, Na_2SO_4, $CaCl_2$, and real seawater using the dead-end filtration method. The results indicated that the piperazine-based membrane exhibited higher rejection of divalent salt ions (>98%) with high

flux. In addition, the m-phenylenediamine-based membrane exhibited higher rejection of divalent and monovalent salt ions (>98% divalent and >96% monovalent) with reasonable flux. The desalination of real seawater results showed that thin film nanofibrous composite membranes were able to retain 98% of salt ions from highly saline seawater without showing any fouling. The electrospun nanofibrous materials proved to be an alternative functional supporting material instead of the polymeric phase-inverted support layer in liquid filtration.

1. Introduction

Demand for fresh water sources is increasing due to a population explosion in the world. Humans need drinkable water, and groundwater resources are decreasing more than ever before. Many countries are facing serious problems regarding this. Several technological methods such as desalination [1, 2] or distillation of seawater [3, 4] have given hope to people in areas of water scarcity. Membrane desalination is an effective technology that produces fresh water from brackish water or seawater using nanofiltration (NF) [5] and reverse osmosis (RO) [6] membrane processes.

Conventional NF and RO membranes consist of a considerably thick phase-inverted polymeric support layer and a relatively thin polyamide (PA) active layer by in situ polymerization of an aqueous solution containing di- or polyfunctional amine and organic solutions containing di- or

trifunctional carboxylic acid chloride at their interface [7–12]. Recently, an electrospun nanofibrous layer has been prepared as an alternative supporting layer to form a thin PA active layer using electrospinning methods. In this method, the polymer solutions are spun directly onto nonwoven fabrics to prepare the nanofibres [13, 14] and a PA active layer is formed over the nanofibrous layer. The final structure is called a thin film nanofibrous composite (TFNC) membrane. One of the greatest advantages of the TFNC membrane is its extremely high permeate flux due to its high surface area and direct channel structure [15–18]. Besides the high flux performance, TFNC membranes have shown excellent rejection in both mono- and divalent salt ions, indiscriminately [19].

Despite the high salt rejection and permeate flux performance of TFNC membranes, the weak mechanical properties of the nanofibrous layer and insufficient adhesion between the nonwoven layer and the nanofibres have become the main

limitations of the nanofiltration process. In the literature there are various attempts to overcome the mechanical problem of nanofibres [20–22]. Some of the studies have focused on increasing interfibre adhesion to improve the mechanical properties of the entire membrane [23, 24]. For instance, a mixed solvent system (dimethylformamide (DMF) and N-methyl-pyrrolidinone (NMP)) was used to prepare a solution of polyethersulfone (PES) by Yoon et al. [25]. A PES polymer solution has been electrospun using needle electrospinning. A different solvent mixed system contained solvents with various vapour pressures. Therefore, the nanoweb on the supporting material was still partly wetted because of the high vapour pressure of NMP, and this could lead to adhesion between the fibres. However, the average fibre diameter increased directly proportional to the mechanical strength [16]. In other studies, to increase the strength and integrity of the nonwoven and nanofibrous composite supporting layer, heat and pressure were applied [26]. These above-mentioned methods influenced the morphology of the nanofibrous layer in a negative way (e.g., there is an increase in the fibre diameter or nonfibrous area). Moreover, the needle electrospinning method, which is a small-scale nanofibres production system, used the studies mentioned above. Hence, the commercialization of those nanofilters is improbable.

The primary purpose of the researcher is to prepare a membrane with the best rejection and flux performance in the area of desalination. In the literature, there are many attempts to increase membrane performance by using various kinds of additives in an aqueous or organic phase to obtain a better IP process [27–29]. Petersen reported that, to obtain higher rejection performance in piperazine-based (PIP) membranes, the presence of an acid acceptor was necessary in an aqueous solution. However, this was not the case for m-phenylenediamine-based (MPD) membranes [10]. The reaction rate of a PIP solution into the trimesoyl chloride (TMC) solution was rather low and requires a higher concentration of acyl halide along with an acid acceptor to promote the PA active barrier layer. In the case of MPD-based membranes, the high portion of tertiary amine content acts as a built-in acid acceptor. Hermans proved that the use of a tertiary amine base was necessary to obtain a high rejection rate together with surfactants. However, adding each of them separately did not improve the performance [30]. Mansourpanah indicated that adding different kinds of surfactants (anionic, cationic, and nonionic) affects the filtration performance and morphology of the active barrier layer. They reported that an increase in surfactant concentrations in aqueous PIP solutions usually decreases rejection and increases permeate flux with some exceptions [31, 32].

When it comes to desalination technology, the dead-end filtration method is usually applied as a pretreatment for reverse osmosis in seawater desalination using a low-pressure membrane such as microfiltration or ultrafiltration [33, 34]. The polymeric phase-inverted micro- and ultrafiltration membranes have proved themselves to be able to take on this task. However, polymeric phase-inverted membranes tend to show fouling due to their hydrophobic structure. Moreover, most of the common phase-inverted membranes are produced from expensive polymers such as PVDF, PES, or

PSf using highly concentrated polymer solutions via a solvent and nonsolvent exchange system.

Taking into consideration the above information, the objectives of the present work are the following:

(1) To prepare alternative supporting material, which is relatively cheap and applicable to upscale production of liquid filtration or desalination.

(2) To overcome the main issues of nanofibrous membranes (weak mechanical properties) in liquid nanofiltration and prepare the finest possible nanofibrous surface without negatively affecting the morphology of the nanofibres for PA thin active surface.

(3) To desalinate real seawater provided from the Mediterranean Sea using thin film nanofibrous composite membranes under low pressure via dead-end filtration.

In this study, three-layered thin film nanofibrous composite membranes were prepared. The nonwoven and nanofibrous supporting layers were combined using the lamination method by applying heat and pressure. The top PA thin active layer was formed by interfacial polymerization. The characterizations of laminated support layer and prepared thin film nanofibrous composite membrane were done. The long-term filtration performance was evaluated via a dead-end filtration cell using mono- and divalent salt solutions. Finally, real seawater filtration was carried out using the dead-end filtration cell.

2. Experimental

2.1. Materials. The TFNC bottom substrate was a polypropylene/polyethylene (80/20, 18 g/m²) bicomponent spunbond nonwoven fabric (Pegatex S BICO) from Pegas Nonwovens s.r.o. (Czech Republic). The solution used to produce the porous nanofibre layer by electrospinning consisted of polyamide 6 (PA6) (BASF B24) dissolved in acetic acid/formic acid. The selective layer of the TFNC membrane was prepared by interfacial polymerization of two immiscible phases on the porous nanofibre layer. Piperazine (PIP) and m-phenylenediamine (MPD) were purchased from Sigma-Aldrich and prepared in deionised water as aqueous phases, while the organic phase was prepared by dissolving trimesoyl chloride (TMC) (Sigma-Aldrich) in hexane at 40°C. The filtration performance of TFNC membranes was tested using salt solutions containing magnesium sulphate ($MgSO_4$), sodium chloride (NaCl), and calcium chloride ($CaCl_2$) purchased from Penta s.r.o. (Czech Republic) and sodium sulphate (Na_2SO_4) purchased from Lachema, Brno (Chemapol). Triethylamine (TEA) was purchased from Sigma-Aldrich. Sodium hydroxides (NaOH) were chosen as acid acceptor materials and Synferol AH 1241 was used as an anionic surfactant.

2.2. Preparation of the Electrospun PA6 Porous Nanofibrous Layer. A solution of polyamide 6 (8% wt.) was dissolved in acetic acid/formic acid at a ratio of 2/1 at 80°C for
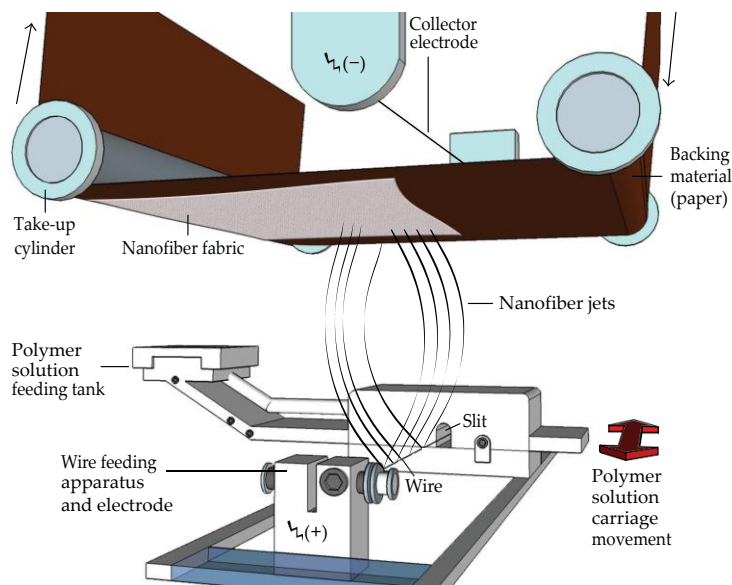
Figure 1: Electrospinning of PA6 nanofibres using the Nanospider Production Line NS 1WS500U.

4 hours to produce a nanofibre layer using wire electrode electrospinning equipment (NS 1WS500U, Elmarco s.r.o., Czech Republic). Wire electrospinning is a new technique that uses an electrical force to spin nanofibres from a free surface liquid towards a collector electrode [35] (Figure 1). A solution carriage feeds the polymer solution around a moving stainless steel wire. The speed of the carriage is 245 mm/s and the rotation speed of the wire is 40.5 cm/h. High voltage suppliers are connected to the wire electrode (55 kV) and the collector electrode (−10 kV). When the applied voltage exceeds a critical value, many Taylor cones are created on the surface of the wire. Polymer solution jets move towards the collector, the solvent evaporates, and the PA6 nanofibrous layer is collected on baking paper moving in front of the collector electrode. The speed of the movement of the baking paper is 9 cm/min.

The distance between the electrodes is 18 cm. The temperature and humidity of input air are set to 23°C and 30% by the air-conditioning system. The volumes of air input and output are 98 and 110 m³/h, respectively.

2.1. Lamination of Nonwoven and Nanofibrous Materials. Bicomponent spunbond nonwoven and PA6 nanofibrous fabrics were laminated using RPS-Mini fusing lamination equipment (Meyer-Germany). This process was carried out tenuously to avoid damaging the structure of the nanofibres such as the fibre diameter and pore size.

The PA6 nanofibrous layer was put onto PP/PE bicomponent nonwoven fabric and inserted between two Teflon belts moving at 2 m/min in the lamination equipment.

The temperature was set at 135°C considering the melting point of PE (120–130°C). The nanofibrous layer adhered to
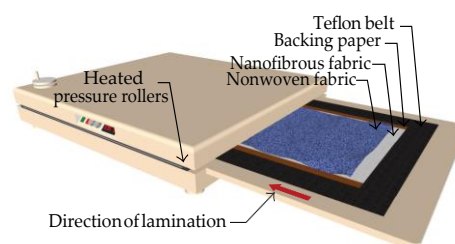
Figure 2: Lamination method and equipment.

the nonwoven fabric under a pressure of 15 N/cm while the PE fibres partly melted. The resulting product is called the nonwoven-nanofibrous composite (NNC) scaffold (Figure 2).

2.2. Preparation of the Active Barrier Layer. The laminated PP/PE bicomponent spunbond nonwoven fabric and the PA6 nanofibrous web were used as supporting material to prepare the TFNC membranes. To form an active barrier layer, interfacial polymerization was carried out using MPD and PIP monomers for an aqueous solution while TMC was used for organic solutions.

To prepare the PIP-based TFNC membranes, TEA [4.0% (w/v)] and NaOH [1.0% (w/v)] were added to a certain amount of PIP [2.0% (w/v)] aqueous solution while the concentration of the TMC was [0.2% (w/v)]. The reaction times selected for the aqueous and organic solutions were 1 min and 45 sec, respectively. The drying time between the solutions was set at 5 min. The temperature and time of curing in the incubator were 110°C and 10 min, respectively.

MPD-based membranes were prepared using an acid acceptor [TEA, 2.0% (w/v)] and surfactants [anionic liquid, 0.2% (w/v)]. The selected concentrations of MPD and TMC were [2.0% (w/v)] and [0.2% (w/v)] in aqueous and organic solutions. The IP reaction for the MPD-based membranes was carried out under the same conditions as the drying, curing time, and curing temperature mentioned above for the PIP-based membranes except that the reaction times were different. The selected reaction time for the MPD aqueous solution was 1 min, whereas the reaction time for the organic solution was 30 sec.

2.1. Characterization of Enhanced TFNC Membranes. The surface morphologies of enhanced MPD- and PIP-based TFNC membranes were investigated using scanning electron microscopy (Tescan-Vega3 SEM). Attenuated total reflectance Fourier transforms infrared spectroscopy (ATR-FTIR) characterization of the MPD- and PIP-based TFNC membrane surfaces was performed with the ATR accessory, using a Nicolet IZ10 (Thermo Fisher Scientific Inc., Waltham, MA). Analysis of samples was carried out by applying the reflection technique using a Germanium crystal. The surface hydrophilicity of the NNC scaffold and MPD- and PIP-based TFNC membranes was evaluated using an optical angle meter (Kruss Drop Shape Analyzer DS4).

2.2. Molecular Weight Cut-Off (MWCO) Test Using Aqueous PEG Solutions. Molecular weight cut-off refers to the lowest molecular weight solute (in daltons) in which 90% of the solute is retained by the membrane. The MWCO of MPD- and PIP-based membranes was evaluated with polyethylene glycol aqueous feed solutions, containing 1000 ppm PEG with different molecular weights (Sigma-Aldrich; Mn: 200, 400, and 600). The permeates and feed solutions were analyzed using a total organic carbon analyzer (direct measurement method, Analytik Jena Multi N/C 2100S, Germany). The filtration performance of PEG solutions was tested using a dead-end filtration cell.

2.3. Liquid Chromatography Analysis. The prepared MPD- and PIP-based membranes were used to determine whether residual compounds such as MPD, PIP, TMC, TEA, or surfactants were released from the membranes to the permeation side. Therefore, the membranes were set into a dead-end filtration cell and only pure water was used as a feed solution. The permeate water samples were stored in a vial specifically for liquid analysis. The existence of residual chemicals that could be released from the membrane itself during the pure water filtration experiments was investigated using ABSciex 3200 QTRAP mass spectrometer and Dionex UltiMate 3000 liquid chromatography.

The amount of salt ions (Na^+, Ca^{+2}, K^+, Mg^{+2}, Cl^-, SO^{-4}, NO^{-2}, and NO^{-3}) in the original feed seawater and filtered seawater was determined through ion chromatography analysis using ICS-90 Dionex.

2.4. Evaluation of Filtration Performance. The dead-end filtration cell was used to investigate the filtration performance

Table 1: Properties of the NNC scaffold.

Smallest pore size (μm)	Bubble point pore size (μm)	Mean flow pore size (μm)	Fibre diameter (nm)
0.469	1.064	0.739	126 ± 29.1

of enhanced MPD- and PIP-based TFNC membranes. All of the filtration experiments were performed to observe the long-term and fouling performance of the TFNC membranes. The experiments were performed using pure water and salt solutions, for example, 2,000 ppm $MgSO_4$, NaCl, $CaCl_2$, and Na_2SO_4 solutions, were used as feed water. The rejection performance was calculated by (1), using a conductivity meter:

$$\text{Rejection (\%)} = \frac{Cf - Cp}{Cf} \times 100, \tag{1}$$

where Cf and Cp are the conductivity of the feed and permeant concentrations.

1. Results and Discussion

3.1. Characteristic of TFNC Membranes. In this study, production of PA6 nanofibres was carried out onto a backing paper substrate using a Nanospider electrospinning device. Subsequently, the PA6 nanofibrous layer was transferred onto a PP/PE spunbond nonwoven fabric by the lamination method. Figure 3 illustrates the top-viewed and cross-sectioned SEM image of the TFNC membranes. The average fibre diameter of the top layer of the NNC scaffold was 126 ± 29.1 nm and the mean flow pore size was 0.739 μm. Further features of the NNC scaffold are listed in Table 1.

The tensile strength tests of the nonwoven fabric, nanofibrous scaffold, and NNC scaffold were measured individually. The nanofibrous layer showed weak mechanical properties of 4.33 N/25 mm (machine direction) and 4.12 N/25 mm (counter-direction), while the tensile strength of the spunbond bicomponent nonwoven fabric was 14.95 N/25 mm (machine direction) and 6.14 N/25 mm (counter-direction). When the lamination method was applied, the tensile strength of the NNC scaffold was increased to 29.17 N/25 mm (machine direction) and 14.42 N/25 mm (counter-direction). The thicknesses of the nanofibrous scaffold and the spunbond bicomponent nonwoven fabric were 38 ± 0.5 μm and 75 ± 1 μm, respectively. After lamination of the fabrics, the total scaffold thickness was 105 ± 5 μm.

The PIP- and MPD-based TFNC membranes were prepared by adding various additives to the aqueous solutions. The addition of an acid acceptor, a strong base, and anionic surfactants to the aqueous solution had a significant effect on the surface morphology of the PIP- and MPD-based TFNC membranes (Figure 4).

It is evident from the SEM images in Figure 4 that the fibrous pattern of the nanofibrous layer disappeared and formed a typical ridge and valley PA structure on the NNC scaffold. The surface structures of the MPD-based
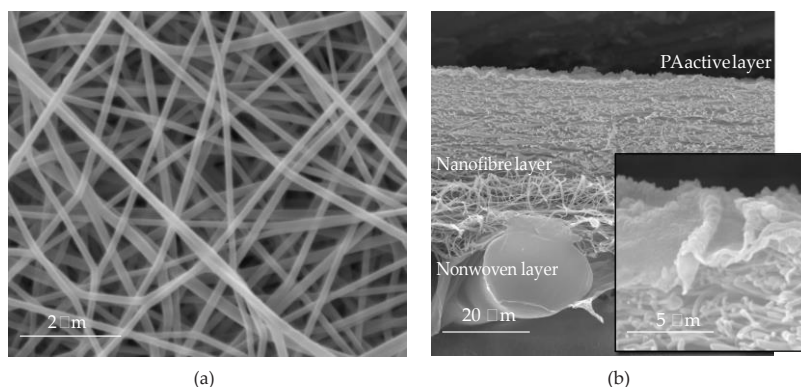
144

Figure 3: SEM images of (a) top view (nanofibres) and (b) cross-sectioned TFNC membranes.
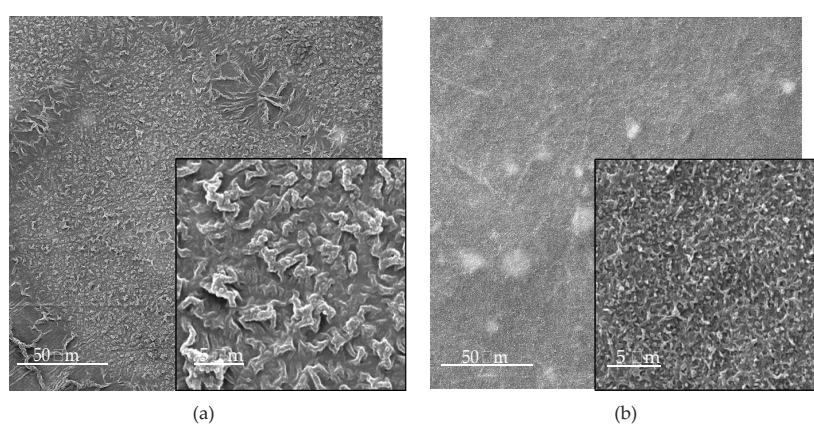

Figure 4: Surface images of (a) PIP-based membranes which were prepared TEA+NaOH and (b) MPD-based membranes which were prepared TEA+Synferol AH.

membranes prepared with the anionic liquid were smooth and homogenous according to the PIP-based membranes. The morphological difference of the MPD- and PIP-based membranes is mainly due to the difference in the chemical structure of the monomers.

The FTIR spectra of the obtained PIP-based PA active layers on the NNC scaffold are shown in Figure 5. The strong and broad signals around the wavelength of $3,405\,cm^{-1}$ were observed with the addition of NaOH, which was assigned to the carboxylic acid group or the hydroxyl group on the surface of the active layer. However, for the membranes coated with MPD-based active layers, the same bond seems weaker. A strong band at $1,620\,cm^{-1}$ is an indicator of the C=O bond of an amide functional group for both membranes.

The FTIR spectra of the prepared MPD-based PA active layers on the NNC scaffold are also given in Figure 5. The characteristic properties of the MPD-based membranes were seen at $1,650\,cm^{-1}$ and $1,550\,cm^{-1}$, which are represented by the C=C bond of the phenyl ring and amide II, respectively. The C-H stretching region for the anionic liquid (Synferol AH) can be observed from the medium peaks at $2,956\,cm^{-1}$ (asymmetric CH_3), $2,923\,cm^{-1}$ (asymmetric CH_2), and $2,854\,cm^{-1}$ (symmetric CH_3). The other peaks observed after $1,000\,cm^{-1}$ indicate C-H bonds in aromatics groups.

The reaction of both MPD (Figure 6) and PIP (Figure 7) monomers with TMC led to the successful formation of a dense layer on the NNC scaffold.

The surface hydrophilicity of the prepared PIP- and MPD-based TFNC membranes is given in Table 2.

The NNC scaffold showed slightly hydrophilic behaviour, while the membranes with the active barrier layer showed more hydrophilic behaviour than the NNC scaffold. The measurement of contact angles of the PIP-based membranes showed superhydrophilic behaviour with the existence of acid acceptors (TEA, NaOH). The measurement of the contact angle of the MPD-based membranes demonstrated that the addition of an acid acceptor and an ionic liquid to the aqueous solution has a significant effect on the surface hydrophilicity of the active layer.
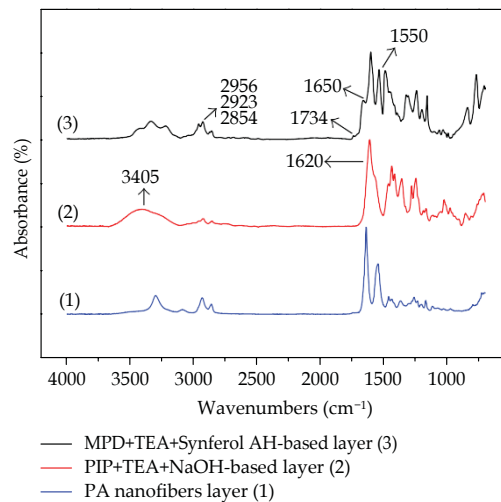
Figure 5: ATR-FTIR of the NNC scaffold (1) and PIP-based (2) and MPD-based (3) membranes.

Table 2: Contact angle properties of NNC and TFNC membranes (specified with reaction time).

Membranes	Contact angle	Images of water droplet
NNC scaffolds	62.7 ±2.74	
PIP+TEA+NaOH+TMC (1 min + 45 sec)	0	
MPD+TEA+Synf+TMC (1 min + 30 sec)	21±1.64	

3.2. Determination of the Molecular Weight Cut-Off of the TFNC Membranes. The filtration of an aqueous PEG solution with different molecular weights was carried out using dead-end filtration to determine the MWCO of the TFNC membrane. Table 3 gives the PEG rejection values of the PIP-based TFNC membrane prepared using TEA + NaOH as an additive and the MPD-based TFNC membrane prepared using TEA + Synferol AH as an additive. 1000 ppm PEG 200, 400, and 600 solutions were used as the test samples during the MWCO tests.

It was found that the MWCO of the PIP+TEA+NaOH-based membrane was 400 Da (the rejection rate was 91.1%). The average solution diameter of PEG-400 was 1.8 nm, which means that the effective pore size of the PIP+TEA+NaOH-based membrane was around 1.8 nm. The MPD+TEA+Sy-AH-based membrane showed a high PEG-200 rejection rate (97.3%). The average solution diameter of PEG-200

Table 3: The rejection values of the TFNC membranes using PEG feed solutions.

Membranes	PEG-200	PEG-400	PEG-600
PIP+TEA+NaOH	61.5%	91.1%	98.9
MPD+TEA+Sy-AH	97.3%	98.9%	99.6

Table 4: Properties of the salt used for the feed solutions.

Type of salt	Conductivity (mS/cm)	pH	Parts per million (ppm)
$MgSO_4$	2.21	5.59	2,000
Na_2SO_4	5.74	6.87	2,000
NaCl	3.52	6.15	2,000
$CaCl_2$	3.62	5.75	2,000

was 1.3 nm (200 Da), which means that the effective pore size of the MPD+TEA+Sy-AH-based membrane was less than 1.3 nm [36]. The TOC analysis showed that the PIP+TEA+NaOH-based membrane was able to retain compounds with a maximum average molecular weight of 400 g/mol. On the other hand, the MPD+TEA+Sy-AH-based membrane was able to retain a compound with a molecular weight of less than 200 g/mol.

3.3. Filtration Performance of TFNC Membranes. The filtration processes in the extended period were carried out using a PIP+TEA+NaOH-based membrane. First, the filtration process was carried out using distilled water to determine the pure water permeate flux and level of compaction of the membrane (Figure 8).

In the early filtration stage of all of the membranes, determination of the pure water flux is necessary in order for the membranes to reach a steady state. In this study, transmembrane pressure was applied to all of the prepared membranes for compaction. Once the membranes reach a steady state using pure water, the filtration process was carried out for the feed solutions. Figure 8 shows the pure water flux of PIP+TEA+NaOH-based membranes for 24 hours. The filtration of the pure water flux began with 78.5 L m⁻² h⁻¹ and was then decreased to 75.9 and 74.7 L m⁻² h⁻¹. Stable flux averaging 73.5 L m⁻² h⁻¹ was obtained after 6 hours. The differences between the steady state and the third-hour flux were not so significant (1.2 L m⁻² h⁻¹). It is also seen from Figure 8 that the amount of compaction on the PIP-based membranes was almost negligible.

After the steady state of the PIP+TEA+NaOH-based membrane was determined and attained using pure water, feed solution experiments were carried out for an extended period. Four kinds of salts, that is, $MgSO_4$, NaCl, $CaCl_2$, and Na_2SO_4, were chosen for the feed solution. The properties of the salt solutions are given in Table 4 and the filtration performances of the four kinds of solution are illustrated in Figure 9.

The flux and rejection performance are shown for the filtration of feed solutions in all of the graphs in Figure 9.
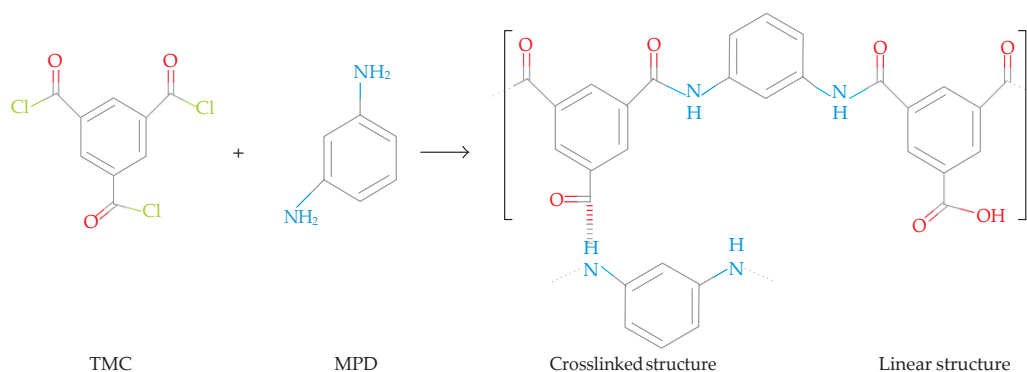
Figure 6: An aromatic polyamide formed with trimesoyl chloride and *m*-phenylenediamine.
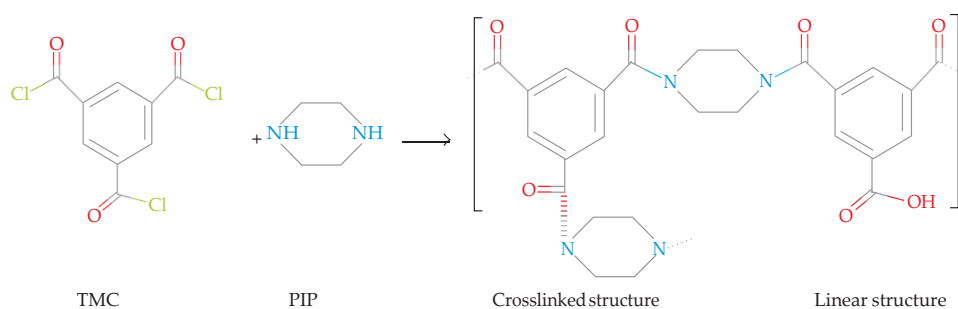
Figure 7: Reaction of trimesoyl chloride and piperazine to aliphatic PA.
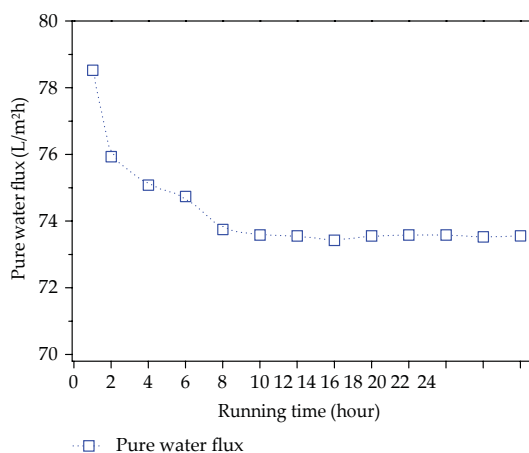
Figure 8: Observation of the filtration process for an extended period of PIP+TEA+NaOH membrane using pure water at 4.8 bar.

In Figure 9(b), the flux performance showed a decreasing trend, which means that the PIP+TEA+NaOH-based membrane showed slightly fouling behaviour during the filtration of the Na_2SO_4 feed solution. Eventually, the

PIP+TEA+NaOH-based membrane showed a high rejection performance for divalent salts. Inherently, the retained monovalent salt ratios were low.

The MPD+TEA+Sy-AH-based membrane used for the pure water filtration over an extended period is shown in Figure 10.

The MPD+TEA+Sy-AH-based membrane began with considerably high pure water flux; after a while the pure water flux becomes stable and reaches a steady state. The pure water flux began around $31.2 \, L \, m^{-2} \, h^{-1}$ and then reached a steady state at $22.3 \, L \, m^{-2} \, h^{-1}$ after 6 hours. The membrane compaction is crucial for the NF and RO membranes and depends on the applied pressure and type of membrane [37, 38]. Flux performance can drop significantly, especially in reverse osmosis membranes [39]. Figures 8 and 10 show that the compaction rate of the TFNC membranes is substantially low due to the advantages of the fibrous structure of the supporting layer.

The filtration experiments of different salt-based feed solutions for the MPD+TEA+Sy-AH-based membrane are given in Figure 11. The rejection rates of divalent salts were higher than 98% and were around 96-97% for monovalent salts. The flux performance of the MPD+TEA+Sy-AH-based membrane showed a slightly decreasing trend. This may be explained by the concentration polarization due to the use of a dead-end filtration cell.
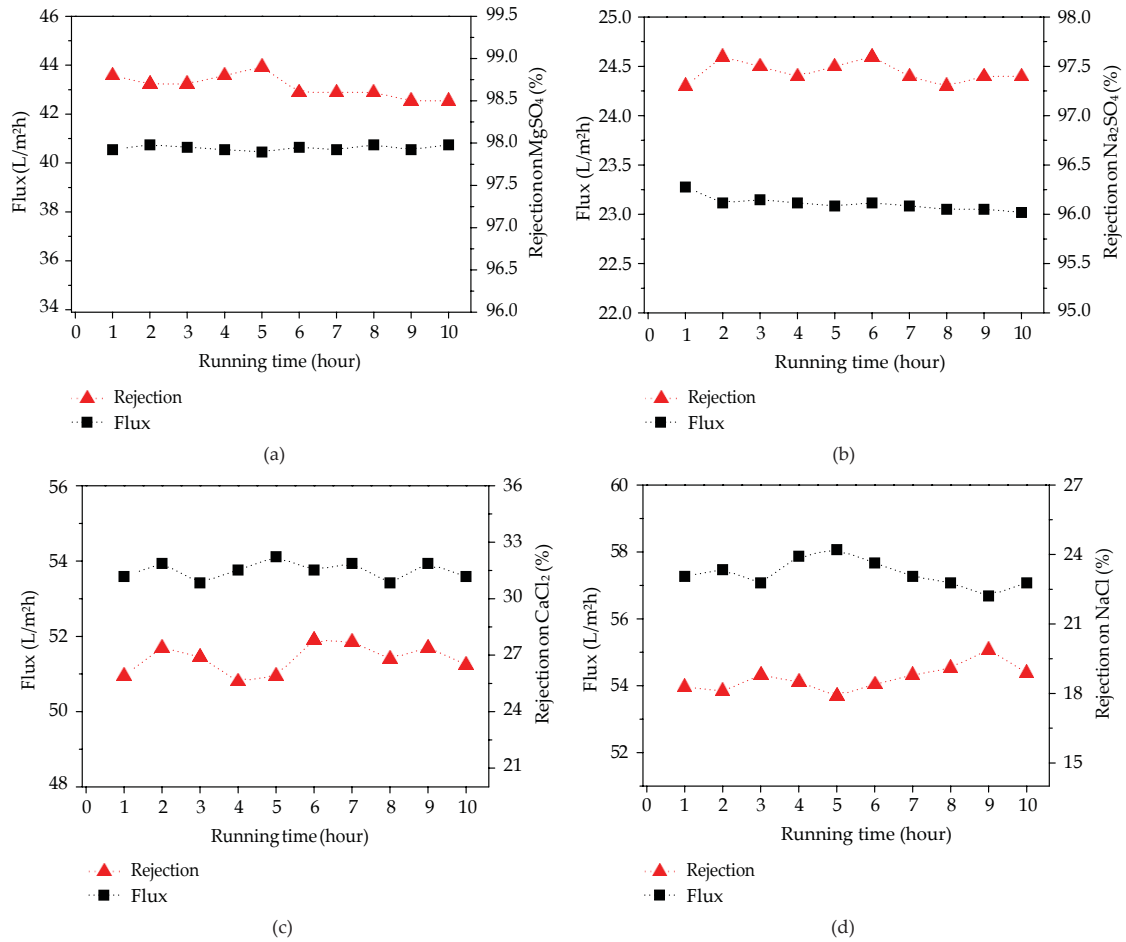
Figure 9: Extended filtration of (a) MgSO₄, (b) Na₂SO₄, (c) CaCl₂, and (d) NaCl feed solutions at 2,000 ppm and 4.8 bar using a dead-end cell.

A specific amount of feed water was used in each experiment, and the circulation of feed water was impossible in the dead-end filtration system. As the water molecules diffuse through the TFNC membrane, the salt ion is retained and the concentration of feed water continuously increases. Due to the fact that the ratio of salt ions increased rapidly, concentrated feed solutions accumulate on the surface of the membrane and lead to salt leakage or fouling. Moreover, the osmotic pressure of the feed water increases proportionally to the concentration of the feed solution. For this reason, the flux of feed water tended to decrease during filtration using the MPD-based membranes.

3.4. Analysis of Real Seawater Filtration. The desalination of seawater using membrane technology is a promising technique, which essentially requires more than one step to produce drinkable water such as prefiltration, microfiltration, and softening. The results of ion-exchange chromatography analysis and conductivity measurements show that the amount of the main dissolved salt ions and the conductivity of the seawater were extremely high for the NF membrane filtration process (Table 5).

The primarily filtration experiment was carried out using PIP+TEA+NaOH- and MPD+TEA+Sy-AH-based membranes by measuring the conductivity of the permeate water only (Figure 12).

The results in Figure 12 show that the conductivity value of permeate water dropped from 53.2 mS/cm to 47 mS/cm and 38 mS/cm, respectively, while the flux performance was 24.6 L m⁻² h⁻¹ and 0.65 L m⁻² h⁻¹, respectively. It is clear that the PIP- and MPD-based membranes remained incapable of retaining an excessive amount of salt ions in the seawater all at once. For this reason, the same feed seawater was circulated and was used more than once while the same membrane was fixed on the dead-end cell.

The filtration experiment of circulated seawater started with the PIP-based membranes and was repeated six times. Subsequently, the same permeate water was used
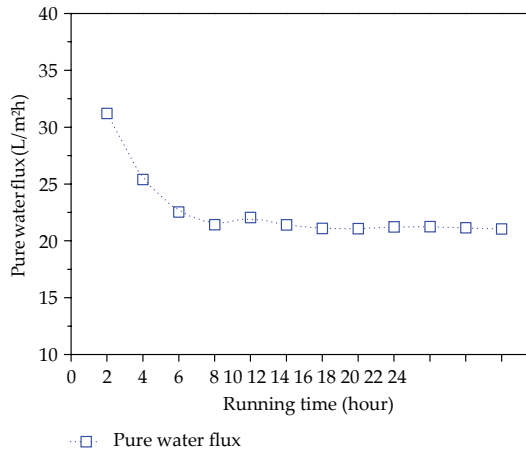
Figure 10: Observation of the filtration process of MPD+TEA+Sy-AH membrane for an extended period using pure water at 4.8 bar.

Table 5: The main dissolved ions in a Mediterranean seawater sample.

Cations	mg/L
Na$^+$	11,741
Mg^{+2}	1,447
Ca^{+2}	433
K$^+$	411
Anions	mg/L
Cl$^-$	21,384
SO$_4$ $^{-2}$	2,357
NO$_2$ $^-$	<100
NO$_3$ $^-$	<100
Conductivity of seawater	53.2 ms/cm

as feed water using the MPD-based membranes and was repeated four times (Figure 13). The flux performance of the PIP+TEA+NaOH-based membranes in the filtration of seawater was higher compared to the MPD+TEA+Sy-AH-based membranes. Moreover, the flux performance of PIP-based membranes increased after each filtration process, while the conductivity of the feed seawater decreased. The conductivity of the feed seawater remained stable after the fifth (32.5 mS/cm) and sixth (32.0 mS/cm) filtration (Figure 13(a)). It was understood that after four filtration cycles using the PIP-based membranes there was none or only trace amounts of divalent salt ions in the feed seawater. The rate of recovery was more than 95% at the end of the filtration processes of seawater using the PIP-based membrane.

Further filtration was continued with MPD+TEA+Sy-AH-based membrane using prefiltered feed seawater, which had a conductivity of 32.0 mS/cm (Figure 13(b)). In the first attempt of filtration, the conductivity dropped to 20 mS/cm while the flux performance was 0.935 L m^{-2} h^{-1}, which was slightly higher than shown in Figure 12. During the second filtration of the feed seawater, the conductivity decreased to

Table 6: Amount of ions in the filtered seawater sample [permeant (4.) in Figure 13(b)].

Cations	mg/L
Na$^+$	219
Mg^{+2}	1.8
Ca^{+2}	9.4
K$^+$	8.6
Anions	mg/L
Cl$^-$	341
SO$_4$ $^{-2}$	4.2
NO$_2$ $^-$	<10
NO$_3$ $^-$	<10
Conductivity of seawater	585.1 ☐S/cm

10.5 mS/cm while the flux performance was more or less the same (0.965 L m^{-2} h^{-1}).

After the fourth attempt at MPD-based filtration, the conductivity of the obtained permeate water was 585.1 ☐S/cm with increased flux (1.12 L m^{-2} h^{-1}), which means that approximately 98.9% of the salt ions were retained from the seawater using TFNC membranes by dead-end filtration. The final recovery rate was around 75% at the end of the seawater filtration process using the MPD-based membrane.

The analysis of ion-exchange chromatography was carried out again, and the amounts of salt ions in the filtered water are given in Table 6.

It is clear from Figure 13 that the rejection ratio of salt ions from seawater was dependent on the number of repetitions of the circulated feed seawater using the dead-end filtration method. We firmly believe that there was a chance to retain the rest of the salt ions from the obtained seawater permeants by increasing the circulation time. However, the flux performance of the MPD-based membranes dropped extremely. It was not reasonable to proceed with the filtration of seawater experiment using a dead-end filtration cell and so we limited the circulation times of the feed seawater to four using the MPD-based membrane.

Another advantage of TFNC membranes was revealed by liquid chromatography analysis of permeate water. The results of the analysis showed that the amount of the residual chemical, which was maybe released from the membrane itself, was not observed except for a trace amount of TEA (0.1 mg/L after 5 hours of pure water filtration).

1. Conclusion

In this study, not only the flux performances but also the rejection performances of MPD- and PIP-based membranes were significantly high using an acid acceptor and surfactants. The addition of TEA as an acid acceptor is necessary for the formation of poly(piperazine amide). The presence of TEA increased the reaction rate of the PIP monomer to the TMC monomers. A strong base (NaOH) was added as a second additive to the aqueous solution and a poly(piperazine amide) active layer formed onto the NNC scaffold. The highest divalent rejection performance
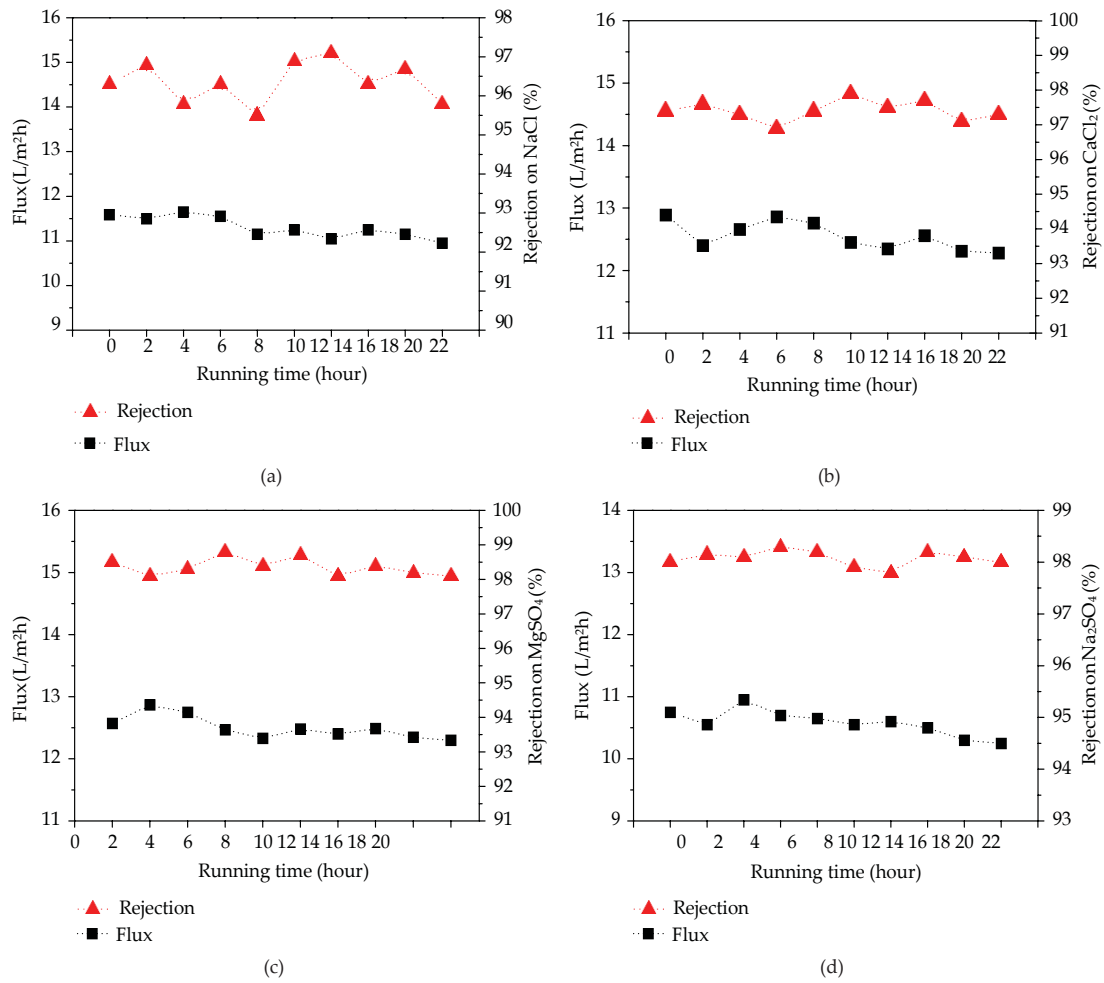
Figure 11: Extended filtration of (a) NaCl, (b) CaCl$_2$, (c) MgSO$_4$, and (d) Na$_2$SO$_4$ feed solutions at 2,000 ppm and 4.8 bar using a dead-end cell.
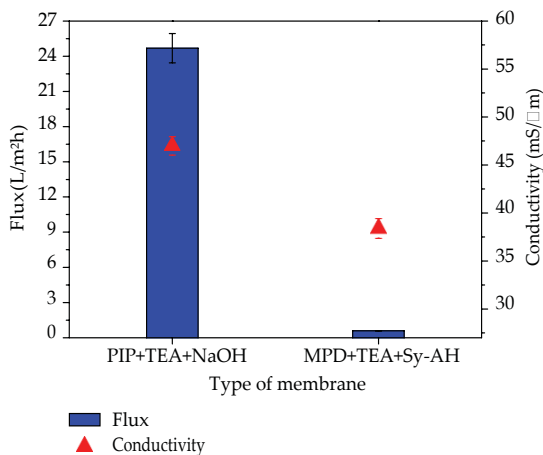
Figure 12: Filtration experiment of seawater using different membranes and a dead-end cell at 4.8 bar.

was obtained using the PIP+TEA+NaOH-based membrane, which was on average 98.8% MgSO$_4$ and 97.4% Na$_2$SO$_4$. Even though the effect of the dead-end filtration method proved to be a disadvantage, the pure water flux and permeate flux of PIP+TEA+NaOH-based membranes were high, that is, 73.5 L m^{-2} h^{-1} and 40.5 L m^{-2} h^{-1}, respectively. The MPD-based membrane showed high flux and rejection performance with the addition of an anionic liquid and TEA. The highest monovalent rejection performance was recorded with the MPD+TEA+Sy-AH-based membrane, which had an average of 97.4% CaCl$_2$ and 96.3% NaCl. The pure water flux and permeate flux of the MPD+TEA+Sy-AH-based membrane were high, that is, 22.5 L m^{-2} h^{-1} and 12.5 L m^{-2} h^{-1}, respectively.

The filtration experiments of the real seawater indicated that the TFNC membranes were not able to retain a sufficient amount of salt ions at the first attempt. For this reason, the combination of circulated feed seawater was used to retain
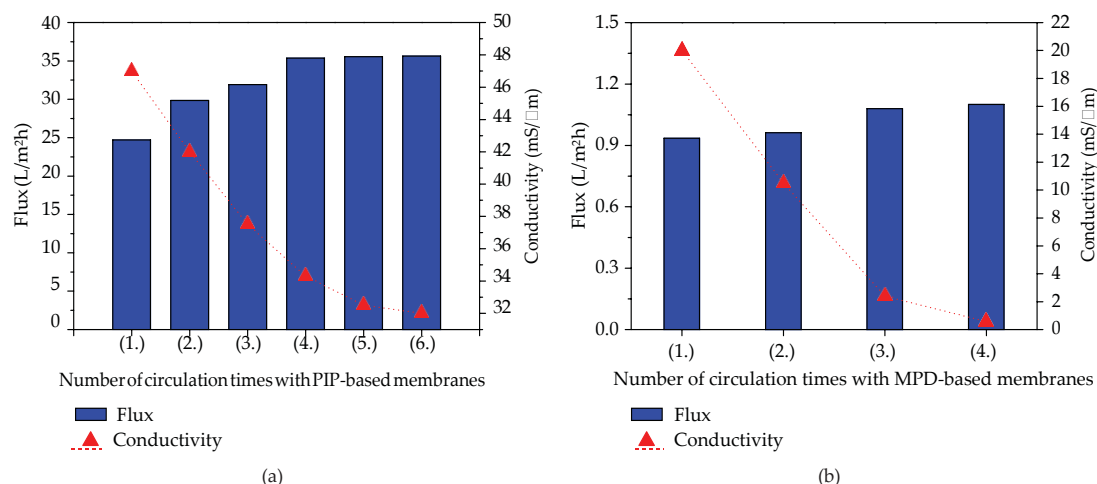
Figure 13: Circulated filtration of seawater using (a) PIP- and (b) MPD-based membranes.

a higher amount of salt ions. As a result, 98.9% of the salt ions were retained from the original seawater. The results of the ion-exchange chromatography analysis of the original and obtained permeate water matched the conductivity values.

The thin film nanofibrous composite membranes exhibited high mechanical properties and resisted an applied pressure of 4.8 bar in all of the filtration experiments. Primary results indicated that electrospun nanofibres are promising candidates for use as new high-performance nanofiltration membranes due to their high flux and ion rejection.

Competing Interests

The authors declare that they have no competing interests.

Acknowledgments

References

[1] H. Ettouney and M. Wilf, "Commercial desalination technologies," in *Seawater Desalination: Conventional and Renewable Energy Processes*, G. Micale, L. Rizzuti, and A. Cipollina, Eds., pp. 77–107, Springer, Berlin, Germany, 2009.

[2] J. Ribeiro, *Desalination Technology: Survey and Prospects*, IPTS, 1996.

[3] M. M. A. Shirazi, A. Kargari, and M. J. A. Shirazi, "Direct contact membrane distillation for seawater desalination," *Desalination and Water Treatment*, vol. 49, no. 1–3, pp. 368–375, 2012.

[4] L. M. Camacho, L. Dumée, J. Zhang et al., "Advances in membrane distillation for water desalination and purification applications," *Water*, vol. 5, no. 1, pp. 94–196, 2013.

[5] A. L. Ahmad, B. S. Ooi, A. W. Mohammad, and J. P. Choudhury, "Development of a highly hydrophilic nanofiltration membrane for desalination and water treatment," *Desalination*, vol. 168, no. 1–3, pp. 215–221, 2004.

[6] L. F. Greenlee, D. F. Lawler, B. D. Freeman, B. Marrot, and P. Moulin, "Reverse osmosis desalination: water sources, technology, and today's challenges," *Water Research*, vol. 43, no. 9, pp. 2317–2348, 2009.

[7] X. Lu, X. Bian, and L. Shi, "Preparation and characterization of NF composite membrane," *Journal of Membrane Science*, vol. 210, no. 1, pp. 3–11, 2002.

[8] A. I. Schäfer, A. G. Fane, and T. D. Waite, *Nanofiltration: Principles and Applications*, Elsevier Advanced Technology, Oxford, UK, 2005.

[9] E. L. Wittbecker and P. W. Morgan, "Interfacial polycondensation. I.," *Journal of Polymer Science Part A: Polymer Chemistry*, vol. 40, no. 137, pp. 289–297, 1959.

[10] R. J. Petersen, "Composite reverse osmosis and nanofiltration membranes," *Journal of Membrane Science*, vol. 83, no. 1, pp. 81–150, 1993.

[11] J. E. Cadotte, "Interfacially synthesized reverse osmosis membrane," US Patents, 1981.

[12] J. E. Cadotte, R. J. Petersen, R. E. Larson, and E. E. Erickson, "A new thin-film composite seawater reverse osmosis membrane," *Desalination*, vol. 32, no. C, pp. 25–31, 1980.

[13] B. Yalcinkaya and F. Cengiz-Callioglu, "The roller electrospinning of poly(vinyl alcohol) nanofibers," in *Proceedings of the 3rd Edition of the International Conference on Intelligent Textiles & Mass Customisation (ITMC '11)*, p. 109, Casablanca, Morocco, October 2011.

[14] F. Yener and B. Yalcinkaya, "Electrospinning of polyvinyl butyral in different solvents," *e-Polymers*, vol. 13, no. 1, pp. 229–242, 2013.

[15] K. Yoon, K. Kim, X. Wang, D. Fang, B. S. Hsiao, and B. Chu, "High flux ultrafiltration membranes based on electrospun

nanofibrous PAN scaffolds and chitosan coating," *Polymer*, vol. 47, no. 7, pp. 2434–2441, 2006.

[16] L. Yung, H. Ma, X. Wang et al., "Fabrication of thin-film nanofibrous composite membranes by interfacial polymerization using ionic liquids as additives," *Journal of Membrane Science*, vol. 365, no. 1-2, pp. 52–58, 2010.

[17] N.-N. Bui, M. L. Lind, E. M. V. Hoek, and J. R. McCutcheon, "Electrospun nanofiber supported thin film composite membranes for engineered osmosis," *Journal of Membrane Science*, vol. 385-386, no. 1, pp. 10–19, 2011.

[18] Z. Fan, Z. Wang, M. Duan, J. Wang, and S. Wang, "Preparation and characterization of polyaniline/polysulfone nanocomposite ultrafiltration membrane," *Journal of Membrane Science*, vol. 310, no. 1-2, pp. 402–408, 2008.

[19] X. Wang, T.-M. Yeh, Z. Wang et al., "Nanofiltration membranes prepared by interfacial polymerization on thin-film nanofibrous composite scaffold," *Polymer*, vol. 55, no. 6, pp. 1358–1366, 2014.

[20] S.-S. Choi, Y. S. Lee, C. W. Joo, S. G. Lee, J. K. Park, and K.-S. Han, "Electrospun PVDF nanofiber web as polymer electrolyte or separator," *Electrochimica Acta*, vol. 50, no. 2-3, pp. 339–343, 2004.

[21] R. Sen, B. Zhao, D. Perea et al., "Preparation of single-walled carbon nanotube reinforced polystyrene and polyurethane nanofibers and membranes by electrospinning," *Nano Letters*, vol. 4, no. 3, pp. 459–464, 2004.

[22] X. Wang, K. Zhang, M. Zhu, B. S. Hsiao, and B. Chu, "Enhanced mechanical performance of self-bundled electrospun fiber yarns via post-treatments," *Macromolecular Rapid Communications*, vol. 29, no. 10, pp. 826–831, 2008.

[23] L. Huang, J. T. Arena, S. S. Manickam, X. Jiang, B. G. Willis, and J. R. McCutcheon, "Improved mechanical properties and hydrophilicity of electrospun nanofiber membranes for filtration applications by dopamine modification," *Journal of Membrane Science*, vol. 460, pp. 241–249, 2014.

[24] L. Huang, S. S. Manickam, and J. R. McCutcheon, "Increasing strength of electrospun nanofiber membranes for water filtration using solvent vapor," *Journal of Membrane Science*, vol. 436, pp. 213–220, 2013.

[25] K. Yoon, B. S. Hsiao, and B. Chu, "Formation of functional polyethersulfone electrospun membrane for water purification by mixed solvent and oxidation processes," *Polymer*, vol. 50, no. 13, pp. 2893–2899, 2009.

[26] S. Kaur, R. Barhate, S. Sundarrajan, T. Matsuura, and S. Ramakrishna, "Hot pressing of electrospun membrane composite and its influence on separation performance on thin film composite nanofiltration membrane," *Desalination*, vol. 279, no. 1–3, pp. 201–209, 2011.

[27] X. Wang, D. Fang, K. Yoon, B. S. Hsiao, and B. Chu, "High performance ultrafiltration composite membranes based on poly(vinyl alcohol) hydrogel coating on crosslinked nanofibrous poly(vinyl alcohol) scaffold," *Journal of Membrane Science*, vol. 278, no. 1-2, pp. 261–268, 2006.

[28] S. Kaur, Z. Ma, R. Gopal, G. Singh, S. Ramakrishna, and T. Matsuura, "Plasma-induced graft copolymerization of poly(methacrylic acid) on electrospun poly(vinylidene fluoride) nanofiber membrane," *Langmuir*, vol. 23, no. 26, pp. 13085–13092, 2007.

[29] S. Kaur, D. Rana, T. Matsuura, S. Sundarrajan, and S. Ramakrishna, "Preparation and characterization of surface modified electrospun membranes for higher filtration flux," *Journal of Membrane Science*, vol. 390-391, pp. 235–242, 2012.

[30] S. Hermans, R. Bernstein, A. Volodin, and I. F. J. Vankelecom, "Study of synthesis parameters and active layer morphology of interfacially polymerized polyamide-polysulfone membranes," *Reactive and Functional Polymers*, vol. 86, pp. 199–208, 2015.

[31] Y. Mansourpanah, K. Alizadeh, S. S. Madaeni, A. Rahimpour, and H. Soltani Afarani, "Using different surfactants for changing the properties of poly(piperazineamide) TFC nanofiltration membranes," *Desalination*, vol. 271, no. 1–3, pp. 169–177, 2011.

[32] Y. Mansourpanah, S. S. Madaeni, and A. Rahimpour, "Fabrication and development of interfacial polymerized thin-film composite nanofiltration membrane using different surfactants in organic phase; study of morphology and performance," *Journal of Membrane Science*, vol. 343, no. 1-2, pp. 219–228, 2009.

[33] J. Guilbaud, A. Massé, F.-C. Wolff, and P. Jaouen, "Seawater pretreatment by dead-end micro and ultrafiltration in pressure-driven inside feed," *Desalination and Water Treatment*, vol. 51, no. 1–3, pp. 416–422, 2013.

[34] S. C. J. M. van Hoof, J. G. Minnery, and B. Mack, "Dead-end ultrafiltration as alternative pre-treatment to reverse osmosis in seawater desalination: a case study," *Desalination*, vol. 139, no. 1–3, pp. 161–168, 2001.

[35] O. Jirsak, F. Sanetrnik, D. Lukas, V. Kotek, L. Martinova, and J. Chaloupek, "Method of nanofibres production from a polymer solution using electrostatic spinning and a device for carrying out the method," US Patents, 2005.

[36] J. K. Lin, M. R. Ladisch, J. A. Patterson, and C. H. Noller, "Determining pore size distribution in wet cellulose by measuring solute exclusion using a differential refractometer," *Biotechnology and Bioengineering*, vol. 29, no. 8, pp. 976–981, 1987.

[37] A. A. Manito Pereira, J. M. Timmer, and J. J. Keurentjes, "Swelling and compaction of nanofiltration membranes in a non-aqueous environment," *Desalination*, vol. 200, no. 1–3, pp. 381–382, 2006.

[38] K. M. Persson, V. Gekas, and G. Trägårdh, "Study of membrane compaction and its influence on ultrafiltration water permeability," *Journal of Membrane Science*, vol. 100, no. 2, pp. 155–162, 1995.

[39] R. K. McGovern, D. McConnon, and J. H. Lienhard V, "The effect of very high hydraulic pressure on the permeability and salt rejection of reverse osmosis membranes," in *Proceedings of the IDA World Congress on Desalination and Water Reuse*, International Desalination Association, San Diego, Calif, USA, 2015.
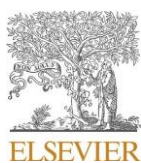
Separation of racemic compound by nanofibrous composite membranes with chiral selector

Jana Gaalova [a], Fatma Yalcinkaya [b], Petra Cuřínová [a], Michal Kohout [c], Baturalp Yalcinkaya [b], Martin Koštejn [a], Jan Jirsák [d], Ivan Stibor [b], Jason E. Bara [e], Bart Van der Bruggen [f,g], Pavel Izak [a,c,*]

[a] Institute of Chemical Process Fundamentals of the CAS, v.v.i, Rozvojova 135, 165 00, Prague, Czech Republic
[b] Technical University of Liberec, Studentsk� 1402/2, 461 17, Liberec 1, Czech Republic
[c] UCT Prague, Technick� 5, 166 28, Prague 6, Dejvice, Czech Republic
[d] Jan Evangelista Purkyn� University in Ústí nad Labem, Pasteurova 1, 400 96, Ústí nad Labem, Czech Republic
[e] Department of Chemical & Biological Engineering, University of Alabama, Tuscaloosa, AL, USA, 35487-0203
[f] Department of Chemical Engineering, KU Leuven, Celestijnenlaan 200F, B-3001, Leuven, Belgium
[g] Faculty of Engineering and the Built Environment, Tshwane University of Technology, Private Bag X680, Pretoria, 0001, South Africa

ARTICLE INFO

ABSTRACT

A series of unique composite membranes formed from a nano&micro fibrous material with different amounts of a chiral selector was used for separation of chiral drugs. The membrane performances were demonstrated through sorption tests, wherein they were soaked in an aqueous solution of racemic D, L-tryptophan (a model chiral drug). The changes in concentration of both enantiomers over time were monitored by HPLC analysis. During 100 days, a blank membrane (without the chiral selector) exhibited no sorption activity. The membranes containing the selector had no influence on the amount of D-enantiomer, while the L-enantiomer was preferentially adsorbed on each membrane. The intensity of the sorption was found to be a direct function of the amount of the selector contained in a particular membrane. The separation of the same model chiral compound was further studied in diffusion cells by pertraction. The preferential sorption of L-tryptophan in the feed underlined the crucial importance of the selector in an active layer in view of chiral recognition of enantiomers. Due to the exclusive membrane material, the retention of L-tryptophan in the membrane materials did not block the passage of D-enantiomer into the permeate at any point during the experiment. Moreover, the nanomaterial in the active layer assured the distribution of the selector to the point that only 50% of (S, S)-1,2-diaminocyclohexane in one part of the active layer was sufficient to achieve 99% of enantioselectivity. The membranes – fresh and used – were analysed by Fourier-transform infrared (FTIR) spectroscopy and characterized by scanning electron microscopy (SEM) confirming the stability of the tested membranes. To complete the study, the role of the polyamide active layer in chiral recognition of tryptophan enantiomers was proposed.

1. Introduction

Currently, nearly 50% of pharmaceuticals on the market are chiral drugs, the majority of which are racemates, i.e., an equimolar mixture of two enantiomers. The enantiomers may cause significantly different physiological effects of the same medicament; e.g., anti-arthritic/mutagenic penicillamine, bitter/sweet asparagine, tuberculostatic/blindness-causing ethambutol or sedative/teratogenic thalidomide [1]. In such drugs, the pharmacologically active enantiomer (eutomer)

metabolizes differently to its diastereomer, which is at best is bio-inert or worse, has undesired (in the case of high dosage of teratogen even fatal) bioactivity. Another "chiral alert" comes from toxicology. Chiral pharmaceuticals are essential in clinical medicine, and demand from widespread applications inevitably results in an increased production. However, overuse also results in the drugs (and their metabolites) becoming environmental pollutants [2]. Bioaccumulation, persistence or toxicity also depends on the enantiomeric composition. There is an ascendant pressure to characterize the effects of both enantiomers or to

replace racemic mixtures by enantiomerically enriched or enantiopure medicinal products. The separation of enantiomers is therefore vital to assure general drug safety.

One approach leading to optically pure enantiomers is the asymmetric synthesis of enantiopure drugs [3–5], while another approach relies on the separation of the enantiomeric mixtures by asymmetric biotransformation, sensors, liquid-liquid extraction (LLEx), chromatography, capillary electrophoresis, or membranes [6,7]. One of the most important technologies applied for high-resolution purification of products is chromatographic enantioseparation [8–10]. However, from an economic point of view, membrane separation processes represent a particularly advantageous option. The benefits of membranes include better mass transfer efficiency, increased flow rates, ease of operation, and the ability to deal with large molecules.

There are multiple methods in which membrane processes can be employed [11]. Membrane-assisted processes and adsorption-enantioselective (liquid and solid) membranes for chiral resolution were summarized in a comprehensive review by Xie et al. [12] The former is based on non-enantioselective membranes which have no enantioselectivity themselves. However, they can assist in an enantioselective process, such as enzyme enhanced ultrafiltration or polymer enhanced ultrafiltration [13]. In an adsorption-type enantioselective membrane, the binding affinity between enantiomers and chiral recognition sites is stronger than that of a diffusion-enantioselective membrane. This interaction force always exists between one enantiomer and one chiral site [14–18]. The separation of racemic mixtures from liquid phases by pertraction, using adsorption-enantioselective membranes is discussed in the paper. Its principle of pertraction is similar to that of LLEx: the feed mixture and extraction agent are in direct contact, and the separation process is based on the solubility/affinity of the substance in both phases. In pertraction, both media are separated by a non-porous polymeric or liquid membrane, which mediates the transport of the individual components between the phases. The separation of mixtures through permeation is controlled by the rates of membrane transport processes. The most common types of membranes for permeation are liquid and composite membranes. The latter exhibit an outstanding proton conductivity, fuel cell durability and performance, when compared to other types of hydrocarbon membranes and the industrial standard Nafion® 212 [19].

In previous works [20,21], a composite three-layer membrane was prepared, with the layers comprising (1) a nonwoven part, functioning as supporting material, (2) a nanofibrous scaffold, forming the porous layer, and (3) an active barrier layer. The selective layer of the thin film membrane was prepared by interfacial polymerization of two immiscible phases on the porous nanofiber layer. In this process either piperazine or m-phenylene diamine (MPD) was dissolved in deionized water to form the aqueous phase, while the organic phase was prepared by dissolving 1,3,5-trimesoyl chloride (TMC) in n-hexane. The active film was obtained by remittent immersion of the fibrous composite in both phases and subsequent thermal treatment. Such membranes are suitable for desalination and ion separation due to the narrow pore size of the membrane.

The innovation of the present work is to use MPD and TMC for the creation of a thin film on the nanofibrous layer substituting variable portions of MPD with a chiral active substance, (S,S)-1,2-diaminocyclohexane (DACH), thus obtaining a membrane suitable for enantiomer separation [22]. To the best of our knowledge, this is the first successful exploration of nonporous composite membranes with the unique combination of nanofibrous and microfibrous structures plus chiral composition at the same time.

This study highlights the membrane-based separation of the enantiomers of D, L-tryptophan (D, L-Trp), a molecule that catabolizes numerous physiological processes and contributes to intestinal and systemic homeostasis in health and disease [23]. There is preliminary evidence that an altered Trp metabolism is related to white matter integrity in schizophrenia [24]. Furthermore, an increased catabolic

turnover of Trp along the kynurenine pathway in patients with major depressive disorder was detected [25]. In 1989, the Japanese company Showa Denko genetically modified bacteria in an attempt to market large quantities of L-Trp [26]. However, this resulted in the death of 37 people and another 1500 disabled by disease causing muscle pain [27] due to the presence of D-Trp. Enantioselective membranes should safely, without produced impurities, separate the two enantiomers of the drug. Tobis et al. reported the facile synthesis of nanophase separated amphiphilic polymer conetworks, which allows the preparation of chiral membranes with precise mesh size and morphology. They demonstrated that variation of composition and phase swelling allows controlling of the selectivity and the permeability by varying the nanostructure. When using tryptophan as substrate in water with a chiral amphiphilic polymer conetworks membrane with 29 wt% of poly((R), (S)–N-(1-hydroxy-butan-2-yl)acrylamide) the L-enantiomer can be completely separated from the D-enantiomer [28].

1. Experimental

1.1. Materials

Polyethylene/polypropylene (PE/PP = 80/20, 18 g/m^2) bicomponent spunbond nonwoven fabric (Pegatex S BICO) was furnished by Pegas Nonwovens s.r.o., Czech Republic. Together with polyamide 6 (PA6) (BASF B24), it was described in previous work [21]. TMC, MPD, DACH and D, L-Trp of purity 99% were purchased from Sigma-Aldrich. Deionized water was produced by an ultrapure water system (Simpli Lab, Millipore S. A., Molsheim, France).

1.2. Membrane preparation

As shown in Fig. 1, the membrane components are:

- Supporting layer: PE/PP bicomponent nonwoven fabric/material
- Nanofiber: PA6 nanofiber. The laminated spunbond nonwoven fabric and the PA6 nanofibrous web were used as a supporting material to prepare the thin film nanocomposite (TFNC) membranes.
- Thin film: MPD/DACH in aqueous phase, TMC in organic phase. To form an active barrier layer, interfacial polymerization was carried out to form a polyamide layer on the PA6 nanofiber using 2% (w/v) MPD with addition of various amount of chiral active substance in aqueous solution while 0.2% (w/v) TMC was used for preparation of organic solutions (hexane). The interfacial polymerization reaction for the membranes was carried out under the same conditions as drying (5 min), curing (10 min) and temperature (100 °C). The reaction time for the MPD/DACH aqueous solution was 60 s, while 30 s for the reaction time of TMC organic solution.
- Chiral active substance: DACH. As the active substance playing the role of the chiral selector for chiral drugs, DACH, in variable amounts was used.
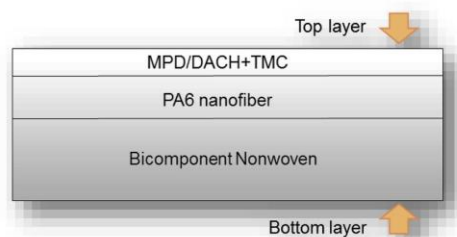

Fig. 1. Membrane components.

154

The commercially available film (PE/PP), used as the support, was covered by micromaterial prepared by electrospinning. The large spe- cific surface area has been stabilized by lamination and the stable tissue thus obtained used as the polymeric support material for the interfacial polymerization process. The active layer was prepared by interfacial

polymerization using a solution of MPD in water with addition of 10–50% of chiral selector (cs) - DACH (calculated on total diamine). The organic phase was prepared by dissolving TMC in hexane. The sup- porting membrane was immersed in the aqueous and then in the organic phase, and the preparation process was finalized by subsequent thermal treatment, resulting in the chiral membrane [20].

The quality of the membrane depends on a number of factors: pri- marily the concentration of solutions, the contact time of the fabric with both solutions and the conversion of the reaction at the interface. Finally, membranes with excellent material properties (mechanical stability and flexibility) were prepared. The membranes were denoted on the basis of cs content: 10%cs, 20%cs, 30%cs, 40%cs and 50%cs.

1.1. Experimental set-up, mode and evaluation terminology

2.3.1. Preferential sorption

The preferential sorption of D, L-Trp is depicted in Fig. 2. The ex- periments were performed in dark glass bottles. 50 mL of D, L-Trp (the racemic mixture) in water (c_{Trp} = 0.01 M) were put in contact with a membrane (time = 0) and were agitated at 25 °C on a GLF 3005 rotator at 130 rpm. The active area of the chiral membrane was 9 cm^2 with average thickness 0.4 mm. The solution - 1 mL - was sampled at regular time intervals and analysed by high-performance liquid chromatog- raphy (HPLC). UltiMate3000 spectrometer (Thermo Scientific) was used, equipped with a Chiralpak ZWIX(+) (250x 3 mm, ID, 3 μm) column (Diacel). The mobile phase composed of 98% MeOH and 2% H$_2$O, containing 50 mM of formic acid (HCOOH) and 25 mM of dieth- ylamine (Et$_2$NH) as a buffer. The flow was isocratic at the rate of 0.5 mL min^{-1}, total run time of analysis was 25 min. The peaks of both enan- tiomers were detected by a UV diode-array detector at 254 nm. Using the calibration curve, the concentrations of each enantiomers were deter- mined. The complete series of membranes, with different percentages of incorporated CS, was tested.

2.3.2. Pertraction

Pertraction experiments were carried out in a closed, circular stain- less steel cell of 5.8 cm diameter and 6 cm length. In the middle, the cell was divided into two chambers by a membrane, anchored in a stainless
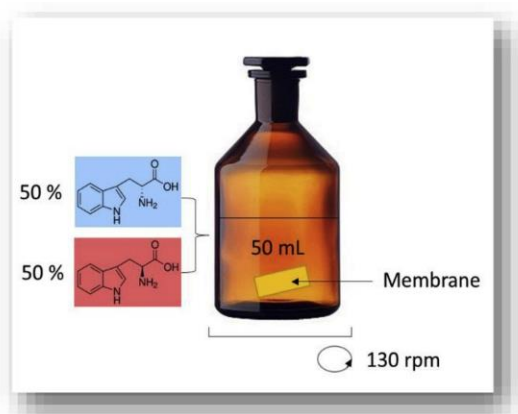

Fig. 2. Preferential sorption of tryptophan racemic mixture (D-enantiomer in blue, L-enantiomer in red). (For interpretation of the references to colour in this figure legend, the reader is referred to the Web version of this article.)

steel disc. The layout of the cell is shown within the scheme of the pertraction set-up in Fig. 3. Experiments were performed at a constant temperature of 25 °C, maintained by recirculating cooler/chiller pumping EtOH through the double wall of the cell.

The membrane was cut to the desired size immediately preceding the experiment, using a round punch of 3 cm diameter, then fixed between two parts of the disc with screws. The cell was then closed from both sides and the chambers were filled with a stripping solution (deionized water) and feed solution (2M aqueous D, L-Trp) simultaneously, so that the pressure was kept equal on both sides of the membrane. Both chambers were equipped with a PTFE- coated magnetic stirrer and constantly stirred using external rotating magnets. The samples for analysis of the composition were extracted through septa from the feed (1 mL) and permeate side of the pertraction cell (1 mL) at regular time intervals by disposable sanitary syringes; with higher frequency at the beginning of the experiment (0, 5, 15, 30, 60 min), then at longer time intervals, depending on the rate of separation. The sampling was first performed from the stripping solution, then from the feed. While the sample was taken, another needle was stuck through the septum to prevent a pressure change in the chamber. Samples were then analysed by HPLC as described above.

The amounts of D- and L-Trp transported through the membrane were determined according to Eqn. (1), where flux, J (mol·cm^{-2}·h^{-1}), is defined as

$$J = Q/At \qquad (1)$$

where Q (mol) represents the amount of transported Trp, A (cm^2) stands for the active membrane area, and t (h) is the time. The permselectivity (α) is defined as the flux ratio (J_D/J_L) and in case that feed solution was Trp racemate the permselectivity is defined in Eqn. (2).

$$\alpha = J_D / J_L \qquad (2)$$

1.2. Analysis and characterization of the membrane materials

The membranes, fresh and used, were analysed by Fourier-transform infrared spectroscopy (FTIR) and characterized by scanning electron microscopy (SEM). An FTIR spectrometer Avatar 360 (Nicolet) was used to measure IR spectra of samples in the range of 508 and 4000 cm^{-1} (resolution 1.93 cm^{-1}, 200 scans, 1 s per scan). FTIR in ATR mode was used to obtain spectra from the membrane pressed against the ZnSe crystal. An SEM (Tescan Indusem) was used to image the surface morphology (top view) of the membranes and their cross-section. Im- aging was carried out with an accelerating voltage of 15 kV. A thin layer of gold was sputtered on the membranes to impart better conductivity to the samples. Samples for cross-section imaging were prepared by immersing the partially cut membrane into LN$_2$ followed by fracturing into two pieces. The necessary drying of samples prior the measurement resulted in cracks on the superficial layer. SEM images were manually processed by a measuring tool, which is standard part of Tescan soft- ware, in order to determine a diameter of nanofibers. Fifty nanofibers were measured and the average was evaluated statistically.

2. Results and discussion

2.1. Scanning electron microscopy observations

As-prepared membranes were characterized by SEM. Fig. 4 A shows the cross section and Fig. 4 B shows the detailed top view SEM micro- photograph of the membrane with 20%cs. The carrier fabric of the membrane is about 430 μm thick (Fig. 4 A). The fabric has a micro- fibrous structure with fibers of ~15 μm diameter and this support is responsible for the good mechanical properties of the membrane. On top of the carrier fabric, there is an observable nanofibrous layer with
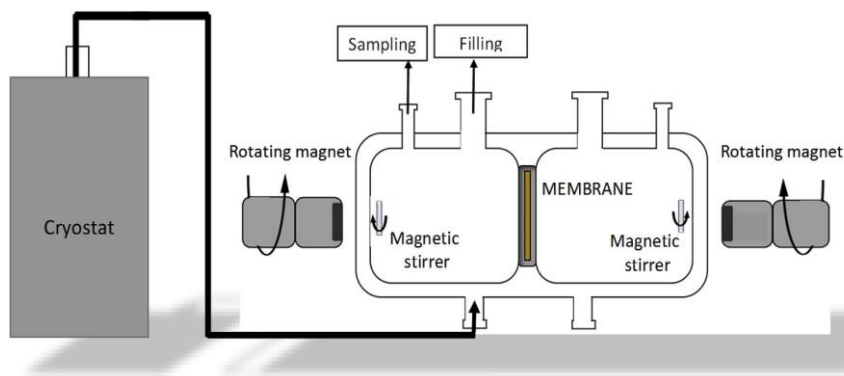
Fig. 3. Pertraction set up.
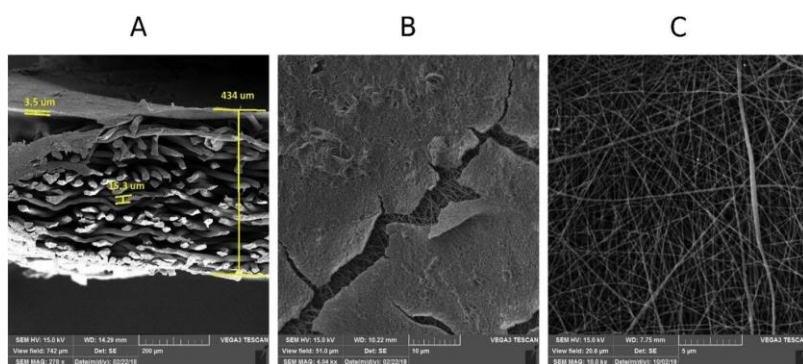
Fig. 4. (A) SEM cross section microphotograph of the as-prepared membrane with 20%cs, composed of PE/PP bicomponent nonwoven fabric with diameter around 15 μm. The mem- brane thickness varies between 400 and 450 μm.
PA6 nanofibers, where MPD/TMC + chiral selector (DACH) was introduced in different %, form the top layer with thickness around 3.5 μm. (B) SEM top view micrograph of as-prepared membrane with 20%cs. On top of PA6 nano- fibers, a thin submicron layer is formed, comprised of MPD/TMC + chiral selector (DACH). (C) SEM top view micrograph of orig- inal membrane.

thickness of about 3.5 μm. These values are practically the same for all tested membranes. The top view of the membrane (Fig. 4 B) shows the nanofibrous structure of PA6 with fibers of ~250 nm diameter. These nanofibers impart the material with a superior dispersion. The top view revealed a complete coverage of nanofibers by a thin layer. It is composed of compact material, MPD/TMC + chiral selector DACH playing the main role in the separation process. The thickness of this superficial layer is > 1 μm. The crack in the layer enabling observation of
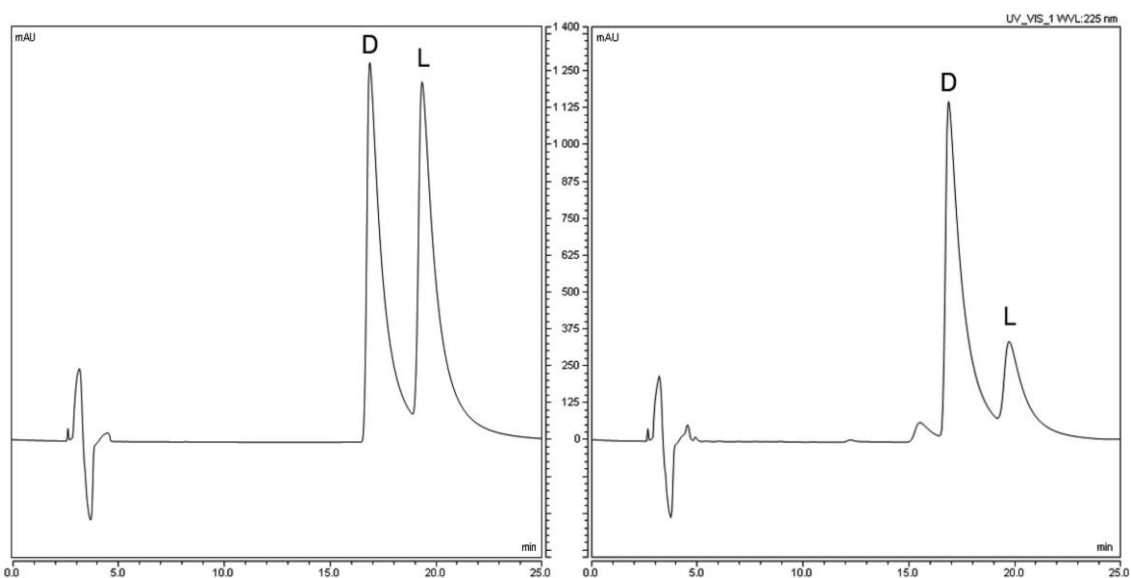
Fig. 5. HPLC spectra: racemic mixture of D, L-Trp, time zero, (left), mixture of D, L-Trp after a preferential sorption of L-Trp, 110 days, membrane with 50% of chiral selector, peak ratio approximately 70:30 D:L form (right).

nanofibers originates from the drying process of the membrane, which is inevitable for placing the membrane into the SEM.

A top view of the original membrane without any chemical treatment (Fig. 4C) shows detailed image of PA6 fibers with diameter from 100 to 250 nm. The average diameter of nanofibers is 150 nm.

1.1. Preferential sorption experiments

The preferential sorption experiments of D, L-Trp by membranes with various amounts of cs were monitored by HPLC analysis. Fig. 5 shows two exemplary spectra of a Trp solution. Both images reveal the peak at retention time 15.5 min, attributed to D-Trp, as well as the peak at 18 min linked to L-Trp. The left spectra of Fig. 5 gives similar peak areas of two Trp enantiomers, with area ratio close to 50:50 D:L form, illustrating the composition of the racemic mixture which is present at the start of the preferential sorption experiments (i.e., t = 0). During the course of the sorption experiments, for the membranes containing the chiral selector, the peak attributed to the L-enantiomer decreased, while the peak of the D-enantiomer remained constant. Simply put, L-Trp was preferentially adsorbed in the membrane, while D-Trp was not. An example of the spectra with nearly depleted L-Trp is shown on the right side of Fig. 5.

The evolution of the peak ratio matching the two Trp enantiomers relative to the experimental time is shown in Fig. 6.

The increasing amount of chiral selector in membranes (from 0 to 50%) is illustrated by an increasing intensity of the appropriate colour (L-Trp = red, D-Trp = blue). The peak areas correspond to the amount of enantiomer in the solution and it can be seen that the proportion of each enantiomer is changing and the gap between their percentages is growing. The membrane with 50%cs causes the largest gap between the area ratio of the enantiomers, and the membrane without cs the lowest one. That proves the highest selectivity in the preferential sorption experiments for the membrane with 50%cs, the lowest selectivity for the membrane without cs, and for the entire series: 0%cs < 10%cs < 20%cs < 30%cs < 40%cs < 50%cs.

The diverging values of peak area ratio during the sorption experiments and the broadening of the gap between D- and L-Trp gave the base for enantiomeric excess values, presented in Fig. 7. This figure shows an increase of enantiomeric excess in time of preferential sorption with the amount of cs. In fact, L-Trp is preferentially adsorbed into all membranes where cs is present, while D-Trp remains in the solution during the entire experiment. This effect increases with an increasing percentage of chiral selector in the membrane: 0%cs < 10%cs < 20%cs < 30%cs < 40%cs <

Fig. 7. Dependence of enantiomeric excess on time of preferential sorption and of the amount of cs.

50%cs. Therefore, for the chosen interval of %cs, the amount of adsorbed L-Trp is proportional to the fraction of chiral selector in the membrane. Fig. 8 traces the peak area loss at the end of the preferential sorption experiments comparing to the ones at t = 0 as a function of %cs in the membrane's top layer. The sorption activity of all membranes was negligible towards the D-enantiomer, although the sorption of L-Trp correlated to an essentially linear trend with increasing fraction of cs in membrane.

1.2. Pertraction experiments

3.3.1. Pertraction of tryptophan

An enantiomeric separation of the model chiral drug D, L-Trp was performed during 1 month in diffusion cells in the pertraction membrane process (see Table 1). Fig. 9 describes the ratio D-Trp and L-Trp concentrations at the permeate side, for whole series of membranes at 4th day, again the series of membranes at 6th day etc., for the duration of the pertraction experiment. The values for D-Trp are in blue, those for
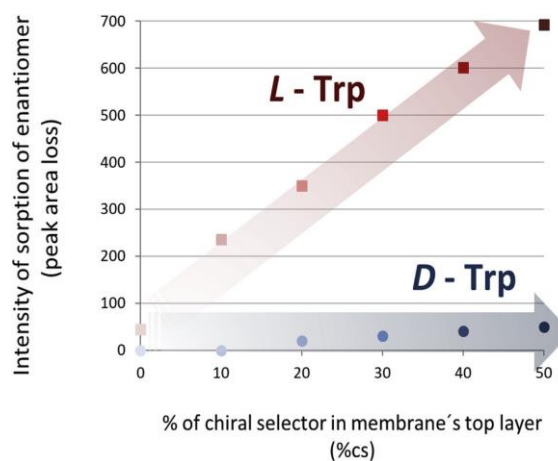
Fig. 8. Preferential sorption activity of membranes towards D-Trp (blue rounds) and L-Trp (red squares) in a function of the amount of cs in the membrane's top layer (in % versus one part of the top layer, described in the part of membrane preparation above). (For interpretation of the references to colour in this figure legend, the reader is referred to the Web version of this article.)
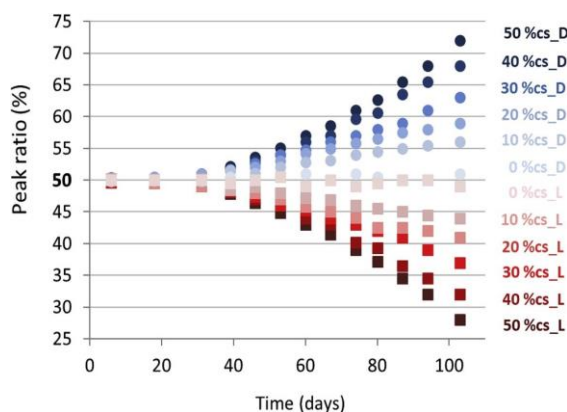

Fig. 6. Area ratio of HPLC peaks corresponding to D-Trp enantiomer (noted as "D" and marked as blue rounds for each membrane) and L-Trp enantiomer (noted as "L" and marked as red squares for each membrane) in a function of the time of the sorption process. (For interpretation of the references to colour in this figure legend, the reader is referred to the Web version of this article.)
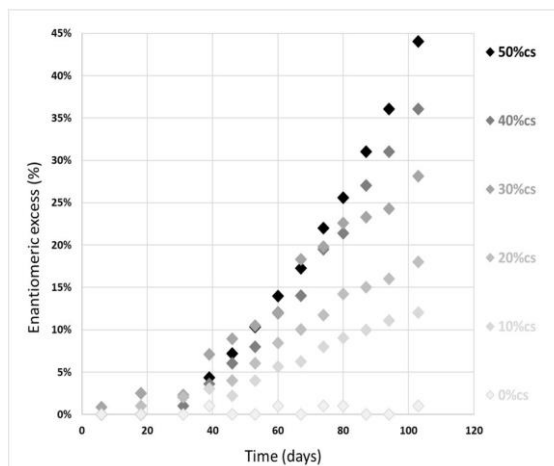
the L-Trp are in red, and deeper shades symbolize an increasing fraction of chiral selector (a lighter color for a lower amount of cs, a darker color for a higher amount of cs in the membrane etc.). The permeation of each membrane remains stable within the error of 2% during whole experiment. The separation ability of the membrane was increasing (similarly to the sorption process) as follows: 0%cs < 10%cs < 20%cs < 30%cs < 40%cs < 50%cs. Corresponding final enantiomeric ratios were 50:50, 59:41, 70:30, 82:18, 91:9 and 99:1.

During pertraction experiments, Trp flowed through the membrane at a rate of 3.25 mmol m^{-2} h^{-1} during the first hour, and the flux declines to ~0.07 mmol m^{-2} h^{-1} during the last hours due to the decrease of the concentration gradient, which is the driving force of the separation. In accordance with the preferential sorption, L-Trp was adsorbed proportionally to the fraction of the chiral selector in the active layer of corresponding membranes. However, a decreased amount of D-Trp in the feed was also observed. Here, the diverse behavior of the membranes towards each enantiomer during permeation underlines the crucial importance of the selector in the active layer[17]. The chiral recognition of enantiomers causes the retention of L-Trp in the membranes, while D-Trp passed through the separating material. The result of such permeation is an excess of D-Trp in the permeate, visible in Fig. 9. The excess was again proportional to the amount of the chiral selector in the membranes: 0%cs < 10%cs < 20%cs < 30%cs < 40%cs < 50%cs. Due to the exclusive membrane material, the retention of L-Trp in the membrane materials did not block the transport of D-Trp into the permeate during the entire experimental time. Moreover, only 50% of DACH in the active layer is required to achieve 99% enantioselectivity.

1.1. Analysis of membranes by fourier-transform infrared spectroscopy

Two membranes – one unused membrane, in "as-prepared" state and the "used" membrane after the 3 month sorption experiment - were analysed from both sides using FTIR. The spectrum of the top side covered by nanofibres corresponds to PA6 with pronounced amidic vibrations at 1640 and 1540 cm^{-1}. At 1715 cm^{-1}, a weak valence vibration of a carbonyl group (C═O) was observed. The shape of the spectra at 3300 cm^{-1} (not shown) indicates the presence of mainly 2° amides as
there is only one band present. IR data thus indicate that this side of the membrane did not change during use, revealing a good stability of the material (Fig. 10).

The spectrum of the bottom side of the as-prepared membrane (Fig. 11) shows amidic vibrations at 1640 and 1540 cm^{-1} with very low intensity. On the other hand, C═O group vibrations were well pronounced (1715 and 1240 cm^{-1}). After the usage, the C═O signal
significantly decreases and the intensity of amidic vibrations remain the same. The shape of the spectra at 3300 cm^{-1} shows only the presence of 2° amides; however, the intensity is much lower than for the top side of the membrane. The presence of halides was not observed (1780-1820 cm^{-1}).

Figs. 10 and 11 indicate that the spectrum of the nanofibrous side of membrane can be clearly assigned to PA6. The polymerization of the chiral selector in the top layer is almost quantitative, leaving only a very small amount of residual free carboxylic acid units. This layer forms only a thin film on the nanofibers, and this side of the membrane remains

Table 1
The composition of D: L enantiomers in feed side and permeate side of pertraction cell after 29 days of the experiment. The composition at time 0 was 2.00 mml/ml in feed side (60 ml) and 0 mmol/ml in permeate side (60 ml) of pertraction cell.

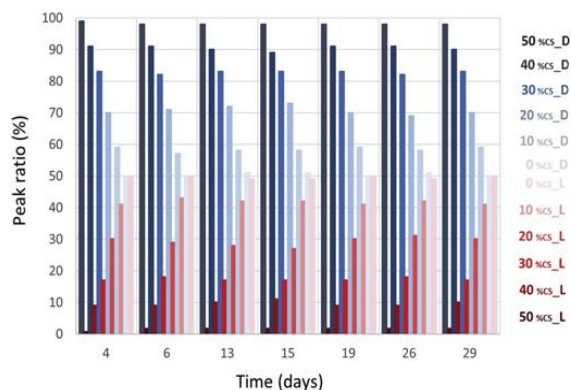| Amount of Chiral selector (%)	0	10	20	30	40	50
Feed D: L (mmol/ml)	1.92 : 1.84	1.78 : 1.64	1.65 : 1.40	1.62 : 1.38	1.58 : 1.29	1.51 : 1.22
Permeate D: L (mmol/ml)	0.01 : 0.01	0.10 : 0.07	0.25 : 0.11	0.27 : 0.05	0.25 : 0:03	0.34 : 0.01

Fig. 9. Ratio of D-Trp (in blue) and L-Trp (in red) concentration as a function of time in permeate side for all membranes. An increasing fraction of chiral selector in membranes is illustrated by growing intensity of colours. (For interpretation of the references to colour in this figure legend, the reader is referred to the Web version of this article.)

unchanged during the sorption process.

At the bottom layer of the fresh membrane, well pronounced signals of a C═O group are clearly visible, indicating that the polymerization reaction at this surface takes place with rather low conversion, forming a defective resin. Nevertheless, residual halide signals can be observed, indicating that all the starting acid chloride was converted into amide or hydrolyzed to the corresponding carboxylic acid. After the membrane was used, the signals of carboxylic acid are diminished, probably due to gradual dissolution of these non-polymerized species into the permeate. Indeed, minor impurities were observed in the obtained chromatograms (see Fig. 5 (right) the unassigned peak). The spectrum of the layer, after the sorption process, corresponds to a compact polyamide layer.

1.2. Mechanism of chiral recognition

To complete the study, the role of the polyamide active layer in chiral recognition of Trp enantiomers was elucidated. The mechanism of chiral recognition has been conventionally described in terms of the three-point interaction model [29]. Although often challenged as too simplistic and not sufficiently general [30], the three-point model usually provides a useful insight into the enantioselective binding geometry without the need of detailed computational modelling, and it has been frequently applied in an intuitive way to explain chiral separation in various systems [30].

In an attempt to explain the role of TMC + MPD/DACH PA6 active layer in chiral recognition of Trp enantiomers, a binding mechanism between (presumably zwitterionic) Trp molecules and the
TM–DACH–TM moiety is proposed (Fig. 12).

The three interactions required by the three-point model are assumed to be the following: (i) a π–π stacking between the aromatic rings of the indole and trimesoyl moieties possibly aided by N–H (Trp) … C═O antiparallel dipole–dipole interaction, (ii) the (Trp)–NH$_3^+$ … O═C interaction, and (iii) the (Trp)–CO$_2^-$ … H–N interaction. Interactions (ii) and (iii) between ionic and polar groups possess a variable degree of H-bonding character depending on particular bonding geometry; nonetheless, in any case they involve a strong electrostatic ion–dipole component. In addition, the steric fit into the assumed binding pockets created within the polymeric structure of the selector has to be taken into account.

For the (S,S) configuration of DACH, the spatial arrangement of interaction sites conforms to L-Trp, whereas D-Trp cannot simultaneously engage in all bonds (i), (ii), and (iii), see Fig. 12.

In order to provide the proposed intuitive model with stronger theoretical support, MOPAC2016 package [31] was used to optimize the
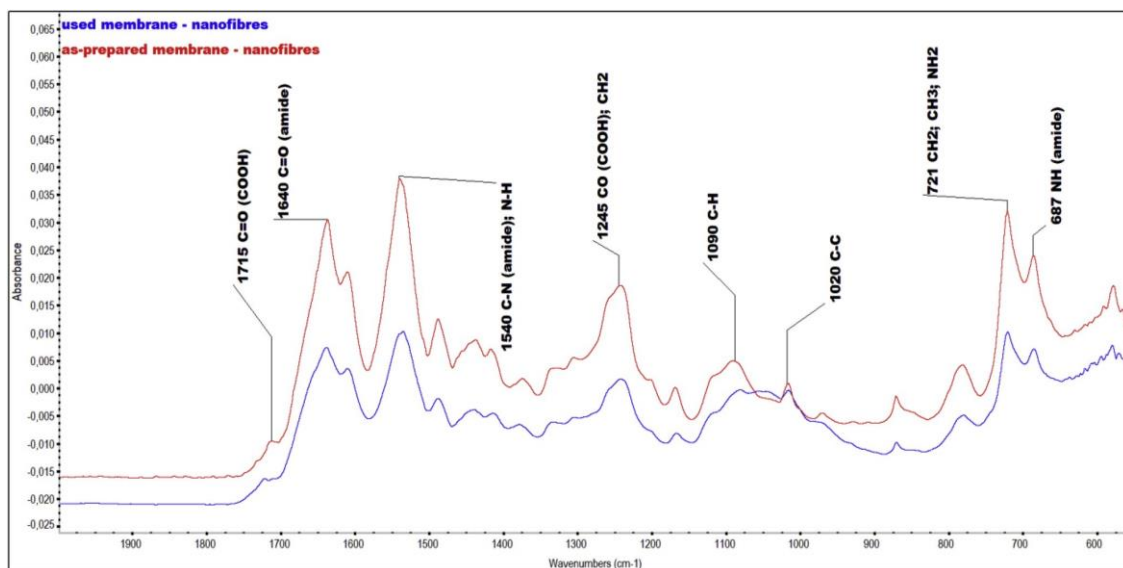
Fig. 10. FTIR spectra of membranes as-prepared and used, top side.
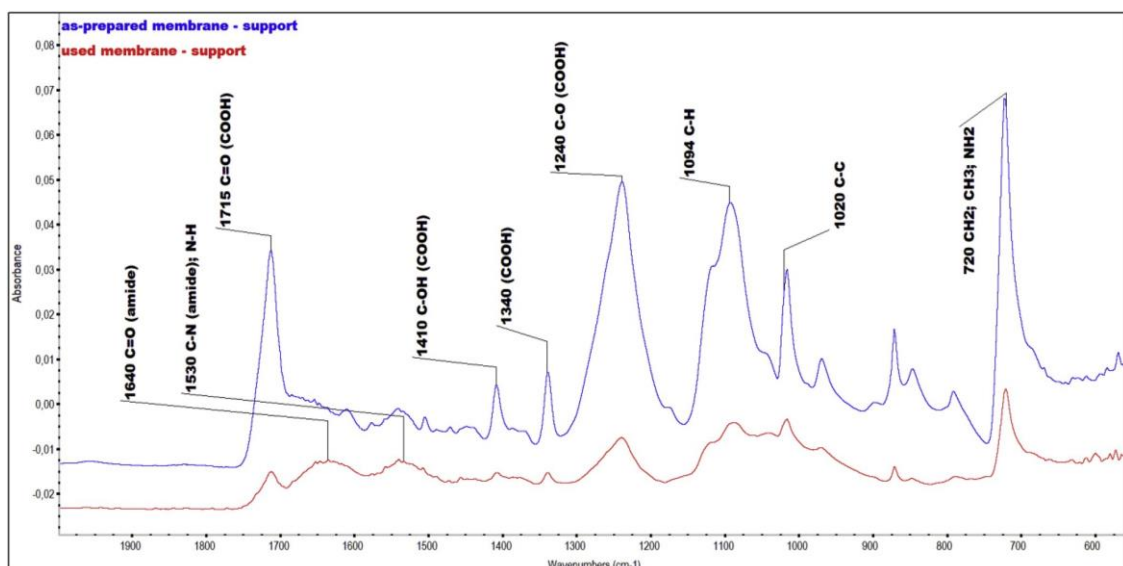
Fig. 11. FTIR spectra of membranes as-prepared and used, bottom side.

structures of the respective complexes of tryptophan and the selector fragment. The semiempirical PM6 method was used in the PM6-D3H4 variant of Rezac and Hobza [32] designed specifically to treat non-covalent complexes.

Fig. 13 Shows the structures resulting from the PM6-D3H4 optimization. One can see that the binding of L-tryptophan is in accordance with the proposed mechanism and involves all four interactions suggested, whereas D-tryptophan is only able to maintain two hydrogen bonds losing the alignment needed for a π–π stacked configuration.

PM6-D3H4 in MOPAC2016 was also employed to calculate gas-phase heats of formation of the optimized complexes of L- and D-Trp with the selector fragment, yielding -531.00 and -520.97 kJ/mol, respectively, corroborating the assumed stronger binding in the case of L-Trp. The

difference of ca 10 kJ/mol accounts for the marked preference of the selector to L-enantiomer.

1. Conclusion

A series of membranes was prepared and successfully applied in both sorption and pertraction experiments. The unique composition nano-&micro fibrous composition of the membrane material assures stability and superior dispersion of the active surface layer. The crucial part of the barrier is formed by the chiral selector, which was added in different proportions into the top layer. New membranes underwent sorption tests, soaked in an aqueous solution of the model chiral drug D, L-Trp. The evolution of enantiomeric concentration over time was monitored
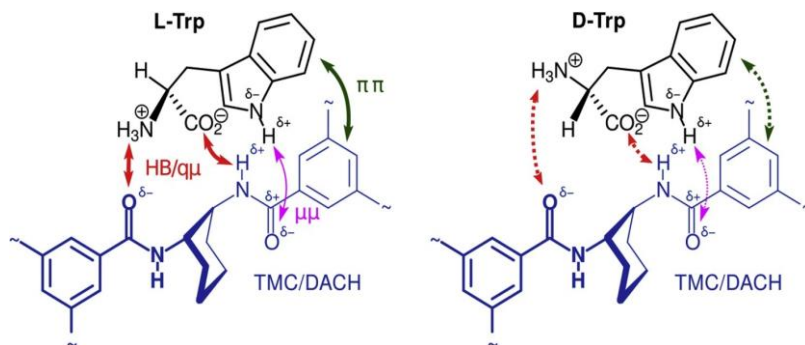
Fig. 12. The proposed chiral recognition mech- anism of Trp by TM–DACH–TM selector moiety in the TMC + MPD/DACH polyamide active layer. Trimesoyl amide groups depicted with thinner bonds are farther from the observer, behind Trp molecule in its binding position. Left — binding of L-Trp to the selector; right — binding of D-Trp to the selector. Arrows indicate interactions assumed within the three-point model: red (HB/qμ) — strong H-bonding and/or ion–dipole interactions; green (ππ) — a π–π stacking interaction; magenta (μμ) – an "auxiliary" dipole–dipole interaction in antiparallel alignment. (For interpretation of the references to colour in this figure legend, the reader is referred to the Web version of this article.)
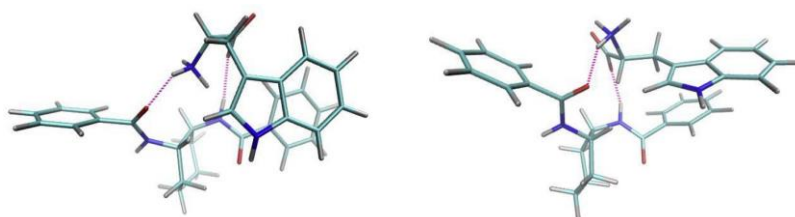

Fig. 13. Final geometries of the (L/D)-Trp–selector complexes resulting from PM6-D3H4 optimization. Left — L-Trp; right — D-Trp. Hydrogen bonds are drawn in magenta. Visualization was made by Visual Molecular Dynamics [33].

by HPLC analysis and revealed no sorption activity for a blank membrane – i.e., one lacking a chiral selector. On the contrary, the membranes containing the selector demonstrated preferential sorption activity towards one enantiomer. The sorption of L-Trp was found to be proportional to the fraction of the chiral selector in the active layer of the membrane, while an unchanged concentration of D-Trp was detected in the solution during the entire testing time interval. In addition, an enantiomeric separation of the same model chiral drug was performed in by pertraction in diffusion cells. The preferential sorption of L-Trp from the feed underlined the crucial importance of the selector in the active layer to achieve chiral recognition of enantiomers. Due to the exclusive membrane material, the retention of L-Trp in the membrane materials did not block the transport of D-Trp into the permeate during the entire experimental time. Moreover, only 50% of DACH in one part of the active layer was sufficient to achieve an enantioselectivity of 99%. Fresh and used membranes were analysed by FTIR spectroscopy and characterized by SEM. The role of the PA active layer in chiral recognition of Trp enantiomers was elucidated. This study demonstrates that such membranes can be an effective tool for the separation of enantiomers.

Declaration of competing interest

There is no conflict of Interest.

Symbols used

cs   chiral selector
DACH   (S,S)-1,2-diaminocyclohexane
Exp.   experiment
FTIR   Fourier-transform infrared spectroscopy
HPLC   high-performance liquid chromatography
J   pervaporate flow
m   mass
MPD   m-phenylene diamine
PA6   polyamide 6
rpm   rotation per minute
SEM   scanning electron microscopy
TMC   1,3,5-trimesoyl chloride
Trp   tryptophan
w   mass fraction
Δt   time change

Appendix A. Supplementary data

Supplementary data to this article can be found online at https://doi.org/10.1016/j.memsci.2019.117728.

References

[1] I.K. Reddy, R. Mehvar, Chirality in Drug Design and Development, CRC Press, 2004.
[2] Y. Zhou, S. Wu, H. Zhou, H. Huang, J. Zhao, Y. Deng, H. Wang, Y. Yang, J. Yang, L. Luo, Chiral pharmaceuticals: environment sources, potential human health impacts, remediation technologies and future perspective, Environ. Int. 121 (2018) 523–537.
[3] A. Nag, Asymmetric Synthesis of Drugs and Natural Products, CRC Press, 2018.
[4] Y.-P. Xue, C.-H. Cao, Y.-G. Zheng, Enzymatic asymmetric synthesis of chiral amino acids, Chem. Soc. Rev. 47 (4) (2018) 1516–1561.
[5] A. Hölzl-Hobmeier, A. Bauer, A.V. Silva, S.M. Huber, C. Bannwarth, T. Bach, Catalytic deracemization of chiral allenes by sensitized excitation with visible light, Nature 564 (7735) (2018) 240–243.
[6] I. Agranat, H. Caner, J. Caldwell, Putting chirality to work: the strategy of chiral switches, Nat. Rev. Drug Discov. 1 (2002) 753.
[7] H. Lorenz, A. Seidel-Morgenstern, Processes to separate enantiomers, Angew. Chem. Int. Ed. 53 (5) (2014) 1218–1250.
[8] J. Shen, Y. Okamoto, Efficient separation of enantiomers using stereoregular chiral polymers, Chem. Rev. 116 (3) (2016) 1094–1138.

[9] X.-Y. Huang, D. Pei, J.-F. Liu, D.-L. Di, A review on chiral separation by counter-current chromatography: Development, applications and future outlook, J. Chromatogr. A 1531 (2018) 1–12.

[10] L. Candelaria, L.V. Frolova, B.M. Kowalski, K. Artyushkova, A. Serov, N.G. Kalugin, Surface-modified three-dimensional graphene nanosheets as a stationary phase for chromatographic separation of chiral drugs, Sci. Rep. 8 (1) (2018) 14747.

[11] C. Fernandes, M.E. Tiritan, M.M.M. Pinto, Chiral separation in preparative scale: a brief overview of membranes as tools for enantiomeric separation, Symmetry 9 (10) (2017) 206.

[12] R. Xie, L.-Y. Chu, J.-G. Deng, Membranes and membrane processes for chiral resolution, Chem. Soc. Rev. 37 (6) (2008) 1243–1263.

[13] A.H. Ölçeroğlu, P. Çalık, L. Yılmaz, Development of enhanced ultrafiltration methodologies for the resolution of racemic benzoin, J. Membr. Sci. 322 (2) (2008) 446–452.

[14] K. Singh, P.G. Ingole, J. udhari, H. Bhrambhatt, A. Bhattacharya, H.C. Bajaj, Resolution of racemic mixture of alpha-amino acid derivative through composite membrane, J. Membr. Sci. 378 (1-2) (2011) 531–540.

[15] P.G. Ingole, H.C. Bajaj, D.N. Srivastava, B. Rebary, Preparation of thin film polymer composite membranes for optical resolution of racemic mixture of α-amino acids, Separ. Sci. Technol. 48 (12) (2013) 1777–1787.

[16] P.G. Ingole, H.C. Bajaj, K. Singh, Membrane separation processes: optical resolution of lysine and asparagine amino acids, Desalination 343 (2014) 75–81.

[17] K. Singh, S. Devi, H.C. Bajaj, P. Ingole, J. Choudhari, H. Bhrambhatt, Optical resolution of racemic mixtures of amino acids through nanofiltration membrane process, Separ. Sci. Technol. 49 (17) (2014) 2630–2641.

[18] L.M. Yuan, Y.Q. Su, A.H. Duan, Y. Zheng, P. Ai, X.X. Chen, Optical resolution of D, L-Phenylglycine and chiral separation mechanism using an enantioselective membrane of vancomycin, Chem. J. Chin. Univ. 37 (11) (2016) 1960–1965.

[19] X. Liu, Y. Li, J. Xue, W. Zhu, J. Zhang, Y. Yin, Y. Qin, K. Jiao, Q. Du, B. Cheng, X. Zhuang, J. Li, M.D. Guiver, Magnetic field alignment of stable proton-conducting channels in an electrolyte membrane, Nat. Commun. 10 (1) (2019) 842.

[20] B. Yalcinkaya, F. Yalcinkaya, J. Chaloupek, Optimisation of thin film composite nanofiltration membranes based on laminated nanofibrous and nonwoven supporting, Mater. Desalin. Water Treat. 59 (2017) 19–30.

[21] B. Yalcinkaya, F. Yalcinkaya, J. Chaloupek, Thin film nanofibrous composite membrane for dead-end seawater desalination, J. Nanomater. 2016 (2016) 12.

[22] K. Singh, P.G. Ingole, H.C. Bajaj, H. Gupta, Preparation, characterization and application of β-cyclodextrin-glutaraldehyde crosslinked membrane for the enantiomeric separation of amino acids, Desalination 298 (2012) 13–21.

[23] H.M. Roager, T.R. Licht, Microbial tryptophan catabolites in health and disease, Nat. Commun. 9 (1) (2018) 3294.

[24] J. Chiappelli, T.T. Postolache, P. Kochunov, L.M. Rowland, S.A. Wijtenburg, D. K. Shukla, M. Tagamets, X. Du, A. Savransky, C.A. Lowry, A. Can, D. Fuchs, L. E. Hong, Tryptophan metabolism and white matter integrity in schizophrenia, Neuropsychopharmacology 41 (2016) 2587.

[25] T. Teraishi, H. Hori, D. Sasayama, J. Matsuo, S. Ogawa, M. Ota, K. Hattori, M. Kajiwara, T. Higuchi, H. Kunugi, 13C-tryptophan breath test detects increased catabolic turnover of tryptophan along the kynurenine pathway in patients with major depressive disorder, Sci. Rep. 5 (2015) 15994.

[26] E.A. Belongia, C.W. Hedberg, G.J. Gleich, K.E. White, A.N. Mayeno, D. A. Loegering, S.L. Dunnette, P.L. Pirie, K.L. MacDonald, M.T. Osterholm, An investigation of the cause of the eosinophilia–myalgia syndrome associated with tryptophan use, N. Engl. J. Med. 323 (6) (1990) 357–365.

[27] L.J. Crofford, J.I. Rader, M.C. Dalakas, R.H. Hill, S.W. Page, L.L. Needham, L. S. Brady, M.P. Heyes, R.L. Wilder, P.W. Gold, L-tryptophan implicated in human eosinophilia-myalgia syndrome causes fasciitis and perimyositis in the Lewis rat, J. Clin. Investig. 86 (5) (1990) 1757–1763.

[28] J. Tobis, L. Boch, Y. Thomann, J.C. Tiller, Amphiphilic polymer conetworks as chiral separation membranes, J. Membr. Sci. 372 (2011) 219–227.

[29] A. Berthod, Chiral recognition mechanisms, Anal. Chem. 78 (7) (2006) 2093–2099; (a) K. Jozwiak, R. Moaddel, S. Ravichandran, A. Plazinska, J. Kozak, S. Patel, R. Yamaguchi, I.W. Wainer, Exploring enantiospecific ligand–protein interactions using cellular membrane affinity chromatography: chiral recognition as a dynamic process, J. Chromatogr. B 875 (1) (2008) 200–207.

[30] M. Lämmerhofer, Chiral recognition by enantioselective liquid chromatography: mechanisms and modern chiral stationary phases, J. Chromatogr. A 1217 (6) (2010) 814–856.

[31] J.P. Stewart, Stewart Computational Chemistry, Colorado Springs, CO, USA, 2016.

[32] J. Řezáč, P. Hobza, J. Chem. Theory Comput. 8 (1) (2012) 141–151 ([RHref]).

[33] W. Humphrey, A. Dalke, K. Schulten, J. Mol. Graph. 14 (1996) 33–38 ([VMDref]).

161

5. CONCLUSION

The "nanotechnology" has been introduced to literature by the Nobel Prize scientist Richard Feynman with his speech "There's Plenty of Room at the Bottom" in the meeting of the American Physical Society at Caltech, in December of 1959 [80]. He predicted that one day scientists would make things at the atomic level, and since then, nanotechnology builds upwards, and we are able to make them more precisely and controllable as we want.

Nanofiber has been widely used in various applications due to its unique structure, surface properties, and functionality. There is significantly grown in both pilot and industrial-scale nanofiber production devices. Considering the high technical developments and advantages, nanofibers are expected to take part in a wide variety of markets. One application area that will receive countless benefits from these developments and will continue to profit in the future is nanofiber membranes in water treatment. Nanofibers have great potential in different water purification processes such as microfilters, UF, NF, desalination, distillation, and removal of microbial, heavy metals, dyes, and other toxic substances. Some of the technical obstacles of nanofibers, given in "*Chapter 1-Main problems*", limit their application in the water domain area.

In this thesis, first, we tried to determine the main obstacles and problem of nanofibers to apply to membrane technology, and then demonstrate some achievements to justify and improve existing research in the literature. This thesis suggests various approaches that have the potential to solve many of the problems introduced in "*Chapter 1-Main problems*".

This thesis discusses the role of nanofiber membranes that are suitable for use in water treatment in the different water purification process.

REFERENCES

1. Hutten, I.M. CHAPTER 1 - Introduction to Nonwoven Filter Media. In *Handbook of Nonwoven Filter Media*; Hutten, I.M., Ed.; Butterworth-Heinemann: Oxford, 2007; pp. 1–28 ISBN 978-1-85617-441-1.
2. Nanofiber Technology in Filtration – The American Filtration and Separations Society (AFS) Available online: https://www.afssociety.org/nanofiber-technology-in-filtration/ (accessed on Sep 9, 2020).
3. Gilbert, W. *De Magnete*; Courier Corporation, 1958; ISBN 978-0-486-26761-6.
4. Cooley, J.F. Improved methods of and apparatus for electrically separating the relatively volatile liquid component from the component of relatively fixed substances of composite fluids. *United Kingdom Patent* **1900**, *6385*, 19.
5. Yener, F. New Methods in the Study of Roller Electrospinning Mechanism. Ph.D. thesis, Technical University of Liberec: Liberec, 2014.
6. Jirsak, O.; Sanetrnik, F.; Lukas, D.; Kotek, V.; Martinova, L.; Chaloupek, J. A Method of Nanofibres Production from a Polymer Solution Using Electrostatic Spinning and a Device for Carrying Out the Method 2005.
7. Yalcinkaya, F.; Yalcinkaya, B.; Jirsak, O. Dependent and Independent Parameters of Needleless Electrospinning. In *Electrospinning*; Haider, S., Haider, A., Eds.; IntechOpen: Rijeka, 2016.
8. Shenoy, S.L.; Bates, W.D.; Frisch, H.L.; Wnek, G.E. Role of chain entanglements on fiber formation during electrospinning of polymer solutions: good solvent, non-specific polymer–polymer interaction limit. *Polymer* **2005**, *46*, 3372–3384, doi:10.1016/j.polymer.2005.03.011.
9. Barnes, H.A. *A Handbook of Elementary Rheology*; University of Wales, Institute of Non-Newtonian Fluid Mechanics, 2000; ISBN 978-0-9538032-0-0.
10. Filatov, V.; Budyka, A.; Kirichenk, V. Electrospinning of Micro-and-Nanofibers: Fundementals and Applications in Seperation and Filtration Process. 2007. *Bgell House Inc. Danbury, Connecticut, United states*.
11. Fallahi, D.; Rafizadeh, M.; Mohammadi, N.; Vahidi, B. Effects of feed rate and solution conductivity on jet current and fiber diameter in electrospinning of polyacrylonitrile solutions. *e-Polymers* **2009**, *9*, doi:10.1515/epoly.2009.9.1.1250.
12. Bhattacharjee, P.K.; Schneider, T.M.; Brenner, M.P.; McKinley, G.H.; Rutledge, G.C. On the measured current in electrospinning. *Journal of Applied Physics* **2010**, *107*, 044306, doi:10.1063/1.3277018.
13. Theron, S.A.; Zussman, E.; Yarin, A.L. Experimental investigation of the governing parameters in the electrospinning of polymer solutions. *Polymer* **2004**, *45*, 2017–2030, doi:10.1016/j.polymer.2004.01.024.
14. Demir, M.M.; Yilgor, I.; Yilgor, E.; Erman, B. Electrospinning of polyurethane fibers. *Polymer* **2002**, *43*, 3303–3309, doi:10.1016/S0032-3861(02)00136-2.
15. Yalcinkaya, F. Preparation of various nanofiber layers using wire electrospinning system. *Arabian Journal of Chemistry* **2019**, *12*, 5162–5172, doi:10.1016/j.arabjc.2016.12.012.
16. Anton, F. Process and apparatus for preparing artificial threads 1934.
17. Kny, E.; Ghosal, K.; Thomas, S. *Electrospinning: From Basic Research to Commercialization*; Royal Society of Chemistry, 2018; ISBN 978-1-78801-100-6.
18. Bechold, H. Investigations on colloids by filtration methods. *Biochem. Z* **1907**, *6*, 379.
19. Loeb, S.; Sourirajan, S. Sea water demineralization by means of an osmotic membrane. In; ACS Publications, 1962.
20. Muralidhara, H.S. Chapter 2 - Challenges of Membrane Technology in the XXI Century. In *Membrane Technology*; Cui, Z.F., Muralidhara, H.S., Eds.; Butterworth-Heinemann: Oxford, 2010; pp. 19–32 ISBN 978-1-85617-632-3.
21. Overview of Membrane Science and Technology. In *Membrane Technology and Applications*; John Wiley & Sons, Ltd, 2012; pp. 1–14 ISBN 978-1-118-35968-6.

22. Abdullah, N.; Rahman, M.A.; Dzarfan Othman, M.H.; Jaafar, J.; Ismail, A.F. Chapter 2 - Membranes and Membrane Processes: Fundamentals. In *Current Trends and Future Developments on (Bio-) Membranes*; Basile, A., Mozia, S., Molinari, R., Eds.; Elsevier, 2018; pp. 45–70 ISBN 978-0-12-813549-5.

23. Purkait, M.K.; Sinha, M.K.; Mondal, P.; Singh, R. Chapter 1 - Introduction to Membranes. In *Interface Science and Technology*; Purkait, M.K., Sinha, M.K., Mondal, P., Singh, R., Eds.; Stimuli Responsive Polymeric Membranes; Elsevier, 2018; Vol. 25, pp. 1–37.

24. Yalcinkaya, F. A review on advanced nanofiber technology for membrane distillation. *Journal of Engineered Fibers and Fabrics* **2019**, *14*, 1558925018824901, doi:10.1177/1558925018824901.

25. Hwang, K.-J.; Lin, T.-T. Effect of morphology of polymeric membrane on the performance of cross-flow microfiltration. *Journal of Membrane Science* **2002**, *199*, 41–52, doi:10.1016/S0376-7388(01)00675-5.

26. Koenhen, D.M.; Mulder, M.H.V.; Smolders, C.A. Phase separation phenomena during the formation of asymmetric membranes. *Journal of Applied Polymer Science* **1977**, *21*, 199–215, doi:10.1002/app.1977.070210118.

27. Cadotte, J.E.; Petersen, R.J.; Larson, R.E.; Erickson, E.E. A new thin-film composite seawater reverse osmosis membrane. *Desalination* **1980**, *32*, 25–31, doi:10.1016/S0011-9164(00)86003-8.

28. Gohil, J.M.; Choudhury, R.R. Chapter 2 - Introduction to Nanostructured and Nano-enhanced Polymeric Membranes: Preparation, Function, and Application for Water Purification. In *Nanoscale Materials in Water Purification*; Thomas, S., Pasquini, D., Leu, S.-Y., Gopakumar, D.A., Eds.; Micro and Nano Technologies; Elsevier, 2019; pp. 25–57 ISBN 978-0-12-813926-4.

29. Fleischer, R.L.; Price, P.B.; Walker, R.M.; Walker, R.M. *Nuclear tracks in solids: principles and applications*; Univ of California Press, 1975; ISBN 0-520-02665-9.

30. Tasselli, F. Membrane Preparation Techniques. In *Encyclopedia of Membranes*; Drioli, E., Giorno, L., Eds.; Springer: Berlin, Heidelberg, 2015; pp. 1–3 ISBN 978-3-642-40872-4.

31. Tiyek, I.; Gunduz, A.; Yalcinkaya, F.; Chaloupek, J. Influence of Electrospinning Parameters on the Hydrophilicity of Electrospun Polycaprolactone Nanofibres. *J Nanosci Nanotechnol* **2019**, *19*, 7251–7260, doi:10.1166/jnn.2019.16605.

32. Membrane Transport Theory. In *Membrane Technology and Applications*; John Wiley & Sons, Ltd, 2004; pp. 15–87 ISBN 978-0-470-02039-5.

33. Yalcinkaya, B.; Yalcinkaya, F. *12. Nanofibers in liquid filtration*; De Gruyter, 2019; ISBN 978-3-11-058139-3.

34. Ferry, J.D. Ultrafilter Membranes and Ultrafiltration. *Chemical reviews* **1936**, *18*, 373–455.

35. Renkin, E.M. Filtration, diffusion, and molecular sieving through porous cellulose membranes. *The Journal of general physiology* **1954**, *38*, 225.

36. Luis, P. Chapter 1 - Introduction. In *Fundamental Modelling of Membrane Systems*; Luis, P., Ed.; Elsevier, 2018; pp. 1–23 ISBN 978-0-12-813483-2.

37. Khulbe, K.C.; Feng, C.Y.; Matsuura, T. Surface modification of synthetic polymeric membranes for filtration and gas separation. *Recent Patents on Chemical Engineering* **2010**, *3*, 1–16.

38. Morgan, P.W. *Condensation polymers: by interfacial and solution methods*; Interscience Publishers, 1965; Vol. 10;.

39. Lau, W.-J.; Ong, C.-S.; Nordin, N.; Sani, N.A.A.; Mokhtar, N.M.; Gohari, R.J.; Emadzadeh, D.; Ismail, A.F. Surface Modification of Polymeric Membranes for Various Separation Processes. *Surf. Treat. Biol. Chem. Phys. Appl* **2016**, 115–180.

40. Al-Jumaili, A.; Alancherry, S.; Grant, D.; Kumar, A.; Bazaka, K.; Jacob, M.V. Chapter 8 - Plasma Treatment of Polymeric Membranes. In *Non-Thermal Plasma Technology for Polymeric Materials*; Thomas, S., Mozetič, M., Cvelbar, U., Špatenka, P., K.m., P., Eds.; Elsevier, 2019; pp. 211–240 ISBN 978-0-12-813152-7.

41. Abd El-Ghaffar, M.; Tieama, H.A. A review of membranes classifications, configurations, surface modifications, characteristics and Its applications in water purification. *Chemical and Biomolecular Engineering* **2017**, *2*, 57.

42. Salmani, L.; Nouri, M. Electrospun Silk Fibroin Nanofibers with Improved Surface Texture. *Journal of Textiles and Polymers* **2016**, *4*, 75–81.

43. Chen, L.; Cheng, H.-H.; Xiong, J.; Zhu, Y.-T.; Zhang, H.-P.; Xiong, X.; Liu, Y.-M.; Yu, J.; Guo, Z.-X. Improved Mechanical Properties of Poly(butylene succinate) Membrane by Co-electrospinning with Gelatin. *Chin J Polym Sci* **2018**, *36*, 1063–1069, doi:10.1007/s10118-018-2112-0.

44. Sen, R.; Zhao, B.; Perea, D.; Itkis, M.E.; Hu, H.; Love, J.; Bekyarova, E.; Haddon, R.C. Preparation of Single-Walled Carbon Nanotube Reinforced Polystyrene and Polyurethane Nanofibers and Membranes by Electrospinning. *Nano Lett.* **2004**, *4*, 459–464, doi:10.1021/nl035135s.

45. Bilge, K.; Yorulmaz, Y.; Javanshour, F.; Ürkmez, A.; Yılmaz, B.; Şimşek, E.; Papila, M. Synergistic role of in-situ crosslinkable electrospun nanofiber/epoxy nanocomposite interlayers for superior laminated composites. *Composites Science and Technology* **2017**, *151*, 310–316, doi:10.1016/j.compscitech.2017.08.029.

46. Nissilä, T.; Hietala, M.; Oksman, K. A method for preparing epoxy-cellulose nanofiber composites with an oriented structure. *Composites Part A: Applied Science and Manufacturing* **2019**, *125*, 105515, doi:10.1016/j.compositesa.2019.105515.

47. Wang, X.; Zhang, W.-J.; Yu, D.-G.; Li, X.-Y.; Yang, H. Epoxy Resin Nanofibers Prepared Using Electrospun Core/Sheath Nanofibers as Templates. *Macromolecular Materials and Engineering* **2013**, *298*, 664–669, doi:10.1002/mame.201200174.

48. Jahanbaani, A.R.; Behzad, T.; Borhani, S.; Darvanjooghi, M.H.K. Electrospinning of cellulose nanofibers mat for laminated epoxy composite production. *Fibers Polym* **2016**, *17*, 1438–1448, doi:10.1007/s12221-016-6424-9.

49. Tang, X.; Yan, X. Dip-coating for fibrous materials: mechanism, methods and applications. *J Sol-Gel Sci Technol* **2017**, *81*, 378–404, doi:10.1007/s10971-016-4197-7.

50. Cai, J.; Zhang, Q.; Lei, M.; He, J.; Liu, G. The use of solvent-soaking treatment to enhance the anisotropic mechanical properties of electrospun nanofiber membranes for water filtration. *RSC Adv.* **2016**, *6*, 66807–66813, doi:10.1039/C6RA11020G.

51. Choi, S.-S.; Lee, Y.S.; Joo, C.W.; Lee, S.G.; Park, J.K.; Han, K.-S. Electrospun PVDF nanofiber web as polymer electrolyte or separator. *Electrochimica Acta* **2004**, *50*, 339–343, doi:10.1016/j.electacta.2004.03.057.

52. Huang, L.; Manickam, S.S.; McCutcheon, J.R. Increasing strength of electrospun nanofiber membranes for water filtration using solvent vapor. *Journal of Membrane Science* **2013**, *436*, 213–220, doi:10.1016/j.memsci.2012.12.037.

53. Yoon, K.; Hsiao, B.S.; Chu, B. Formation of functional polyethersulfone electrospun membrane for water purification by mixed solvent and oxidation processes. *Polymer* **2009**, *50*, 2893–2899, doi:10.1016/j.polymer.2009.04.047.

54. Byron, J.J.; Nicholas, M. Method and apparatus for ultrasonic welding 1965.

55. Trejo, N.K.; Reyes, C.G.; Sanchez, V.; Zhang, D.; Frey, M.W. Developing composite nanofibre fabrics using electrospinning, ultrasonic sewing, and laser cutting technologies. *International Journal of Fashion Design, Technology and Education* **2016**, *9*, 192–200, doi:10.1080/17543266.2016.1154111.

56. Wirth, E.; Sabantina, L.; Weber, M.O.; Finsterbusch, K.; Ehrmann, A. Preliminary Study of Ultrasonic Welding as a Joining Process for Electrospun Nanofiber Mats. *Nanomaterials* **2018**, *8*, 746, doi:10.3390/nano8100746.

57. Bernstein, R.; Kaufman, Y.; Freger, V. Membrane Characterization. In *Encyclopedia of Membrane Science and Technology*; American Cancer Society, 2013; pp. 1–41 ISBN 978-1-118-52231-8.

58. Li, M.; Li, J.; Zhou, M.; Xian, Y.; Shui, Y.; Wu, M.; Yao, Y. Super-hydrophilic electrospun PVDF/PVA-blended nanofiber membrane for microfiltration with ultrahigh water flux. *Journal of Applied Polymer Science* **2020**, *137*, 48416, doi:10.1002/app.48416.

59. Gopal, R.; Zuwei, M.; Kaur, S.; Ramakrishna, S. Surface Modification and Application of Functionalized Polymer Nanofibers. In *Molecular Building Blocks for Nanotechnology: From Diamondoids to Nanoscale Materials and Applications*; Mansoori, G.A., George, T.F.,

Assoufid, L., Zhang, G., Eds.; Topics in Applied Physics; Springer: New York, NY, 2007; pp. 72–91 ISBN 978-0-387-39938-6.

60. Yalcinkaya, F. Effect of argon plasma treatment on hydrophilic stability of nanofiber webs. *Journal of Applied Polymer Science* **2018**, *135*, 46751, doi:10.1002/app.46751.

61. Yusof, M.R.; Shamsudin, R.; Zakaria, S.; Azmi Abdul Hamid, M.; Yalcinkaya, F.; Abdullah, Y.; Yacob, N. Electron-Beam Irradiation of the PLLA/CMS/β-TCP Composite Nanofibers Obtained by Electrospinning. *Polymers* **2020**, *12*, 1593, doi:10.3390/polym12071593.

62. Boyraz, E.; Yalcinkaya, F.; Hruza, J.; Maryska, J. Surface-Modified Nanofibrous PVDF Membranes for Liquid Separation Technology. *Materials* **2019**, *12*, 2702, doi:10.3390/ma12172702.

63. Torres-Mendieta, R.; Yalcinkaya, F.; Boyraz, E.; Havelka, O.; Wacławek, S.; Maryška, J.; Černík, M.; Bryjak, M. PVDF nanofibrous membranes modified via laser-synthesized Ag nanoparticles for a cleaner oily water separation. *Applied Surface Science* **2020**, *526*, 146575, doi:10.1016/j.apsusc.2020.146575.

64. Bryjak, M.; Hodge, H.; Dach, B. Modification of porous polyacrylonitrile membrane. *Angew. Makromol. Chem.* **1998**, *260*, 25–29.

65. Cécile, C.; Hsieh, Y.-L. Hydrophilic polystyrene/maleic anhydride ultrafine fibrous membranes. *Journal of Applied Polymer Science* **2010**, *115*, 723–730, doi:10.1002/app.31003.

66. Yalcinkaya, F.; Siekierka, A.; Bryjak, M. Surface modification of electrospun nanofibrous membranes for oily wastewater separation. *RSC Advances* **2017**, *7*, 56704–56712, doi:10.1039/C7RA11904F.

67. Yalcinkaya, F.; Siekierka, A.; Bryjak, M. Preparation of Fouling-Resistant Nanofibrous Composite Membranes for Separation of Oily Wastewater. *Polymers (Basel)* **2017**, *9*, doi:10.3390/polym9120679.

68. Guarino, V.; Varesano, A. Electrospinning Technology for Filtering Membranes Fabrication. In *Filtering Media by Electrospinning: Next Generation Membranes for Separation Applications*; Focarete, M.L., Gualandi, C., Ramakrishna, S., Eds.; Springer International Publishing: Cham, 2018; pp. 1–24 ISBN 978-3-319-78163-1.

69. Jiao, L.; Yan, K.; Wang, J.; Lin, S.; Li, G.; Bi, F.; Zhang, L. Low surface energy nanofibrous membrane for enhanced wetting resistance in membrane distillation process. *Desalination* **2020**, *476*, 114210, doi:10.1016/j.desal.2019.114210.

70. Jiříček, T.; Komárek, M.; Lederer, T. Polyurethane Nanofiber Membranes for Waste Water Treatment by Membrane Distillation Available online: https://www.hindawi.com/journals/jnt/2017/7143035/ (accessed on Apr 8, 2020).

71. Li, M.; Wang, D.; Xiao, R.; Sun, G.; Zhao, Q.; Li, H. A novel high flux poly(trimethylene terephthalate) nanofiber membrane for microfiltration media. *Separation and Purification Technology* **2013**, *116*, 199–205, doi:10.1016/j.seppur.2013.05.046.

72. Ding, Y.; Wu, J.; Wang, J.; Wang, J.; Ye, J.; Liu, F. Superhydrophilic carbonaceous-silver nanofibrous membrane for complex oil/water separation and removal of heavy metal ions, organic dyes and bacteria. *Journal of Membrane Science* **2020**, *614*, 118491, doi:10.1016/j.memsci.2020.118491.

73. Huang, X.; Zhang, S.; Xiao, W.; Luo, J.; Li, B.; Wang, L.; Xue, H.; Gao, J. Flexible PDA@ACNTs decorated polymer nanofiber composite with superhydrophilicity and underwater superoleophobicity for efficient separation of oil-in-water emulsion. *Journal of Membrane Science* **2020**, *614*, 118500, doi:10.1016/j.memsci.2020.118500.

74. Wang, Y.; Zhang, X.; He, X.; Zhang, W.; Zhang, X.; Lu, C. In situ synthesis of MnO2 coated cellulose nanofibers hybrid for effective removal of methylene blue. *Carbohydrate Polymers* **2014**, *110*, 302–308, doi:10.1016/j.carbpol.2014.04.008.

75. Rahaman, S.; Chen, T.; Islam, M.S.; Ma, W. Membranes for Forward Osmosis and Membrane Distillation and Process of Treating Fracking Wastewater 2020.

76. Bahmani, P.; Maleki, A.; Daraei, H.; Khamforoush, M.; Rezaee, R.; Gharibi, F.; Tkachev, A.G.; Burakov, A.E.; Agarwal, S.; Gupta, V.K. High-flux ultrafiltration membrane based on electrospun polyacrylonitrile nanofibrous scaffolds for arsenate removal from aqueous solutions. *Journal of Colloid and Interface Science* **2017**, *506*, 564–571, doi:10.1016/j.jcis.2017.07.086.

77. Li, R.; Li, M.; Li, Z.; Zhu, Q.; Zhong, W.; Liu, K.; Wang, D. A thin film composite membrane supported by a hydrophilic poly(vinyl alcohol-co-ethylene) nanofiber membrane: Preparation, characterization, and application in nanofiltration. *Journal of Applied Polymer Science* **2018**, *135*, 46261, doi:10.1002/app.46261.

78. Schinwald, A.; Murphy, F.A.; Prina-Mello, A.; Poland, C.A.; Byrne, F.; Movia, D.; Glass, J.R.; Dickerson, J.C.; Schultz, D.A.; Jeffree, C.E.; et al. The threshold length for fiber-induced acute pleural inflammation: shedding light on the early events in asbestos-induced mesothelioma. *Toxicol. Sci.* **2012**, *128*, 461–470, doi:10.1093/toxsci/kfs171.

79. 14:00-17:00 ISO/TR 13121:2011 Available online: https://www.iso.org/cms/render/live/en/sites/isoorg/contents/data/standard/05/29/52976.html (accessed on Sep 24, 2020).

80. Feynman, R.P. Plenty of Room at the Bottom.; 1959.

APPENDIX-LIST OF PUBLICATIONS

A.1. Publications in WoS -impacted journals

1. F. Yener, O. Jirsak, 'Comparison between the Needle and Roller Electrospinning of Polyvinylbutyral', Journal of Nanomaterials, Vol. 2012, Article ID 839317, 6 pages DOI:10.1155/2012/839317, 2012.

2. F. Yener, O. Jirsak, R. Gemci, Using a Range of PVB Spinning Solution to Acquire Diverse Morphology for Electrospun Nanofibres, IJCCE, Vol.31, No:4, pages:49-58, 2012.

3. F. Yener, B.Yalcinkaya, 'Electrospinning of Polyvinyl Butyral in Different Solvents', e-Polymers, Vol. 13, Issue 1, pp. 229–242, 2013.

4. F. Yener, B.Yalcinkaya, O. Jirsak, 'On the Measured Current in the Needle- and Needleless Electrospinning', Journal of Nanoscience and Nanotechnology, Vol. 13, Issue 7, pp. 4672-4679, DOI: 10.1166/jnn.2013.7189, 2013.

5. B. Yalcinkaya, F. Yener, O. Jirsak, F. Cengiz-Callioglu, 'On the Nature of Electric Current in the Electrospinning Process', Journal of Nanomaterials, Vol. 2013, Article ID 538179, 10 pages, DOI: 10.1155/2013/538179, 2013.

6. B. Yalcinkaya, F. Cengiz-Callioglu, F. Yener, Measurement and Analysis of Jet Current and Jet Life in Roller Electrospinning of Polyurethane, Textile Research Journal, March, Vol. 84, no 16, pages: 1720-1728, DOI: 0040517514528563, 2014.

7. F. Yalcinkaya, B. Yalcinkaya, O. Jirsak, Influence of Salts on Electrospinning of Aqueous and Nonaqueous Polymer Solutions, Journal of Nanomaterials, vol. 2015, Article ID 134251, 12 pages, DOI:10.1155/2015/134251, 2015.

8. F.Yalcinkaya, Effect of Current on Polymer Jet in Electrospinning Process, Tekstil ve Konfeksiyon, Vol. 25, Issue 3, pages: 201-206, 2015.

9. F. Yalcinkaya, Experimental Study on Electrospun Polyvinyl Butyral Nanofibers Using a Non-solvent System, Fibers and Polymers, Vol. 16, Issue 12, pp. 2544-2551, DOI: 10.1007/s12221-015-5525-1, 2015.

10. F. Yalcinkaya, M. Komarek, D. Lubasova, F. Sanetrnik, J. Maryska, Preparation of Antibacterial Nanofibre/Nanoparticle Covered Composite Yarns, Journal of Nanomaterials, Volume 2016 (2016), Article ID 7565972, 7 pages, DOI: 10.1155/2016/7565972, 2016.

11. F. Yalcinkaya, B. Yalcinkaya, A. Pazourek, J. Mullerova, M. Stuchlik, J. Maryska, Surface Modification of Electrospun PVDF/PAN Nanofibrous Layers by Low Vacuum Plasma Treatment, International Journal of Polymer Science, Volume 2016, Article ID 4671658, 9 pages, DOI: 10.1155/2016/4671658, 2016.

12. B. Yalcinkaya, F. Yalcinkaya, J. Chaloupek, Thin Film Nanofibrous Composite Membrane for Dead-End Seawater Desalination, Journal of Nanomaterials, Volume 2016, Article ID 2694373, 12 pages, DOI: 10.1155/2016/2694373, 2016.

13. F. Yalcinkaya, B. Yalcinkaya, O. Jirsak, Analysis of the Effects of the Rotating Roller Speed on a Roller Electrospinning System, Textile Research Journal, DOI: 10.1177/0040517516641362, Vol 87, Issue 8, pages 913-928, 2017.

14. F. Yalcinkaya, D. Lubasova, Quantitative Evaluation of Antibacterial Activities of Nanoparticles (ZnO, TiO2, ZnO/ TiO2, SnO2, CuO, ZrO2, AgNO3) Incorporated into Polyvinyl Butyral Nanofibres, Polymers for Advanced Technologies, Vol. 28, Issue 1, pp. 137-140, DOI: 10.1002/pat.3883, 2017.

15. F.Yalcinkaya, B. Yalcinkaya, J. Hruza, P. Hrabak, Effect of Nanofibrous Membrane Structures on the Treatment of Wastewater Microfiltration, Science of Advanced Materials, Volume 9, issue 5, pp.747-757, DOI:10.1166/sam.2017.3027, 2017.

16. B. Yalcinkaya, F. Yalcinkaya, J. Chaloupek, Optimisation of Thin Film Composite Nanofiltration Membranes Based on Laminated Nanofibrous and Nonwoven Supporting Material, Desalination and Water Treatment, Volume 59, pages 19-30, DOI: 10.1155/2016/2694373, 2017.

17. F. Yalcinkaya, A. Siekierka, M. Bryjak, Preparation of Fouling-Resistant Nanofibrous Composite Membranes for Separation of Oily Wastewater, Polymers, Volume 9, Issue 12, Article number 679, DOI: 10.3390/polym9120679, 2017.

18. F. Yalcinkaya, A. Siekierka, M. Bryjak, Surface Modification of Electrospun Nanofibrous Membranes for Oily Wastewater Separation, RSC Advances, Volume 7, Issue 89, pp. 56704-56712, DOI: 10.1039/C7RA11904F, 2017.

19. M. R. Yusof, R. Shamsudin, Y. Abdullah, F. Yalcinkaya, N. Yaacob, Electrospinning of Carboxymethyl Starch/Poly (L-Lactide) Acid Composite Nanofibers, Polymers for Advanced Technologies, Volume 29, Issue 6, pp. 1843-1851, DOI:10.1002/pat.4292, 2018. IF=2.137.

20. F. Yalcinkaya, J. Hruza, Effect of Laminating Pressure on Polymeric Nanofibre Composite

21. Membranes for Liquid Filtration, Nanomaterials, Volume 8, Issue 5, Article number 272, DOI: 10.3390/nano8050272, 2018. IF=3.504.

22. F. Yalcinkaya, The Effect of Argon Plasma Treatment on Hydrophilic Stability of Nanofibre Webs, Journal of Applied Polymer Science, Volume 135, Issue 38, DOI: 10.1002/app.46751, 2018. IF=1.901.

23. R. Roche, F. Yalcinkaya, Incorporation of PVDF Nanofiber Multilayers into Functional Structure for Filtration Applications, Nanomaterials, Volume 8, Issue 10, 771, DOI: 10.3390/nano8100771, 2018. IF=3.504.

24. I. Tiyek, A. Gunduz, F. Yalcinkaya, J. Chaloupek, Influence of Electrospinning Parameters on the Hydrophilicity of Electrospun Polycaprolactone Nanofibers, Journal of Nanoscince and Nanotechnology, Volume 19, pp. 1-10, 2019, DOI: 10.1166/jnn.2019.16605. IF=1.354.

25. F. Yalcinkaya, B. Yalcinkaya, J. Hruza, Electrospun Polyamide-6 Nanofiber Hybrid Membranes for Wastewater Treatment, Fibers and Polymers, Volume 20, Issue 1, pp 93-99, 2019. IF=1.353.

26. F.Yalcinkaya, A Review on Advanced Nanofiber Technology for Membrane Distillation, Journal of Engineered Fibers and Fabrics, 2019, DOI: 10.1177/1558925018824901. IF=0.678.

27. R. Roche, F. Yalcinkaya, Electrospun Polyacrylonitrile Nanofibrous Membranes for Point-of-Use Water and Air Cleaning, ChemistryOpen, Volume 8, Issue 1, pp. 97-103, 2019, DOI: 10.1002/open.201800267. IF=2.801.

28. E. Boyraz, F. Yalcinkaya, J. Hruza, J. Maryska, Surface-Modified Nanofibrous PVDF Membranes for Liquid Separation Technology, Materials, Volume 12, Issue 17, pp. 2702, 2019, DOI: 10.3390/ma12172702. IF= 2.972.

29. Mohd Reusmaazran Yusof, Roslinda Shamsudin, Sarani Zakaria, Muhammad Azmi Abdul Hamid, Fatma Yalcinkaya, Yusof Abdullah, Norzita Yacob, Fabrication and Characterization of Carboxymethyl Starch/Poly (L-Lactide) Acid/β-Tricalcium Phosphate Composite Nanofibers via Electrospinning, Polymers, Volume 11, Issue 9, pp. 1468, 2019, 10.3390/polym11091468. IF= 3.164.

30. F. Yalcinkaya, M. Komarek, Polyvinyl Butyral (PVB) Nanofiber/Nanoparticle Covered Yarns for Antibacterial Textile Surfaces, International Journal of Molecular Sciences, 2019, Volume 20, Issue 17, pp. 4317, DOI: 10.3390/ijms20174317. IF=4.183.

31. F. Yalcinkaya, Preparation of Various Nanofiber Layers Using Wire Electrospinning System, Arabian Journal of Chemistry, Volume 12, Issue 8, Pages 5162-5172, DOI: 10.1016/j.arabjc.2016.12.012, 2019. IF=3.298.

32. Jana Gaalova, Fatma Yalcinkaya, Petra Curinova, Michal Kohout, Baturalp Yalcinkaya, Martin Kostejn, Jan Jirsak, Ivan Stibor, Jason E. Bara, Bart Van der Bruggen, Pavel Izak, Separation of racemic compound by nanofibrous composite membranes with chiral selector, Journal of Membrane Science, 2020, Volume 596, IDOI: 10.1016/j.memsci.2019.117728. IF=7.015.

33. F. Yalcinkaya, E. Boyraz, J. Maryska, K. Kucerova, A Review on Membrane Technology and Chemical Surface Modification for the Oily Wastewater Treatment, Materials, 2020, Volume 13, Issue 2, pp 493, DOI: 10.3390/ma13020493. IF= 2.972 .

34. R. Torres-Mendieta, F. Yalcinkaya, E. Boyraz, O. Havelka, S. Wacławeka, J. Maryška, M.Černik, M.Bryjak, PVDF nanofibrous membranes modified via laser-synthesized Ag nanoparticles for a cleaner oily water separation, Applied Surface Science, Volume 256, 2020, DOI: 10.1016/j.apsusc.2020.146575. IF= 5.155.

35. Mohd Reusmaazran Yusof, Roslinda Shamsudin, Sarani Zakaria, Muhammad Azmi Abdulhamid, Fatma Yalcinkaya, Yusof Abdullah, Norzita Yacob, Electron Beam Irradiation of the PLLA/CMS/β-TCP Composite Nanofibers Obtained by Electrospinning, Polymers, 12 (7), 2020, DOI: 10.3390/polym12071593. IF= 3.426.

A.2. Published in refereed journals, technical notes, letters to the editor, discussion, case reports and a summary of publications other than the type of article

1. F. Yener, O. Jirsak, B. Yalçinkaya, 'Effects of Material Parameters on Electrospun Polyvinyl Butyral Nanofiber Web', Electronic Journal of Textile Technologies, Issue: 5, Volume: 2, Pages: 26-34, 2011.

2. R. Gemci, F. Yener, H. Solak, 'The Relationship between Applied Voltage and Diameter of PVB Nanofibers', KSU. Journal of Engineering Sciences, 14(1), 2011.

3. F. Yalcinkaya, B. Yalcinkaya, O. Jirsak, Dependent and Independent Parameters of Needleless Electrospinning, Fibers and Textiles, ISSN 1335-0617, 1, pages: 75-79, 2015.

4. F. Yalcinkaya, B. Yalcinkaya, J. Maryska, Preparation and Characterization of Polyvinyl Butyral Nanofibers Containing Silver Nanoparticles, Journal of Materials Science and Chemical Engineering, Vol.4, no 1, pp. 8-12. doi:10.4236/msce.2016.41002, 2016.

5. F. Yalcinkaya, A. Siekierka, M. Byjak, J. Maryska, Preparation of various nanofibrous composite membranes using wire electrospinning for oil-water separation, IOP Conf. Ser.: Mater. Sci. Eng., Volume 254, Article no 102011, 17th World Textile Conference AUTEX, DOI: 10.1088/1757-899X/254/10/102011, 2017.

6. F. Yalcinkaya, Mechanically enhanced electrospun nanofibers for wastewater treatment, E3S Web of Conferences, International Conference on Advances in Energy Systems and Environmental Engineering (ASEE17), Volume 22, Article no 00193, 7 pages, DOI: 10.1051/e3sconf/20172200193, 2017.

A.3. International conference by presenting papers published in full text

1. F.Yener, O.Jirsak, 'Improving Performance of Polyvinyl Butyral Electrospinning', 3th Nanocon, ISBN978-80-87294-23-9, Brno, Czech Republic, 2011.

2. F.Yener, O.Jirsak, B.Yalçinkaya, "The Determination of Anionic and Non-Ionic Surfactant Effect on Electrospun Nanofibers", 18th Strutex, Liberec-Czech Republic, 2011.

3. F.Yener, O.Jirsak, B.Yalçinkaya," Effect of Additives on Needle Electrospinning system, 18th Strutex, Liberec-Czech Republic, 2011.

4. B.Yalçinkaya, F.Yener, O.Jirsak, F. CengizÇallioğlu, 'Influence of NaCl Concentration on the Taylor Cone Number and Spinning Performance', 18th Strutex Liberec-Czech Republic, 2011.

5. B.Yalçinkaya, O.Jirsak, F.Cengiz Çallioğlu, F.Yener, ' The Effect of Concentration on Spinning Performance Using Roller Electrospinning ', 18th Strutex, Liberec-Czech Republic, 2011.

6. N.Duyar, B.Yalçinkaya, F.Yener, "Preparation of Electrospun fibers PVB/CNT Composite Fibers", 18th Strutex, Liberec-Czech Republic, 2011.

7. H.G. Sevgisunar, F.Yener, B.Yalçinkaya, "Comparision of Needle and Rod Electrospinning System", 18th Strutex, Liberec-Czech Republic, 2011.

8. F. Yener, O. Jirsak, 'Optimization and Characterization of Polyvinyl Butyral Nanofibers in Different Acetalisation Degree', 12th Autex, ISBN 978-953-7105-47-1,pp. 251-256, Croatia, Zadar 2012.

9. F. Yener, O. Jirsak, "Effect of Nonsolvent on Electrospinning Performance and Nanofiber Properties", 4th Nanocon, ISBN 978-80-87294-35-2, Brno, pp 471-475, Czech Republic, 2012.

10. B. Yalçinkaya, F. Yener, F. CengizCallioglu, O. Jirsak, "Effect of Solution Concentration and Additive on taylor cone Structure", 4th Nanocon, ISBN 978-80-87294-35-2, 1st edition, pp 200-203, Brno, Czech Republic, 2012.

11. O. Jirsak, K. Farana, F. Yener, 'Electrospinning Studies: Jet Forming Force', 19th Strutex, Liberec-Czech Republic, 2012.

12. F. Yener, O. Jirsak, "Development of New Methods for Study of Mechanism of Electrospinning", 19th Strutex, Liberec-Czech Republic, 2012.

13. F. Yener, B. Yalcınkaya, O. Jirsak, 'Roller Electrospinning System: A Novel Method to Producing Nanofibers', The International Istanbul Textile Congress, ISBN: 978-605-4057-37-5, pp. 917-922, Istanbul, Turkey, 2013.

14. B. Yalçinkaya, F. Yener, F. Cengiz-Callioglu, O. Jirsak, 'Relation between number of Taylor Cone and life of jet on the roller electrospinning', The International Istanbul Textile Congress, ISBN: 978-605-4057-37-5, pp. 213-218, Istanbul, Turkey, 2013.

15. F. Yener, B. Yalcınkaya, O. Jirsak, 'New Measurement Methods for Studying of Mechanism of Roller Electrospinning System', 5th Nanocon, Brno, ISBN 978–80–87294–47–5, pp808-812, Czech Republic, 2013.

16. F. Yalcinkaya, B. Yalcinkaya, O. Jirsak, Experimental Investigation of Salt Effect on Electrospinning Parameters and Nanofiber Morphology, 6th Nanocon, Brno, Czech Republic, ISBN 978-80-87294-53-6, 1st edition, pp 785-790, 2014.

17. F. Yalcinkaya, M. Komarek, D. Lubasova, F. Sanatrnik, J. Maryska, Producing Antibacterial Textile Material by Weaving PVB/CuO Nanocomposite Fiber Covered Yarn, 6th Nanocon, Brno, Czech Republic, ISBN 978-80-87294-53-6, 1st edition, pp 421-426, 2014.

18. F. Yalcinkaya, B. Yalcinkaya, O. Jirsak, Dependent and Independent Parameters of Needleless Electrospinning, 20th Strutex, Liberec-Czech Republic, 2014.

19. F. Yalcinkaya, B. Yalcinkaya, J. Maryska, Preparation and Characterization of Polyvinyl butyral Nanofibers Containing Silver Nanoparticles, (abstract) The 5th Conference on Nanomaterials (CN 2016), 14-16 January, Bangkok, page 59, 2016.

20. F. Yalcinkaya, B. Yalcinkaya, J. Hruza, P. Hrabak, J. Maryska, Nanofibrous Composite Membranes for Microfiltration, 8th Nanocon-International conference on Nanomaterials, Brno, Czech Republic, October 17 2016.

21. E. Boyraz, F. Yalcinkaya, Polymeric Nanofibers Produced by Needleless Electrospinning, 22th Strutex, Liberec-Czech Republic, 2018.

22. F. Yalcinkaya, Ondrej Hofman, Jiri Maryska, Surface Properties of Lowvacuum Plasma Modıfıed Polyvınylıdene Fluorıde (PVDF) Nanofıber Membranes, 18th World Textile Conference AUTEX, 20-22 June 2018, Istanbul, Turkey.

23. E. Boyraz, F. Yalcinkaya, Oily Wastewater Separation by Using Nanofibrous Membrane, 47th Textile Research Symposium, June 17-19, Liberec, Czech Republic, ISBN 978-80-7494-473-4, 2019.

A.4. International conference by presenting papers published in abstract

1. F. Yalcinkaya, B. Yalcinkaya, J. Hruza, P. Hrabak, Mechanically Enhanced Electrospun Polyamide-6 Nanofiber Composite Membranes for Liquid Filtration, MELPRO-Membrane and Electrosmembrane Process, 13-16 May 2018, Prague, Czech Republic.

2. F. Yalcinkaya, A. Siekierka, Modified PVDF Nanofibrous Membranes for the Separation of Oil-Water Emulsion, NART-Nanofiber, Applications and Related Technologies, 18-20 Sept 2019, Liberec, Czech Republic.

3. F. Yalcinkaya, J. Hruza, J. Maryska, Functional Electrospun Nanofiber Webs for the Separation of Oily Wastewater, Nanocon 2019- 11th International Conference on Nanomaterials - Research & Application, 16-18th October 2019, Brno, Czech Republic.

A.5. Patents

1. Method for Application of a Cosmetic Composition Containing at least One Active Substrate to Skin and a Means for Carrying out this Method for Application of the Cosmetic Composition. Nafigate Cosmetic a.s.; Ladislav Mares, Jana Svobodova, Fatma Yalcinkaya. International Patent No: PCT/CZ2015/000111, WO/2016/050227, 07.04.2016.

2. J. Gaálová, Fatma Yalcinkaya, P. Cuřínová, M. Kohout, I. Stibor, P. Izák: Separation of Chiral Drugs by Composite Chiral Membrane Based on 1,2- diaminocyclohexane and 1,3-diaminobenzene, CZ 308513 (2020).

A.6. Book Chapters

1. F. Yalcinkaya, B. Yalcinkaya, O. Jirsak, Dependent and Independent Parameters of Roller Electrospinning System, Electrospinning, Material, Techniques, and Biomedical Applications, book edited by Sajjad Haider and Adnan Haider, ISBN 978-953-51-2822-9, Print ISBN 978-953-51-2821-2, http://dx.doi.org/10.5772/65838, DOI: 10.5772/62860, IntechOpen publisher, Published: December 21, 2016.

2. B. Yalcinkaya, F. Yalcinkaya, Nanofibers in Liquid Filtration, Green electrospinning, book edited by Nesrin Horzum, Mustafa M. Demir, Rafael Munoz-Espi, Danieal Crespy, ISBN 978-3-11-058139-3, De Gruyter publisher, July 2019.

3. F. Yalcinkaya, A. Gul, E. Boyraz, M. Bryjak, Nanofibers for oil-water separation and coalescing filtration, "Electrospun and Nanofibrous Membranes: Principles and Applications" to be published by Elsevier (submitted), 2020.